Conjugated Polymer Nanoparticles by Direct Arylation Polycondensation

A thesis submitted to

The University of Manchester

for the degree of

Doctor of Philosophy

in the Faculty of

Science & Engineering

2021

Sebastian P. Broll

School of Natural Sciences

Department of Chemistry

Blank Page

Table of Contents

word count 40397

List of Figures

List of Tables

List of Schemes

List of Equations

List of Abbreviations

°C	degrees Celsius
Đ	molar mass dispersity
δ	chemical shift
λ	wavelength
μ	field-effect mobility
ADF	Annular Dark Field
AFM	Atomic Force Microscopy
BDT	Benzo[1,2-b:4,5-b']dithiophene
BT	2,1,3-Benzothiadiazole
BuOH	1-Butanol
CB	Chlorobenzene
$CDCl_3$	Deuterated chloroform
$CHCl_3$	Chloroform
CMC	Critical Micelle Concentration
CMD	Concerted Metalation Deprotonation
CMT	Critical Micelle Concentration
CPN	Conjugated Polymer Nanoparticle
COSY	Correlation Spectroscopy
DArP	Direct Arylation Polycondensation
DCB	Dichlorobenzene
DCM	Dichloromethane
DFT	Density Functional Theory
DLS	Dynamic Light Scattering
DPP	Diketopyrrolopyrrole
DSC	Differential Scanning Calorimetry
EDOT	3,4-Ethylenedioxythiophene
E_g	Band gap
eq.	equivalent
EtOH	Ethanol
eV	Electron Volts
FRET	Förster Resonance Energy Transfer
F4	1,2,4,5-Tetrafluorobenzene
F2BT	5,6-Difluoro-2,1,3-benzothiadiazole
g	gram
GCA	Gradual Channel Approximation
GPC	Gel Permeation Chromatography

h	hour
HD	hexadecane
HOMO	Highest Occupied Molecular Orbital
HSQC	Heteronuclear Single Quantum Correlation
HMBC	Heteronuclear Multiple Bond Correlation
HMQC	Heteronuclear Multiple Quantum Correlation
HT	High Temperature
Hz	Hertz
i	Iso
I	Current
(IPr*)$PdCl_2$(TEA)	1,3-Bis[2,6-bis-(diphenylmethyl)-4-methylphenyl]imidazole-2-ylidine
J	Coupling Constant
LogM	Log Molecular weight
LUMO	Lowest Unoccupied Molecular Orbital
m/z	Mass-to-charge ratio
MALDI-TOF	Matrix Assisted Laser Desorption Ionisation - Time of Flight
MeOH	Methanol
min	Minute
mL	Millilitre
M_n	Number average molecular weight
MMA	Methyl Methacrylic Acid
MWCO	Molecular Weight Cut-Off
MMW	Micelle Molecular Weight
mol	Mole
MS	Mass Spectrometry
M_w	Weight average molecular weight
n	normal
NDI	Naphthalene Diimide
NHC	N-Heterocyclic Carbene
nm	Nanometre
NMR	Nuclear Magnetic Resonance
n-type	Negative charge carrier semiconductor
o	Ortho
OFET	Organic Field-Effect Transistor
OLED	Organic Light-Emitting Diode
OSC	Organic Semiconductor
p	Para
PEO	Poly(ethylene oxide)
PEDOT	Poly(3,4-ethylenedioxythiophene)
PEG	Polyethylene Glycol

PDI	Polydispersity Index of particle size distribution
PIE	Phase Inversion Emulsification
PIT	Phase Inversion Temperature
PL	Photo Luminescence
PLQY	Photoluminescence Quantum Yield
PMMA	Poly(methyl methacrylic acid)
ppm	Parts per Million
PPV	Poly(p-phenylene vinylene)
PrOH	Propanol
PS	Polystyrene
PTFE	Poly(tetrafluoroethylene)
p-type	Positive charge carrier semiconductor
rpm	Revolutions per minute
rt	Room Temperature
SDS	Sodium Dodecyl Sulphate
STEM	Scanning Transmission Electron Microscopy
T	Temperature
TCB	1,2,4-trichlorobenzene
TEM	Transmission Electron Microscopy
TFT	Thin Film Transistor
TGA	Thermogravimetric Analysis
THF	Tetrahydrofuran
TPD	Thieno[3,4-c]pyrrole-1,4-dione
TT	Thieno[3,2-b]thiophene
UV/Vis	Ultraviolet/Visible
V	Volt
XPS	X-ray Photoelectron Spectroscopy
^{1}H	Hydrogen
^{13}C	Carbon-13
^{19}F	Fluorine

Abstract

Conjugated polymer nanoparticles can be successfully prepared by conventional C-C cross couplings (e.g Suzuki-Miyaura, Stille etc.) in aqueous emulsion and miniemulsions.[1,2,3] This thesis investigates the preparation of these conjugated polymer nanoparticle dispersions by novel C-C cross couplings utilising C(sp^2)-H bonds. This direct arylation polycondensation (DArP) approach[4] enables a more atom efficient preparation of semiconducting polymers in fewer synthesis steps. Judicious reaction parameter screening facilitated the formation of stable nanoparticle dispersions in the sub-micron regime with particle size dispersities (PDI) < 0.30 by increasing the hexadecane concentration. A comprehensive understanding of the influence of the reaction parameters on the molecular weight of the polymer prepared by this *in-situ* miniemulsion polymerisation technique was developed. Polymer molecular weights of $M_n \geq 10$ kg mol^{-1} were controlled reproducibly by adjusting the pivalic acid and potassium carbonate concentration.

The microstructure of the polymers in these nanoparticle dispersions have been analysed and the identity of any polymer backbone defects investigated. DArP is known to introduce homo coupling defects into the polymer backbone that are less prevalent in polymers prepared by more conventional C-C coupling methods.[4] Hence, different analytical methods such as mass spectrometry (MALDI-TOF-MS) and NMR techniques (^1H, ^{13}C, ^{19}F and 2D experiments) were employed to identify and quantify the defects.

As a proof of principle for the applicability of the prepared dispersions, organic field effect transistors were fabricated using the aqueous dispersions. Comparison between the holistic synthesis to device fabrication in water presents a greener and scalable process for the printing of electronic devices with measured electron mobilities of $\mu_e = 0.05$ cm^2 V^{-1} s^{-1} for PDPPF4.

Declaration

No portion of the work referred to in the thesis has been submitted in support of an application for another degree or qualification of this or any other university or other institute of learning.

Copyright Statement

Acknowledgements

First and foremost, I would like to express my gratitude to Prof. Dr. Michael L. Turner for the support and freedom he granted for the realisation of this research project. I also would like to thank Dr. Benjamin Lidster and Dr. Andrew Foster for their advice along the way. My appreciation for their supervision and support during my time at VISTEC go to Prof. Dr. Vinich Promarak, Assoc. Prof. Dr. Daniel Crespy, Dr. Taweesak "Nueng" Sudyoasuk, and Dr. Pichaya Pattanasattayavong.

I acknowledge the support of the administrative staff of the Department of Chemistry at the University of Manchester and of VISTEC for realising this joint programme and the financial support of VISTEC and Chromition Ltd.

Many thanks go to the technical staff at the University of Manchester, namely Emma Enston, Mohammed "Mac" Maqsood and Gareth Smith (mass spectrometry laboratory), Dr. Carlo Bawn and Dr. Ralph Adams (NMR facility), Martin Jennings (elemental analysis), Mark Mullin, Alan Beaver, Tim Neale and Willie Opone (chemistry stores). I wish my collaboration partners Usman Khan and Evan Tillotson good luck in their professional endeavours and acknowledge their contribution to this body of work.

Unforgotten are the moments of witty humour and laughter in OMIC's offices and laboratories and the pubbing after work. Special thanks go to Jair Esquivel Guzman, Seong Hyun Park, Raymundo Marcial Hernandez, Joshua Moore, Jaruphat Wongpanich, Michael "17" Chan, Vanessa Tischler, Emma Poole, Gleen Sunley Saez, Robyn Worsley, Vaiva Nagyte, Matthew Boyes, Junru Zhang and all those who I have not mentioned.

To my friends outside of academia, Loulou and David which made our time in Manchester so enjoyable with countless barbeques and Canasta games. David, we must admit that our missuses play a couple of leagues above us.

Bei meiner ganzen Familie möchte ich mich von Herzen für Rat und Tat über all die Jahre bedanken. Vor allem meinen Eltern Annette und Peter Broll und meiner besseren Hälfte Luna verdanke ich, dass ich mir diesen Traum erfüllen konnte. Ihnen widme ich dieses Werk.

- Common sense is not so common. -

Voltaire

1. Introduction

1.1. Organic Semiconductors

The invention of transistors in the middle of the 20th century led to inorganic semiconductors, such as silicon and germanium, developing a predominant position in the manufacturing of electronic components. Electronic devices based on vacuum tubes were gradually replaced leading to an omnipresence of microelectronic components in our everyday lives. At the beginning of the 21st century, a new electronic revolution is on the horizon that will realise electronic components, displays and photovoltaics based on organic semiconductors. Tremendous progress in this area has been achieved ever since the discovery of the conductivity of doped polyacetylene in 1977.[5] Alan Heeger, Alan MacDiarmid and Hideki Shirakawa were awarded the Nobel Prize in Chemistry in 2000 for the discovery of conducting polymers. Further developments in the 1980s induced an elevated interest in the use of organic semiconductors, such as in organic photovoltaics.[6] At the same time, the first thin film transistors based on conjugated oligomers and polymers were published.[7–9] The breakthrough in the field of organic semiconductors was achieved by vapour deposition of conjugated small molecules for use in highly efficient electroluminescent diodes.[10,11] Due to great efforts in both academia and industry, organic light emitting diodes (OLEDs) were integrated into commercially available products within the last decade.

An evolution of conjugated polymers is depicted in figure 1.1 starting from poly(sulphur nitride) (**1.1**) towards poly acetylene (**1.2**), poly(thiophene) (**1.3**) and donor-acceptor conjugated polymers (-**D**-**A**-).[12] Poly(sulphur nitride) is depicted as precursor of poly acetylene since Alan MacDiarmid stated that his research on polyacetylene was inspired by poly(sulphur nitride) and its intrinsic metallic properties. Poly(sulphur nitride) itself was not subject to lasting research since it is synthesised by sublimation forming explosive S_2N_2 as intermediate.

A common feature of those materials is the alternating single and double bond. The π-orbitals of the double bond overlap leading to delocalisation of the electrons along the polymer backbone. Amongst these materials, polythiophenes have been extensively

studied due to their ease of structural modification and solution processibility by incorporation of aliphatic side chains into the polymer backbone.[13]

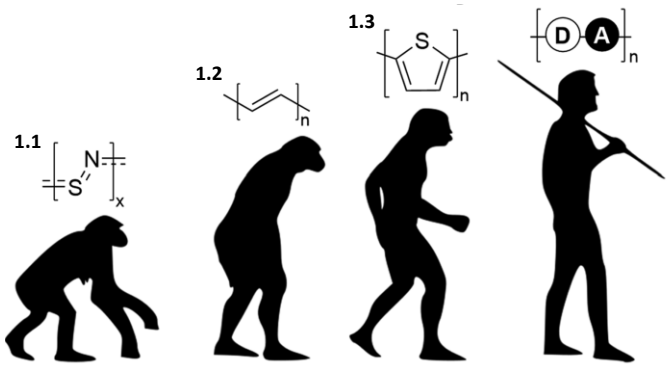

Figure 1.1: Evolution of conjugated polymers starting from poly(sulphur nitride) (**1.1**) towards poly acetylene (**1.2**) and poly(thiophene) (**1.3**) and donor acceptor conjugated polymers (-**D**-**A**-).[12]

During the past two decades, electron donors (D) (scheme 1.1, **1.4** and **1.5**) and acceptors (A) (scheme 1.1, **1.6** and **1.7**) have been developed for their use in donor-acceptor (DA) conjugated copolymers. The bandgap of DA polymers can be fine-tuned since the donor lowers the LUMO and the acceptor elevates the HOMO of the organic semiconductor (OSC).[14] Moreover, interactions between the two moieties planarise the polymer backbone and improve upon intrachain packing leading to greater charge carrier mobilities.[15] Hence, alternating DA Polymers have emerged as a leading class of high-performance materials in organic electronics.[16,17]

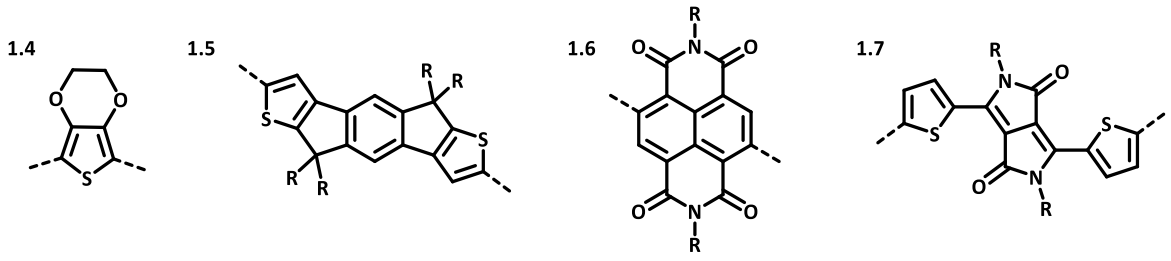

Scheme 1.1: Examples of common building blocks of semiconducting polymers.[15,18,19] 3,4-ethylenedioxythiophene **1.4** , indaceno dithiophene **1.5**, naphthalene diimide **1.6** and diketopyrrolopyrrole **1.7**.

1.1.1. Organic Field Effect Transistors

Conjugated organic polymers are commonly employed in organic field effect transistors (OFET). OFETs are fabricated by deposition of thin films of conjugated polymers on an insulating substrate. Various deposition techniques are available: Doctor blading, spray and spin-coating, physical vapour deposition (PVD) and inkjet printing.[20] Amongst these techniques, PVD is commonly utilised for electrode deposition whereas solution processable dielectrics and OSCs are prepared by spin coating in research and development environments. OFET devices are made up of three main components, which are the dielectric material, semiconductor and electrodes. Three electrodes are required; a gate electrode which is separated from the semiconductor by the dielectric material, while the semiconductor layer connects the source and drain electrodes. Figure 1.2 illustrates the most common device architectures.

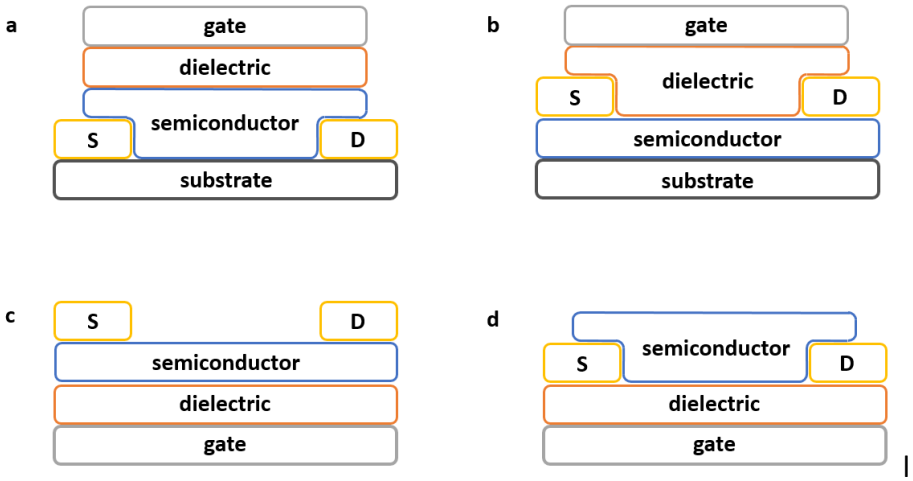

Figure 1.2: Common OFET architectures: top-gate, top-contact (TGTC, a); top-gate, bottom-contact (TGBC, b); bottom-gate, top-contact (BGTC, c); bottom-gate, bottom-contact (BGBC, d).

Charge accumulation between the source and drain contacts is achieved by applying a bias between the gate and drain electrodes and is explained by Schockley's gradual channel approximation (GCA) for thin film field effect transistors (TFTs).[21] Thus, TFTs operate when two electric fields are applied: (i) between the gate electrode and the source contact (V_G) and (ii) between the source and drain contacts (V_D). The GCA simplifies this

2-dimensional problem into two 1-dimensional equations for each electric field applied. Several assumptions are made by GCA such as zero channel thickness, no contact resistance and that charge mobility is independent of bias.[22,23] The drain current V_D depends on several parameters. The following equation is applicable in case of $V_D < V_G - V_T$, where V_G is the gate voltage and V_T the threshold voltage (equation 1). V_T accounts for charge accumulation/depletion that facilitates/hinders charge transport along the OSC-dielectric interface. If the OFET device operates within this "linear regime", the charge accumulation along the channel is evenly distributed (figure 1.3).

$$I_{D,lin} = \frac{W\ \mu\ C_i}{L}\ (V_G - V_T)\ V_D \qquad (1)$$

W and L are the channel width and length, C_i is the areal capacitance and μ is the charge carrier mobility.

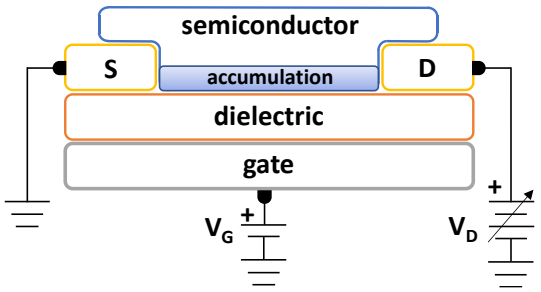

Figure 1.3: FET operates in accumulation mode within the linear regime where $V_D < V_G - V_T$.

When $V_D \geq V_G - V_T$, the field strength between the source and drain contact is insufficient (V_D) causing a depletion area and the conducting channel is pinched off (figure 1.4). The device operates in the saturation regime. Under this condition, the drain current becomes V_D independent.

$$I_{D,sat} = \frac{W\ \mu\ C_G}{2L}\ (V_G - V_T)^2 \qquad (2)$$

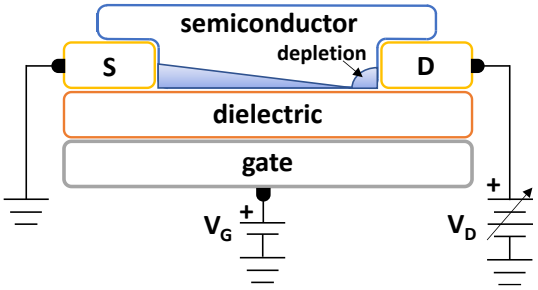

Figure 1.4: FET operates in accumulation mode within the saturation regime where $V_D > V_G - V_T$.

Figure 1.5 depicts the transfer and output characteristics of a transistor. As explained above, the output curve (a) exhibits linear behaviour for I_D at small values of V_D at constant V_G. Beyond the pinch-off point, the channel current saturates and I_D is independent of V_D. Superlinear behaviour indicates charge injection barriers and parasitic contact resistance. The transfer curve (figure 1.5, right) illustrates I_D against V_G at constant V_D.

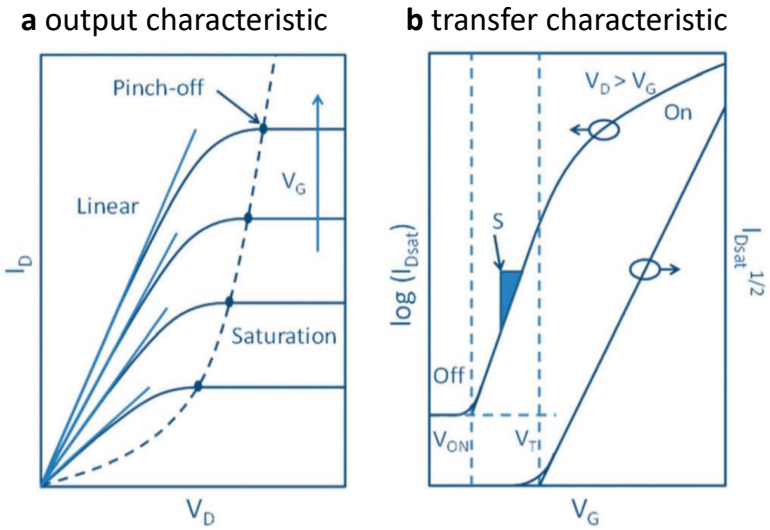

Figure 1.5: Transfer curve: Drain current I_D versus gate current V_G (a) and output curve I_D versus gate current V_D (b).[24]

Several important device metrics are deduced from experimentally acquired transfer curves: For example, by differentiating equation 2 to equation 3, the device mobility can be extracted. Equation 3 indicates that by plotting the square root of the drain saturation current ($I_{D,sat}^{1/2}$) versus V_G, the square of the slope of the resulting straight line

is proportional to μ. The charge carrier mobility μ is arguably the most popular benchmark of a material's performance in an OFET and describes how quickly a charge can move through a semiconductor if an external field is applied. Other parameters determined from the transfer curve are the threshold voltage V_T and the subthreshold swing S. V_T is derived by extrapolation of the linear curve to the intercept with the V_G axis. The subthreshold swing (S in figure 1.5 a) can be extracted from the logarithmic I_D plot. The subthreshold swing indicates how quickly a TFT undergoes a transition from an off to on state and gives, together with V_T, an estimate of the trapping density of states (DOS) at the OSC-dielectric interface. Additionally, the current on/off ratio is derived by comparing the current baseline at a specified onset voltage V_{on}.

$$\mu_{sat} = \frac{2L}{W\ C_G}\left(\frac{\partial\sqrt{I_{D,sat}}}{\partial\ V_G}\right)^2 \qquad (3)$$

Semiconductors are distinguished between those in which electrons are the charge carrier (n-type) and those in which holes are the charge carriers (p-type). In addition, there are examples of oligomers and polymers that exhibit ambipolar behaviour as well (e.g. poly(diketopyrrolopyrrole benzothiadiazole), P(DPPBT)).[25] Due to this observation, both mobilities in an OFET are commonly measured.[26] Whether an OSC is p- or n-type depends on the respective HOMO/LUMO levels, the Fermi level, and the work function between OSC and electrode. In recent years, mobilities in excess of 10 $cm^2\ V^{-1}\ s^{-1}$ have been reported for p-type but n-type materials have yet to achieve these values.[27]

Real-life devices deviate from ideal behaviour due to impurities, ambient oxygen, trapping sites caused by disordered microstructures, various modes of charge carrier transportation and contact resistance R_c on the organic semiconductor/electrode contacts.[27] The contact resistance is the result of the energetic difference Δϕ between the work functions of the OSC and the metal electrode, this causes charge carriers to move across the OSC/metal interface forming a Schottky barrier. Since the measured transconductance depends on the sum of the channel and contact resistances, inaccurate determination of the charge carrier mobility can arise if the transfer characteristics deviate from reality.[28] As a consequence, the mobility can be overestimated if non-ideal OFET

characteristics are observed and caution should be applied to some mobility values reported in the literature. The issue is described in detail in Anthopoulos' review.[27] Moreover, intrinsic charge transconductance highly depends on device architecture and processing renders comparison and reproducibility challenging.[29,30]

1.2. Conjugated Polymer Nanoparticles (CPNs)

The preparation of nanoparticles by emulsion polymerisation is a well-established procedure to obtain coatings and paints.[31] Nanoparticles of conjugated polymers, sometimes referred to as conjugated polymer dots, are of special interest for various applications in life sciences[32,33,34] organic electronics[35,36] and catalysis[37,38].

Solutions of pre-formed conjugated polymers can be emulsified to produce stable aqueous nanoparticle dispersions. This approach requires the use of a multistep procedure in which the conjugated polymer is initially prepared and isolated and subsequently dispersed. There are two common methods, either the miniemulsion (figure 1.6, **a**) or reprecipitation method (figure 1.6, **b**).

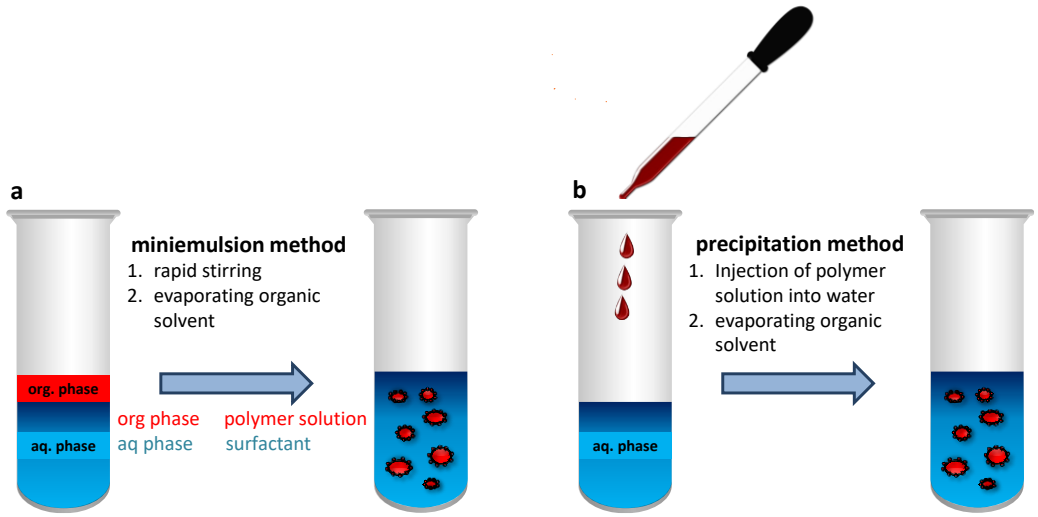

Figure 1.6: Post polymerisation method to obtain CPNs in emulsion by using surfactants and a solvent immiscible in water (a) or by reprecipitation with a water miscible solvent (b).[39]

In order to obtain CPNs by the miniemulsion route, the polymer is dissolved in a "good" solvent that is immiscible in water. The polymer solution is then injected into an aqueous solution containing an appropriate surfactant.[40] The mixture is emulsified by

stirring, ultrasonication or homogenisation, which forms surfactant-stabilised small droplets of the polymer solution within the aqueous phase. The organic solvent is subsequently evaporated to obtain a dispersion of CPNs in water that are stabilised by the surfactant. The initial droplets can flocculate due to Oswald ripening and coalescence.[31] Oswald ripening can be avoided by adding a hydrophobe to the dispersed phase that counteracts the Laplace pressure.[41,42] The reprecipitation method (figure 1.6, **b**) requires a "good" water miscible solvent for the hydrophobic conjugated polymer, which is usually THF. The polymer solution is then added to the aqueous phase and stirred rapidly or sonicated to from solid nanoparticles. After removal of the solvent, water dispersed nanoparticles are obtained, without the presence of surfactant. The formation of particles is favoured by the hydrophobic effect which usually leads to spherical shapes due to minimal exposure of the polymer chains to water. A limitation of the reprecipitation and miniemulsion routes is the scalability due to the limited solubility of conjugated polymers in organic solvents. Particularly in the reprecipitation approach only very dilute solutions and thus dispersions with low solid content are obtained. To improve the scalability of the reprecipitation and miniemulsion routes, the formation of conjugated polymers through *in-situ* polymerisation during the emulsifying process has been researched and are presented in the next section.

1.2.1. Polymerisation of Conjugated Polymers in Heterophasic Systems

The first polymerisations of conjugated polymers in emulsion were reported by Weder and coworkers in an one pot approach to form hyperbranched poly(phenylene ethynylene) particles in 2004 (figure 1.7, **1.11**).[43] The polymerisation was performed *via* a palladium catalysed Sonogashira coupling with $A_2 + B_2 + A_3$ monomers of which monomers A (figure 1.7, **1.8** and **1.10**) contain bromine and iodine functionalities and monomer B (figure 1.7, **1.9**) contains ethynyl end groups. The catalyst system employed was $Pd(PPh_3)_4$, CuI and diisopropylamine, and the organic phase was toluene that was emulsified into the aqueous phase.

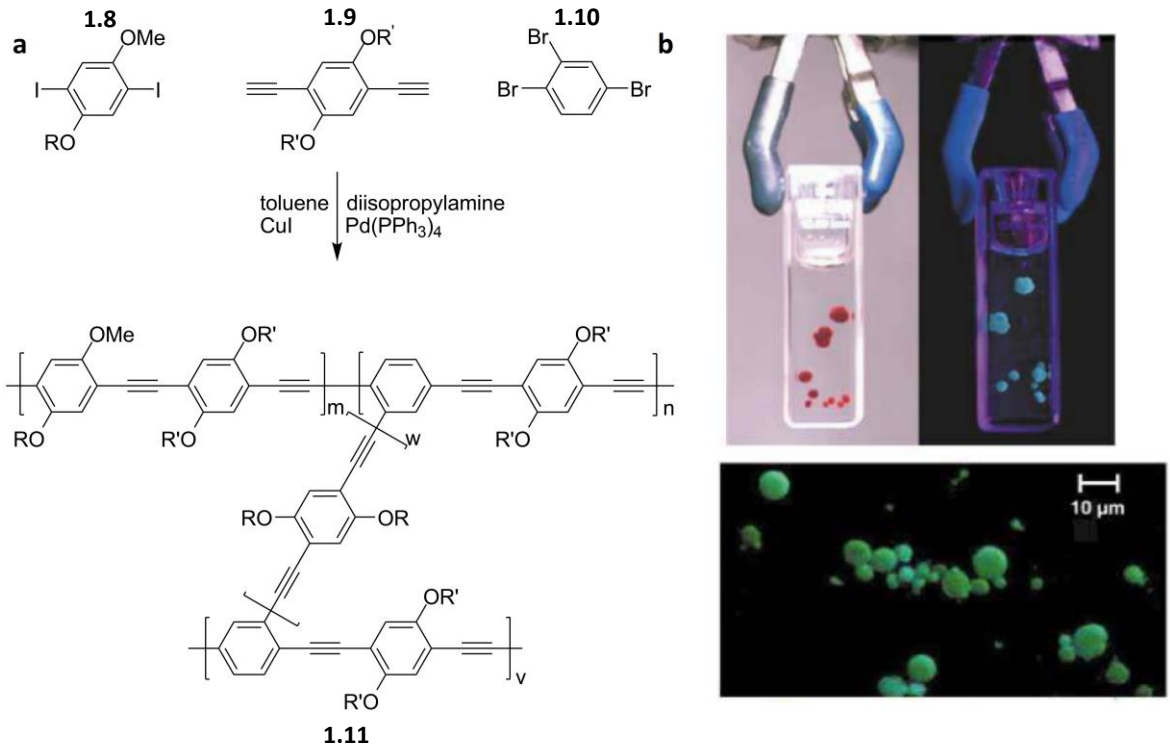

Figure 1.7: Synthesis of crosslinked PPEs (a). Photographs and optical micrographs of the micrometer-sized particles obtained by Weder and coworker (b).[43]

In 2006, Mecking and coworkers addressed the processability challenge of polyacetylene[44,45,46] and reported a polyinsertion within hexane/ethanol nanoparticles in an aqueous continuous phase.[47] The catalytic system used was $Pd(OAc)_2$ and tBu$_2$P(CH$_2$)$_3$PtBu$_2$ (1,3-bis(di-tert-butyl)phosphino-propane) due to the high activity of this mixture to polymerise acetylene in aqueous media. The authors explained the small particle sizes obtained (e.g. 20 nm, determined by transition electron microscopy, TEM) *via* a dispersion polymerisation mechanism: Initially polymerised acetylene precipitated from the hexane/ethanol droplets and are subsequently stabilised by surfactant. Hence, the polymerisations can continue for prolonged reaction times as long as an acetylene atmosphere is maintained.

This report followed a publication within the same year by Müllen and coworkers which presented the formation of polyacetylene and poly(3,4-ethylenedioxythiophene) (PEDOT) nanoparticles in a non-aqueous oil-in-oil emulsion polymerisation.[48] Poly(isoprene-*block*-poly(methyl methacrylate)) P(PI-b-PMMA) was used as surfactant and cyclohexane as the continuous phase. In the case of PEDOT synthesis, an iron (III) catalyst was dissolved in acetonitrile and polymerisation of EDOT monomer yielded isotropic

polymer particles below 30 nm (determined by TEM). Polyacetylene was polymerised using the Luttinger catalyst (i.e sodium borohydrate and cobalt (II) nitrate hexahydrate) resulting in spherical particles with a diameter of 43 ± 10 nm.

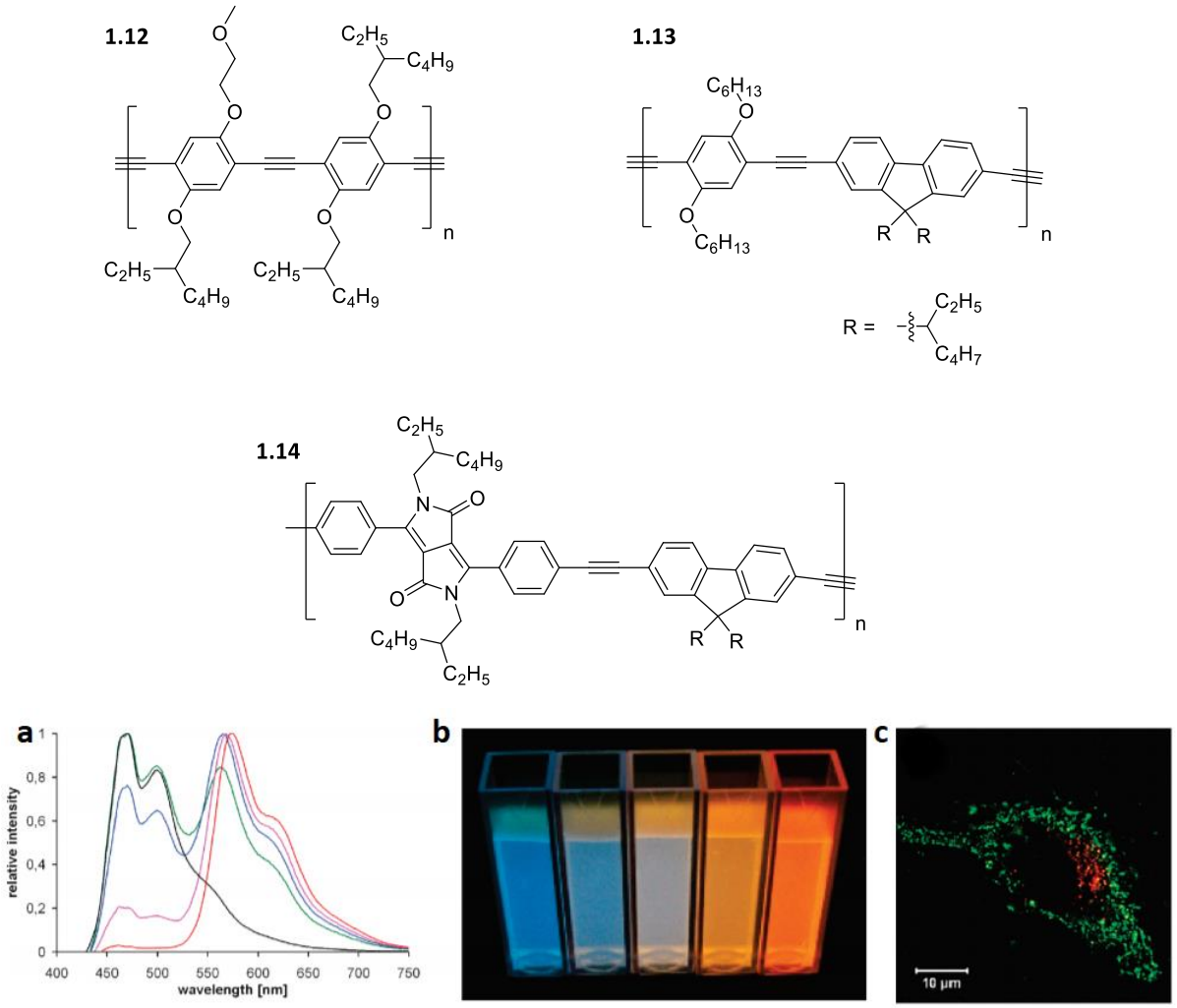

Figure 1.8: Polymers prepared as CPNs by Mecking and coworker (**1.12** – **1.14**) and fluorescence spectra ($\lambda_{excitation}$ = 398 nm, a). Visual appearance of aqueous nanoparticle dispersions under UV light illumination ($\lambda_{excitation}$ = 366 nm, b). Micrographs of fixed HeLa cells labelled with conjugated polymer nanoparticles excited at 458 nm (c).[49]

Mecking and co-workers extended the miniemulsion polymerisation method to an aqueous solution for the preparation of poly(2,5-dialkoxyphenylene diethynylene) (figure 1.8, **1.12**) and poly(9,9'-dihexylfluorene diethynylene) (figure 1.8, **1.13**) nanoparticles *via* a Glaser coupling, using $Pd(PPh_3)_4$ as a catalyst and sodium dodecyl sulphate (SDS) as the surfactant.[50] The molecular weights of the polymers obtained were measured to be in the range of $M_n = 10^4$ to 10^5 g mol^{-1} by gel permeation chromatography (GPC) and the particle

diameter was determined to be about 30 nm by TEM. Covalent incorporation of electron withdrawing building blocks into the poly(2,5-dialkoxyphenylene diethynylene) (figure 1.8, **1.14**) showed effective energy transfer to the dye, which resulted in long wavelength emission for *in vitro* and *in vivo* applications. Ionic surfactants are particularly favourable since their micellar molecular weights (MMWs) are lower than those of non-ionic surfactants for miniemulsion polymerisations and enable removal of the surfactant micelles by dialysis possible.

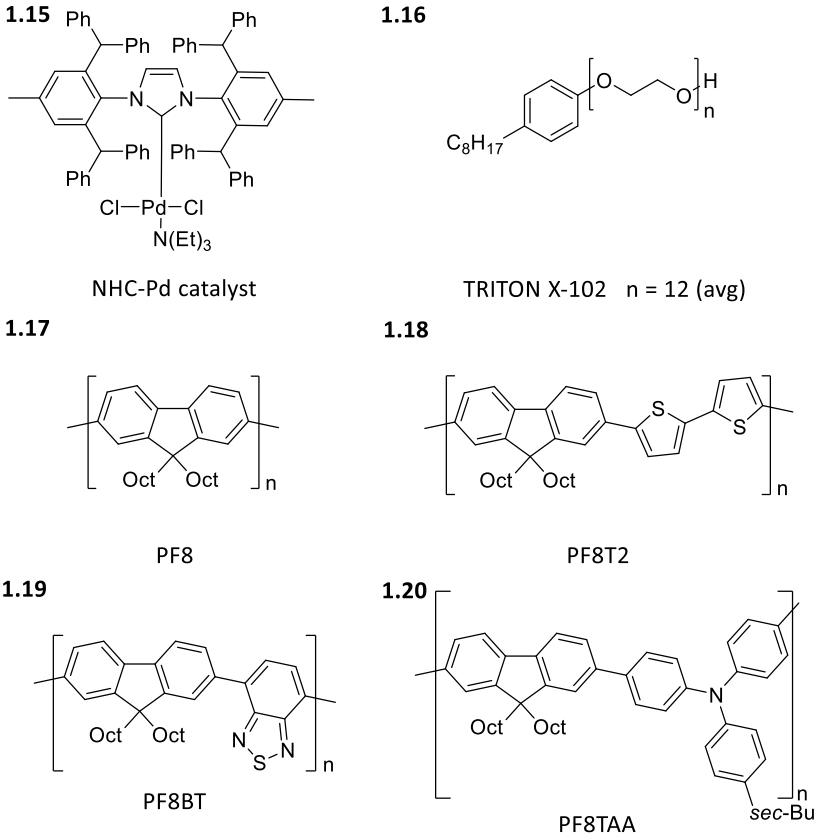

Figure 1.9: NHC based Pd catalyst (IPr*)$PdCl_2$(TEA) **1.15** applicable for polymerisations at room temperature and Triton X102 surfactant **1.16**. Poly(9,9-dioctylfluorene-*alt*-benzothiadiazole) PF8BT **1.17**, poly(9,9-dioctylfluorene-*alt*-bithiophene) PF8T2 **1.18**, poly(9,9-dioctylfluorene) PF8 **1.19**, poly(9,9-dioctylfluorene-*alt*-4-s-butylphenyldiphenylamine) PF8TAA **1.20**.

The palladium catalysed Suzuki-Miyuara cross coupling reaction is favourable for polymerisations in miniemulsion as it avoids the use of highly air sensitive or toxic organometallic reagents. It also enables the incorporation of a range of structurally diverse moieties into the backbone of the polymers. Usually, this reaction is carried out at elevated temperatures using palladium catalysts in a temperature range above the cloud point of

most non-ionic surfactants. Although ionic surfactants exhibit higher cloud points than their non-ionic counterparts, they are disadvantaged by their sensitivity towards the ionic strength of the solution, which is a crucial issue for in vitro and in vivo applications. In order to circumvent this issue, catalysts such as the N-heterocyclic carbene (NHC) based Pd complexes (figure 1.9, **1.15**) have been developed that enable the Suzuki-Miyaura cross coupling reactions to be conducted at room temperature.[51,52] Aqueous dispersions of polyfluorene copolymer nanoparticles can be prepared employing the (IPr*)$PdCl_2$(TEA) catalyst **1.15** in aqueous dispersions using the non-ionic surfactant Triton X-102 (figure 1.9, **1.16**).[1]

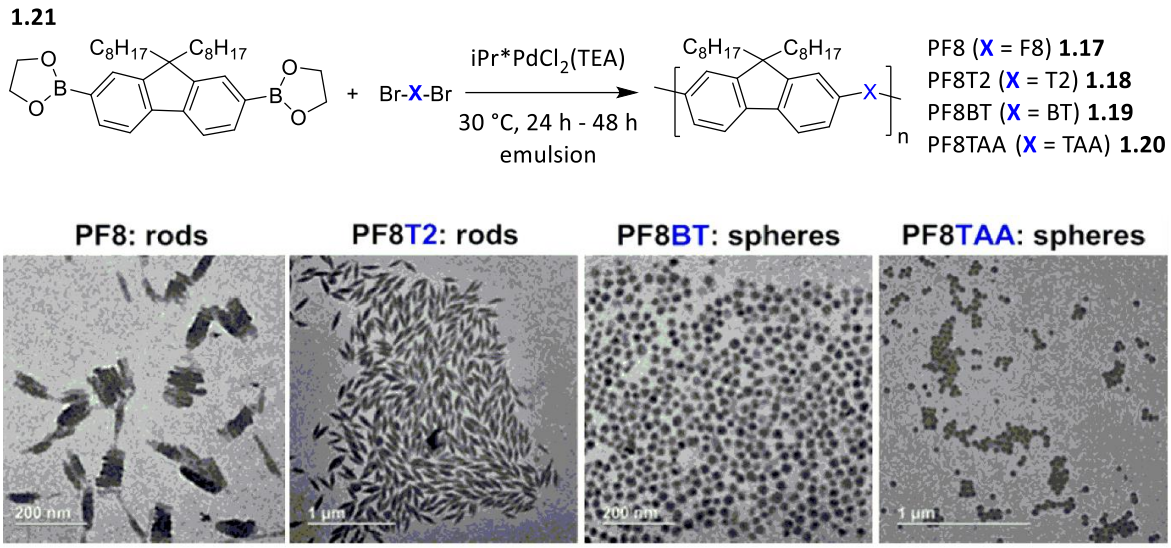

Figure 1.10: Reaction scheme and the particles obtained via a miniemulsion Suzuki-Miyaura cross polymerisation protocol at room temperature reported by Muenmart and Turner.[1]

Nanoparticles derived from poly(9,9-dioctylfluorene) (PF8, **1.17**) and poly(9,9-dioctylfluorene-*alt*-bithiophene) (PF8T2, **1.18**), revealed an anisotropic rod shape of 200 nm length in TEM analysis. In contrast, polyfluorene copolymers that contain benzothiadiazole (PF8BT, **1.19**) or triarylamine (PF8TAA, **1.20**) showed spherical particles with diameters of 20 – 40 nm. UV/Vis absorption spectra of the PF8 dispersions revealed high levels of ordered β-phase polyfluorene. Most notably, conjugated polymer concentrations were achieved in aqueous emulsions up to 11 mg mL^{-1}, which renders these dispersions suitable for applications in large area electronics.

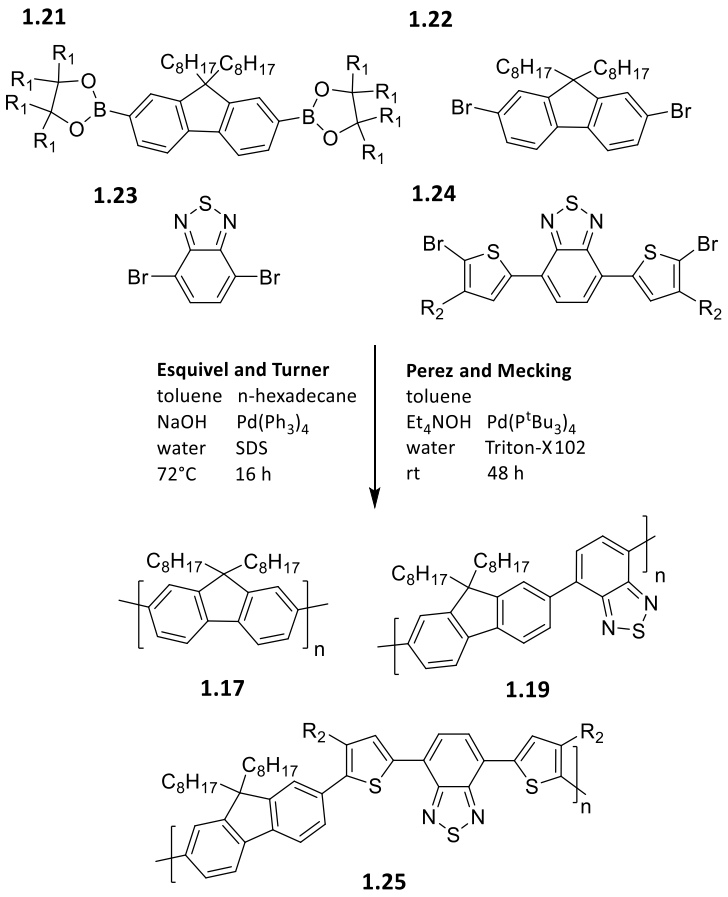

Figure 1.11: Overview of monomers in miniemulsion polymerisation reaction obtained by Esquivel *et al*. (entries **1.17**, **1.19** and **1.25**, R_1, R_2 = H) and Perez *et al*. (entries **1.17** and **1.25**, R_1 = CH_3 and R_2 = C_6H_{13}).[2,3]

A further contribution from Esquivel *et al*. investigated the effect of varying the co-monomer ratios on the optical properties of the CPNs obtained.[2] Hence, fluorene monomers with either boronic pinacol ester **1.21** or bromine groups **1.22** were polymerised with dibromobenzothiadiazole **1.23** or brominated dithienylbenzothiadiazole **1.24** giving molecular weights up to 15 kg mol^{-1} (figure 1.11). The particles **1.19a** and **1.19b** were prepared by adding **1.21** and **1.22** with 5 and 10 mol% of **1.23**, respectively. The UV/Vis absorption spectra of both samples are similar due to the abundance of fluorene-fluorene segments. These segments give rise to β-phase polyfluorene segments and result in increased photoluminescence quantum yields (PLQYs) for these polymers (table 1.1). The photoluminescence (PL) emission spectra of these polymers is dominated by the intramolecular energy transfer (FRET) to the fluorene-benzothiadiazole (BT) segments resulting in an increased Stokes shift and green emission of the polyfluorene based CPNs. These features are not found in case of the alternating polymer nanoparticles **1.19c** that

exhibit a moderate PLQY. Similar properties were found for **1.25a** and **1.25b** containing the thiophene-benzothiadiazole-thiophene (TBTT) co-monomer **1.24**. PL emission was observed in the FR/NIR region due to the low bandgap of the resulting polymer. The polymerisation was performed at dispersed/continuous phase ratios of 1: 20 and 1: 10. The nanoparticles prepared at the latter loadings flocculated after surfactant removal using porous polystyrene resin (Amberlite XAD-2).

Table 1.1: Optical Properties of CPNs in water (excited at 465 nm) reported by by Esquivel *et al*.[2]

entry	comonomer content	λ_{max} [nm]	λ_{em} [nm]	ϕ [%]
1.17a	-	405	440	38
1.17b	-	405	440	23
1.19a	5 mol% BT	380	534	41
1.19b	10 mol% BT	379	534	56
1.19c	50 mol% BT	334, 466	537	12
1.25a	5 mol% TBTT	382	631	34
1.25b	10 mol% TBTT	380	633	19

λ_{max} absorption maximum, λ_{em} emission maximum, ϕ quantum yield..

Mecking and coworkers confirmed the findings reported by Esquivel *et al*. using the same procedure with the exception of employing $Pd(PtBu_3)_2$ instead of the previously reported NHC catalyst.[3] The molecular weights of the polymers were reported to amount to 40 kg mol^{-1} and the particle lengths are, as reported by Muenmart and Turner, between 100 and 200 nm (table 1.2). Cryo-TEM verifies that the anisotropic shapes observed are an intrinsic property of the CPNs rather than being the results of TEM sample preparation. Notably, low incorporation of monomer **1.24** (0.5 and 1 mol%, figure 1.11) revealed well-defined ellipsoidal shapes whereas particle shape homogeneity decreased with increasing content of **1.24**. The authors concluded a relation between polymer backbone alignment and particle shape homogeneity.

Table 1.2: Polymer properties reported by Perez *et al*.

entry	TBT content [mol %]	λ_{max} [nm]	λ_{em} [nm]	ϕ [%]	M_n[1] [kg mol^{-1}]	Đ[1]	length[2] /v [nm]	ar[3] /v
1.25a	0.5	402	619	71	34	3.0	115 /0.12	3.2 /0.13
1.25b	1.0	405	624	77	33	3.2	141 /0.15	2.7 /0.15
1.25c	2.0	404	627	72	19	2.7	109 /0.24	2.5 /0.15
1.25d	5.0	404	634	78	31	3.0	91 /0.44	1.7 /0.21

TBT thiophene flanked benzothiadiazole with $R_2 = C_6H_{13}$, λ_{max} absorption maximum, λ_{em} emission maximum, ϕ quantum yield. [1] GPC in THF at 50 °C. Particle dimensions were determined by TEM: [2] Mean value of length and [3] mean aspect ratio (ar) and coefficient of variation v in either case.

An additional contribution to obtain CPNs of polymers **1.17** and **1.19** (figure 1.11) by a Suzuki-Miyaura polycondensation protocol in heterogenous phases is a dispersion polymerisation technique reported by Kühne *et al*.[53] Propan-1-ol was chosen as continuous phase since it acts as good solvent for the conjugated monomers **1.21**, **1,22** and **1.23** and as non-solvent for the resulting polymers. Upon a critical chain length, the polymer chains precipitate from the continuous phase forming nucleating particles due to phase separation from the solvent.[54] The particles were stabilised by Triton X-45 and poly(1-vinylpyrrolidone-co-vinyl acetate) and yielded large particles (167 nm up to < 1 µm) when compared to the previously discussed protocols.

Table 1.3: Miniemulsion polymerisation of PIDTBT and PDPPBT reported by Rahmanudin *et al*.

entry	polymer	method	T [°C]	M_n[3] [kg mol^{-1}]	Đ[3]	Yield [%]
1.29a	PIDTBT	conventional[1]	90	21	2.2	83
1.29b			55	1.2	1.2	32
1.29c		mini-emulsion[2]	90	17	1.9	82
1.29d			55	21	2.3	79
1.30a	PDPPBT	conventional[1]	80	90	1.7	85
1.30b		mini-emulsion[2]		72	1.6	81

Polymerisation was performed [1] with Aliquat 336 in toluene/H_2O (1:4, v/v). [2] with SDS and hexadecane in toluene/H_2O (1:10, v/v). [3] HT-GPC in TCB at 160 °C.

The miniemulsion polymerisation of state-of-the-art conjugated polymers **1.29** and **1.30** by the Suzuki-Miyaura cross coupling protocol has recently been reported by

Rahmanudin *et al*. (figure 1.12).[55] In this work a conventional bulk Suzuki-Miyaura reaction employing a phase transfer reagent (i.e Aliquat 336) was also carried out to directly compare with the reaction conducted in presence of a surfactant and hydrophobe. In case of PIDTBT **1.30**, the miniemulsion protocol yields comparable molecular weights at lower reaction temperature rendering this protocol less energy intensive than its biphasic (conventional) counterpart (table 1.3).

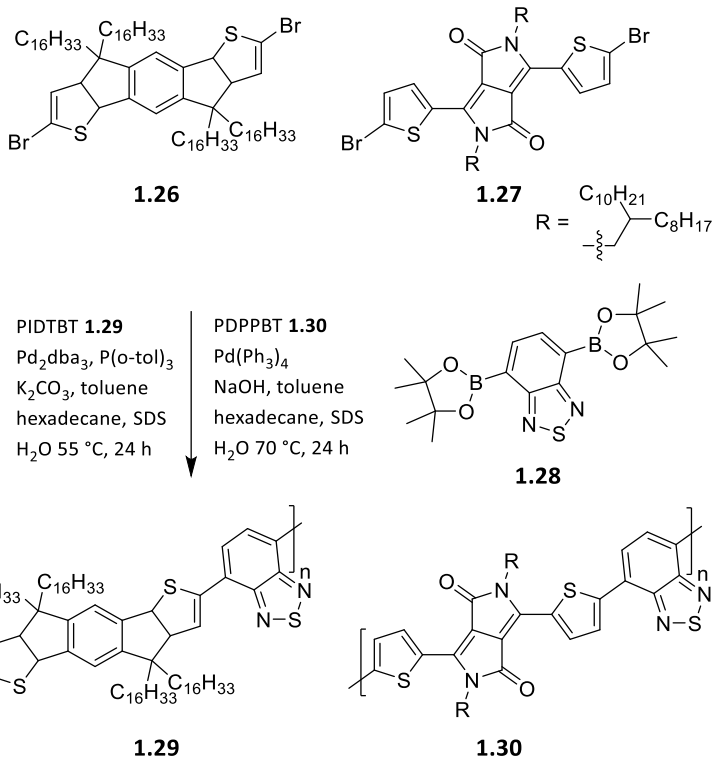

Figure 1.12: Preparation of PIDTBT and PDPPBT by miniemulsion Suzuki-Miyaura cross coupling polymerisation reported by Rahmanudin *et al*.[55]

1.2.2. Properties and Applications of Conjugated Polymer Nanoparticles

The optical properties of the conjugated polymer in nanoparticles have been compared to those of the equivalent polymer in the solid state deposited from organic solvents. It has been shown that nanoparticles obtained by post-polymerisation techniques reveal a hypsochromic shift in their absorption due to the conformation of the polymer chains which may contain twists and bends.[56] These twists and bends of the polymer chain are a consequence of the smaller volume the polymer chains have to occupy within the

nanoparticle. This effectively reduces the conjugation length. Especially in case of particles obtained by nanoprecipitation the particle formation occurs very quickly which prevents the polymers adopting an ordered conformation.[57,58] When the particles are formed over a longer period of time, a red shift of the conjugated polymer absorption can be observed. The size of the nanoparticles has an effect on this red shift, tending to increase the absorption wavelength as the dimension of the particles increase.[59] It has been reported that a red shift is observed upon annealing of CPNs which is attributed to the ordering of the twisted polymer chains within the nanoparticles.[60] Moreover, a significant change in the emission properties were observed when comparing solutions and dispersions of polyfluorene.[61] The PLQY of a poly(9,9-dihexyl-9H-fluorene) solution (ϕ = 83 %) was greater than of the dispersions since emission of the solution occurs through a radiative process of non-aggregated polymer chains. On the contrary, comparison of the PLQY between thin films drop casted from either solution (ϕ = 43 %) or dispersion showed the opposite trend. In case of thin films made from the polyfluorene CPNs, the PLQY depended on the particle size, with smaller particles tending to feature a higher PLQY (ϕ = 68 %, 5 – 30 nm particle diameter) compared to bigger particles (ϕ = 43 %, 5 – 70 nm particle diameter). This was explained by the reduction of non-radiative losses of the emission caused by interchain aggregation whereas non-radiative processes are even more suppressed within the smaller particles. Numerous reports on CPNs have discussed the excellent photostability and high brightness of these particles that make these materials promising candidates in imaging applications.[36,37]

Conjugated microporous polymers (CMPs) combine extended conjugated systems with microporous structure and are utilised in a plethora of light-promoted chemical transformations, chemosensors and biological applications.[64] One synthesis strategy for the preparation of porous polymer skeletons is polymer cross-linking by incorporating tri or multi-functional monomers. The synthesis of cross-linked conjugated polymers in heterogenous phases enables processing of otherwise insoluble material: Li *et al*. reported the synthesis of borylated dioctylfluorene **1.21** with the trifunctional monomer **1.31** and demonstrated that cross-linked polymer obtained by a miniemulsion polymerisation confines the polymerisation in each nano droplet reactor (figure 1.13).[65] Hence, the miniemulsion polymerised batch remained soluble in organic solvents whereas the conventional cross-coupling method gave insoluble material. The branched structure

within the nanoparticles improved the fluorescence sensitivity towards the presence of picric acid.

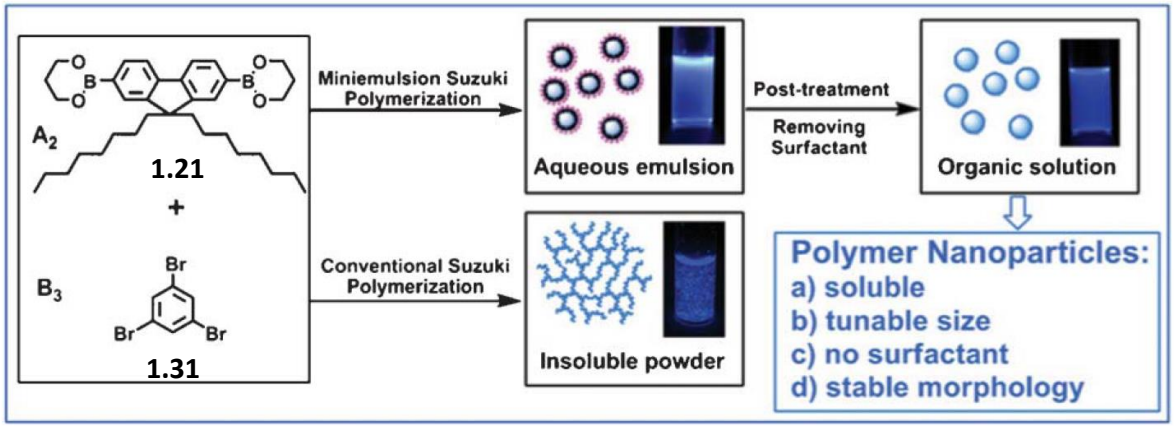

Figure 1.13: Comparison of hyperbranched conjugated polymers polymerised via solution and miniemulsion protocol.[65]

In terms of processing, OSCs entered large scale production in recent years leading to challenges of reducing volatile organic compounds (VOCs). Hence, aqueous dispersions of conjugated polymers offer a cradle to grave approach (i.e from polymer synthesis to application) by direct processing into electronic devices.[66,67,68,69,70] Figure 1.12 (a – d) presents the spin coating of dialysed aqueous dispersions of PIDTBT **1.29** and PDPPBT **1.30** reported by Rahmanudin *et al*.[55] The granular particle morphologies are observed as cast films (a and b) and change to a continuous amorphous film in case of PIDTBT upon annealing at 150 °C (c). Whereas for PDPPBT thermal annealing of the thin film at 150 °C (d) led to only minor changes. Thin films of these aqueous CPN dispersions were formed *via* spin-coating and fabricated in BGTC OFETs using PMMA as gate dielectric. Figure 1.12 (e) compares the charge carrier mobilities measured for OSC thin films from aqueous processing (i) and from dichloro benzene (DCB) dispersion/solution (iii). The inferior charge carrier mobilities measured for the OSC thin films processed from aqueous dispersions are explained by charge trapping sides introduced by the surfactant SDS. Thermal annealing at 150 °C only did not improve charge carrier mobilities to levels obtained by DCB coated OSC thin films. To remove the remaining surfactant within the thin films sufficiently, an ethanol washing step was performed with subsequent spin coating and annealing at 100 °C leading to an increase in charge carrier mobilities. X-ray photoelectron spectroscopy (XPS) confirms

the removal of SDS by decreased sulphate peaks (signal * in figure 1.12 (f)) for the post-wash batches. This extra washing step circumvents thermal treatments at elevated temperatures to remove SDS (i.e. 270 °C) improving the compatibility for flexible substrates.

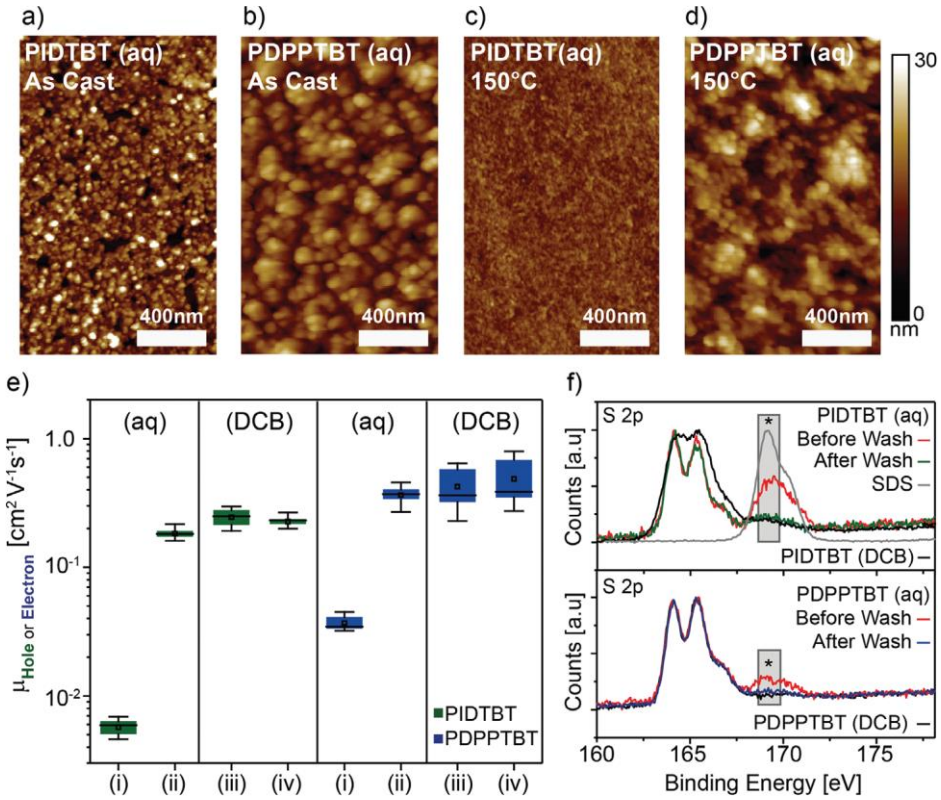

Figure 1.14: AFM thin-film images of aqueous processed CPN dispersions of PIDTBT and PDPPTBT: as-cast (a,b), annealed films at 150 °C for 30 min (c,d). Summary of saturation mobility values: aqueous processed CPN dispersions before (i) and after (ii) solvent wash and DCB dispersions of polymers synthesised from mini-emulsion (iii) and conventional (iv) protocols (e). Aqueous processed thin-film before (red lines) and after the post-washing process. Grey box with (*) indicates the region of the 2p sulphate peak including DCB-processed semiconducting polymer thin films (black line) (f).[55]

1.3. Direct (Hetero)Arylation Polycondensation (DArP)

A challenge to render conjugated polymers more competitive in optoelectronic applications is the development of shorter monomer syntheses and increased atom economy to decrease the ecologic profile and the costs of production.[16] Hence, novel polymerisation methods such as direct (hetero)arylation polycondensation (DArP) are an

ongoing topic of research. The discovery of DArP facilitates this approach for the synthesis of conjugated polymers, since it circumvents functionalisation of the monomers with costly organometallic and potentially toxic moieties. Moreover, the formation of stoichiometric organometallic by-products renders tedious purification redundant. The development of DArP arose from pioneering investigations on C-H bond activation on small molecules, which aided to understand reactivity and selectivity. Research on DArP provided insights into side reactions causing defects in the backbone (figure 1.15). Since numerous monomers contain more than one C-H bond with similar dissociation energies, regioselectivity issues can lead to kinks in the polymer backbone. Additionally, α,α-homo couplings can occur during the polymerisation leading to homo coupling defects in the polymer backbone.

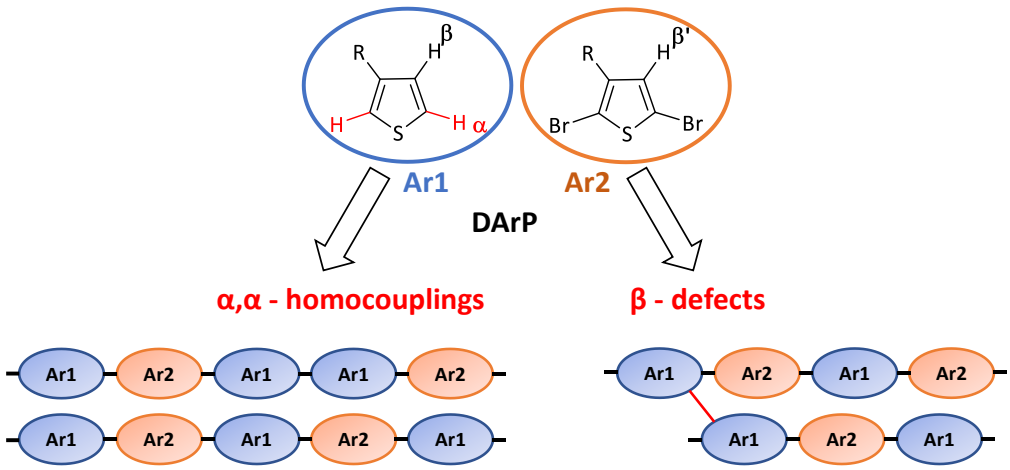

Figure 1.15: Structural defects as result of side reactions upon DArP.[71]

The DArP catalyst cycle is depicted in figure 1.16 using bromobenzene and thiophene as an example.[72] As with most palladium catalysed cross couplings, the DArP cycle starts with the oxidative addition of the Pd(0) species to bromobenzene. The halogen ligand on the formed Pd(II) intermediate is subsequently exchanged by the carboxylate anion. Complex **1.32** undergoes a transmetalation with the concerted cleavage of the C-H bond of the thiophene substrate occurring, leading to **1.32-TS**. This transition state is called concerted metalation deprotonation (CMD) and is commonly recognised as the likeliest mechanism amongst other proposed mechanisms. The CMD mechanism was elucidated by combining theoretical calculations and experimental data when carboxylate bases or

carbonates are involved.[73] The catalyst cycle ends by the reductive elimination of the product regenerating the Pd(0) complex. Additionally, the carboxylate is regenerated either by pathway 1 *via* reaction with the base or pathway 2 in case the carboxylate remains coordinated to the Pd complex throughout the entire process.

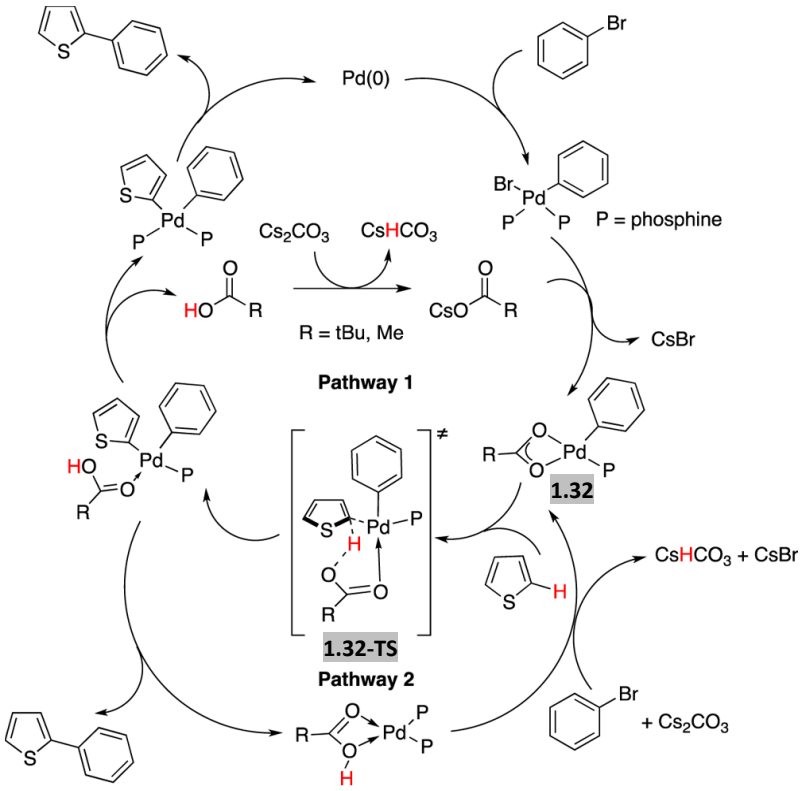

Figure 1.16: DArP catalytic cycle.[72]

To elucidate the CMD transitions state, Fagnou *et al*. deconstructed the enthalpic contributions into bond distortions and interactions between the catalyst and the substrates.[74] The distortion originates from the distortion of the ground states **I** of the palladium catalyst and **II** of the (hetero)aromatic substrate. This is indicated by the red arrow in figure 1.17 as the result of the out-of-plane bending and elongation of the C-H bond E_{dist}(ArH) and the deformation of the palladium-ligand bond E_{dist}(PdL). The interaction energy E_{int} arises from the interaction between the palladium atom (**III**) and the π–orbitals of the substrate (**IV**) and is illustrated as the green arrow in figure 1.17. E_{int} counteracts E_{dist} by stabilising the transition state **V**. E_{dist}(ArH) becomes more important for electron-poor compounds, which exhibit a lower barrier due to the acidity of the C-H bond.

On the contrary, electron-rich compounds feature a higher π-nucleophilicity. For those compounds the E_{int} contribution becomes dominant.

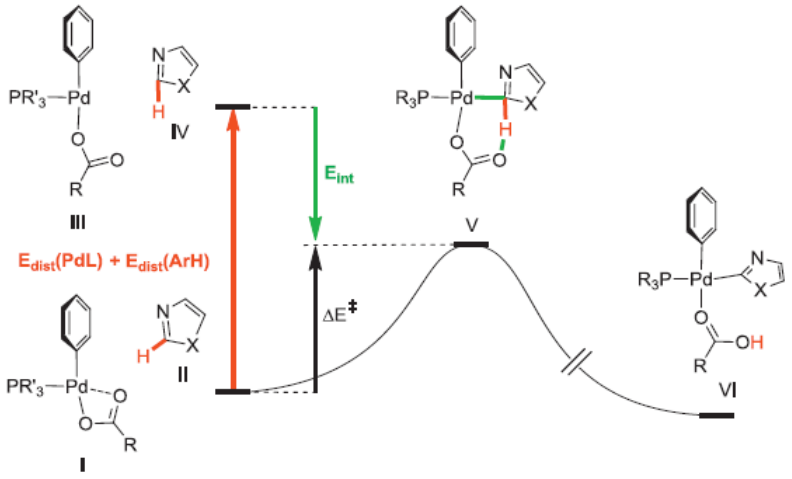

Figure 1.17: Energy diagram of the CMD transition state with ground states **I** and **II** and fragments **III** and **IV**. An azole and $[Pd(C_6H_5)(PMe_3)(OAc)]$ were used as example.[75]

The selectivity can be predicted by DFT calculations taking the counteracting energy contributions into account.[74] Gorelsky and Fagnou could classify (hetero)arenes into three different classes regarding their selectivity.

A. If E_{dist}(ArH) is the determining factor, the reaction typically occurs at the most acidic C-H bond. This applies for the class A compounds in figure 1.18.
B. Class B compounds are governed by their E_{int} contribution at the most nucleophilic site.
C. For class C compounds, both contributions are crucial and hence their reactivity can be difficult to predict. Typical monomers used to construct conjugated polymers, such as thiophene, indoles and pyrroles, belong to this category. Substituents on the δ-position can enhance or decrease the reactivity without a clear correlation of their electronic influence. Fortunately, most five membered heterocycles tend to react on their α-position which facilitates their polymerisation.

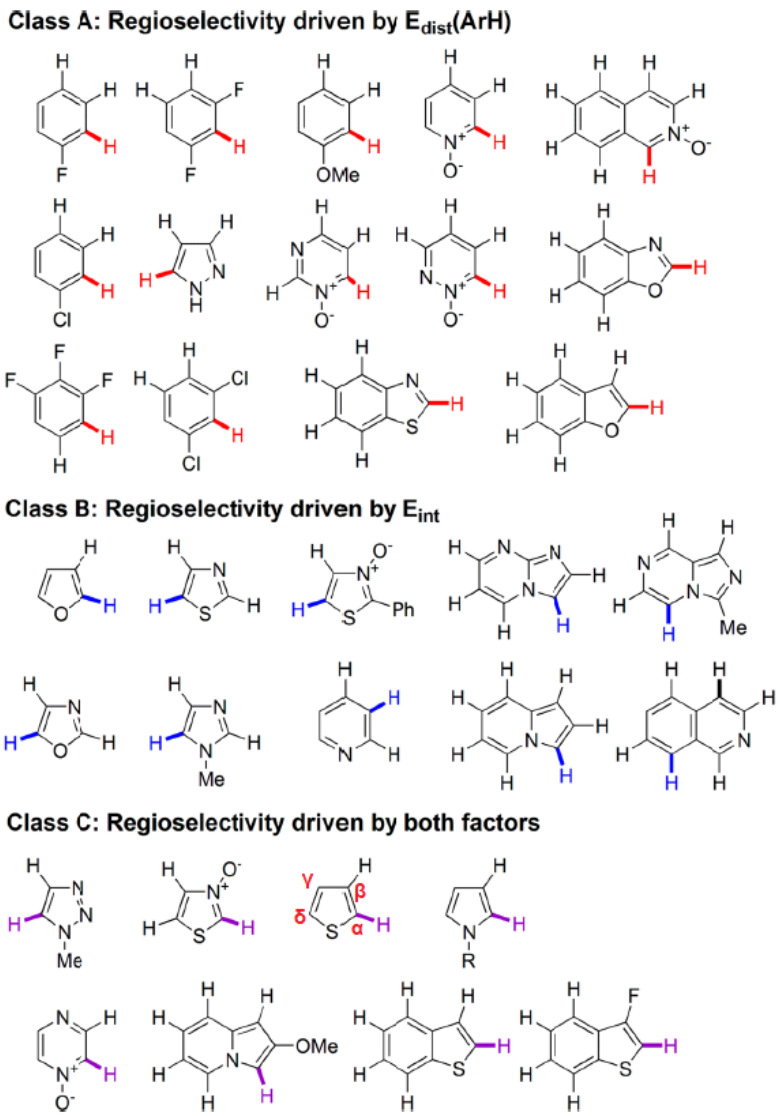

Figure 1.18: Classification of various (hetero)arenes distinguished by their regioselectivity. The most favoured site for CMD is labelled in colour. The α – δ positions are labelled on the thiophene ring.[16]

The choice of which monomer should be halogenated was investigated by Leclerc *et al*. For example a benzodithiophene (BDT, figure 1.19, **1.33**) as polymerised with dithienyl diketopyrrolopyrrole monomer (DPP, **1.27**).[71] The brominated BDT monomer **1.34** was reacted with DPP **1.35** for reaction denoted as **1** and vice versa for reaction **2**. Lower molecular weight polymers were obtained via route **2** in comparison to **1,** regardless of the nature of the ligand. The measured UV/Vis spectra of the polymer obtained by route **1** resembled UV/Vis spectra of defect-free PDPPBDT obtained *via* Suzuki-Miyaura cross coupling polymerisations. In contrary, the UV/Vis spectra **2** indicated the presence of defects introduced by route **2**.

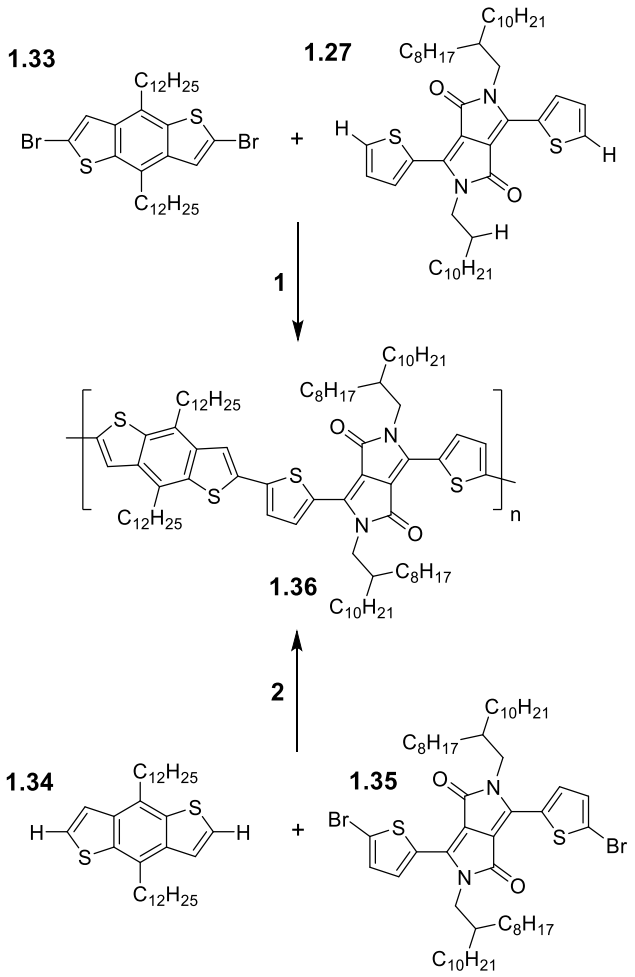

Figure 1.19: DArP of DPP and BDT with 5% $Pd(OAc)_2$, ligand (20 mol%), Cs_2CO_3 (3 eq.), pivalic acid (1 eq.) in toluene at 125 °C.[71]

The findings were explained by DFT calculations at the B3LYP/TZVP (DZVP for palladium) level. The Gibbs free energy of the activation barrier for the C–H bond activation were calculated by comparing different C–H bonds of each substrate. The activation energy refers to the Gibbs free energy (ΔE_a) of the CMD transition state, referenced to the substrate and the model catalyst [$(PMe_3)Pd(Ph)(CH_3COO^-)$]. In case of pathway **1** in figure 1.19 the difference in the activation energy (ΔE_a) between H_α and H_β of the DPP monomer **1.27** is found to be 4.4 kcal mol^{-1} (24.5 vs. 28.9 kcal mol^{-1}, figure 1.20 a). Using Arrhenius' law, a selectivity ratio of the α-position compared to the β-position can be estimated as of 250:1 favouring H_α at the polymerisation temperature (125 °C) to obtain **1.36**. The ΔE_a between H_α of DPP **1.27** (24.5 kcal mol^{-1}) and H_β of BDT **1.33** (28.2 kcal mol^{-1}, figure 1.20 b) are respectively 3.7 kcal mol^{-1}, giving a selectivity of about 100:1. Both results indicate that β-coupling is rather unlikely which is further confirmed by experimental data.

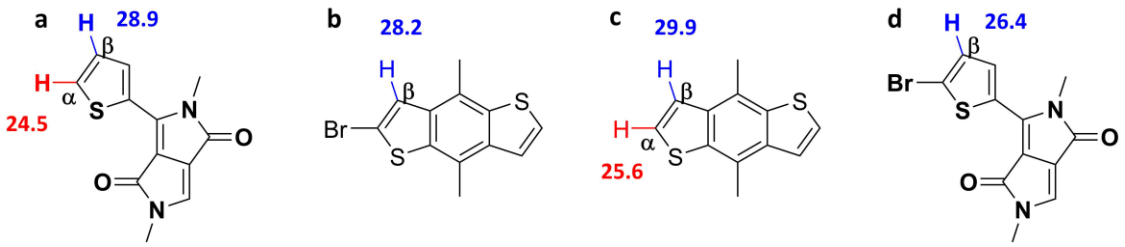

Figure 1.20: Activation barriers E_a of H-DPP-H **1.27** (a), Br-BDT-Br **1.33** (b), H-BDT-H **1.34** (c) and Br-DPP-Br **1.35** (d). [71]

DFT calculations performed for pathway **2** in figure 1.19 calculate ΔE_a between H_α (25.6 kcal mol^{-1}) and H_β (29.9 kcal mol^{-1}) of H-BDT-H **1.34** as 4.3 kcal mol^{-1} (figure 1.20 c), indicating an excellent selectivity for the activation of H_α of **1.34**. However, the ΔE_a between H_β of the Br-DPP-Br **1.35** (26.4 kcal mol^{-1}, figure 1.20 d) and H_α of H-BDT-H **1.34** (25.6 kcal mol^{-1}) is only of 0.8 kcal mol^{-1}, suggesting poor selectivity which leads to significant degree of unwanted β-defects. These calculations coincide with experimental data which shows that the choice of functionalisation of the substrates is crucial for DArP. It is concluded that the bromine atom decreases E_a of the vicinal protons, which favours β-coupling and hence kinks in the polymer backbone. The DFT calculations are also applicable for other monomers in additional publications.[76,77] It is worth noting that these calculations explain the α versus β selectivity for possible β-defects but do not give any prediction about potential α-α homo couplings.

Wang and coworkers have investigated both synthetic pathways to obtain PDPPF4 **1.38** by interchanging the functionalities on the respective monomers (figure 1.21).[78] Thorough reaction parameter screening was required for both pathways to obtain the reported molecular weights. Pathway **2** resulted in polymers exhibiting multiple broad peaks in their GPC elution diagrams resulting in enormous polydispersities. The presence of structural defects was further corroborated by high temperature NMR analyses and UV/Vis absorption measurements. PDPPF4 polymerised via pathway **2** shows a bathochromic shift (14 nm) in its absorption spectrum compared to PDPPF4 synthesised via pathway **1**. Moreover, an additional absorption above 800 nm is indicative of DPP-DPP homo couplings previously reported by Hendriks *et al*.[4] Both contributions from Wang *et al*. and Leclerc and coworkers conclude that the selection of monomer functionalities are crucial for the successful DArP to obtain conjugated polymers without structural defects.

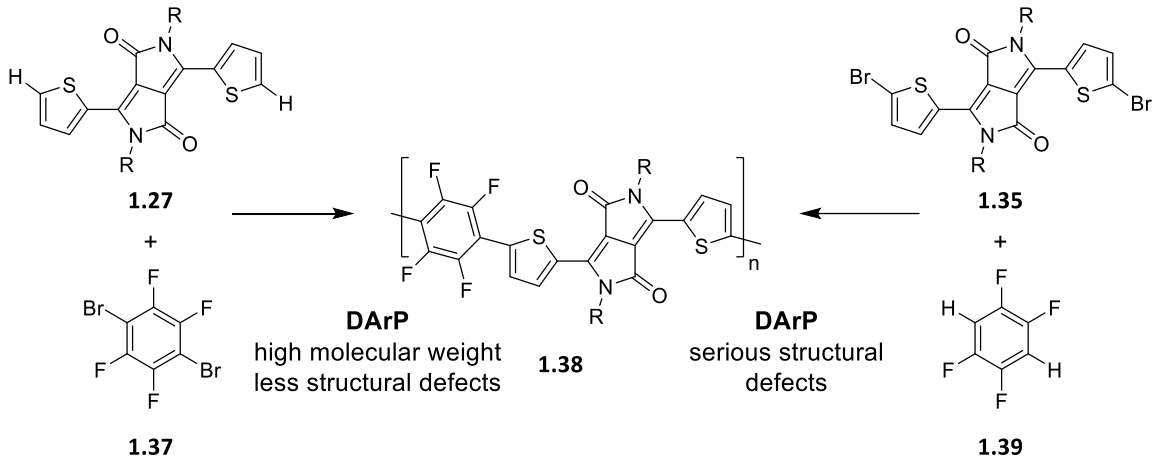

Figure 1.21: Solution DArP of PDPPF4 **1.38** reported by Wang *et al*.[78] M_n and Đ were determined by GPC in THF at 30 °C.

1.3.1. Direct(Hetero)Arylation in Biphasic Systems

Leclerc and coworkers reported a DArP protocol in a biphasic system consisting of water and toluene.[79] Both electron-rich and electron-poor thienyl- or phenyl-based substrates were polymerised with the conditions shown in figure 1.22. The reaction conditions were optimised after thorough screening of the reaction parameters, particularly for PTPD2T **1.40**. In order to optimise the reaction conditions and the molecular weights obtained, the palladium pre-catalysts were screened and $PdCl_2(PPh_3)_2$ reproducibly gave the highest molecular weights. Furthermore, the ligands, solvents and phase transfer agents were screened and P(*o*-anisyl)$_3$, toluene and tetrabutylammonium bromide (TBAB) gave the best results, however, the polymer molecular weights and yields of the polymers obtained were not satisfactory. The authors demonstrated that the critical parameters in polymerisation is accessibility of the water-soluble reagents, namely the base and carboxylic acid additive. Hence, polymerisations with 40 equivalents of K_2CO_3 gave the highest molecular weight (M_n = 72 kg mol^{-1}, Đ = 1.9). Changing the quantity of pivalic acid, showed that it was not involved in the rate-limiting step. Additionally, thorough mixing of the reaction mixture appeared to be crucial as well. Based on the results of the optimisation on DArP of PTPD2T, the scope of the method was investigated on a variety of other conjugated monomers (figure 1.22).

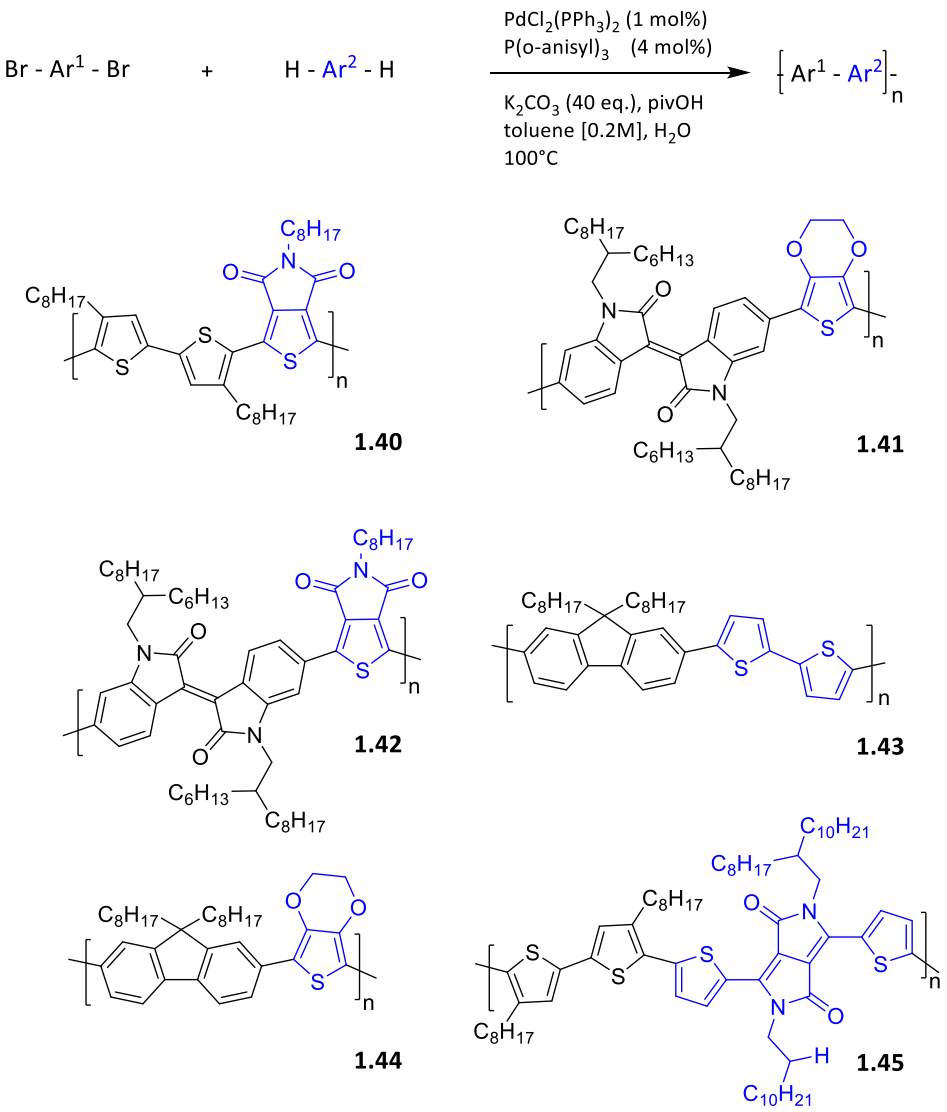

Figure 1.22: Synthesis of various polymers *via* DArP in biphasic conditions giving PTPDT2 **1.40**, PIIEDOT **1.41**, PIITPD **1.42**, PFT2 **1.43**, PFEDOT **1.44** and PDPPT2(C8) **1.45**.[79]

Additionally, scalability was demonstrated by upscaling the polymerisation of PIIEDOT **1.41** with a reaction scale of 2.0 mmol (table 1.4 entry **1.41c**). An airtight reactor with a mechanical stirrer was used for the 2.0 mmol reaction which gave a polymer with a high molecular weight of M_n = 137 kg mol^{-1} and an almost quantitative yield. The fluorene based polymers **1.43** and **1.44** were synthesised by this method demonstrating the scope of this procedure although further optimisation was required. Complete characterisation from differential scanning calorimetry and ^{1}H NMR spectroscopy and absorption spectroscopies demonstrated that this DArP protocol offers comparable or better molecular weights than related reports. High molecular weights were obtained using low-cost, "wet" reagents

performed at ambient pressure and 100 °C presenting a robust DArP protocol applicable in heterogenous phases.

Table 1.4: Various polymers obtained using the optimised reaction conditions of PTPD2T(C8) (as presented in figure 1.22).[79]

entry	polymer	c(M) [mmol]	M_n[1] [kg mol^{-1}]	Đ[1]	Yield [%]
1.40	PTPDT2	0.1	72	1.9	97
1.41a	PiIEDOT	0.1	93	2.9	77
1.41b	PiIEDOT	0.3	93	2.4	95
1.41c	PiIEDOT	2.0	137	2.6	98
1.42	PiITPD	0.1	34	3.2	92
1.43	PF2T	0.1	32	4.6	90
1.44	PFEDOT	0.1	63	3.0	97
1.45	PDPP2T(C8)	0.1	58	1.8	97

[1] Measured by HT-GPC in TCB at 110 °C.

2. Aims

The aim of this thesis is to present a pathway to obtain conjugated polymers using novel C-C cross couplings in emulsion by utilising C(sp^2)-H bonds on the monomers, in particular direct arylation polycondensation (DArP). This new approach targets an atom efficient preparation of semiconducting polymers in less synthesis steps while avoiding toxic organometallic by-products. Additionally, conducting DArP in emulsion provides the benefit of avoiding chloroaromatic solvents for the printing of electronic devices.

Extensive reaction parameter screening was employed to develop systems capable of the polymerisation of conjugated polymers ($M_n \geq 10$ kg mol^{-1}) in heterogenous phases and to facilitate the formation of stable nanodroplets in the sub-micron regime with moderate particle size dispersities (PDI < 0.30). The optimised miniemulsion DArP conditions were used to conduct an investigation of the co-monomer structure on the miniemulsion DArP outcomes and demonstrated the scope of this new polymerisation protocol.

The microstructure of the polymers in these nanoparticle dispersions was analysed to identify potential polymer backbone defects. DArP is known to introduce homo coupling defects into the polymer backbone (i.e the coupling of one monomer species with itself) that are less prevalent in polymers prepared by more conventional C-C coupling methods (e.g Suzuki-Miyaura and Stille cross couplings).[4] Hence, different analytical methods such as mass spectrometry (MALDI-TOF-MS) and NMR techniques (^{1}H, ^{13}C, ^{19}F and 2D experiments) were employed to identify and quantify the defects.

Aqueous dispersions of conjugated polymers were used to fabricate OFETs to investigate the applicability of these nanoparticulate dispersions of conjugated polymers for use in electronic devices. Direct comparison of charge carrier mobility between OFET OSC layers deposited from either aqueous dispersion or chloroform solutiondemonstrated the effect of this novel deposition method upon device performance.

3. Miniemulsion Polymerisations of PDPPF4 by Direct Arylation Polycondensation

This Chapter focuses on the optimisation of the direct arylation polycondensation (DArP) to poly((3,6-dithienyl-2,5-di(2-octyldodecyl)pyrrolo[3,4c]pyrrolo-1-4-dione)-alt-(tetrafluorobenzene)) (PDPPF4, entry **3.3**, scheme 3.1) conducted in a miniemulsion. Initial work focused on the synthesis of the alkylated DPP monomer (entry **3.1)** and the reproducibility of the polymer nanoparticle preparation throughout the body of this work. The optimised reaction conditions in miniemulsion are then compared with bulk solution polymerisations. An overview of the most impactful reaction parameters in terms of polymer molecular weights obtained and the particle size and dispersities are presented in conclusion.

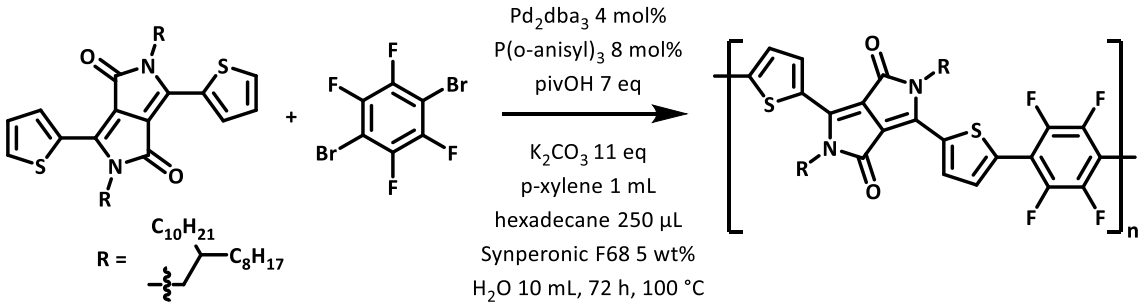

Scheme 3.1: General reaction scheme of the direct arylation polymerisation of PDPPF4.

3.1. DPP Monomer Synthesis

The synthesis of the alkylated DPP monomer was performed according to reported procedures and consisted of 3 steps (scheme 3.2).[80,81] Since the DPP core exhibits low solubility in common organic solvents, the inclusion of the side chain 2-(R/S)-octyldodecyl has been chosen to improve solubility. Long and branched side chains improve the solubility of conjugated polymers drastically and are in most cases superior to linear side chains.[82] Since 1-iodo-2-octyl-dodecane (**3.7**) is not readily commercially available, the

alcohol was halogenated in an Appel-type reaction (scheme 3.2). The product was characterised by ^{1}H NMR spectroscopy and the yields obtained were very good. The side chain 1-iodo-2-octyl-dodecane (**3.8**) was subsequently reacted by a S_N2 reaction with **3.6** to give the alkylated DPP monomer (**3.1**) with improved solubility in common organic solvents.

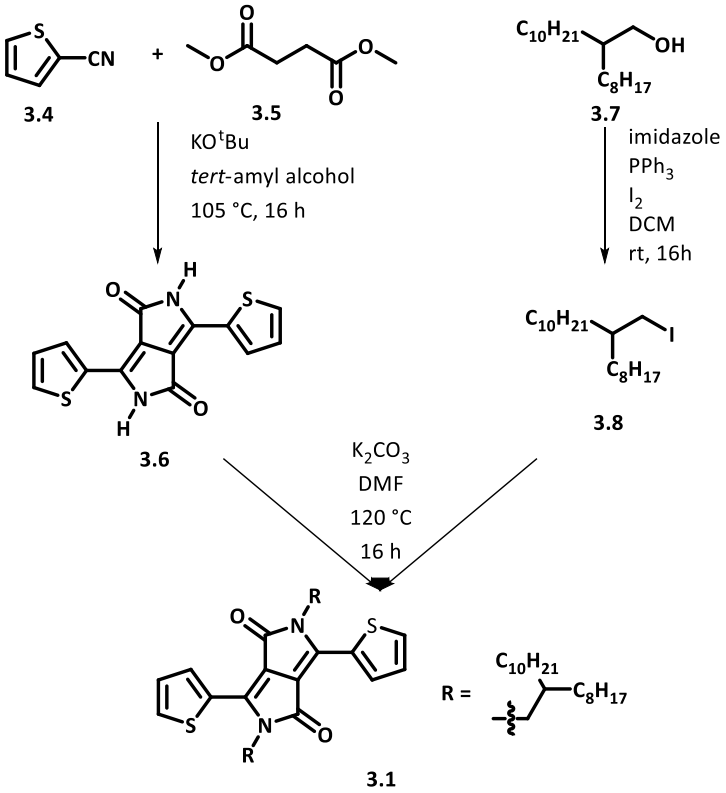

Scheme 3.2: Synthesis overview of the DPP monomer synthesis with N-alkylation with 2-octyldocedyl chains.

The ^{1}H NMR spectrum of **3.1** (figure 3.1, top) shows the thienyl protons **a**,**b** and **c**. H_b reveals two ^{3}J coupling to its vicinal located protons (e.g. ^{3}J = 4 and 5 Hz), while a smaller ^{4}J = 1 Hz coupling can be observed for the peripheral protons H_a and H_c. The bottom ^{1}H NMR spectrum in figure 3.1 shows additional signals that were observed for the crude alkylated DPP monomer and material collected after column chromatographic purification. Repeated crystallisation from dichloromethane with methanol (1 – 3 times) was adequate to remove the remaining impurity giving the alkylated DPP monomer in good quality but poor yields (≤ 40 %).

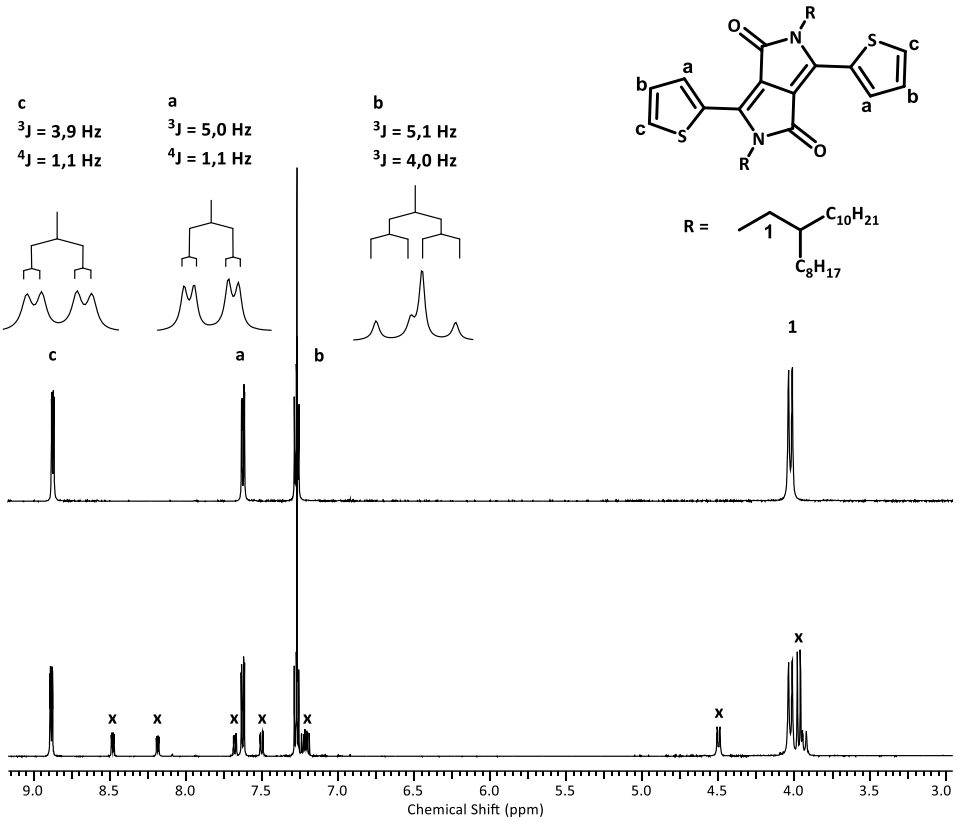

Figure 3.1: ^{1}H NMR spectrum of the alkylated DPP monomer, region below 3.0 ppm emitted for clarity that are associated with the alkyl chains. The top ^{1}H NMR spectrum presents purified alkylated DPP monomer after column chromatographic purification and twofold crystallisation. The bottom ^{1}H NMR spectrum shows additional peaks for the purified alkylated DPP monomer after column chromatographic purification only. The additional peaks (x) were designated as O,N-alkylated DPP tautomer signals.[83]

Zhao *et al*. reported the origin of the impurity signals (marked as **x** in figure 3.1) as the methylene hydrogens of the alkyl chain of an O-alkylated tautomer that forms during the DPP alkylation in DMF.[83] The degree of the tautomerisation has been found to depend on reaction temperature, time and steric hindrance of the halogenated side chains. Higher reaction temperatures (140 °C compared to 100 °C reaction temperature) and less sterically demanding alkyl halides increase the yield of the desired N-alkylated DPP. Due to those findings, the following reaction mechanism was proposed by the authors (scheme 3.3) whereby nucleophilic addition of the alkyl bromide occurs either on the nitrogen or oxygen of the DPP core. This is crucial to understand why standard silica column chromatographic purification was not sufficient (ΔR_f < 0.1 between the dialkylated DPP monomer and its tautomer (chloroform/petroleum ether 1:1, v/v)) and recrystallisation from dichloromethane and methanol of the chromatographically purified crude-product was necessary.

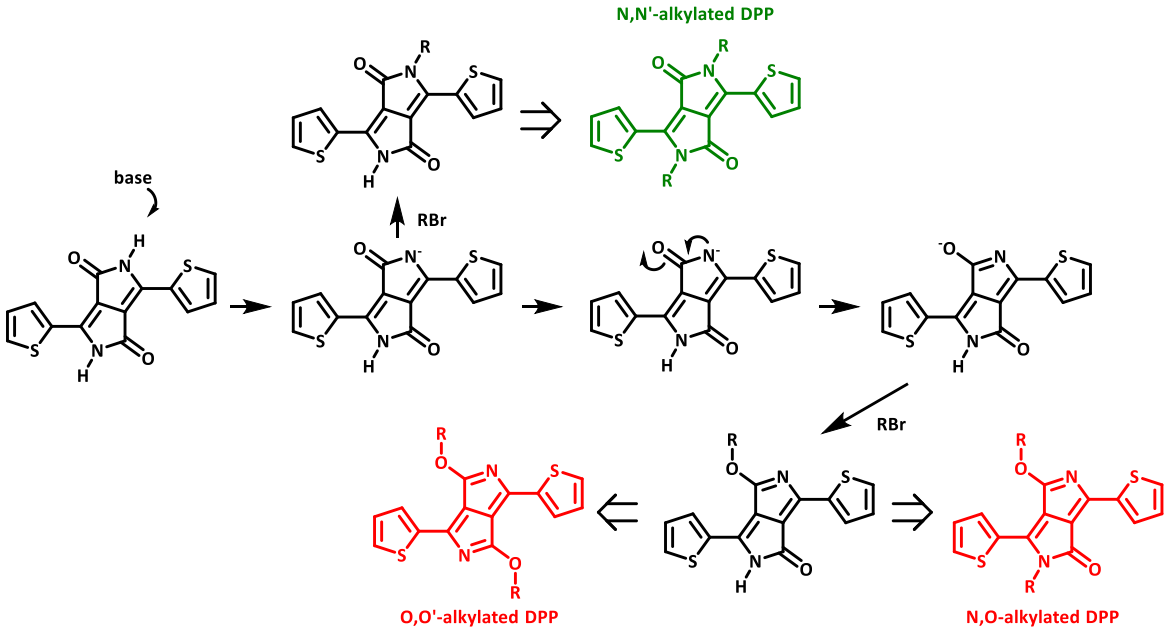

Scheme 3.3: Mechanism of the alkylation and tautomerisation of DPP proposed by Zhao *et al*.[83]

3.2. Miniemulsion Polymerisations with the Ionic Surfactant SDS

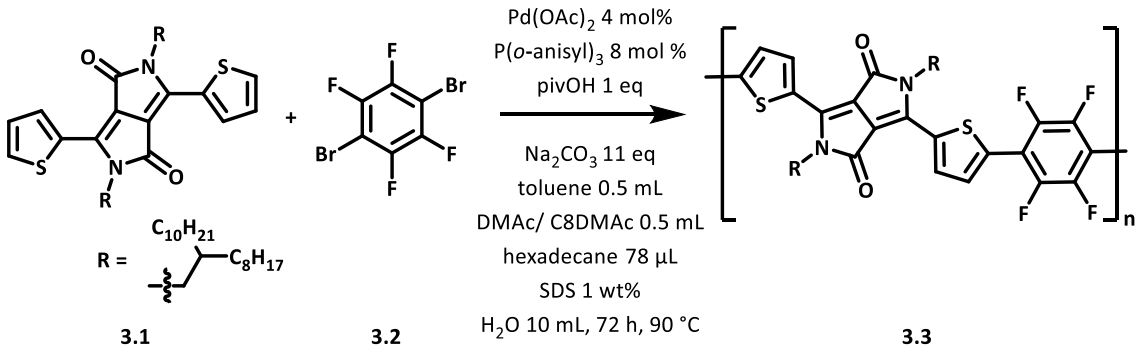

Scheme 3.4: Reaction scheme of the direct arylation polymerisation of PDPPF4 with reagents employed in section 3.2.1.

In this entire Chapter, DArP was performed to C-C cross couple DPP and dibromo tetrafluorobenzene in emulsion. Scheme 3.4 lists the reagents and solvents employed in section 3.2.1 and figure 3.2 indicates in which phase those compounds were prepared. The biphasic system was emulsified by sonication with a 6 mm tapered microtip at 21 % intensity for 10 min. The resulting miniemulsion consisted of the organic phase dispersed in the aqueous phase in a ratio of 1:10. By definition, droplets in an miniemulsion are supposed to be stable over the course of the reaction. This is accomplished by suppressing

Ostwald ripening by adding hexadecane as hydrophobe. A concentration of 78 $\mu L_{hexadecane}$ $mL_{solvent}^{-1}$ was chosen for initial screenings since this hydrophobe concentration has been reported to give reliable results in terms of particle size dispersity and emulsion stability.[84] The monomers reveal no solubility in water (colourless aqueous phase), hence no migration is considered to occur through the continuous phase and each droplet functions as nanoreactor. Whether this rigid push-pull polymer exhibits isotropic or anisotropic shapes are part of the characterisation in Chapter 5.5.

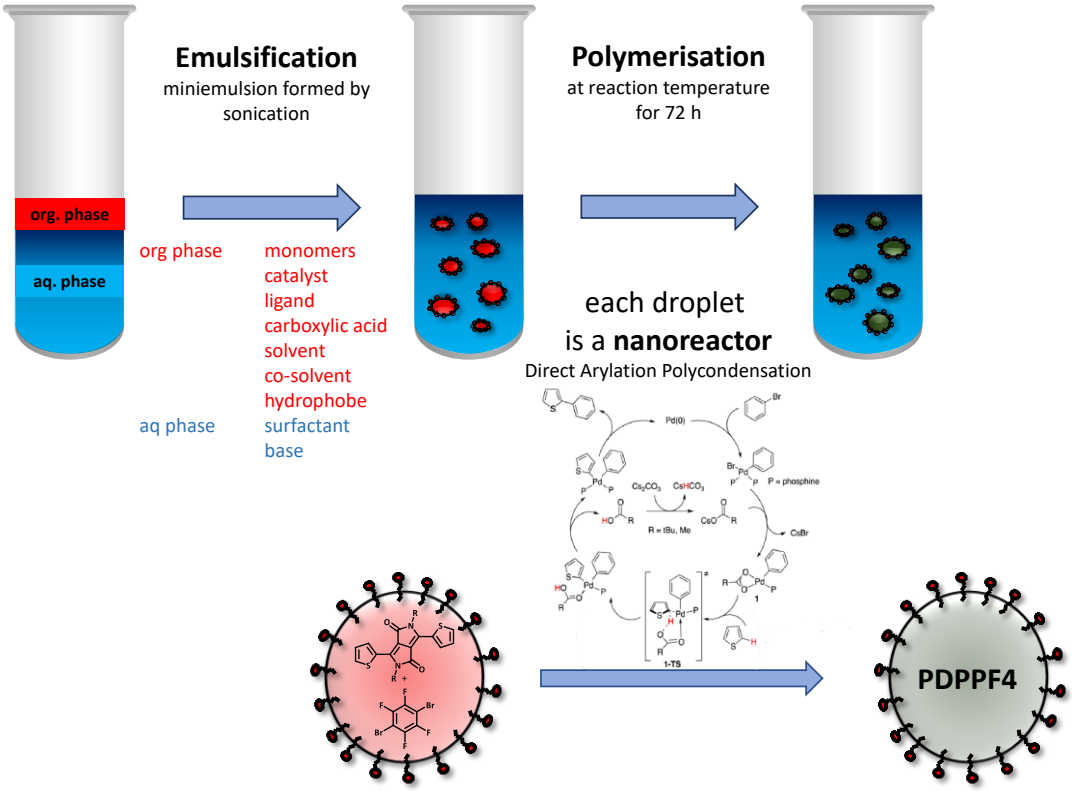

Figure 3.2: Setup of direct arylation polycondensation (DArP) in emulsion. A detailed procedure can be found in the experimental section (Chapter 8.4).

To polymerise DPP and tetrafluorobenzene *via* the DArP protocol in aqueous emulsion, several challenges had to be addressed. (i) The miniemulsion polymerisation was performed in water and under inert conditions, therefore the catalytic system needed to be stable towards the aqueous phase. (ii) The Sommer group reported that the molecular weights obtained for PDPPF4 by DArP critically depended on the monomer concentration with increased concentrations resulting in polymers with greater molecular weights (e.g. [monomer] = 0.2 – 0.5 M).[85] Solubility is a limiting parameter in the case of miniemulsion

polymerisations since neither the monomers nor the resulting polymer dissolve readily again once precipitated. Therefore, initial parameter screening was performed with decreased monomer concentration of [monomer] = 0.2 M. (iii) The Sommer group has also reported that solution polymerisations of PDPPF4 gave greater molecular weights when polar aprotic co-solvents were employed due to their ligating nature. It has been anticipated that polar conditions utilising DMAc as co-solvent might destabilise the resulting emulsion due to its partition into the aqueous phase.

Non-brominated DPP was chosen to be polymerised with dibrominated tetrafluorobenzene since Wang *et al*. elucidated that PDPPF4 obtained by synthesising brominated DPP and tetrafluorobenzene are more susceptible to homo coupling defects (figure 1.21).[78]

3.2.1. Miniemulsion Polymerisations with Polar co-Solvents

The polar co-solvent, DMAc, was employed for the initial polymerisation of PDPPF4 in emulsion (table 3.1, entries **3.9** and **3.10**). Entry **3.9** indicates that no polymerisation occurred which was confirmed by the red colour of the alkylated DPP monomer remaining at the end of the reaction. The elevated particle size dispersity indicated that the emulsion obtained was not stable and this was shown by the presence of macroscopic lumps. This was attributed to the polarity of DMAc and its partition into the aqueous phase ($\log K_{oct}$ = -0.58). A PDI ≤ 0.3 was considered desirable since values greater than 0.3 resulted in unreproducible results. The particle diameters in table 3.1 and onwards are presented for each distinguishable peak analysed by the MALVERN® distribution analysis rather than quoting the mean size (z-average diameter) for each sample because of the multimodal distributions observed.

To decrease the partition into the aqueous phase, DMAc was replaced by the aliphatic derivative C_8DMAc ($\log K_{oct}$ = 2.59).[86] Nonetheless, an unstable emulsion was obtained for entry **3.10** and no reaction was observed.

Tris(*o*-methoxyphenyl)phosphine (P(*o*-anisyl)$_3$) is a commonly utilised ligand for DArP reactions conducted in solution.[16,17] P(*o*-anisyl)$_3$ is in particular used for DArP

protocols conducted in non-polar solvents and has been anticipated to facilitate the polymerisation due to its reported reactivity with palladium in solvents of different polarity.[16,17,87] Therefore, P(*o*-anisyl)$_3$ was added instead of DMAc to a polymerisation reaction (table 3.1, entry **3.11**) resulting in an increased molecular weight for the polymer with an elevated polymer dispersity Đ and distinguishable oligomer peaks (figure 3.3). The particle size and dispersity measurements hide the fact that macroscopic aggregates were observed as for entry **3.9**.

Table 3.1: Miniemulsion polymerisations with polar co-solvents.

entry	co-solvent[1]	M_n[3] [kg mol^{-1}]	Đ[3]	size distribution[4] [nm]	PDI[4]
3.9	DMAc	1.0	1.1	203 ± 128 (96 %) 5119 ± 541 (4 %)	0.44
3.10	C8DMAc	0.9	1.1	-	-
3.11[2]	C8DMAc	5.9	3.1	207 ± 76 (99 %) 5375 ± 325 (1 %)	0.27

$Pd(OAc)_2$ 4 mol%, [monomer] 0. 25 M, [hexadecane] 78µL$_{HD}$ mL$_{solvent}^{-1}$, Na_2CO_3 3 eq., pivalic acid 1 eq., SDS 100 mg in 10 mL water at 90 °C for 72 h. [1] Solvent mixture of toluene: co-solvent 1:1, 0.5 mL each. [2] P(*o*-anisyl)$_3$ 8 mol%. [3] GPC in THF vs. narrow polydispersity polystyrene standards. [4] DLS analysis of the size distribution and polydispersity index (PDI) at 25 °C. Integral ratios are presented in brackets.

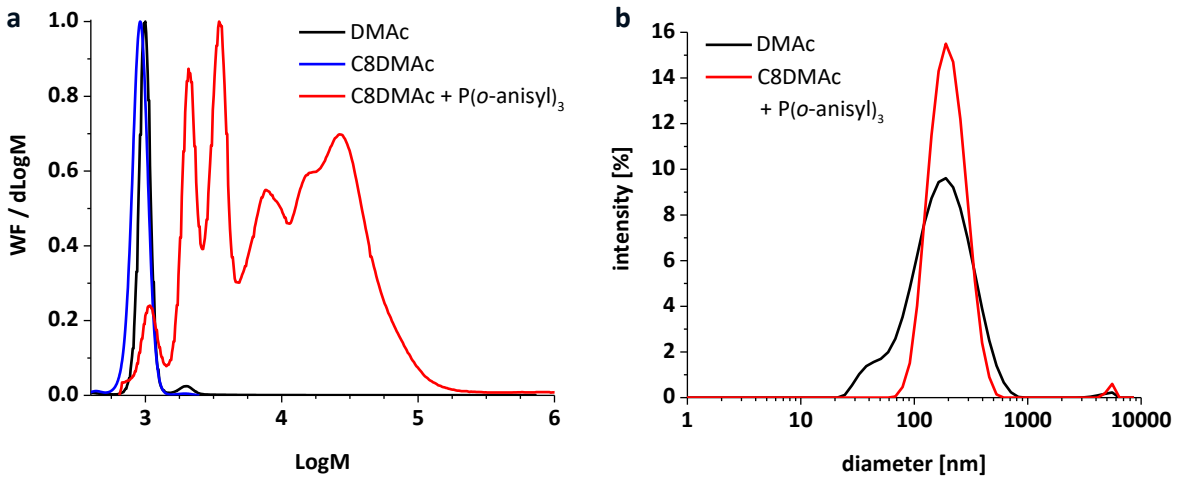

Figure 3.3: Normalised GPC traces of entries **3.9** - **3.11** (a) and DLS intensity distributions of entries **3.9** and **3.11** (b).

3.2.2. Minimemulsion Polymerisations using Non-Polar Solvents

Polymerisations in emulsion performed in exclusively non-polar solvents resulted in non-stable emulsions as with the previous attempts. Entries **3.12** - **3.14** show that the particle size dispersities did not improve when conducted in the absence of DMAc or C_8DMA (table 3.2). In agreement with the previous section, addition of P(*o*-anisyl)$_3$ facilitated a reaction between the monomers as no reaction is observed in the absence of this ligand. A solvent alteration from toluene to *o*-xylene (entries **3.13** and **3.14**) did not show any significant changes and distinguishable oligomer peaks were observed for the GPC traces (figure 3.4 a, entries **3.13** and **3.14**) as in section 3.2.1.

Table 3.2: Miniemulsion polymerisations in toluene and xylene.

entry	solvent	M_n[2] [kg mol^{-1}]	Đ[2]	size distribution[3] [nm]	PDI[3]
3.12	toluene	1.0	1.0	197 ± 117 (100 %)	0.28
3.13[1]	toluene	1.8	1.2	312 ± 290 (97 %) 4309 ± 982 (3 %)	0.53
3.14[1]	*o*-xylene	1.2	1.2	231 ± 179 (95 %) 4354 ± 1012 (5 %)	0.43

$Pd(OAc)_2$ 4 mol%, solvent 1 mL, [monomer] 0. 25 M, [hexadecane] 78µL$_{HD}$ mL$_{solvent}^{-1}$, Na_2CO_3 3 eq., pivalic acid 1 eq., SDS 100 mg in 10 mL water at 90 °C for 72 h. [1] P(*o*-anisyl)$_3$ 8 mol%. [2] GPC in THF vs. narrow polydispersity polystyrene standards. [3] DLS analysis of the size distribution and polydispersity index (PDI) at 25 °C. Integral ratios are presented in brackets.

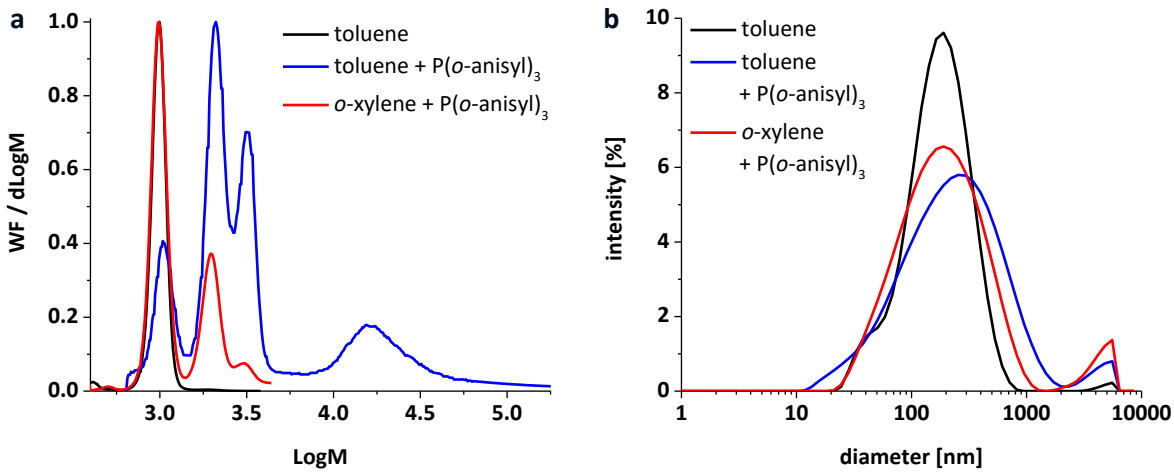

Figure 3.4: Normalised GPC traces (a) and DLS intensity distributions (b) of entries **3.12** - **3.14**.

3.3. Miniemulsion Polymerisations with the Non-Ionic Surfactant Series Triton X

As unstable emulsions were observed when employing SDS as surfactant, a different series of surfactants was screened to investigate the outcome of the C-C couplings in emulsion. Although there are very few publications applying non-ionic surfactants for the synthesis of conjugated polymers in emulsion, Kuehne *et al*.[53], Perez *et al*.[3] and Muenmart *et al*.[1] reported that the Triton X surfactant series help to facilitate Suzuki-Miyaura cross coupling miniemulsion polymerisations. Hence, surfactants from the Triton X series were examined for DArP reactions.

3.3.1. Application of the Non-Ionic Surfactant Triton X305

Table 3.3: Miniemulsion polymerisations with Triton X305 and comparison with SDS.

entry	surfactant	solvent	M_n[1] [kg mol^{-1}]	Đ[1]	size distribution[2] [nm]	PDI[2]
3.14	SDS	*o*-xylene	1.2	1.2	231 ± 179 (95 %) 4354 ± 1012 (5 %)	0.43
3.15	Triton X305	*o*-xylene	3.1	2.2	155 ± 64 (100 %)	0.15
3.16	Triton X305	*p*-xylene	4.8	2.7	162 ± 92 (95 %) 17 ± 4 (5 %)	0.36

$Pd(OAc)_2$ 4 mol%, P(*o*-anisyl)$_3$ 8 mol%, solvent 1 mL, [monomer] 0. 25 M, [hexadecane] 78 μL_{HD} mL_{xyl}^{-1}, Na_2CO_3 3 eq., pivalic acid 1 eq., surfactant 100 mg in 10 mL water at 90 °C for 72 h. [1] GPC in THF vs. narrow polydispersity polystyrene standards. [2] DLS analysis of the size distribution and polydispersity index (PDI) at 25 °C. Integral ratios are presented in brackets.

Reactions conducted using Triton X305 (table 3.3, entries **3.15** and **3.16**) were compared to those using SDS as the surfactant (entry **3.14**). The particle size dispersity decreased for entries **3.15** and **3.16** indicating that Triton X305 stabilises the polymer emulsions better than SDS. Moreover, the molecular weights increased for entry **3.15** (*o*-xylene, M_n = 3.1 kg mol^{-1}) and showed the best value for entry **3.16** (*p*-xylene, M_n = 4.8 kg mol^{-1}). Hence, the combination of Triton X305 and p-xylene was chosen for

subsequent parameter screening. Nonetheless, distinguishable oligomer peaks were observed for all GPC traces (figure 3.5 a) as observed in section 3.2.

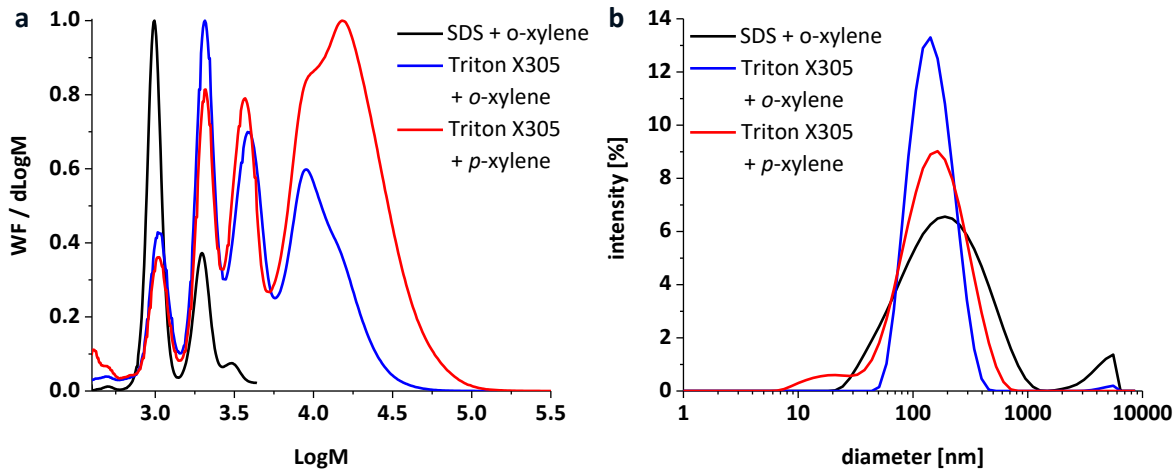

Figure 3.5: Normalised GPC traces (a) and DLS intensity distributions (b) of entries **3.14** - **3.16**.

3.3.2. Screening of the Ethoxylate Chain Length within the Triton X Series

Surfactants within the Triton X series were screened to investigate the impact of the ethoxylate chain length on emulsion stability while the hydrophobic tail remains the same. Therefore, Triton X165 with an average ethoxylate chain length of n = 16 (figure 3.6) was compared with Triton X305 (n = 30) and Triton X405 (n = 35).[88] The extended ethoxylate chain causes an increase in HLB indicating an improved solubility in the aqueous phase. In theory, an increased solubility of the surfactant in water as continuous phase results in increased stabilisation of oil in water (o/w) emulsions.[31]

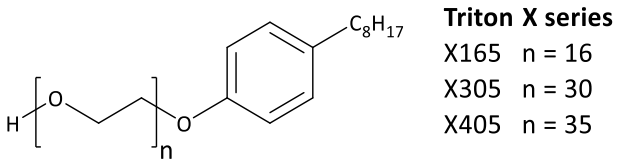

Figure 3.6: Structure of Triton X and number of repeating units (n) of Triton X165, X305 and X405.

Table 3.4: Screening of the PEG chain length within the Triton X series.

entry	surfactant	HLB	M_n[1] [kg mol^{-1}]	Đ[1]	size distribution[2] [nm]	PDI[2]
3.17	Triton X165	16.0	1.6	1.3	238 ± 107 (90 %) 50 ± 12 (7 %)	0.40
3.18	Triton X305	17.3	8.4	3.4	147 ± 71 (91 %) 25 ± 7 (9 %)	0.31
3.19	Triton X405	17.6	3.5	4.7	148 ± 68 (96 %) 19 ±5 (4 %)	0.27

$Pd(OAc)_2$ 4 mol%, P(*o*-anisyl)$_3$ 8 mol%, p-xylene 1 mL, [monomer] 0.25 M, [hexadecane] 78 μL_{HD} mL_{xyl}^{-1}, Na_2CO_3 3 eq., pivalic acid 1 eq., surfactant 100 mg in 10 mL water at 90 °C for 72 h. [1] GPC in THF vs. narrow polydispersity polystyrene standards. [2] DLS analysis of the size distribution and polydispersity index (PDI) at 25 °C. Integral ratios are presented in brackets.

A decrease in particle size dispersities correlated with an increase in the surfactant HLB values with Triton X305 (entry **3.18**) and X405 (entry **3.19**) resulting in fair PDIs (table 3.4). Triton X165 (entry **3.17**) on the contrary, led to an unstable emulsion with macroscopic lumps despite the high cloud point of the surfactant (≤ 100 °C). It is noteworthy, that aggregation was observed for polymerisations conducted with SDS but was entirely absent for experiments conducted with Triton X305 or Triton X405. There seems to be an optimum in observed molecular weight and ethoxylate chain length with Triton X305. As in all previous sections of Chapter 3, distinguishable oligomer peaks were observed for all three GPC traces (figure 3.7 a).

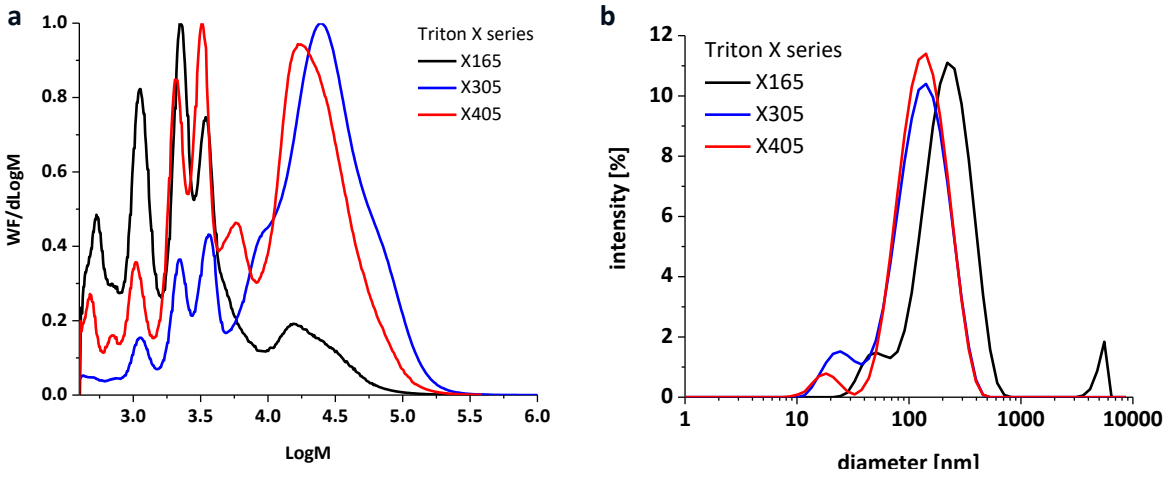

Figure 3.7: Normalised GPC traces (a) and DLS intensity distributions (b) of entries **3.17** - **3.19**.

3.3.3. Surfactant Loading of Triton X305 and Impact upon Emulsion Stability and Polymerisation

Table 3.5 Surfactant loading screening of Triton X305.

entry	surfactant loading		M_n[2]	Đ[2]	size distribution[3]	PDI[3]
	[mg]	[wt. %][1]	[kg mol^{-1}]		[nm]	
3.18	100	1	8.4	3.4	147 ± 71 (91 %) 25 ± 7 (9 %)	0.31
3.20	200	2	4.8	2.7	145 ± 79 (95 %) 16 ± 5 (5 %)	0.37
3.21	500	5	3.9	3.0	144 ± 68 (96 %) 18 ± 6 (3 %) 9 ± 1 (1 %)	0.27

$Pd(OAc)_2$ 4 mol%, P(*o*-anisyl)$_3$ 8 mol%, p-xylene 1 mL, [monomer] 0.25 M, [hexadecane] 78 μL_{HD} mL_{xyl}^{-1}, Na_2CO_3 3 eq., pivalic acid 1 eq. in 10 mL water at 90 °C for 72 h. [1] Weight ratio relative to 10 mL water. [2] GPC in THF vs. narrow polydispersity polystyrene standards. [3] DLS analysis of the size distribution and polydispersity index (PDI) at 25 °C. Integral ratios are presented in brackets.

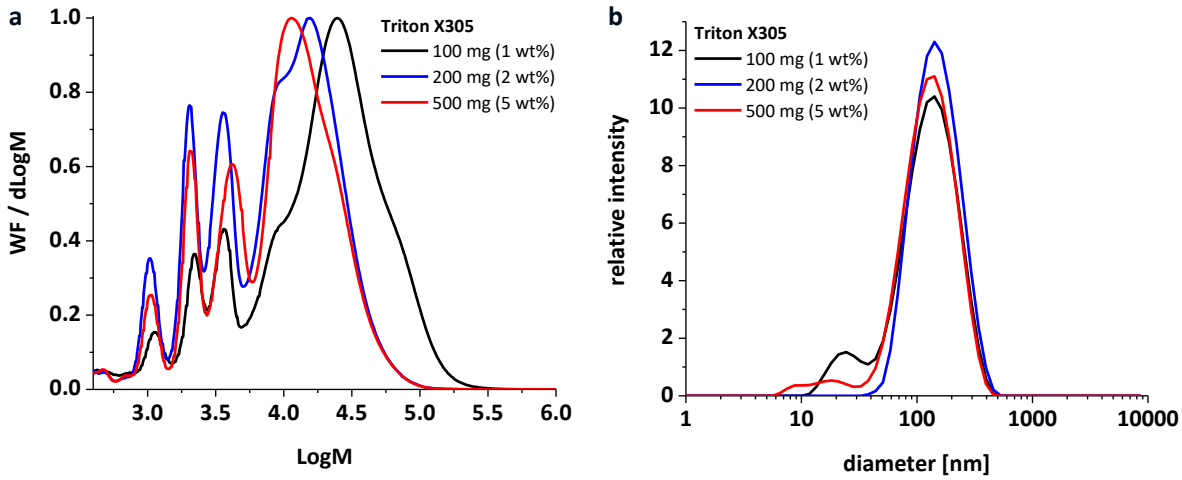

Figure 3.8: Normalised GPC traces (a) and DLS intensity distributions (b) of entries **3.18**, **3.20** and **3.21**.

The surfactant loading of Triton X305 was modified to investigate its impact upon emulsion stability and polymerisation. Table 3.5 shows that the molecular weights of the polymers decrease with increasing surfactant loading. As opposed to that, the particle size dispersities decreased with increasing surfactant loading. Although entry **3.20** gave a lower

dispersity emulsion compared to entries **3.18** and **3.21**, 100 mg of Triton X305 (1 wt%) was used for sections 3.3.4 and 3.3.5. The low molecular weights obtained by employing 200 mg and 500 mg surfactant would have made a differentiation of M_n difficult for the screening to follow due to the low molecular weights obtained for entries **3.20** and **3.21**.

3.3.4. Decrease of Monomer Concentration

Figure 3.9: Miniemulsion after sonication with [monomer] = 0.25 M. The formation of monomer aggregates after sonication was not observed for [monomer] = 0.20 M.

Table 3.6: Miniemulsion polymerisations with decreased monomer concentration.

entry	**monomer concentration** [M]	**M_n**[1] [kg mol^{-1}]	**Đ**[1]	**size distribution**[2] [nm]	**PDI**[2]
3.22	0.20	3.2	2.5	160 ± 66 (99 %) 4385 (1 %)	0.15
3.18	0.25	8.4	3.4	141 ± 66 (97 %) 17 ± 5 (3 %)	0.31

$Pd(OAc)_2$ 4 mol%, P(*o*-anisyl)$_3$ 8 mol%, p-xylene 1 mL, [hexadecane] 78 $\mu L_{HD} mL_{xyl}^{-1}$, Na_2CO_3 3 eq., pivalic acid 1 eq., Triton X305 100 mg in 10 mL water at 90 °C for 72 h. [1] GPC in THF vs. narrow polydispersity polystyrene standards. [2] DLS analysis of the size distribution and polydispersity index (PDI) at 25 °C. Integral ratios are presented in brackets.

Figure 3.9 shows a sonicated miniemulsion prior to being heated to the required reaction temperature. The formation of dark aggregates was visually observed. Due to this, the monomer concentration was decreased from 0.25 M to 0.20 M in 1 mL of p-xylene.

With decreased monomer concentration, no lumps were observed after dispersing the sample indicated by a decreased particle size dispersity for entry **3.22** (table 3.6). Unfortunately, the molecular weight obtained for entry **3.22** decreased as well due to the relationship between monomer concentration and M_n (figure 3.10).

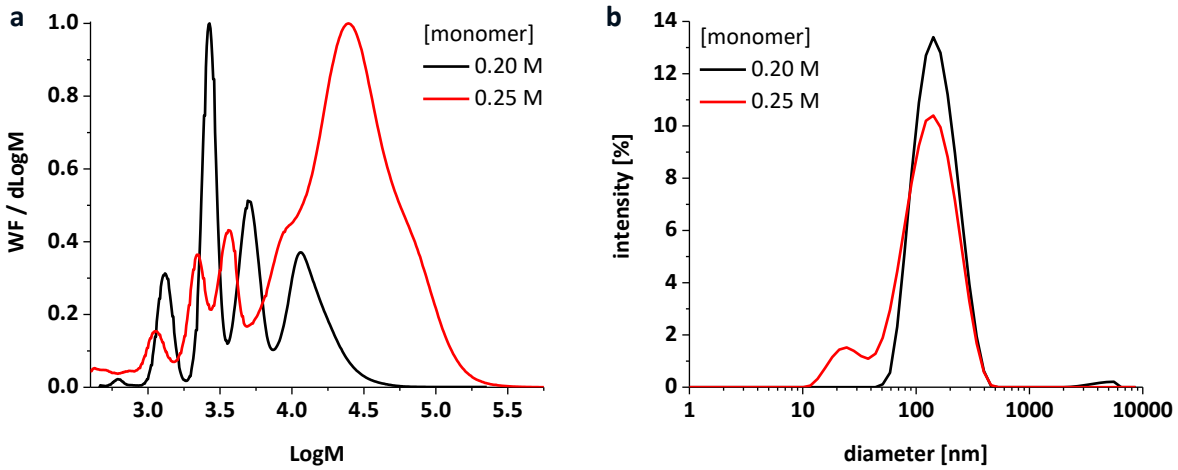

Figure 3.10: Normalised GPC traces (a) and DLS intensity distributions (b) of entries **3.18** and **3.22**.

3.3.5. Palladium(II) Acetate Batch Comparison

Among the Pd(II) acetate batches used in this body of work, materials supplied by Acros Organics gave the greatest molecular weights and most reproducible results when compared to materials supplied by Alfa Aesar and Sigma Aldrich. Table 3.8 and figure 3.12 show that even for two different batches from the same supplier divergent results can be obtained. Reproducibility, activity and selectivity issues with Pd(II) acetate pre-catalysts are reported from several sources in industry and academia.[89] The "non trivial behaviour of Pd(II) acetate" is attributed to the incorporation of nitrite.[90] Its incorporation depends on the procedure used to prepare Pd(II) acetate and can be readily determined by several analytical methods.[91] Due to this, the two pre-catalyst batches were analysed by ^{1}H NMR spectroscopy and elemental analysis and their performance in miniemulsion DArP of PDPPF4.

The ^{1}H NMR spectrum of Pd(II) acetate batch A0400881 (entry **3.23**) in figure 3.11 shows the acetate methyl protons at δ = 1.95 ppm. Three additional peaks are present at

δ = 2.07, 1.97 and 1.87 ppm and were reported to be impurities due to hydrolysis. The bottom spectrum in figure 3.11 shows additional signals at δ = 2.02, 1.99, 1.92 and 1.87 ppm as well as the aforementioned hydrolysis peaks. These shifts are attributed to the substitution of at least one acetate ligand by a nitrite ligand.

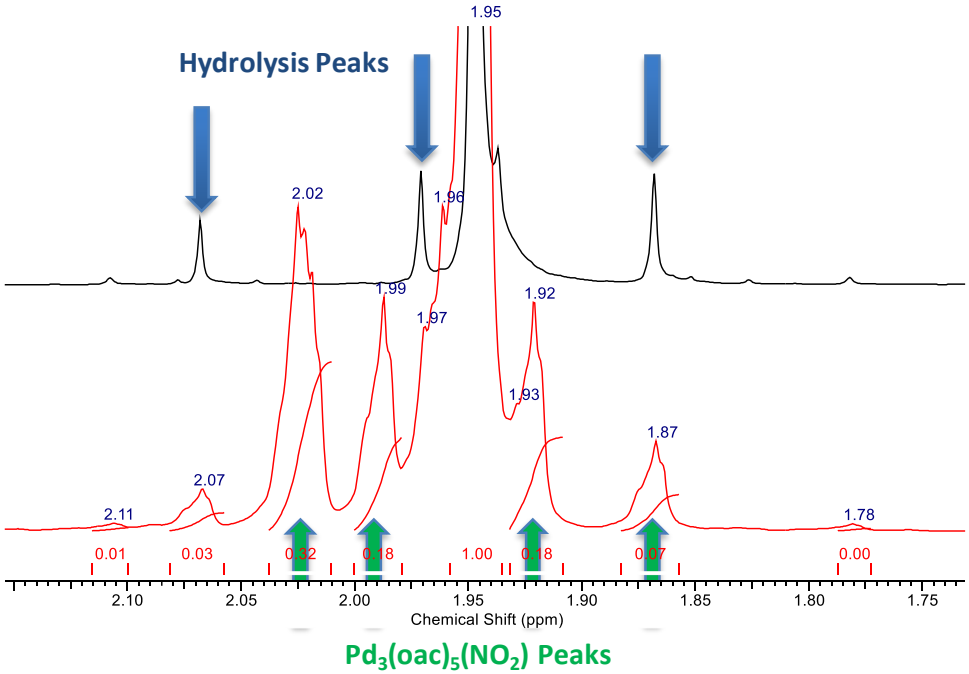

Figure 3.11: ^{1}H NMR spectra of batches A0400881 (top) and A0392692 (bottom). The samples were prepared in a Young tube within a glovebox using anhydrous CD_2Cl_2. The integrals in the lower spectrum were normalised against the acetate methyl protons (δ = 1.95 ppm).

Table 3.7: Elemental analysis of the two Pd(II) acetate batches.

	C [%]	H [%]	N [%]	Pd [%]
$Pd_3(Oac)_6$[1]	20.6	2.6	-	51.8
$Pd_3(Oac)_5(NO_2)$[1]	18.2	2.3	2.1	48.3
A0392692	19.8	2.4	1.0	51.9
A0400881	21.4	2.7	-	47.4

[1]Expected by calculation.

. The two batches were further analysed by elemental analysis (table 3.7). The contents of carbon, hydrogen, nitrogen and palladium were calculated for trinuclear Pd(II)

acetate and an impurity containing one NO_2-ligand. Batch A0392692 (entry **3.22**) contains 1 % nitrogen indicating that about every second trinuclear Pd complex bears a nitrite ligand which confirms the findings from the ^{1}H NMR spectrum. Batch A0400881 (entry **3.23**) on the contrary, shows no presence of a nitrite impurity.Comparison of the molecular weights of the polymers obtained with both Pd(II) acetate batches indicates that batch A0400881 (entry **3.22**) demonstrated a greater catalyst performance (table 3.8 and figure 3.12). Hence, the analyses by ^{1}H NMR spectroscopy and elemental analysis confirm that higher Pd(II) acetate purities yield in superior results in terms of polymerisations outcomes. According to the results, batch A0400881 was used for further work.

Table 3.8: Pd(II) acetate batch comparison.

entry	batch	M_n[1] [kg mol^{-1}]	Đ[1]	size distribution[2] [nm]	PDI[2]
3.22	A0392692	3.2	2.5	160 ± 66 (99 %) 4385 (1 %)	0.15
3.23	A0400881	4.3	2.5	141 ± 66 (97 %) 17 ± 5 (3 %)	0.27

$Pd(OAc)_2$ 4 mol%, P(*o*-anisyl)$_3$ 8 mol%, p-xylene 1 mL, [monomer] 0.20 M, [hexadecane] 78 μL_{HD} mL_{xyl}^{-1}, Na_2CO_3 3 eq., pivalic acid 1 eq., Triton X305 100 mg in 10 mL water at 90 °C for 72 h. [1] GPC in THF vs. narrow polydispersity polystyrene standards. [2] DLS analysis of the size distribution and polydispersity index (PDI) at 25 °C. Integral ratios are presented in brackets.

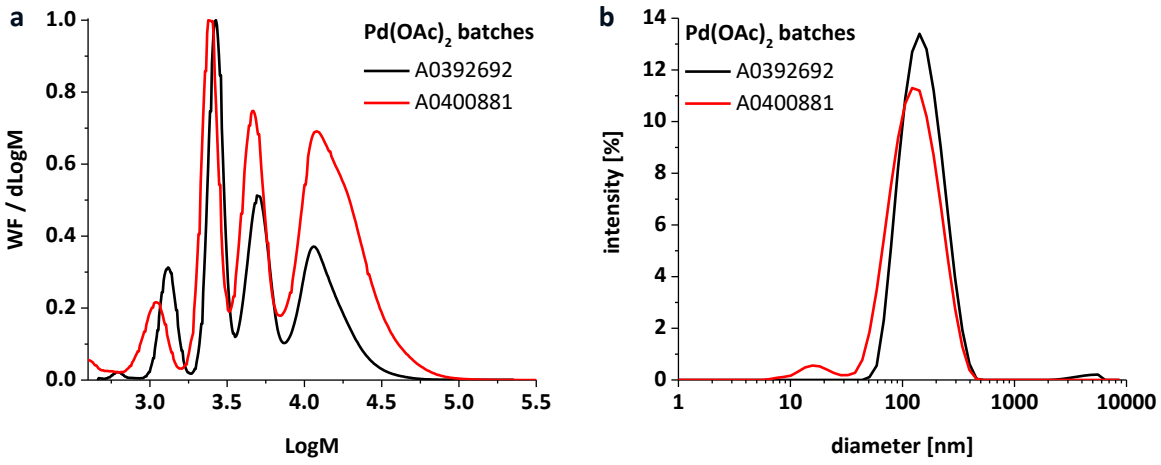

Figure 3.12: Normalised GPC traces (a) and DLS intensity distributions (b) of entries **3.22** (batch A0392692) and **3.23** (batch A0400881).

3.4. Miniemulsion Polymerisations with the Non-Ionic Surfactant Series Synperonic F

Polymerisations conducted with Triton X305 peaked at molecular weights of 8.4 kg mol^{-1} (entry **3.18**). To try and improve the molecular weight of the polymers, surfactants of the Synperonic F series were investigated. The Synperonic surfactants are poloxamers known by different trade names and consist of BAB tri-block copolymers. The central polymer block is composed of poly(propylene oxide) (PPO) that is flanked by water-soluble poly(ethylene oxide) (PEO, PEG) blocks.[92] A notation indicates the length of the PPO block and PPO/PEO ratio within the Synperonic surfactant family: The first (two) digits signify the weight of the PPO block (divided by 100) and the last digit specifies the PEO weight ratio (in percentage, divided by 10). A letter describes the physical from: L for liquid, P for paste and F for flake.

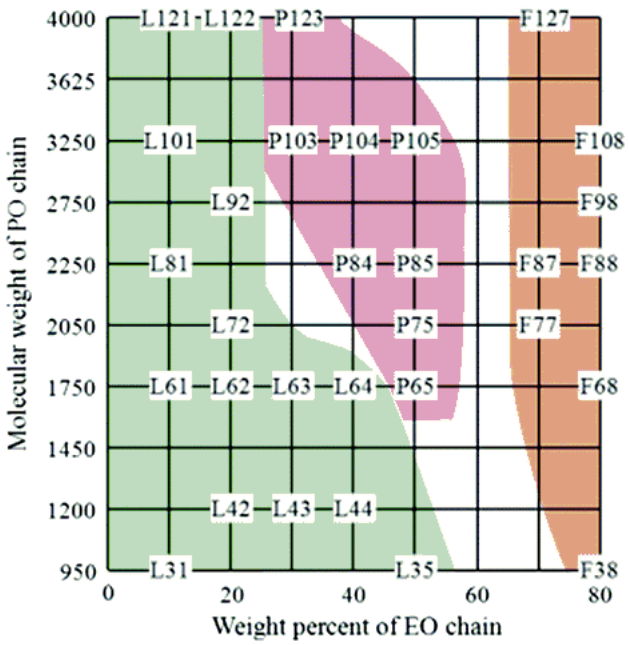

Figure 3.13: Pluronic grid indicating physical form by colour: green = liquid, red = paste, orange = flake.[93]

This is clearly presented in the Pluronic Grid (figure 3.13).[93] Horizontal lines belong to surfactants of the same PPO block length and vertical lines indicate the same PPO/PEO

ratio. In this body of work, Synperonic F 38, 68 and 108 were used due to their extended PEO blocks. Increasing the PEO block length enhances the water solubility as well as the cloud point of the surfactant taking in account the elevated reaction temperatures of the DArP protocol employed.

3.4.1. Comparison between Triton X305 and the Synperonic F Surfactant Series

Table 3.9: Comparison between TritonX-305 and the Synperonic F surfactant series.

entry	surfactant	HLB	M_n[1] [kg mol^{-1}]	Đ[1]	size distribution[2] [nm]	PDI[2]
3.24	Triton X305	17	9.2	2.7	122 ± 66 (92 %) 14 ± 5 (7 %) 3 ± 1 (1 %)	0.49
3.25	Synperonic F38	25	17	2.9	145 ± 94 (94 %) 13 ± 4 (5 %) 4367 ± 944 (1 %)	0.50
3.26	Synperonic F68	29	15	3.1	125 ± 75 (91 %) 11 ± 4 (8 %) 4240 ± 991 (1 %)	0.47
3.27	Synperonic F108	27	7.5	2.6	136 ± 81 (94 %) 12 ± 4(6 %)	0.43

$Pd(OAc)_2$ 4 mol%, P(*o*-anisyl)$_3$ 8 mol%, p-xylene 1 mL, [monomer] 0.20 M, [hexadecane] 78 $\mu L_{HD}\, mL_{xyl}^{-1}$, Na_2CO_3 3 eq., pivalic acid 1 eq., surfactant 500 mg in 10 mL water at 90 °C for 72 h. [1] GPC in THF vs. narrow polydispersity polystyrene standards. [2] DLS analysis of the size distribution and polydispersity index (PDI) at 25 °C. Integral ratios are presented in brackets.

Table 3.9 presents the polymer and emulsion parameters obtained from the surfactant screening. Comparison of the GPC results reveals a trend within the Synperonic F series with the greatest M_n (17 kg mol^{-1}, entry **3.25**) obtained for the shortest poloxamer (Synperonic F38, M = 4.7 kg mol^{-1}). On the contrary, the lowest molecular weight for PDPPF4 was measured for entry **3.27** (M_n = 7.5 kg mol^{-1}) to which the largest surfactant (Synperonic F108, M = 14.6 kg mol^{-1}) was added. The GPC traces of entries **3.25** and **3.26** (figure 3.14) exhibit a second peak at ~ 10^2 kg mol^{-1} suggesting a second C-C coupling mechanism. The particle size dispersities are elevated (PDI > 0.3) for all entries indicating that none of these surfactants stabilise the emulsions sufficiently.

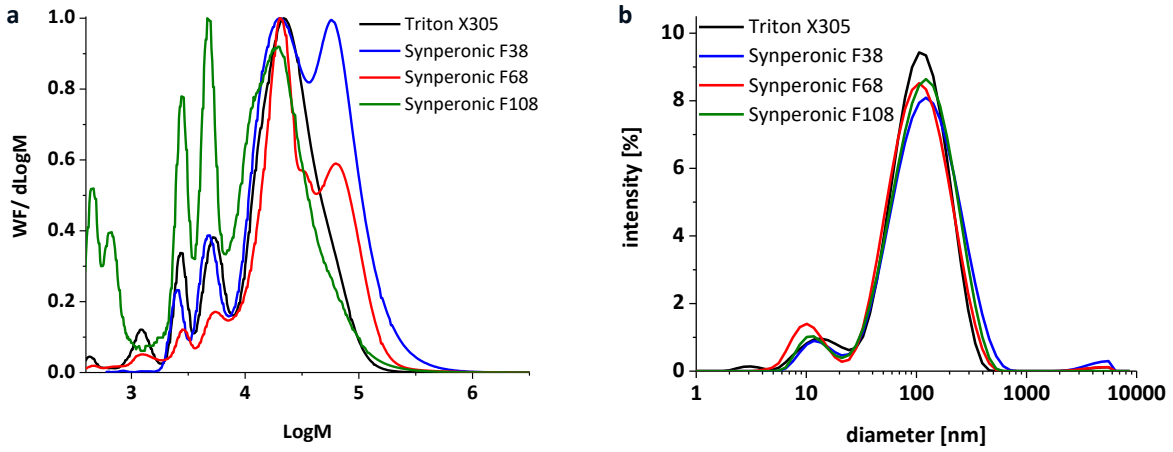

Figure 3.14: Normalised GPC traces (a) and DLS intensity distributions (b) of entries **3.24** – **3.27**.

Isolation of the polymers prepared using Synperonic surfactants required an alteration of the precipitation protocol. Typically, emulsions stabilised by SDS and the Triton series were precipitated by using a 1:4 emulsion to methanol ratio prior to centrifugation. Synperonic F68 and F108 based emulsions required a larger amount of alcohol to precipitate the polymer. Hence, larger centrifuge tubes (Nalgene, 50 mL) were used to allow the precipitation of reasonable sample sizes for subsequent sample analyses. Methanol, ethanol, isopropanol and n-butanol were screened against the three Synperonic surfactants (example depicted in figure 3.15). Amongst these alcohols, methanol precipitated only Synperonic F38 emulsions while n-butanol tended to dissolve the monomer and hence both solvents were not ideal for sample preparations. Thus, ethanol and isopropanol can be used indifferently to precipitate the polymer out of emulsion.

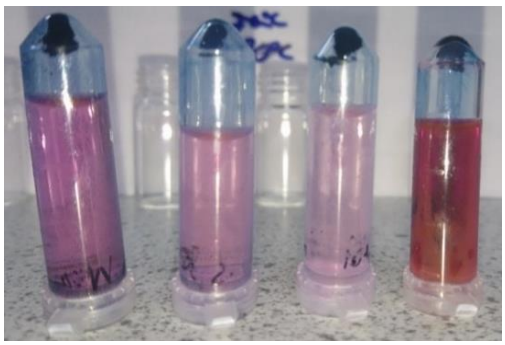

Figure 3.15: Left to right: Synperonic F38 PDPPF4 emulsions (entry **3.25**) precipitated in MeOH, EtOH, iPrOH and n-BuOH. Polymer pellets were observed in all 1.5 mL centrifuge tubes.

In case larger polymer sample amounts were required, the precipitation protocol was modified. Since the decantation of the supernatant tends to re-emulsify the pellet, a small volume of the supernatant was left. The centrifugation tube was then refilled with more alcohol in order to repeat the shake-centrifugation-decantation cycle. Quantification of surfactant removal is discussed in detail in section 5.2.

3.4.2. Effect of Hydrophobe Concentration upon Emulsion Stability and Dispersity

None of the surfactants employed in this body of work (i.e SDS, Triton X305, Synperonic F series) were able to give stable emulsions with moderate particle size dispersities (PDI < 0.30) for the concentration of hydrophobe added ([hexadecane] = 78 μL_{HD} mL_{xyl}^{-1}). Hence, the concentration of hydrophobe and its impact upon emulsion stability was investigated. The monomer was observed to marginally dissolve in hexadecane (pink stain) whereas the polymer exhibited no solubility.

Table 3.10: Impact of hydrophobe concentration upon emulsion stability.

entry	hexadecane concentration [M]	M_n[1] [kg mol^{-1}]	Đ[1]	size distribution[2] [nm]	PDI[2]
3.26	0.27	15	3.1	125 ± 75 (91 %) 11 ± 4 (8 %) 4240 ± 991 (1 %)	0.47
3.28	0.51	18	2.4	222 ± 181 (99 %) 4617 ± 823 (1 %)	0.47
3.29	0.85	15	2.7	182 ± 94 (96 %) 26 ± 7 (4 %)	0.28

$Pd(OAc)_2$ 4 mol%, P(*o*-anisyl)$_3$ 8 mol%, p-xylene 1 mL, [monomer] 0.20 M, Na_2CO_3 3 eq., pivalic acid 1 eq., Synperonic F68 500 mg in 10 mL water at 90 °C for 72 h. [1] GPC in THF vs. narrow polydispersity polystyrene standards. [2] DLS analysis of the size distribution and polydispersity index (PDI) at 25 °C. Integral ratios are presented in brackets.

Table 3.10 presents three entries with varying hexadecane concentration. For entry **3.26**, 78 µL of hexadecane was added into 1 mL of a p-xylene monomer solution corresponding to a concentration of 0.27 M. The amount of hexadecane was increased to

150 and 250 µL according to the concentrations listed in table 3.10 for entries **3.28** and **3.29**, which equates to 0.51 and 0.85 M. The particle size dispersity of entry **3.28** is still elevated for 0.51 M hexadecane suggesting that the osmotic pressure does not suffice to prevent Oswald ripening. Hence, both DLS intensity distributions for entries **3.26** and **3.28** in figure 3.16 (b) should be interpreted with caution. Entry **3.29** on the contrary exhibits a decreased PDI that was subsequently observed for the entirety of experiments conducted with a hydrophobe concentration of 0.85 M except for a few outliers. Stabilisation of miniemulsion polymerisations upon hexadecane addition is reported in the literature for non-conjugated polymers such as poly(styrene) or poly(methyl methacrylate).[94,95,41,42] However, the listed publications contradict each other whether varying concentrations of hydrophobe impact polymer particle diameter. The reported monomer to hexadecane ratios ($n_{monomer}\ n_{HD}^{-1}$) are in a range from 15 - 111 for methyl meth acrylate (MMA)[42] and minimum 250 for styrene[41]. The molar ratio $n_{PDPPF4}\ n_{HD}^{-1}$ presented for entry **3.29** (c(HD) = 0.85 M) is 0.24 indicating that more hydrophobe than monomer is present. Compared to the ratios reported for MMA and styrene, the amount/molar ratio of hydrophobe added in this body of work is orders of magnitude higher to stabilise the PDPPF4 polymer particles. It is noteworthy that this is the only screening of hydrophobe concentrations reported for miniemulsion polymerisations of conjugated polymers so far.

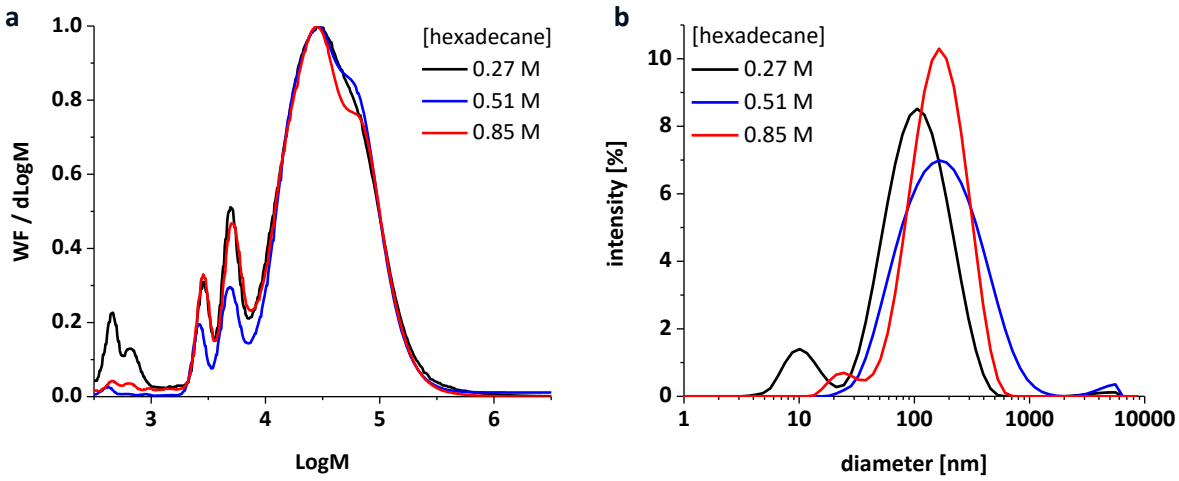

Figure 3.16: Normalised GPC traces (a) and DLS intensity distributions (b) of entries **3.26**, **3.28** and **3.29**.

Control samples were prepared and measured by DLS in order to evaluate the contribution of the monomers/polymer upon the emulsion parameter. The samples contained water, surfactant, solvent, hydrophobe and carbonate salt and were sonicated for 10 min. Figure 3.17 shows from left to right the blank samples with increasing hexadecane content. The sample containing no hexadecane exhibits phase separation, an elevated droplet dispersity (table 3.11) and bimodal intensity distribution (Figure 3.18 right) presenting an unstable miniemulsion. The four following samples reveal a trend of decreasing PDIs for increasing hexadecane contents while the particle sizes do not suggest a correlation. The pure hexadecane sample (c(HD) = 3.40 M) was almost translucent due to a smaller difference of refractive indices between hexadecane and water. Comparing the particle size dispersity and sizes of the blank sample with entry **3.29** (c(HD) = 0.85 M), the blank sample shows a similar particle size but decreased PDI.

Figure 3.17: Blank samples of Synperonic F38 emulsions with different hexadecane concentrations with increasing hexadecane content from left to right according to table 3.11.

Table 3.11: Impact of hydrophobe concentration upon reference sample emulsion parameter.

hexadecane concentration		**size distribution**	**PDI**
c(HD)	$\mu L_{HD}\ mL_{xyl}^{-1}$	[nm]	
-	-	292	0.49
0.27	78	103	0.20
0.85	250	125	0.18
1.70	500	132	0.14
3.40	-	121	0.13

Na_2CO_3 127 mg, p-xylene 2 mL, Synperonic F38 1.00 g in 20 mL water were sonicated for 5 x 2 min at 21 % sonicator amplitude.

The DLS intensity distribution for the blank sample depicts a unimodal distribution (figure 3.18 b) compared to the polymer containing samples in figure 3.16 b. The more intense peak for smaller particle diameter samples in figure 3.16 b is indicative of surfactant micelles in the presence of polymer particles (presented in the next Chapter). Removal of micelles is discussed in section 5.2.

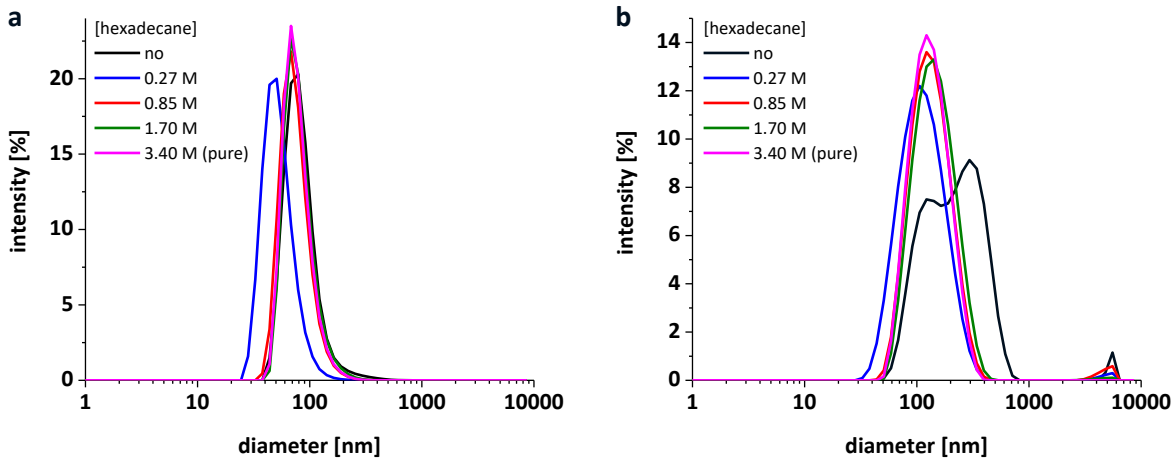

Figure 3.18: DLS number (a) and intensity (b) distributions of the sonicated blank samples.

3.4.3. Comparison between Triton X305 and the Synperonic F Surfactant Series with Increased Hydrophobe Concentration

The surfactant screening was repeated with the increased hydrophobe concentration suggested by the previous results (section 3.4.2). Compared to the entries with lower hexadecane concentrations, all particle size dispersities in table 3.12 are below 0.3 for the 4 surfactants presented (figure 3.19 right). This indicated that c(HD) = 0.85 M or 250 μL_{HD} mL_{xyl}^{-1} is a sufficient quantity of hydrophobe to counteract the Laplace pressure in order to reduce Ostwald ripening leaving coalescence as the cause of particle aggregation. No correlations are derivable between molecular weights, particle sizes and dispersities with the surfactant HLB values. However, Triton X305 and Synperonic F108 gave repeatedly inferior molecular weights for both hydrophobe concentrations. Synperonic F68 was chosen amongst the other two surfactants since it gave the highest molecular weight for c(HD) = 0.85 M. Moreover, Synperonic F68 has reportedly the highest

cloud point amongst the Synperonic Fxx8 series[96] rendering it an optimal choice for emulsion stability investigation (temperature and salt concentration).

Table 3.12: Comparison between Triton X305 and the Synperonic F surfactant series with increased hydrophobe concentration of c(HD) = 0.85 M.

entry	surfactant	HLB	M_n[1] [kg mol^{-1}]	Đ[1]	size distribution[2] [nm]	PDI[2]
3.30	Triton X305	17	9.2	2.3	163 ± 78 (99 %) 24 ± 6 (1 %)	0.25
3.31	Synperonic F38	25	11	2.4	257 ± 175 (98 %) 4514 ± 2 (2 %)	0.25
3.29	Synperonic F68	29	15	2.7	182 ±94 (96 %) 26 ±7 (4 %)	0.28
3.32	Synperonic F108	27	8.9	2.6	167 ± 113 (99 %) 457 ± 831 (1 %)	0.24

$Pd(OAc)_2$ 4 mol%, P(*o*-anisyl)$_3$ 8 mol, p-xylene 1 mL, [monomer] 0.20 M, [hexadecane] 250 μL_{HD} mL_{xyl}^{-1}, Na_2CO_3 3 eq., pivalic acid 1 eq., surfactant 500 mg in 10 mL water at 90 °C for 72 h. [1] GPC in THF vs. narrow polydispersity polystyrene standards. [2] DLS analysis of the size distribution and polydispersity index (PDI) at 25 °C. Integral ratios are presented in brackets.

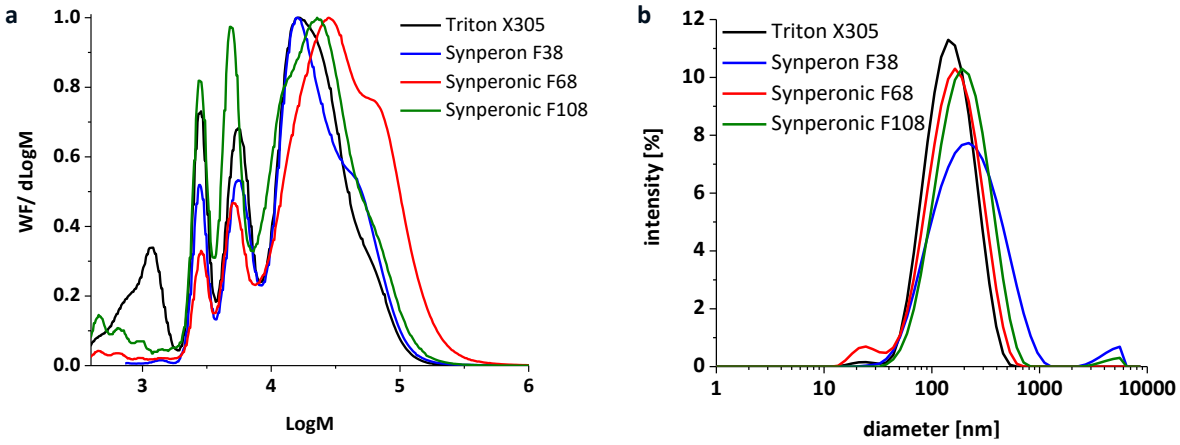

Figure 3.19: Normalised GPC traces (a) and DLS intensity distributions (b) of entries **3.29** - **3.32**.

The DLS number distribution show bimodal distributions except for the Synperonic F108 based miniemulsion (Figure 3.20). The unimodal number distribution for Synperonic F108 is unexpected given that the critical micelle concentrations and temperatures tend to decrease with increasing molecular weight of the poloxamer.[96,97] Furthermore, the

molarities of the Synperonic surfactants employed in entries **3.29**, **3.31** and **3.32** decrease with increasing molecular weight of the surfactant since the same mass (0.5 g) was employed for all entries (table 3.13). The reported area per molecule parameters for the Synperonic Fxx8 series onto polystyrene particles is the highest for Synperonic F108 (6.51 nm^2, 15.1 nm^2 and 24.3 nm^2, respectively)[98]. Taking this value in account, the total surface area of a monolayer of 0.5 g Synperonic F108 is estimated to be 500 m^2. Compared to the reported data, the total surface area for isotropic particles of 1 mL dispersed phase with a diameter of 167 nm is 0.19 m^2 suggesting that an abundant excess of surfactant has been used. This excess should result in the formation of micelles as observed for the other entries in this Chapter. On the other hand, Synperonic F108 exhibits the highest specific adsorption on polystyrene latices.[99]

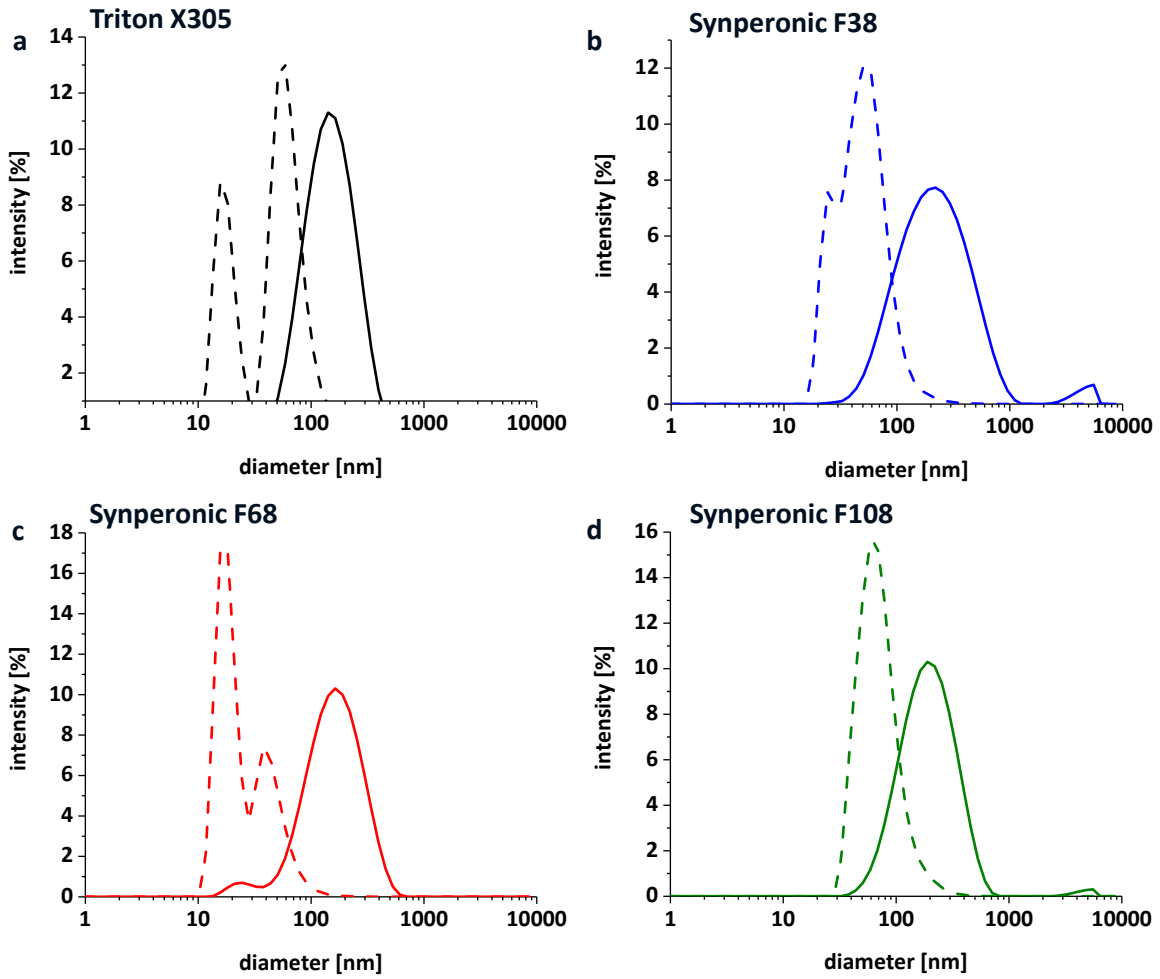

Figure 3.20: DLS number (dashed line) and intensity (straight line) distributions of entries **3.30** (a), **3.31** (b), **3.29** (c) and **3.32** (d).

Table 3.13: Molecular weights, molarity of the surfactant employed in entries **3.29** - **3.32** and CMC of each surfactant.

entry	surfactant	$M_{n,\ surfactant}$ [kg mol^{-1}]	[surfactant] [M]	CMC[1] [M]	CMT[2] [C]
3.30	Triton X305	1.5	$3.3 \cdot 10^{-2}$	$6.5 \cdot 10^{-4}$	-
3.31	Synperonic F38	4.7	$1.1 \cdot 10^{-2}$	-	77
3.29	Synperonic F68	8.4	$6.0 \cdot 10^{-3}$	$4.8 \cdot 10^{-4}$	44
3.32	Synperonic F108	14.6	$3.4 \cdot 10^{-3}$	$2.2 \cdot 10^{-5}$	25

[1] CMC values were determined using a pyrene probe.[97] [2] CMT value was determined for 10 wt. % solution of Synperonic surfactant in water by high sensitivity differential scanning calorimetry.[96]

Surface tension measurements of samples **3.29** (Synperonic F68) and **3.32** (Synperonic F108) were conducted by halving the concentration between each measurement that were performed in triplicate (figure 3.21). The CMC determined for entry 3.21 (Synperonic F68, figure 3.21 a) occurs at less dilution (~ ½ c) than for entry **3.24** (Synperonic F108, figure 3.21 b, ~ 1/16 c) and confirmed the presence of micelles but does not explain the absence of a micelle peak of the DLS number distribution for entry **3.32**.

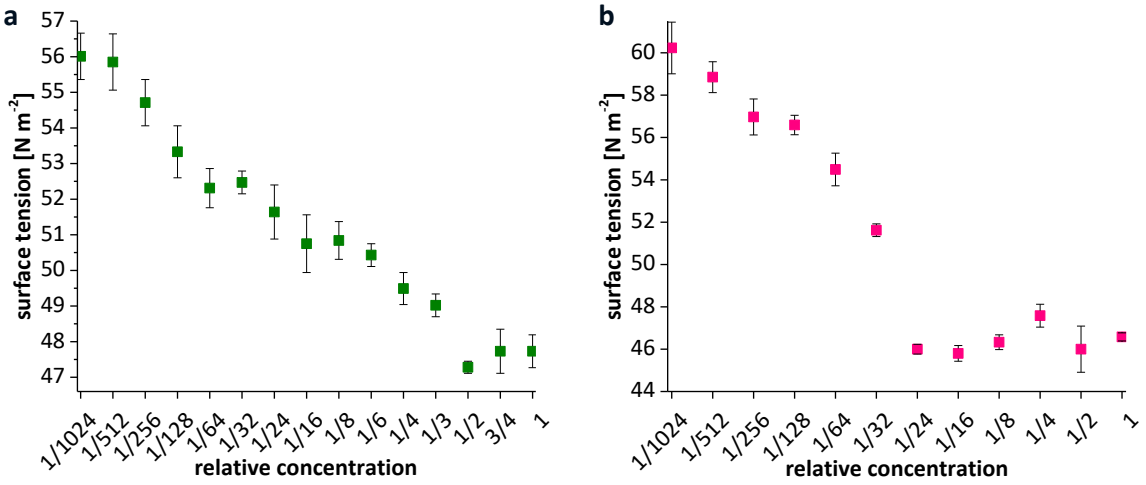

Figure 3.21: Surface tension measurements of entries **3.29** (a, Synperonic F68) and **3.32** (b, Synperonic F108).

3.4.4. Reproducibility between DPP Monomer Batches

Table 3.14: Reproducibility between DPP monomer batches.

entry	DPP batch	number of recrystallisations	M_n[2] [kg mol^{-1}]	Đ[2]	size distribution[3] [nm]	PDI[3]
3.29	**1**	2	15	2.7	182 ± 94 (96 %) 26 ±7 (4 %)	0.28
3.33	**2**	2	5.4	2.0	172 ± 87 (98 %) 4718 ± 793 (2 %)	0.23
3.34	**2**	3	9.8	2.7	168 ± 83 (99 %) 4568 ± 827 (1 %)	0.19
3.35	**2**[1]	1	8.0	2.7	164 ± 97 (98 %) 9 ± 1 (1 %) 4487 ± 885 (1 %)	0.29

$Pd(OAc)_2$ 4 mol%, P(*o*-anisyl)$_3$ 8 mol%, p-xylene 1mL, [monomer] 0.20 M, [hexadecane] 250 μL_{HD} mL_{xyl}^{-1}, Na_2CO_3 3 eq., pivalic acid 1 eq., Synperonic F68 500 mg in 10 mL water at 90 °C for 72 h. [1] Batch contained 2% impurities. [2] GPC in THF vs. narrow polydispersity polystyrene standards. [3] DLS analysis of the size distribution and polydispersity index (PDI) at 25 °C. Integral ratios are presented in brackets.

A reproducibility issue regarding the molecular weights obtained for different alkylated DPP monomer batches was observed throughout this body of work. To elucidate this matter, entry **3.29** was repeated with another DPP monomer batch purified by the same procedure giving a lower molecular weight for entry **3.33** compared to entry **3.29** (table 3.14, figure 3.22 a). Most of the DPP monomer batches were recrystalised twice from dichloromethane and methanol after column chromatographic purification since this gave DPP containing less than 1 % impurities. Quantification of impurities was conducted by ^{1}H NMR spectroscopy as depicted in figure 3.1. For DPP **batch 2**, polymerisations were performed with aliquots after one (entry **3.35**), two-fold (entry **3.33**) and three-fold recrystallisation (entry **3.34**). The DPP batch used for entry **3.34** underwent one additional recrystallisations although no impurities were observed after two-fold crystallisation of **batch 2** (entry **3.33**). The molecular weight obtained for entry **3.34** was the greatest (M_n = 9.8 kg mol^{-1}) amongst the **batch 2** polymerisations in table 3.14. Entry **3.35** was conducted with a DPP batch containing 2 % impurities yielding surprisingly a greater molecular weight

than obtained for entry **3.33** (figure 3.22 c). These results suggest that removal of impurities is crucial to achieve good polymerisations outcomes despite random outliers.

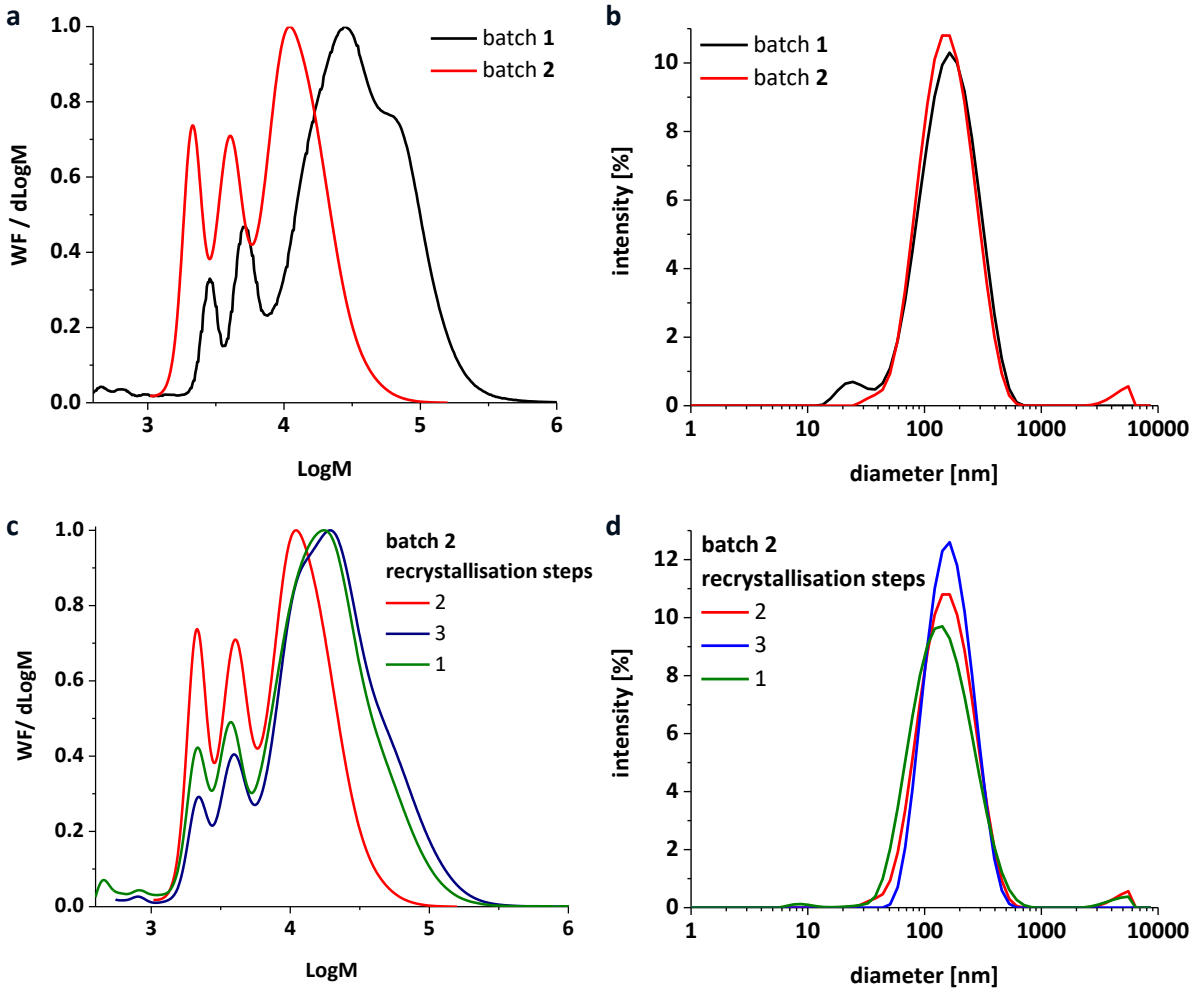

Figure 3.22: Normalised GPC traces (a and c) and DLS intensity distributions (b and d) of entries **3.29** and **3.33** – **3.35**.

Elemental analysis of the DPP batches revealed weight ratios close to the calculated values for DPP indicating there are no substantial impurities which might have not been observed by ^{1}H NMR spectroscopy (table 3.15). Hence, the cause of the batch-to-batch reproducibility issue regarding the molecular weights cannot be determined. As a conclusion, direct comparison for each new batch was conducted to evaluate the performance of each batch. The subsequent work will present systematically lower molecular weights than the previous sections as DPP **batch 2** gave lower molecular weight polymers than **batch 1**.

Table 3.15: Elemental analysis of DPP batches 1 and 2.

	C [%]	H [%]	N [%]	S [%]
calculated	75.3	10.3	3.25	7.44
batch 1	74.5	10.1	3.19	7.19
batch 2	75.5	10.3	3.18	7.31
batch 2[1]	75.2	10.7	3.24	7.24

[1] Batch contained 2% impurities as determined by 1H NMR integral analysis (exemplified in figure 3.1).

3.4.5. Utilisation of Pd_2dba_3 as Pre-Catalyst and Reaction Temperature Screening

Table 3.16: Utilisation of Pd_2dba_3 as precatalyst and reaction temperature screening.

entry	T [°C]	M_n[1] [kg mol^{-1}]	Đ[1]	size distribution[2] [nm]	PDI[2]
3.36	90	5.2	2.0	167 ± 66 (100 %)	0.16
3.37	100	5.4	2.2	174 ± 77 (100 %)	0.30
3.38	110	6.4	2.1	152 ± 66 (99 %) 20 ± (1 %)	0.24

$Pd_2(dba)_3$ 4 mol%, P(*o*-anisyl)$_3$ 8 mol%, p-xylene 1mL, [monomer] 0.20 M, [hexadecane] 250 $\mu L_{HD} mL_{xyl}^{-1}$, K_2CO_3 3 eq., pivalic acid 1 eq., Synperonic F68 500 mg in 10 mL water at reaction temperature for 72 h. [1] GPC in THF vs. narrow polydispersity polystyrene standards. [2] DLS analysis of the size distribution and polydispersity index (PDI) at 25 °C. Integral ratios are presented in brackets.

Palladium(II) acetate is a commonly utilised pre-catalyst for the synthesis of conjugated polymers including DArP. However, the reaction conditions presented so far were not applicable for other comonomers screened in this body of work. Other pre-catalysts were considered for further screening to address an enhanced monomer scope for the optimised reaction conditions. Amongst them, Pd_2dba_3 has been numerously reported for DArP of electron deficient monomers in apolar solvents.[100,101,102,103] Moreover, K_2CO_3 was employed since it was reported to give superior molecular weights for a range of conjugated polymers in conjunction with Pd_2dba_3. The carbonate salt screening (i.e Na_2CO_3, K_2CO_3 and Cs_2CO_3) is discussed in section 3.4.7. Entries **3.36** to **3.38** in table 3.16 show reduced oligomer peaks for increased reaction temperatures (figure 3.23 a)

increasing their M_n marginally. The particle size dispersities for entries **3.36** to **3.38** were below 0.3 (PDI ≤ 0.3) after reaction time since c(HD) = 0.85 M was employed.

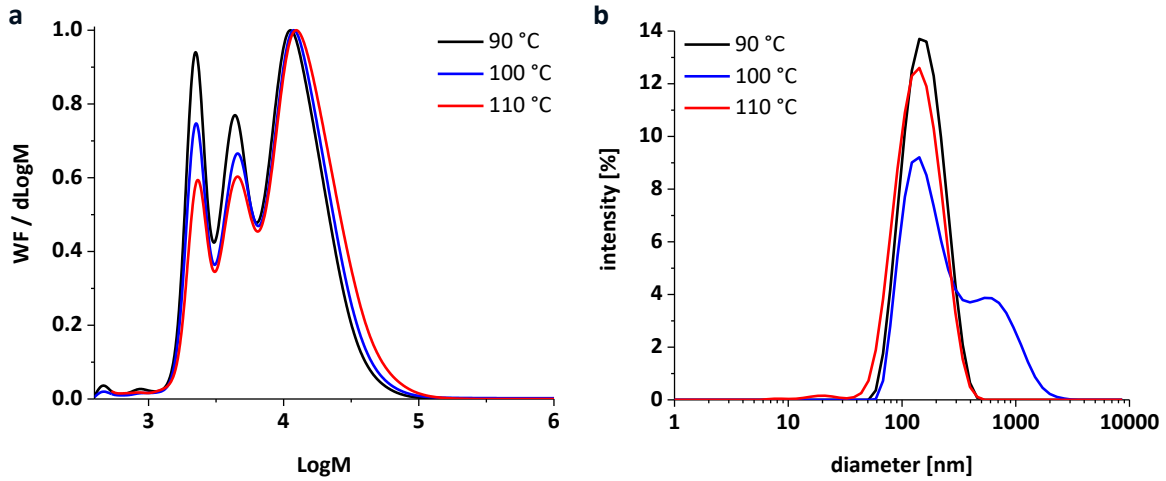

Figure 3.23: Normalised GPC traces (a) and DLS intensity distributions (b) of entries **3.36** - **3.38**.

For entry **3.38**, the formation of two phases was observed during heating up to reaction temperature between 100 °C and 110 °C in an oil bath. The cloud point of Synperonic F68 has been reported to be 110 °C for 5 wt. % surfactant in water.[96] The cloud point itself is subject to several parameters in a heterogeneous phases system and depends on the salt concentration, hydrophobicity of the oil (dispersed) phase and the surfactant itself. Hence, the observation of a somewhat decreased cloud point is the result of those parameters interacting. The two phases observed are attributed to a phase transition from a o/w emulsion to a w/o system. Phase transitions of this kind are abundantly reported for ethoxylated surfactants such as alkyl ethoxylates[104,105,106,107,] (e.g. Brij surfactants) and alkyl phenyl ethoxylates[106,108,109] (e.g Triton X). Poly ethoxylates show a strong temperature dependent behaviour where the interactions between water and the hydrophilic part decrease with increasing temperature until a phase inversion occurs. This temperature is commonly described as phase inversion temperature (PIT) and is identical with the cloud point of the surfactant. The formation of the two phases observed is attributed to the inversed ratio of dispersed to continuous phase beyond the PIT: The ratio changes from 1:10 (organic: aqueous phase v/v) below PIT to 10:1 above PIT. Since the amount of organic continuous phase (above PIT) does not suffice to disperse the larger water phase, a third, non-dispersed, water phase formed. This kind of phase inversion emulsification is classified

as transitional phase inversion and is commonly utilised in the formation of nano-emulsification processes without sonication.[109,110] Nonetheless, the reaction temperature chosen for the next Chapters was 100 °C since the extent of phase inversion to obtain stable o/w emulsions was not entirely understood to this point.

3.4.6. Screening of pre-Catalyst loading and pre-Catalyst to Phosphine Ligand Ratio

The amount of pre-catalyst and its impact upon the molecular weights obtained for entries **3.37**, **3.39** and **3.41** was investigated. The molecular weights in table 3.17 and the GPC traces in figure 3.24 (a) clearly indicated that more pre-catalyst leads to a greater M_n. Additionally, the ratio between palladium pre-catalyst and phosphine ligand was decreased 1:1 (0.5:1 phosphine to palladium) to investigate whether less phosphine ligand increases the rate of reaction or leads to defects (entry **3.40**). The M_n obtained and GPC trace for entry **3.40** (figure 3.24 c) suggests that the polymerisation is less effective than polymerisations with a 1:1 phosphine to palladium ratio. Equal amounts of phosphine ligand to palladium seem to be the minimum required for a successful polymerisation. Defects for the polymers obtained for both phosphine to palladium ratios are discussed in section 5.1.1.

Table 3.17: Screening of precatalyst loading and precatalyst to phosphine ligand ratio.

entry	**Pd_2dba_3** [mol%]	**M_n[1]** [kg mol^{-1}]	**Đ[1]**	**size distribution[2]** [nm]	**PDI[2]**
3.39	5	8.9	2.4	155 ± 64 (98 %) 35 ± 6 (2 %)	0.17
3.40*	5	4.6	2.4	155 ± 59 (100 %)	0.15
3.37	4	5.4	2.2	174 ± 77 (100 %)	0.30
3.41	2	2.6	1.4	193 ± 71 (100 %)	0.14

P(*o*-anisyl)$_3$ to Pd_2dba_3 ratio 2:1, p-xylene 1mL, [monomer] 0.20 M, [hexadecane] 250 μL_{HD} mL_{xyl}^{-1}, K_2CO_3 3 eq., pivalic acid 1 eq., Synperonic F68 500 mg in 10 mL water at 100 °C for 72 h.* P(*o*-anisyl)$_3$ to Pd_2dba_3 ratio 1:1. [1] GPC in THF vs. narrow polydispersity polystyrene standards. [2] DLS analysis of the size distribution and polydispersity index (PDI) at 25 °C. Integral ratios are presented in brackets.

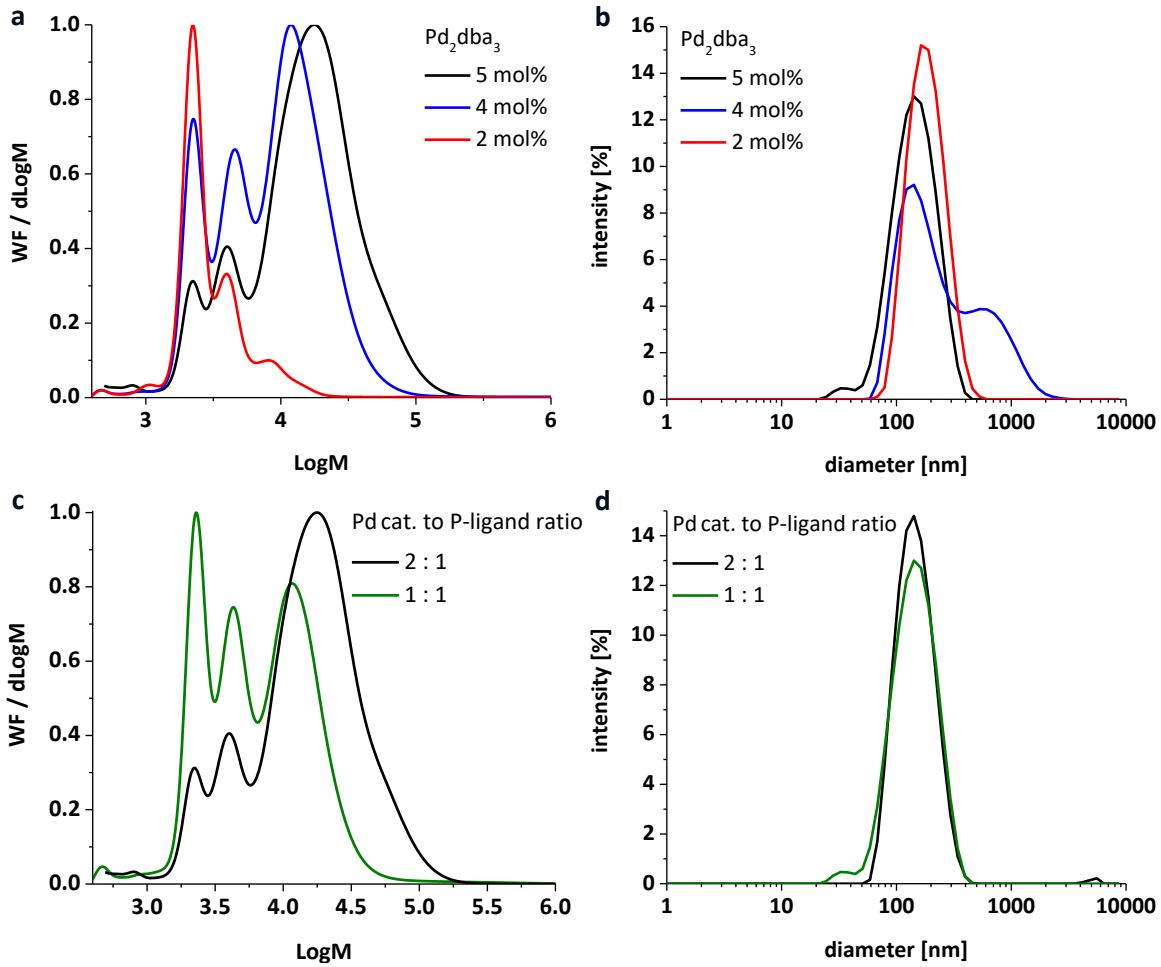

Figure 3.24: Normalised GPC traces of (a) and DLS intensity distributions (b) of the pre-catalyst concentration screening including entries **3.37**, **3.39** and **3.41**. Normalised GPC traces of (c) and DLS intensity distributions (d) of the pre-catalyst to phosphine ligand ratio investigation including entries **3.39** and **3.40**.

3.4.7. Carbonate Salt Screening

Several carbonate salts were reported for DArP of conjugated monomers in solution.[17,72] The most utilised among them are the alkali metal carbonate salts, namely Na_2CO_3, K_2CO_3 and Cs_2CO_3. Table 3.18 presents that an increased M_n was obtained when K_2CO_3 was employed (entry **3.39**) compared to the other carbonate salts. These findings confirm the decision to use K_2CO_3 in the previous two sections and for the parameter screening to follow.

Table 3.18: Carbonate salt screening.

entry	carbonate salt	M_n[1] [kg mol^{-1}]	Đ[1]	size distribution[2] [nm]	PDI[2]
3.42	Na_2CO_3	7.8	2.1	188 ± 99 (98 %) 26 ± 6 (1 %) 4674 ± 794 (1 %)	0.24
3.39	K_2CO_3	8.9	2.4	155 ± 64 (98 %) 35 ± 64 (2 %)	0.17
3.43	Cs_2CO_3	6.5	2.0	163 ± 78 (96 %) 21 ± 5 (3 %) 5641 ± 1042 (1 %)	0.30

Pd_2dba_3 5 mol%, P(*o*-anisyl)$_3$ 10 mol%, p-xylene 1mL, [monomer] 0.20 M, [hexadecane] 250 μL_{HD} mL_{xyl}^{-1}, carbonate salt 3 eq., pivalic acid 1 eq., surfactant 500 mg in 10 mL water at 100 °C for 72 h. [1] GPC in THF vs. narrow polydispersity polystyrene standards. [2] DLS analysis of the size distribution and polydispersity index (PDI) at 25 °C. Integral ratios are presented in brackets.

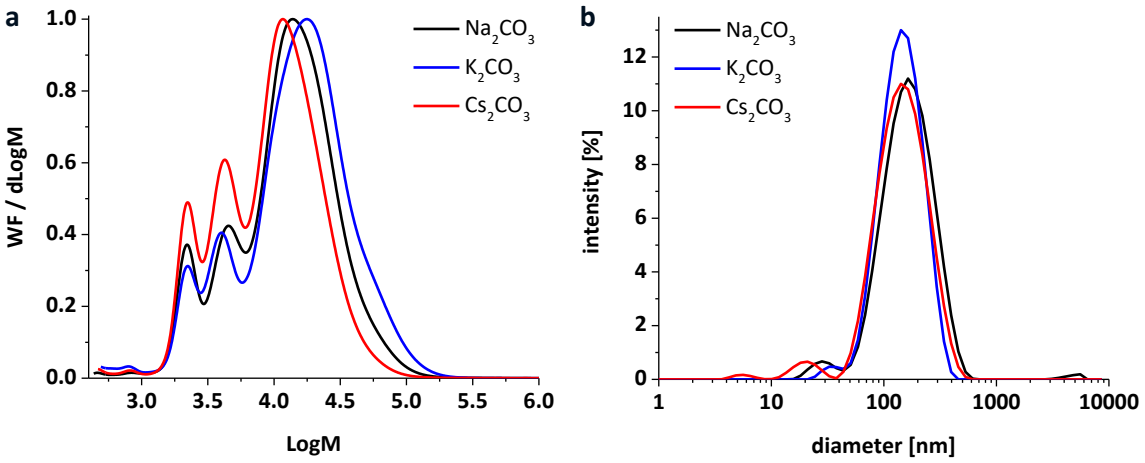

Figure 3.25: Normalised GPC traces (a) and DLS intensity distributions (b) of entries **3.39**, **3.42** and **3.43**.

3.4.8. Screening of Carbonate Salt and Pivalic Acid Loadings

Potassium carbonate salt and pivalic acid were screened since partition of the pivalate into the aqueous phase was anticipated. Partition into the aqueous phase renders the pivalate less accessible in the oil droplets to function as a proton shuttle in the DArP catalyst cycle. As a result, the amount of pivalic acid was increased gradually within one order of magnitude as presented in table 3.19. The ratio of pivalic acid to potassium

carbonate was decreased since the carbonate salt concentration was expected to cause a phase inversion at reaction temperature. Therefore, the pH was kept ≥ 10 to ensure sufficient deprotonation of pivalic acid (pka = 5.0)[111].

Table 3.19: Screening of carbonate salt and pivalic acid loadings.

entry	pivOH : K_2CO_3 eq. (wt. $\%_{K2CO3}$)	pH	M_n[1] [kg mol^{-1}]	Đ[1]	size distribution[2] [nm]	PDI[2]
3.37	1 : 3 (0.8)	10.7	5.4	2.2	174 ± 77 (100 %)	0.30
3.44	3 : 5 (1.4)	10.1	8.2	2.3	166 ± 90 (98 %) 4458 ± 898 (2 %)	0.26
3.45	5 : 8 (2.2)	10.0	10	2.5	178 ± 92 (99 %) 4669 ± 796 (1 %)	0.27
3.46	7 : 11 (3.0)	10.0	9.5	2.2	282 ± 192 (95 %) 4013 ± 1163 (5 %)	0.27
3.47	10: 15 (4.1)	10.0	12	2.7	173 ± 66 (100 %)	0.15

Pd_2dba_3 4 mol%, P(*o*-anisyl)$_3$ 8 mol%, p-xylene 1mL, [monomer] 0.20 M, [hexadecane] 250 μL_{HD} mL_{xyl}^{-1}, Synperonic F68 500 mg in 10 mL water at 100 °C for 72 h. [1] GPC in THF vs. narrow polydispersity polystyrene standards. [2] DLS analysis of the size distribution and polydispersity index (PDI) at 25 °C. Integral ratios are presented in brackets.

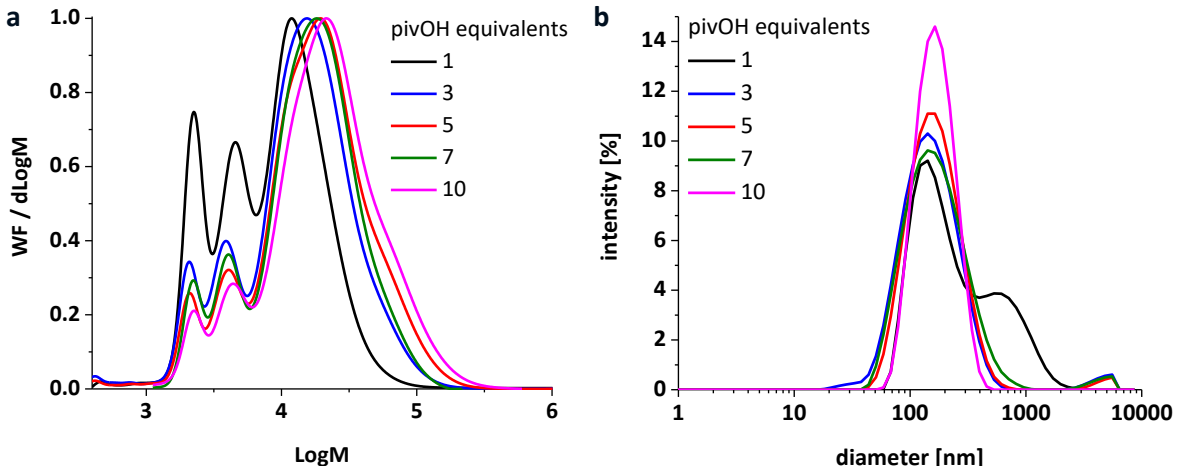

Figure 3.26: Normalised GPC traces (a) and DLS intensity distributions (b) of entries **3.37** and **3.44** – **3.47**.

The molecular weights obtained for entries **3.37** and **3.44** – **3.47** indicate a positive trend for increased pivalate loadings except for entry **3.46** being a marginal outlier. The particle size dispersities for all entries are below 0.3 and hence acceptable. Entries **3.45** and

3.46 with the increased pivalate concentrations are the final optimised reaction conditions in this body of work and were applied for the comonomer scope discussion in Chapter 4. Entry **3.47** exhibited two phases at reaction temperature as observed for entry **3.38** in Chapter 3.4.5. Compared to entry **3.38**, the reaction temperature is 10 °C lower and the pivalic acid and carbonate salt concentrations were increased 10 and 5 times. The phase separations observed at elevated temperatures and/or carbonate salt concentration are explained by the HLD (hydrophilic lipophilic difference) equation.[106]

$$HLD = b(S) - k(EACN) + Cc - \alpha(T - T_{ref}) \quad (4)$$

Where b, k and α are proportionality constants, EACN is the equivalent carbon atom number (i.e. $EACN_{hexadecane}$ = 16), Cc is the characteristic curvature of the surfactant and T the temperature deviating from T_{ref} = 25 °C. An o/w system is by definition HLD < 0 whereas for a w/o system HLD values are greater than 0. For HLD = 0, the emulsion is destabilised and is subject to a transitional phase inversion observed at the PIT. With $T - T_{ref}$ = PIT and α = - 0.06 K^{-1} for ethoxylated surfactants[106,107], the above equation can be converted to

$$PIT = -\frac{b(S) - k(EACN) + Cc}{0.06\ K^{-1}} \quad (5)$$

indicating that the PIT of the CPN emulsions decreases for increased salt concentrations. This relationship between PIT and salt concentration confirmed the observations for entry **3.32** (PIT ~ 110 °C, 0.8 wt. % K_2CO_3) compared to entry **3.39** (PIT ~ 100 °C, 4.1 wt. % K_2CO_3).

To elucidate the reversibility of the transitional phase inversion, 1 mL aliquots of entries **3.31** and **3.36** – **3.39** were heated to 110 °C and then cooled to room temperature (figure 3.27). All samples revealed phase inversions in the temperature regime between 100 °C and 110 °C with an onset at lower temperatures for aliquots containing less carbonate salt. Upon cooling to room temperature, irreversible aggregation was observed for essentially random samples. Those samples showed an increased PDI by DLS measurements at room temperature (presented in red colour in table 3.20). It is

noteworthy that macroscopic aggregates were not observed for the larger polymerisations in emulsion (10 mL of water). There appears to be a scale effect influencing the reversibility of the transitional phase inversion at PIT in favour of larger volumes.

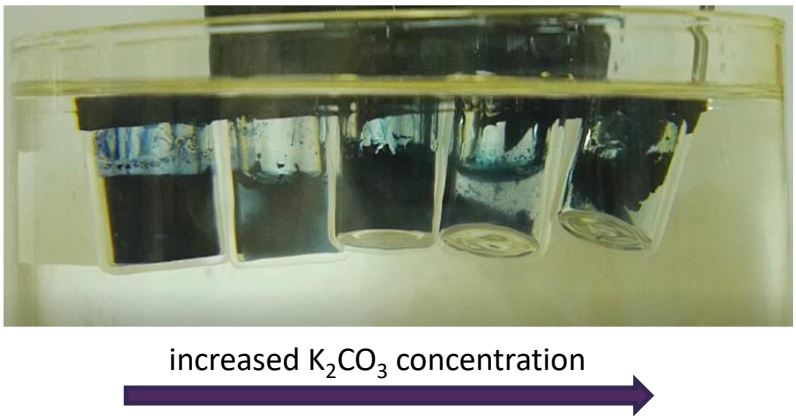

Figure 3.27: From left to right: 1 mL aliquots of entries **3.31** and **3.36** – **3.39** between 100 °C and 110 °C. All samples were stirred during the entire heating/cooling cycle except for the moment the picture was taken.

Table 3.20: Reversibility test of the transitional phase inversion of entries **3.31** and **3.35** – **3.38**.

entry	**pivOH : K_2CO_3** eq. (wt. $\%_{K2CO3}$)	before heating		after heating to PIT	
		size distribution[1] [nm]	**PDI**[1]	**size distribution**[1] [nm]	**PDI**[1]
3.37	1 : 3 (0.8)	194	0.30	198	0.28
3.44	3 : 5 (1.4)	127	0.26	138	0.42
3.45	5 : 8 (2.2)	136	0.27	202	0.36
3.46	7 : 11 (3.0)	145	0.25	140	0.27
3.47	10: 15 (4.1)	148	0.15	138	0.38

Unchanged PDIs after heating to 110 °C are presented in green colour and increased PDIs are indicated in red. [1] DLS analysis of the size distribution and polydispersity index (PDI) at 25 °C. Integral ratios are presented in brackets.

3.4.9. Utilisation of Silver(I) Carbonate

Silver(I) carbonate has been reported as co-catalyst in conjunction with Pd pre-catalysts for DArP on electron deficient monomers.[112] Kinetic investigations indicate that

Ag(I) facilitates the CMD step in the DArP catalyst cycle.[113] For entry **3.48**, 0.4 eq of Ag_2CO_3 was employed due to the solubility limit of Ag_2CO_3 in water (i.e. 0.5 g L^{-1} at 100 °C).[114] Compared to entry **3.46**, the presence of Ag(I) impedes DArP in emulsion (table 3.21 and figure 3.28 a).

Table 3.21: Utilisation of silver(I) carbonate.

entry	K_2CO_3 eq.	Ag_2CO_3 eq.	M_n[1] [kg mol^{-1}]	Đ[1]	size distribution[2] [nm]	PDI[2]
3.46	11.0	-	9.5	2.2	282 ± 192 (95 %) 4013 ± 1163 (5 %)	0.27
3.48	10.6	0.4	1.0	1.6	179 ± 67 (98 %) 4750 ± 754 (2 %)	0.16

Pd_2dba_3 4 mol%, P(*o*-anisyl)$_3$ 8 mol%, p-xylene 1mL, [monomer] 0.20 M, [hexadecane] 250 μL_{HD} mL_{xyl}^{-1}, pivalic acid 7 eq., Synperonic F68 500 mg in 10 mL water at 100 °C for 72 h. [1] GPC in THF vs. narrow polydispersity polystyrene standards. [2] DLS analysis of the size distribution and polydispersity index (PDI) at 25 °C. Integral ratios are presented in brackets.

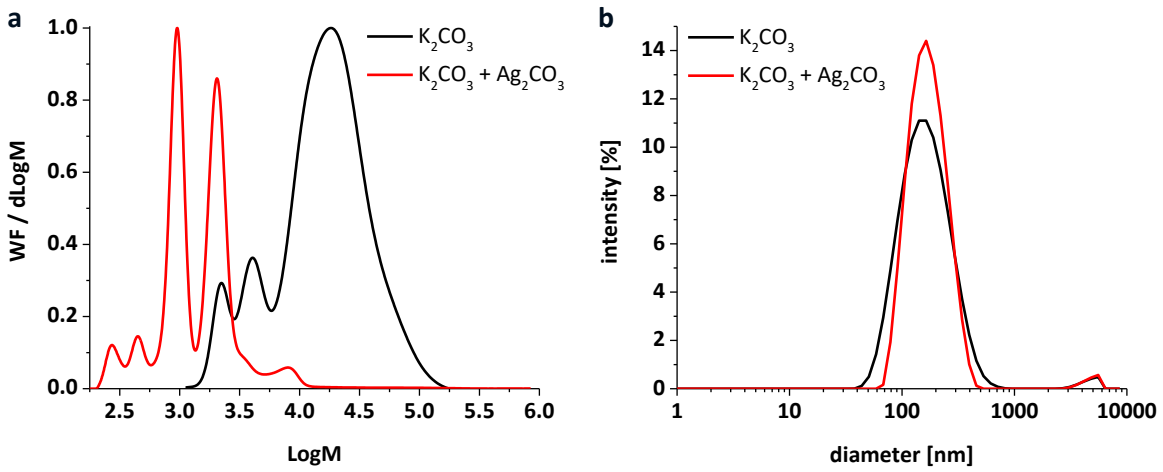

Figure 3.28: Normalised GPC traces (a) and DLS intensity distributions (b) of entries **3.46** and **3.48**.

3.4.10. Transitional Phase Inversion Emulsification

The transitional phase inversion from an o/w to a w/o emulsion was observed at reaction temperatures for entries **3.38** and **3.47**. These observations suggest a possible low-energy method (without sonication) where the temperature behaviour of the

ethoxylated surfactant can result in the formation of an emulsion.[115] The interfacial tension at PIT is low and facilitates the formation of sub-micron particles in a less energy-intensive fashion.[110] Hence, an experimental procedure was employed for entries **3.49** and **3.50** that is identical to previous entries (as listed in table 3.22) with the exception of the absence of a sonication step prior to heating to reaction temperature. Instead, phase inversion emulsification (PIE) was applied before heating at polymerisation temperature (100 °C) for entry **3.49** (figure 3.29 top). Whereas for entry **3.50**, PIE was applied after polymerisation at 110 °C for 3 days (figure 3.29 bottom). The phase inversion is observable when stirring of the sample is temporarily discontinued (figure 3.30).

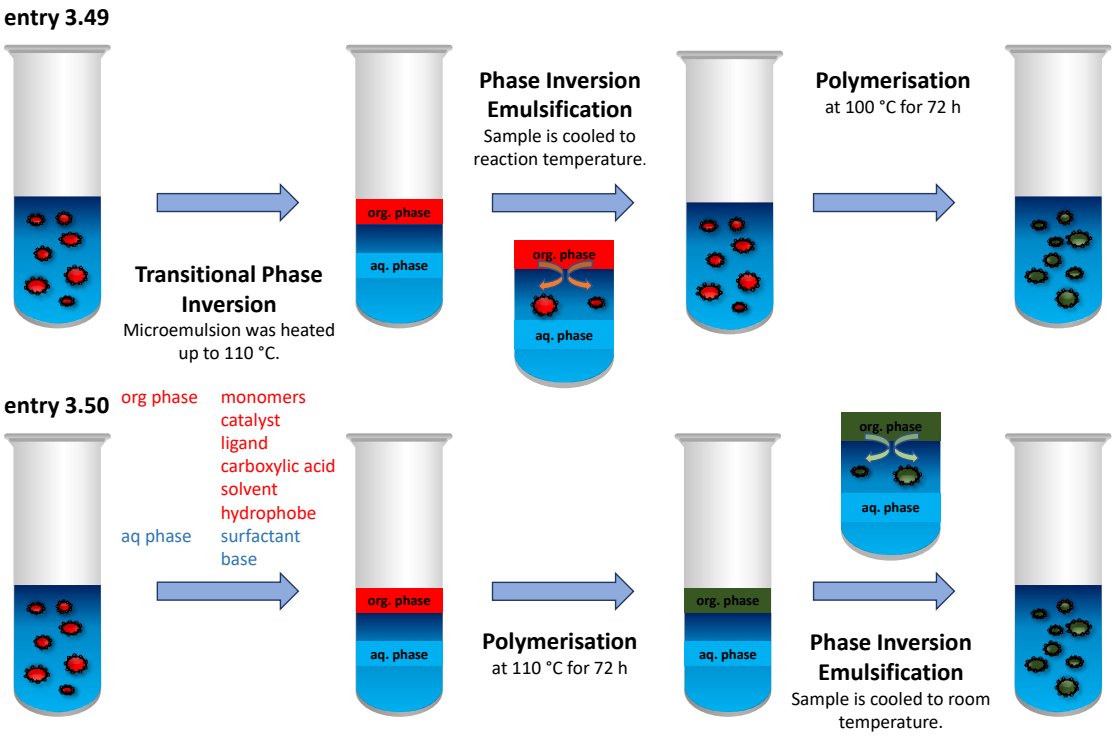

Figure 3.29: Schematic depiction of the phase inversion emulsification of entries **3.49** (top) and **3.50** (bottom).

The GPC and DLS results for entries **3.49** and **3.50** are presented in table 3.22. The molecular weight of entry **3.49** (M_n = 8.6 kg mol^{-1}) is lower than for **3.50** (M_n = 12 kg mol^{-1}) and is comparable to the sonicated reference (entry **3.46**, M_n = 9.5 kg mol^{-1}). The lower molecular weights obtained are attributed to the lower polymerisation temperature (100 °C vs 110 °C). Those results can be compared to the data presented in section 3.4.5; where the increased reaction temperature promoted the polymerisation of PDPPF4 when

Pd_2dba_3 was employed as pre-catalyst. Entry **3.50** exhibits the smallest particle size dispersity and size compared to the other entries in table 3.22. As a control sample, entry **3.51** was prepared without sonication or PIE. The molecular weight obtained for entry **3.51** is the same as entry **3.46** whereas the particle size is increased compared to all entries presented in table 3.22. The increased particle diameter indicates that either sonication or PIE are required to decrease the particle size and that PIE is a valid alternative to sonication.

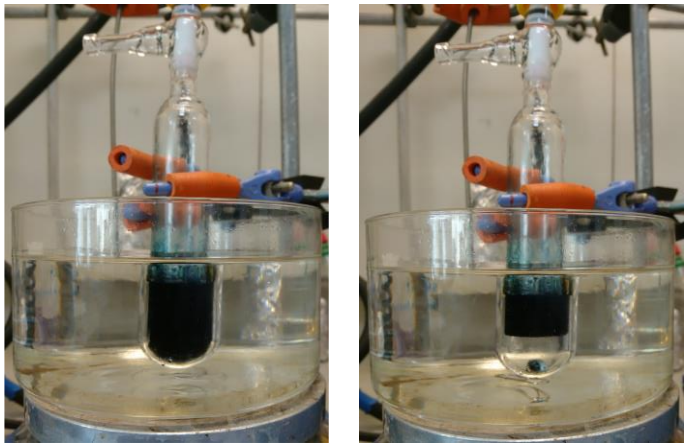

Figure 3.30: Entry **3.50** during polymerisation at 110 °C. The phase inversion to a w/o system above 100 °C is observed when stirring is discontinued giving rise to two distinctive phases.

Table 3.22: Phase inversion technique samples (entries **3.49** and **3.50**) and reference sample (entry **3.51**) compared with a sample prepared by sonication (entry **3.46**).

entry	$T_{reaction}$ [°C]	sonication	M_n[3] [kg mol^{-1}]	Đ[3]	size distribution[4] [nm]	PDI[4]
3.49[1]	100	-	8.6	2.6	291 ± 181 (98 %) 4357 ± 945 (2 %)	0.26
3.50[1,2]	110		12	3.4	270 ± 138 (98 %) (4645 ±822) (2 %)	0.22
3.51	100		9.5	2.7	342 ± 263 (99 %) 4903 ± 670 (1 %)	0.26
3.46	100	5 x 2 min	9.5	2.2	282 ± 192 (95 %) 4013 ± 1163 (5 %)	0.27

Pd_2dba_3 4 mol%, P(*o*-anisyl)$_3$ 8 mol%, p-xylene 1 mL, [monomer] 0.20 M, [hexadecane] 250 μL_{HD} mL_{xyl}^{-1}, K_2CO_3 11 eq., pivalic acid 7 eq., Synperonic F68 500 mg in 10 mL water at reaction temperature for 72 h.[1] Sample was heated to 110 °C until phase separation was observed and subsequently kept at reaction temperature. [2] Transitional phase inversion was observed at reaction temperature. [3] GPC in THF vs. narrow polydispersity polystyrene standards. [4] DLS analysis of the size distribution and polydispersity index (PDI) at 25 °C. Integral ratios are presented in brackets.

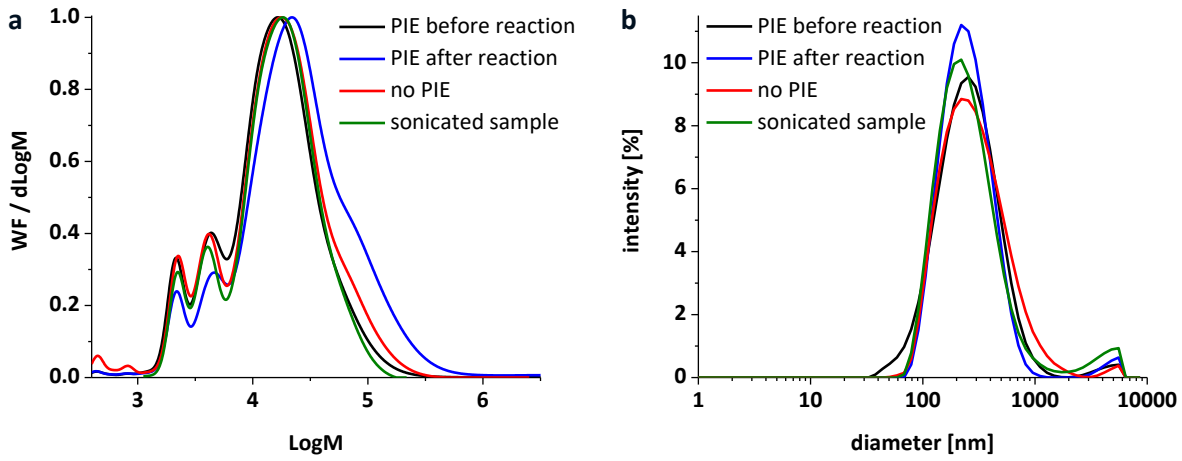

Figure 3.31: Normalised GPC traces (a) and DLS intensity distributions (b) of entry **3.46** and entries **3.49** - **3.51**.

3.5. Bulk Polymerisations Conducted in Solution

Table 3.23: Comparison with solution polymerisations.

entry	reaction	pivOH : K_2CO_3 eq.	[monomer] [M]	M_n[2] [kg mol^{-1}]	Đ[2]
3.37	in emulsion[1]	1 : 3	0.2	5.4	2.2
3.52	solution		0.2	1.7	1.9
3.53	solution		0.2	1.7	1.8
3.54	solution		0.2	1.6	1.6
3.55	solution		0.5	3.2	2.4
3.46	in emulsion[1]	7 : 11	0.2	9.5	2.2
3.56	solution		0.2	1.5	1.5

Pd_2dba_3 4 mol%, P(*o*-anisyl)$_3$ 8 mol%, p-xylene 1mL, [monomer] 0.20 M, K_2CO_3 11 eq, pivalic acid 7 eq at 100 °C for 72 h. [1] [hexadecane] 250 µL$_{HD}$ mL$_{xyl}^{-1}$, Synperonic F68 500 mg in 10 mL water. [2] GPC in THF vs. narrow polydispersity polystyrene standards.

The optimised reaction conditions were performed in solution for comparison. For 3 equivalents of potassium carbonate, the solution polymerisation was prepared in triplicate (entries **3.52** – **3.54**, table 3.23 and figure 3.32 a). The similar molecular weights obtained for those 3 entries are inferior compared to the polymerisation performed in emulsion with analogous reaction conditions (entry **3.37**). The comparison suggests that the optimised conditions in emulsion are less applicable for conventional solution

polymerisations. The Sommer group has reported that the molecular weights obtained for solution polymerisations are lower in the absence of DMAc as co-solvent and if Pd_2dba_3 was used instead of $Pd(OAc)_2$.[85] Since the monomer concentration has a substantial impact upon the polymerisation, a solution polymerisation with [monomer] = 0.5 M was prepared as well. Although the molecular weight obtained for entry **3.55** is higher than the previous entries polymerised with [monomer] = 0.2 M, the obtained M_n was still below compared to the polymerisation in emulsion (entry **3.37**). An additional solution polymerisation was conducted with increased pivOH/K_2CO_3 concentration to investigate if the solution polymerisations are subject to the salt concentration as well (figure 3.32 b). The low molecular weight obtained for entry **3.56** is the same as the other solution polymerisations in this Chapter with [monomer] = 0.2 M indicating that the salt concentration is less crucial than the other parameters mentioned above.

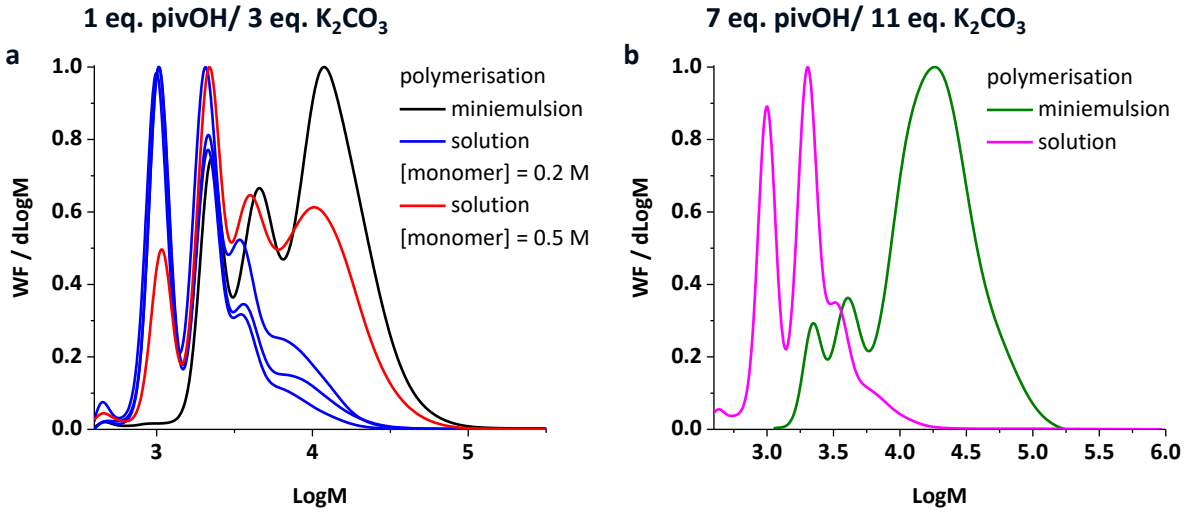

Figure 3.32: Normalised GPC traces of entries **3.37** and **3.52** - **3.55** with K_2CO_3 3 eq. (a) and entries **3.46** and **3.56** with K_2CO_3 11 eq. (b).

In conclusion, DArP in emulsion results in greater molecular weights for the optimised reaction conditions presented in this body of work. Considering the limitations of the miniemulsion polymerisations, i.e. the absence of a polar co-solvent and solubility limits, the molecular weights obtained by DArP in emulsion are still lower than the reported values in the literature for PDPPF4 polymerised in solution (e.g. M_n = 10 – 30 kg mol^{-1}).

3.6. Summary and Outlook

For the DArP of PDPPF4 conducted in an emulsion, several reaction parameters appeared to be crucial to give stable emulsions, reasonable molecular weight and consistent and moderate particle size dispersities. The presence of polar co-solvents destabilised the emulsions and did not facilitate the polymerisations due to partition into the aqueous phase. Although there is an increasing demand for the employment of greener solvents, the absence of coordinating polar solvents limited the molecular weights obtained throughout this body of work. Moreover, non-polar reaction conditions rely on P(*o*-anisyl)$_3$ to promote the polymerisations. The choice of surfactant is crucial as well. Non-ionic surfactants seem to promote DArP in emulsion while the ionic surfactant SDS inhibited any noteworthy reaction. Xylenes gave higher molecular weights than toluene as solvent, this is due to solubility limitations in toluene since elevated concentrations of monomers were employed (e.g. [monomer] = 0.2 M) compared to concentrations reported for the majority of solution polymerisations (0.1 M or less). In addition, previous reports have shown that toluene tends to endcap the polymer chains in the course of the reaction and the solvent C-H reactivity decreases with increased substitution of the aromatic solvent.[116] The hexadecane concentration appeared to be crucial to decrease particle size dispersity. A hexadecane concentration of 0.85 M or 250 $\mu L_{HD}\ mL_{xyl}^{-1}$ is the minimum required to give moderate particle size dispersities (PDI < 0.3) in a reproducible fashion. Larger PDI values were prevented by an increase of the osmotic pressure to counteract the Laplace pressure to inhibit Ostwald ripening. Amongst the alkali metal carbonate salts, potassium carbonate gave superior molecular weights compared to sodium and caesium carbonate. The pivalic acid and carbonate salt concentrations allow control over the molecular weight whereas higher concentrations give greater molecular weights. Scheme 3.5 presents the final optimised reaction conditions for DArP of PDPPF4 in emulsion. Elevated salt concentrations and reaction temperatures also revealed the limits of the miniemulsion system. Phase separations were observed for entries with 110 °C reaction temperature at lower salt concentrations or at 100 °C with increased salt concentrations. The phase separations observed are indicative of an emulsion phase inversion rendering the emulsions subject to particle destabilisation upon cooling depending on batch size. The irreversible aggregation was only observed for smaller aliquots of 1 mL while miniemulsion

polymerisations at 10 mL scale gave stable emulsions at room temperature. Transitional phase inversion emulsification has been demonstrated as an alternative to scale-up approaches by continuous miniemulsion polymerisations.[117] The palladium pre-catalyst screening revealed that more pre-catalyst facilitates the polymerisation. However, economic considerations and industry specifications require a minimum of palladium contamination rendering the amounts of pre-catalyst employed in this body of work improvable. Hence, further investigation with more active pre-catalysts are considered the next optimisation step. NHC based catalysts have been reported for minimising the content of palladium and reducing reaction temperature for Suzuki-Miyaura miniemulsion polymerisations.[1]

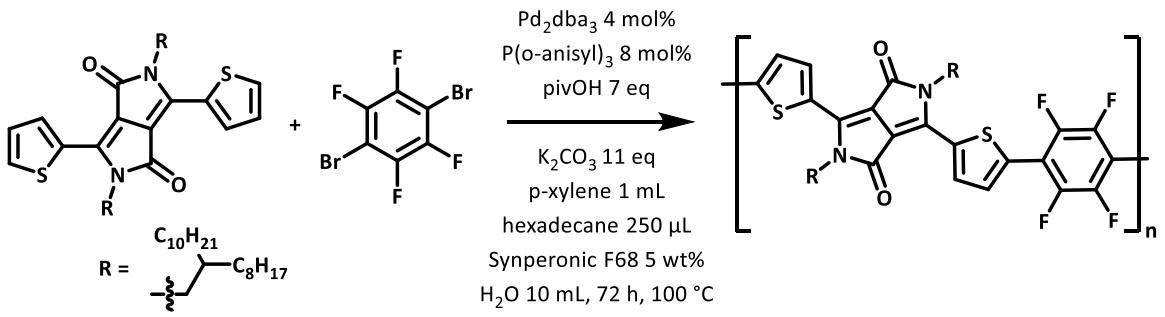

Scheme 3.5: Optimised reaction conditions for DArP of PDPPF4 in emulsion.

As a potential outlook, novel atom efficient C-C cross-couplings methods to react C(sp^2)-H bonds for the synthesis of conjugated polymers were reported in recent years. Those include different co-catalysts[113,118], chain transfer polymerisation (CTP)[119] or oxi-DArP[120]. Those novel methods can be deemed applicable for reactions in heterogeneous phases with the results presented in this body of work regarding the stabilisation of polymer nanoparticle formation and polymerisation optimisation for *in-situ* emulsion polymerisations of C(sp^2)-H bonds.

4. An Investigation of the Influence of Co-Monomer Structure on the Miniemulsion Polymerisations by Direct Arylation Polycondensation

The CMD step in the DArP catalytic cycle requires a low activation barrier for the deprotonation of the C-H bearing monomer (discussed in detail in section 1.3). Hence, electron deficient monomers are expected to perform better in DArP reactions conducted with the optimised conditions developed in Chapter 3. Difluorinated benzothiadiazole (**4.1**, scheme 4.1) was chosen as monomer due to the electron withdrawing nature of its fluorine substituents. The comonomer's electron deficiency are confirmed by the depressed HOMO/LUMO levels reported for PDPPF2BT (-5.48/-4.22 eV) compared to the non-fluorinated analogue PDPPBT (-5.10 /-3.90 eV).[121] An additional benefit is that the solubility of the benzothiadiazole derivatives in p-xylene increases with increasing fluorine content. While only 0.10 M non-fluorinated dibromobenzothiadiazole could be dissolved in p-xylene, mono and difluorinated benzothiadiazoles are readily soluble in the concentration regime required for this reaction protocol (i.e. 0.2 M). The molecular weights of the polymers presented in this Chapter were determined by high temperature GPC (HT-GPC) in trichlorobenzene (TCB) due to the low solubility of the products in the organic solvents (e.g. THF, $CHCl_3$) used for GPC at low temperatures (e.g. 30 - 40 °C). Solution polymerisations were performed for comparison with the corresponding miniemulsion polymerisations. The reagents used for the solution polymerisations were employed at the same concentrations as in case of their miniemulsion analogues except for compounds required to emulsify the reaction mixtures. These are water, the surfactant (Synperonic F68) and the hydrophobe (hexadecane), respectively.

4.1. Diketopyrrolopyrrole (DPP) containing Polymers

4.1.1. with dibromodifluorobenzothiadiazole (PDPPF2BT)

The molecular weights obtained for PDPPF2BT prepared by a miniemulsion polymerisation (entry **4.2**) and in a bulk solution (entry **4.3**) are presented in table 4.1. For comparison, the values obtained for PDPPF4 by miniemulsion polymerisation is also given in table 4.1. The molecular weight distributions presented in figure 4.1 show a decrease in molecular weight for PDPPF4 when compared to PDPPF2BT. The particle size dispersity for entry **4.2** is below 0.3 indicating that the hydrophobe concentration employed is sufficient to stabilise the CPNs regardless of the nature of the polymer backbone. PDPPF2BT prepared in solution (entry **4.3**) also yields increased molecular weights compared to solution prepared PDPPF4 as presented in section 3.5.

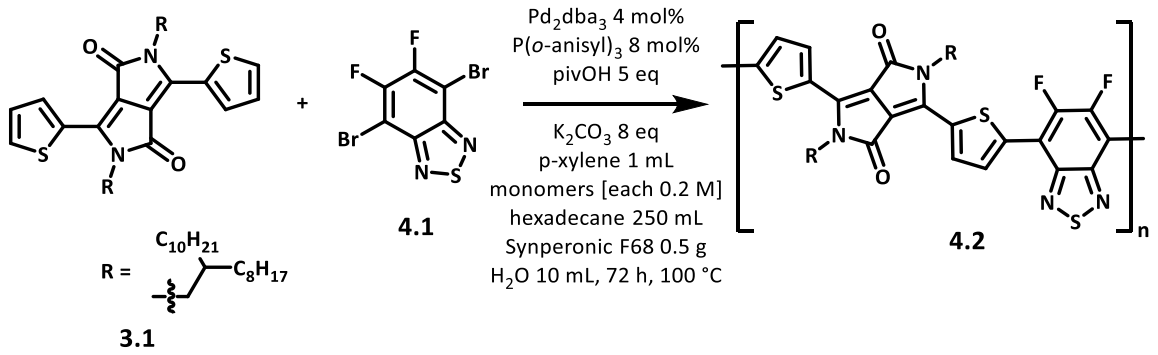

Scheme 4.1: DArP in emulsion of **3.1** and **4.1** to obtain PDPPF2BT **4.2**.

Solution polymerisations of PDPPF2BT were previously reported by Lee *et al*. and polymerisations using a Stille cross coupling protocol (M_n = 25 kg mol^{-1}, Đ = 3.4) were superior to those conducted with a Suzuki-Miyaura polycondensation protocol (M_n = 6.6 kg mol^{-1}, Đ = 1.7) within the same publication.[121] The reported GPC data in this publication were measured in THF at room temperature and hence are not directly comparable with the data presented for entry **4.2** (measured in TCB at 120 °C due to limited solubility in THF). Nonetheless, the DArP protocol presented here is the first report of DArP of PDPPF2BT affording increased molecular weights for PDPPF2BT when compared to a Suzuki-Miyaura polycondensation protocol.

Table 4.1: DArP of PDPPF2BT (entries **4.2** and **4.3**).

entry	polymer	reaction	M_n[2] [kg mol^{-1}]	Đ[2]	size distribution[3] [nm]	PDI[3]
4.2[1]	PDPPF2BT	emulsion	11	2.2	192 ± 96 (100 %)	0.23
3.46	PDPPF4	emulsion	7.2	1.7	282 ± 192 (95 %) 4013 ± 1163 (5 %)	0.27
4.3	PDPPF2BT	solution	4.9	1.6	-	-

Pd_2dba_3 4 mol%, P(*o*-anisyl)$_3$ 8 mol%, p-xylene 1mL, [monomer] 0.20 M, K_2CO_3 8 eq., pivalic acid 5 eq. at 100 °C for 72 h. [1] [hexadecane] 250 μL_{HD} mL_{xyl}^{-1}, Synperonic F68 500 mg in 10 mL water. [2] GPC in TCB at 120 °C vs. narrow polydispersity polystyrene standards. [3] DLS analysis of the intensity size distribution and polydispersity index (PDI) at 25 °C. Integral ratios are presented in brackets.

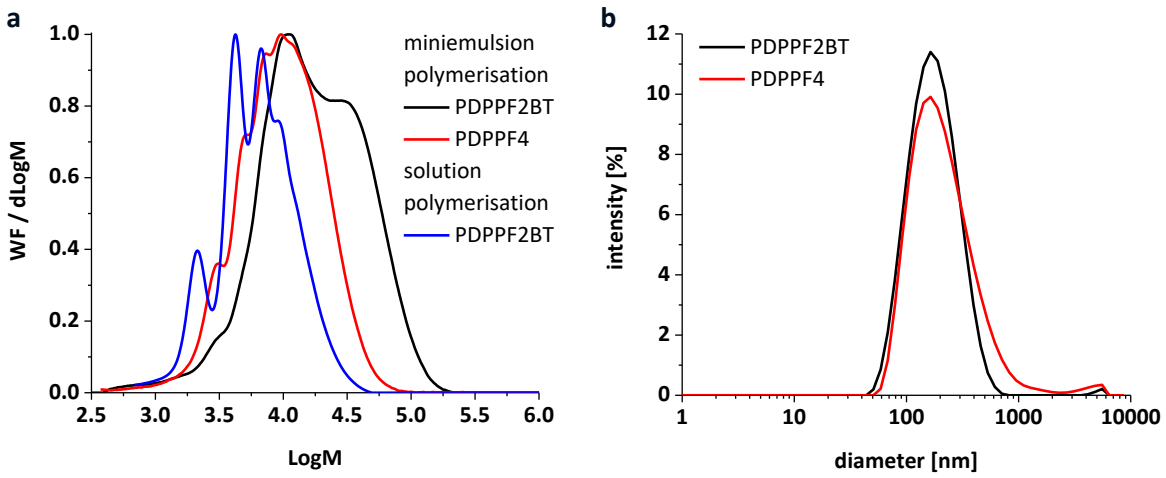

Figure 4.1: Normalised GPC traces of entries **3.46**, **4.2** and **4.3** (a) and DLS intensity distributions of entries **3.46** and **4.2** (b).

4.1.2. with dibromothienothiophene (PDPPTT)

PDPPTT is commonly synthesised by Stille cross coupling polymerisations using organostannane containing monomers and PDPPTT polymers were reported by the Sonar group in 2010 (M_n = 90 kg mol^{-1}, Đ = 2.4, THF GPC) and the Ong group (M_n = 29 – 110 kg mol^{-1}, TCB GPC at 160 °C) in 2012.[122,123] Simultaneously to the Stille method, a Suzuki-Miyaura cross coupling method was reported.[124] Additionally, a phenyl flanked DPP copolymerised with thienothiophene by DArP was reported by Kumada *et al* (scheme 4.2

a). This polymer was isolated with a molecular weight of M_n = 17 kg mol^{-1} and a relatively high polydispersity (Đ = 6.7, $CHCl_3$ GPC). Regioregularity was controlled by blocking the β-position on the thienothiophene monomer with an alkyl group. Moreover, the reaction was carried out solely in DMAc at an elevated monomer concentration of 0.18 M.

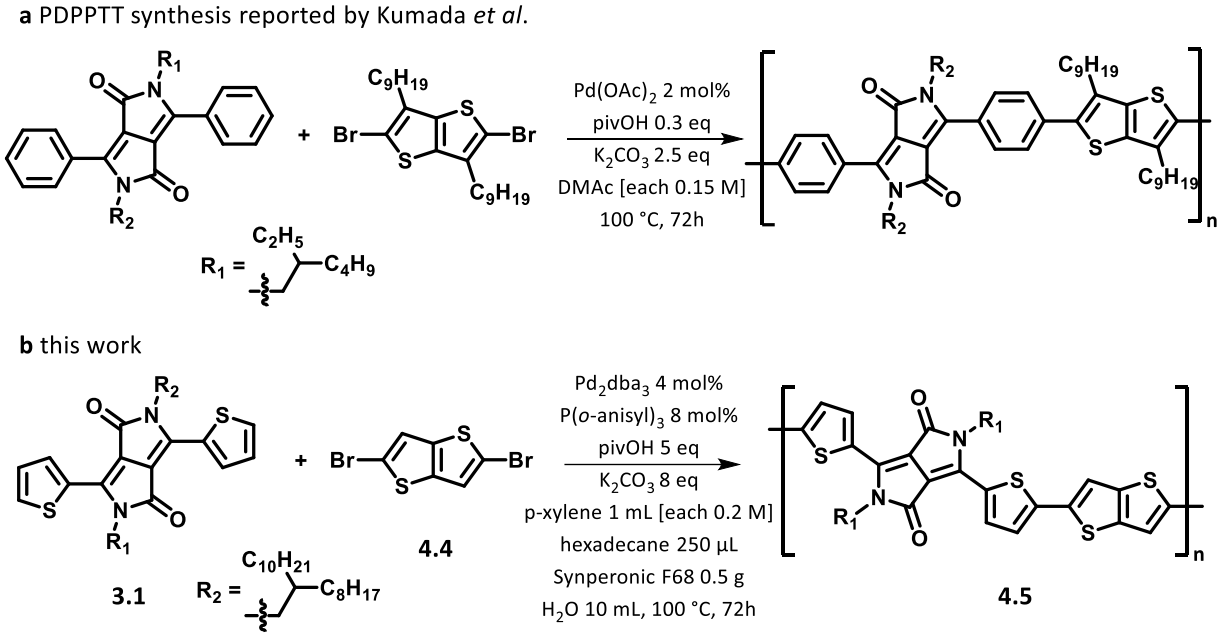

Scheme 4.2: Bulk solution DArP of PDPPTT reported by Kumada *et al*. (a) and DArP in emulsion of **3.1** and **4.4** to obtain PDPPTT **4.5** (b).

Table 4.2: DArP of PDPPTT (entries **4.5** and **4.6**).

entry	reaction	M_n[2] [kg mol^{-1}]	Đ[2]	size distribution[3] [nm]	PDI[3]
4.5[1]	emulsion	11	3.2	351 ± 297 (97 %) 4520 ± 897 (3 %)	0.15
4.6	solution	5.1	1.7	-	-

Pd_2dba_3 4 mol%, P(*o*-anisyl)$_3$ 8 mol%, p-xylene 1mL, [monomer] 0.20 M, K_2CO_3 11 eq., pivalic acid 7 eq. at 100 °C for 72 h. [1] [hexadecane] 250 µL$_{HD}$ mL$_{xyl}^{-1}$, Synperonic F68 500 mg in 10 mL water. [2] GPC in TCB at 120 °C vs. narrow polydispersity polystyrene standards. [3] DLS analysis of the size distribution and polydispersity index (PDI) at 25 °C. Integral ratios are presented in brackets.

The miniemulsion polymerisation protocol presented in this body of work is the only report of PDPPTT **4.5** polymerised by DArP (scheme 4.2 b). Table 4.2 shows that dibromothienothiophene **4.4** polymerises efficiently with DPP despite being a more

electron rich monomer compared to the previously presented moieties (i.e. dibromotetrafluorobenzene **3.2** and dibromobenzothiadiazole **4.1**).

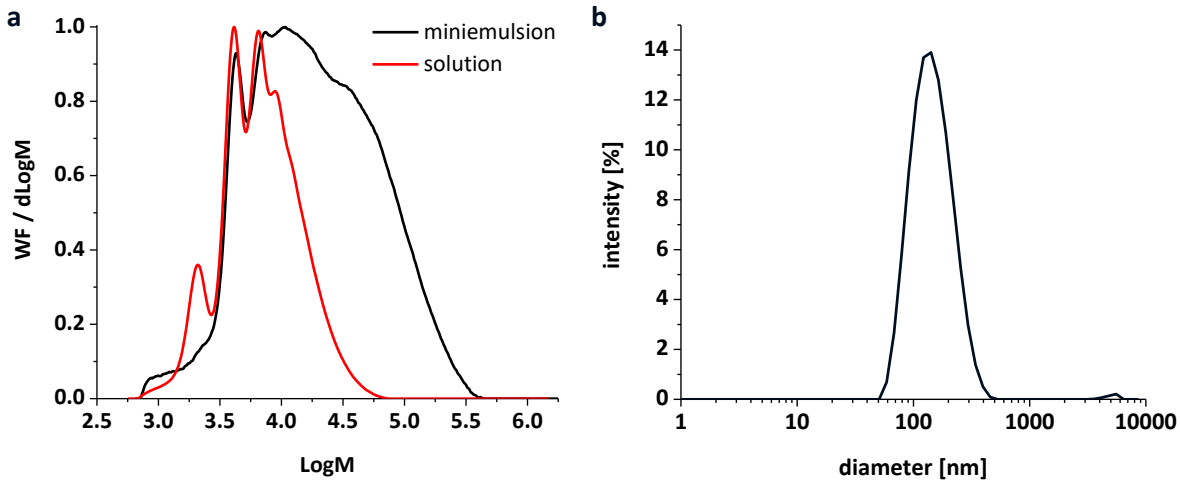

Figure 4.2: Normalised GPC traces of entries **4.5** and **4.6** (a) and DLS intensity distribution of entry **4.5** (b).

4.1.3. with thienopyrrolodione (PDPPTPD)

Table 4.3: DArP of PDPPTPD (entries **4.8** and **4.9**).

entry	reaction	M_n[2] [kg mol^{-1}]	Đ[2]	size distribution[3] [nm]	PDI[3]
4.8[1]	emulsion	4.1	1.4	160 ± 96 (98 %) 4766 ± 758 (2 %)	0.17
4.9	solution	4.1	1.8	-	-

Pd_2dba_3 4 mol%, P(*o*-anisyl)$_3$ 8 mol%, p-xylene 1mL, [monomer] 0.20 M, K_2CO_3 8 eq., pivalic acid 5 eq. at 100 °C for 72 h. [1] [hexadecane] 250 μL_{HD} mL_{xyl}^{-1}, Synperonic F68 500 mg in 10 mL water. [2] GPC in TCB at 120 °C vs. narrow polydispersity polystyrene standards. [3] DLS analysis of the size distribution and polydispersity index (PDI) at 25 °C. Integral ratios are presented in brackets.

The miniemulsion and solution polymerisations of PDPPTPD (entries **4.8** and **4.9**) resulted in low molecular weights (M_n = 4 kg mol^{-1}, table 4.3). These findings are in accordance with a previous report from Pouliot *et al*. when the same substrate pattern is employed (M_n = 3 kg mol^{-1}, Đ = 1.3, TCB GPC at 110, °C, H-DPP-H and Br-TPD-Br ,reagents listed in scheme 4.3 b).[125] Within the same publication, interchanging these functionalities (i.e Br-DPP-Br and H-TPD-H) gave better results (M_n = 21 kg mol^{-1}, Đ = 1.7). Using this set of

monomer functionalities, Wakioka *et al*. reported as well enhanced molecular weights for PDPPTPD (M_n = 25 kg mol^{-1}, Đ = 2.8). The reagents employed were similar to this work (i.e. Pd_2dba_3, P(*o*-anisyl)$_3$, pivOH, Cs_2CO_3, toluene, [monomer] = 0.25 M, 100 °C, 6 h).[102]

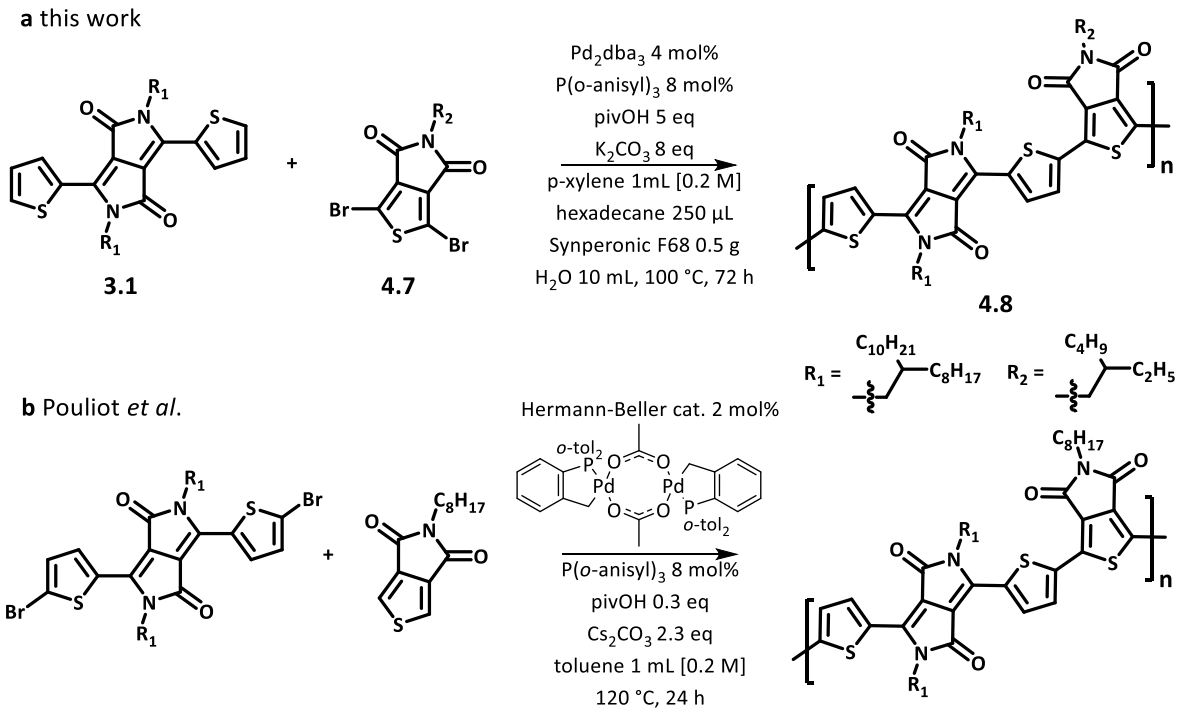

Scheme 4.3: DArP in emulsion of **3.1** and **4.7** to obtain PDPPF2BT **4.8** (a) and bulk solution DArP of PDPPTPD reported by Pouliot *et al*. (b).

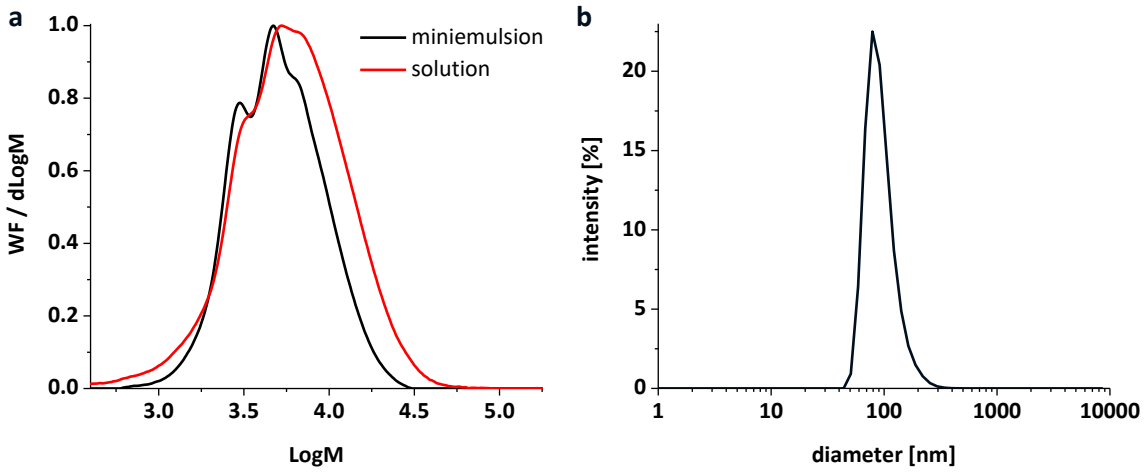

Figure 4.3: Normalised GPC traces of entries **4.8** and **4.9** (a) and DLS intensity distribution of entry **4.8** (b).

4.2. Naphthalene Diimide (NDI) containing Polymers PNDIF4 and PNDIF2BT

A DArP protocol to prepare PNDIF4 was reported by Lucio *et al*. resulting in a polymer with an M_n = 7.2 kg mol^{-1} and Đ = 1.5 (TCB GPC at 150 °C).[126] This DArP protocol employed $Pd(OAc)_2$ and the polar co-solvent DMAc and the monomer solution was heated in a microwave reactor at 100 °C for 2 h. The miniemulsion protocol presented in scheme 4.4 gave a comparable if slightly lower molecular weight (entry **4.11**, table 4.4) and it should be noted that the NDI monomer used in this thesis contained shorter side chains (2-ethylhexyl compared to 2-octyldodecylside chains).

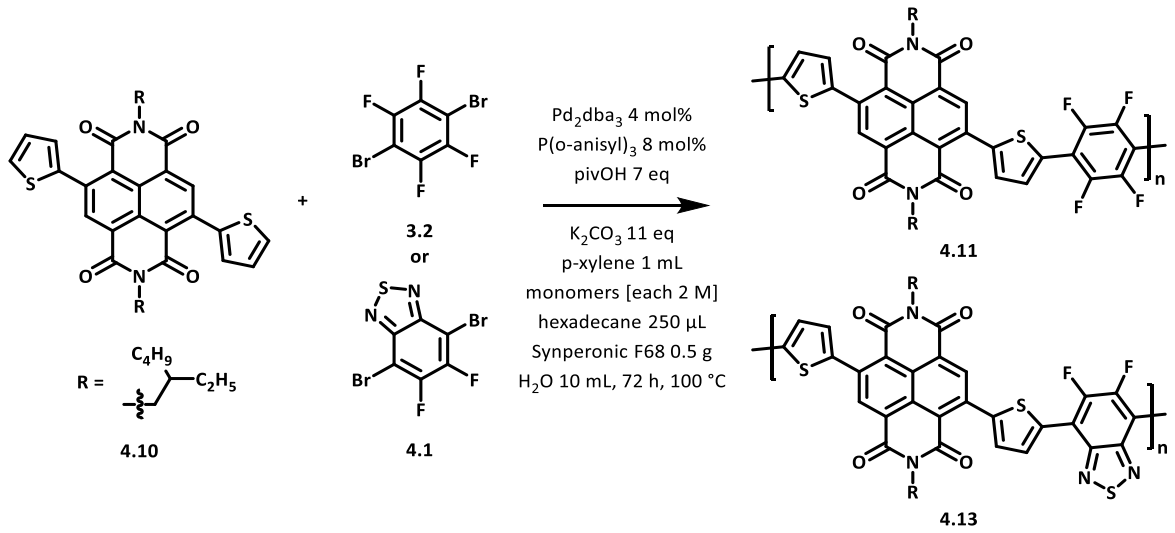

Scheme 4.4: DArP in emulsion of **4.10** with **3.2** and **4.1** to obtain PNDIF4 **4.11** and PNDIF2BT **4.13**.

The PNDIF2BT polymer (entry **4.13**) prepared by DArP showed an increase in molecular weight when compared to PNDIF4 (entry **4.11**). As observed for the equivalent DPP series, the NDI monomer **4.10** polymerises more efficiently with dibromodifluorobenzothiadiazole (**4.1**) than with dibromotetrafluorobenzene (**3.2**). The equivalent solution polymerisations yielded lower molecular weights for the NDI copolymers. The only reported synthesis of PNDIF2BT used a Stille cross coupling method in solution with stannylated thiophene flanked benzothiadiazole moeities.[127] This conventional C-C coupling method gave greater molecular weights (e.g. M_n = 44 kg mol^{-1}, Đ = 2.8, TCB GPC at 150 °C) than the DArP method presented here.

Table 4.4: DArP of PNDIF4 (entries **4.11** and **4.12**) and PNDIF2BT (entries **4.13** and **4.14**).

entry	polymer	reaction	M_n[2] [kg mol^{-1}]	Đ[2]	size distribution[3] [nm]	PDI[3]
4.11[1]	PNDIF4	emulsion	5.6	2.3	208 ± 95 (99 %) 4978 ± 619 (1 %)	0.18
4.12	PNDIF4	solution	1.3	1.5	-	-
4.13[1]	PNDIF2BT	emulsion	8.8	2.1	184 ± 97 (100 %)	0.20
4.14	PNDIF2BT	solution	1.8	2.2	-	-

Pd_2dba_3 4 mol%, P(*o*-anisyl)$_3$ 8 mol%, p-xylene 1mL, [monomer] 0.20 M, K_2CO_3 8 eq., pivalic acid 5 eq. at 100 °C for 72 h. [1] [hexadecane] 250 μL_{HD} mL_{xyl}^{-1}, Synperonic F68 500 mg in 10 mL water.[2] GPC in TCB at 120 °C vs. narrow polydispersity polystyrene standards. [3] DLS analysis of the intensity distribution and polydispersity index (PDI) at 25 °C. Integral ratios are presented in brackets.

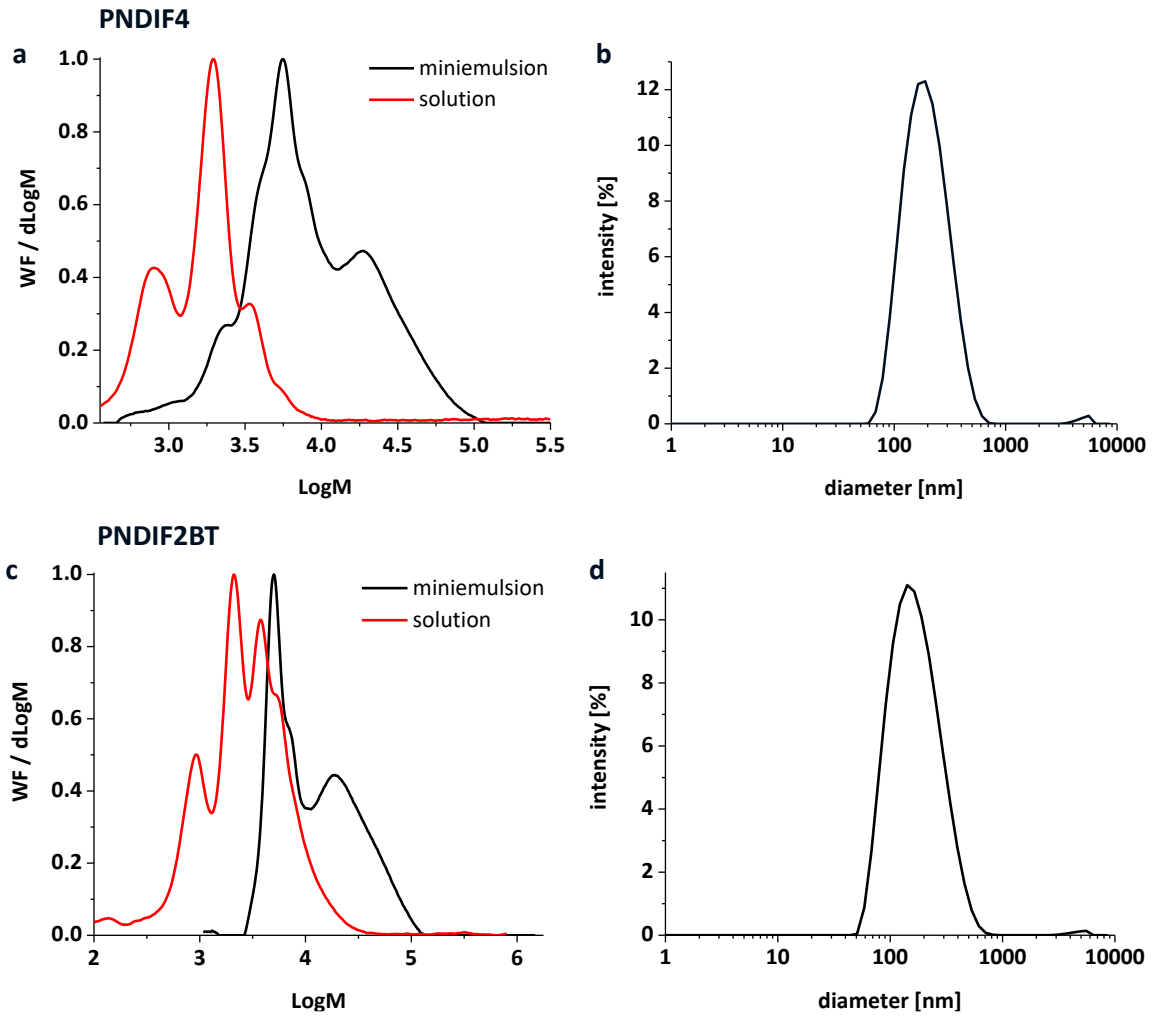

Figure 4.4: Normalised GPC traces of PNDIF4 (entries **4.11** and **4.12**, a) and DLS intensity distributions of entry **4.11** (b). Normalised GPC traces of PNDIF2BT (entries **4.13** and **4.14**, c) and DLS intensity distributions of entry **4.13** (d).

4.3. Thienopyrrolodione (TPD) containing Polymers PTPDF4 and PTPDF2BT

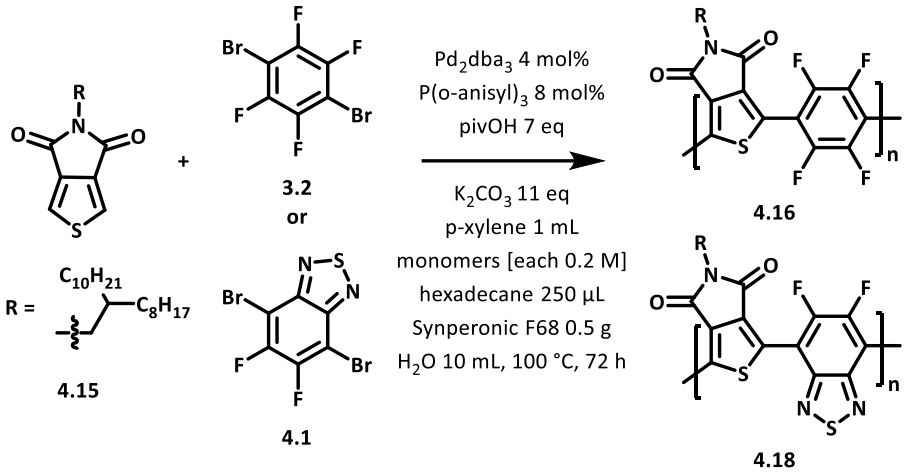

Scheme 4.5: DArP in emulsion of **4.15** with and **3.2** and **4.1** to obtain PTPDF4 **4.16** and PTPDF2BT **4.18**.

Table 4.5: DArP of PTPDF4 (entries **4.16** and **4.17**) and PTPD2BT (entries **4.18** and **4.19**).

entry	polymer	reaction	M_n[2] [kg mol^{-1}]	Đ[2]	size distribution[3] [nm]	PDI[3]
4.16[1]	PTPDF4	emulsion	9.1	1.9	281 ± 156 (99 %) 4796 ± 729 (1 %)	0.23
4.17	PTPDF4	solution	4.3	1.6	-	-
4.18[1]	PTPDF2BT	emulsion	20	1.8	222 ± 95 (73 %) 1881 ± 970 (27 %)	0.38
4.19	PTPDF2BT	solution	11	1.7	-	-

Pd_2dba_3 4 mol%, P(*o*-anisyl)$_3$ 8 mol%, p-xylene 1mL, [monomer] 0.20 M, K_2CO_3 8 eq., pivalic acid 5 eq. at 100 °C for 72 h. [1] [hexadecane] 250 μL_{HD} mL_{xyl}^{-1}, Synperonic F68 500 mg in 10 mL water. [2] GPC in TCB at 120 °C vs. narrow polydispersity polystyrene standards. [3] DLS analysis of the intensity distribution and polydispersity index (PDI) at 25 °C. Integral ratios are presented in brackets.

The thienopyrrolodione monomer **4.15** was reacted with the monomers dibromotetrafluorobenzene (entries **4.16** and **4.17**) and dibromodifluorobenzothiadiazole (entries **4.18** and **4.19**). The molecular weights of the polymers obtained are presented in table 4.5 and this data showed that miniemulsion polymerisations yielded higher molecular weights than the reactions conducted in solution. In accordance with the findings of the previous sections (DPP and NDI based copolymers), dibromodifluorobenzothiadiazole **4.2**

polymerises better than 1,4-dibromotetrafluorobenzene **3.1**. The bimodal distribution for entry **4.18** (M_n = 20 kg mol^{-1}) suggests that stabilisation of particles of especially conjugated polymers of increased molecular weight is challenging for the kind of surfactant (i.e Synperonic F68) and amount of hydrophobe ([hexadecane] 250 μL_{HD} mL_{xyl}^{-1}) employed.

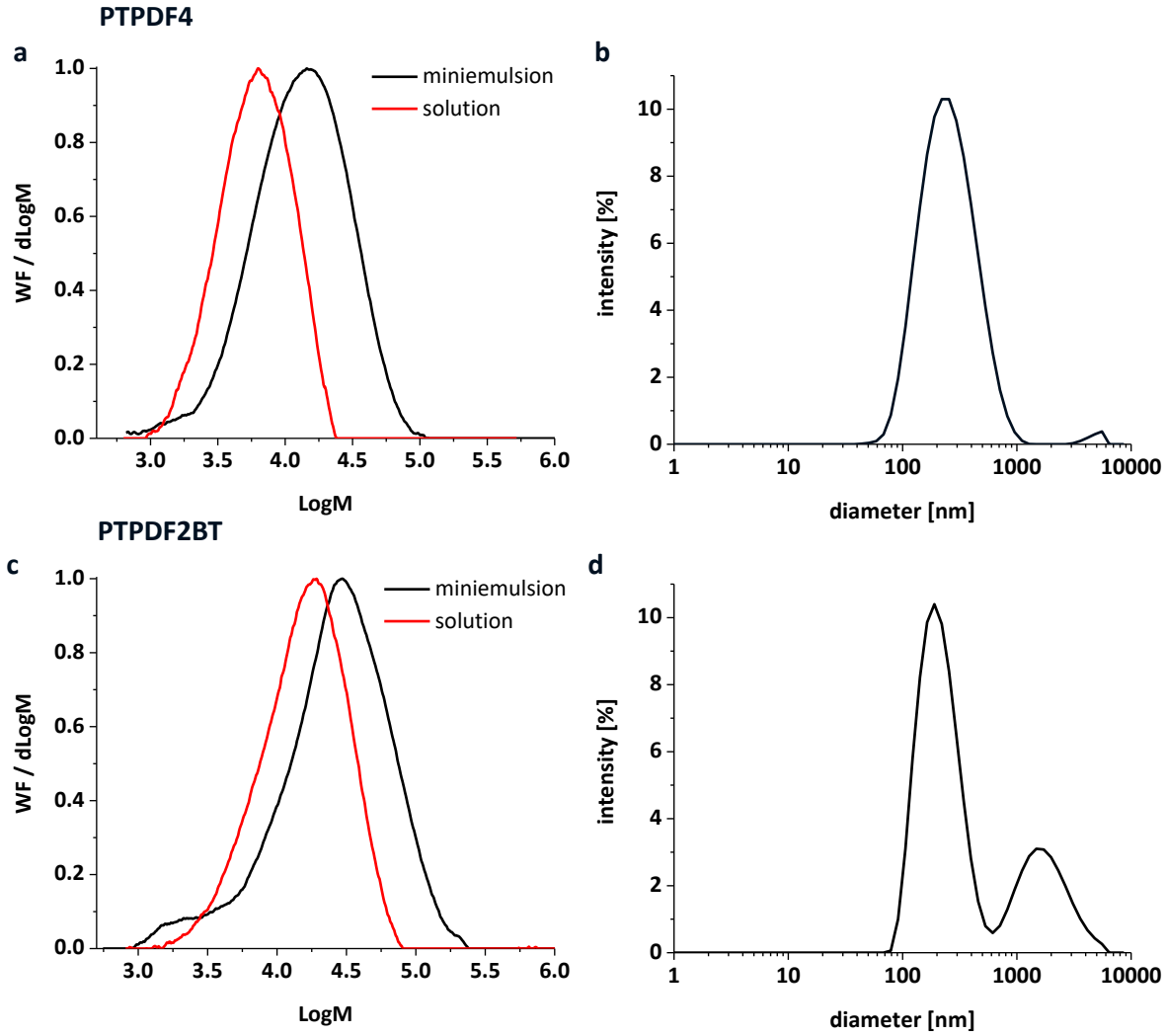

Figure 4.5: Normalised GPC traces of PTPDF4 (entries **4.16** and **4.17**, a) and DLS intensity distributions of entry **4.16** (b). Normalised GPC traces of PTPDF2BT (entries **4.18** and **4.19**, c) and DLS intensity distributions of entry **4.18** (d).

4.4. Benzodithiophene (BDT) containing Polymers PBDTF4 and PBDTF2BT

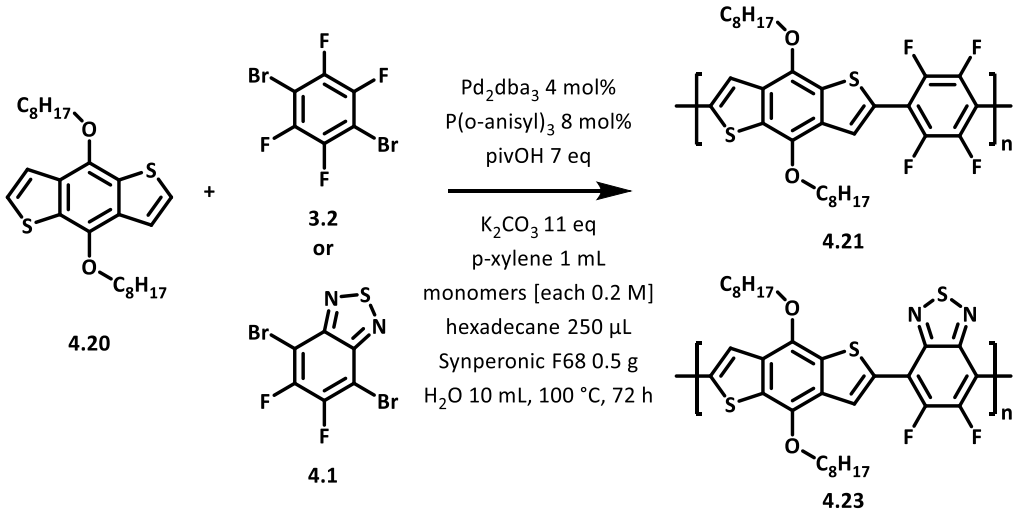

Scheme 4.6: DArP in emulsion of **4.20** with **3.2** and **4.1** to obtain polymers PBDTF4 **4.21** and PBDTF2BT **4.23**.

Table 4.6: DArP of PBDTF4 (entries **4.21** and **4.22**) and PBDT2BT (entries **4.23** and **4.24**).

entry	polymer	reaction	M_n[2] [kg mol^{-1}]	Đ[2]	size distribution[3] [nm]	PDI[3]
4.21[1]	PBDTF4	emulsion	1.7	1.2	180 ± 61 (100 %)	0.11
4.22	PBDTF4	solution	-	-	-	-
4.23[1]	PBDTF2BT	emulsion	1.7	1.4	260 ± 88 (100 %)	0.17
4.24	PBDTF2BT	solution	-	-	-	-

Pd_2dba_3 4 mol%, P(*o*-anisyl)$_3$ 8 mol%, p-xylene 1mL, [monomer] 0.20 M, K_2CO_3 8 eq., pivalic acid 5 eq. at 100 °C for 72 h. [1] [hexadecane] 250 µL$_{HD}$ mL$_{xyl}^{-1}$, Synperonic F68 500 mg in 10 mL water. [2] GPC in TCB at 120 °C vs. narrow polydispersity polystyrene standards. [4] DLS analysis of the size distribution and polydispersity index (PDI) at 25 °C. Integral ratios are presented in brackets.

Benzodithiophene **4.20** was chosen as an electron rich monomer to investigate the scope of the miniemulsion protocol presented in this thesis. Table 4.6 shows that BDT gives inferior molecular weights when polymerisation is conducted in miniemulsion compared to reactions using the monomers DPP, NDI and TPD. For comparison, Nitti *et al*. attempted the polymerisation of BDT and tetrafluorobenzene derivatives *via* both polar and apolar DarP protocol in solution.[128] They found that both methods afford low molecular weight polymers ($M_n \leq 1.6$ kg mol^{-1}, TCB GPC at 90 °C). In comparison, a Stille cross-coupling protocol gave polymers with molecular weights of up to $M_n = 27$ kg mol^{-1} using Pd_2dba_3 as

the catalyst precursor.[129] In case of PBDTF2BT, only polymerisations of thiophene flanked benzothiadiazole derivatives *via* a Stille cross-coupling polymerisation method have been reported.[130,131]

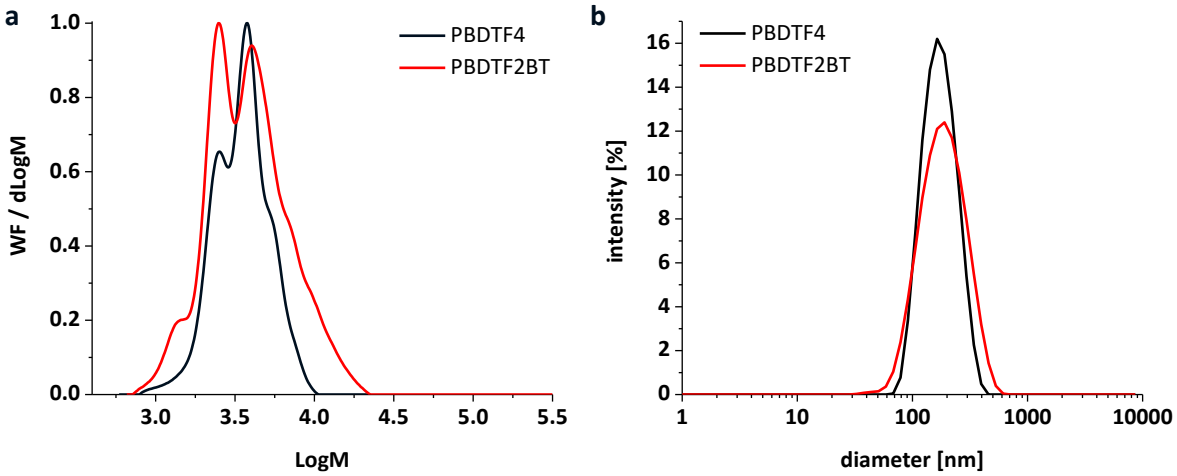

Figure 4.6: Normalised GPC trace (a) and DLS intensity distribution (b) of entries **4.21** and **4.23**.

4.5. Conclusion

Table 4.7: Comparison of degree of polymerisation of the monomers within Chapter 4.

H-M1-H	Br-M2-Br	$\overline{DP}$
DPP	F4	7.2
NDI		7.0
TPD		16
BDT		5.4
DPP	F2BT	11
NDI		8.8
TPD		33
BDT		5.2

In this Chapter the polymerisations of a series of C-H active monomers including DPP, NDI, TPD and BDT with dibromotetrafluorobenzene **3.2** and dibromodifluorobenzo-thiadiazole **4.1** was investigated and the results are summarised in table 4.7. The degree of polymerisation ($\overline{DP}$) was calculated by dividing the M_n (measured by GPC) by the molar mass of the corresponding repeating unit. The trends for the polymerisations involving

both **3.2** and **4.1** are in agreement showing that the TPD containing polymers yield the greatest degree of polymerisation followed by DPP and NDI. Polymers made using a BDT monomer gave only low degree of polymerisations. It appears that the dibromodifluorobenzothiadiazole monomer **4.1** showed an increased reactivity compared to dibromotetrafluorobenzene **3.2**.

5. Characterisation of the Conjugated Polymers and Conjugated Polymer Nanoparticles Prepared by Direct Arylation Polycondensation

5.1. Defect Analyses of the Polymers by MALDI-TOF-MS and HT-NMR

DArP is known to introduce defects into the polymer backbone that are less prevalent in polymers prepared by more conventional C-C coupling methods (e.g Suzuki-Miyaura and Stille cross couplings).[4] The defects alter the HOMO and LUMO levels and hence the bandgap of the organic semiconductor and its properties. Moreover, previous studies demonstrated that thiophene bearing conjugated monomers polymerised by DArP are prone to homo couplings rather than β-proton C-C couplings (figure 1.15).[85,122,132] Therefore, the produced copolymers were analysed for potential backbone defects. The most important analytical methods to identify and quantify backbone defects are NMR spectroscopy and mass spectrometry (MALDI-TOF). MALDI-TOF-MS is a facile method to evaluate the presence of homo coupling defects due to the different masses arising from different polymer backbone compositions. Whereas NMR spectroscopy enables quantification of different species within both the polymer backbone and end groups by ^{1}H NMR resonance integration. NMR end group analysis allows for absolute determination of the number average molecular weights of the polymers obtained. If end group proton signals can be unequivocally assigned, the ratio of chain terminal groups with either comonomer A or B can be calculated and determined. Additionally, homo couplings can be quantified by comparing homo coupling proton integral intensities with their backbone proton counterparts. The NMR measurements presented in this Chapter were performed at elevated temperatures (120 °C) in d2-tetrachloroethane to increase solubility and to overcome the rotational barrier of the rigid conjugated polymer backbone.[133] The proton assignments start with protons adjacent to the thiophene containing monomer moiety and continue towards the polymer end groups. Common distinguishable proton spin systems are listed in figure 5.1

Table 5.1: Proton assignments of the distinguishable backbone and terminal spin systems.

--Th-**M1**-Th--

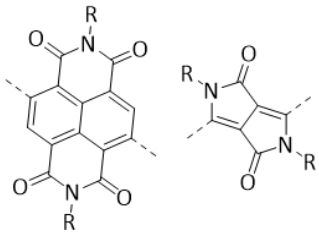

--**M2**--

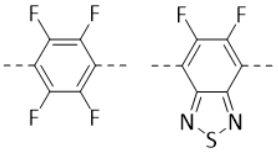

spin system	structure	spin system	structure
polymer backbone	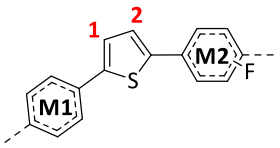	terminal --Th-**M1**-**Th**-H	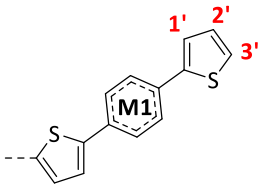
terminal --**Th**-**M2**-X	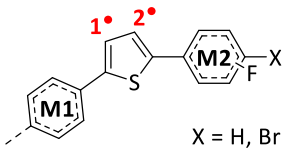 X = H, Br	internal --**Th**-**M1**-Th-H	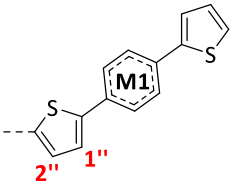

5.1.1. Poly(diketopyrrolopyrrole-*alt*-tetrafluorobenzene) - PDPPF4

NMR spectroscopy of PDPPF4 was performed by gradually increasing the measurement temperature from 25 °C to 120 °C (figure 5.1). Proton signals, in particular of the aromatic region were observed to narrow at elevated temperatures, which facilitated peak interpretation and integration. The proton signals were assigned according to a former report on polymers prepared in organic solvents.[85] The signal assignment was confirmed by COSY revealing correlations for the polymer backbone spin system and the 3 terminal spin systems •, ‘ and ‘’ (figure 5.2). Noteworthy is the absence of bromine end groups in case of the miniemulsion polymerised sample. The unintended substitution of a halogen by a hydrogen (i.e. hydrodehalogenation) as side reaction in palladium mediated C-C couplings has been addressed in the literature.[134,135,136] The moderate molecular weight of entry **3.46** (M_n = 9.5 kg mol^{-1}, THF GPC) suggests that debromination occurs at a slower rate than DArP.

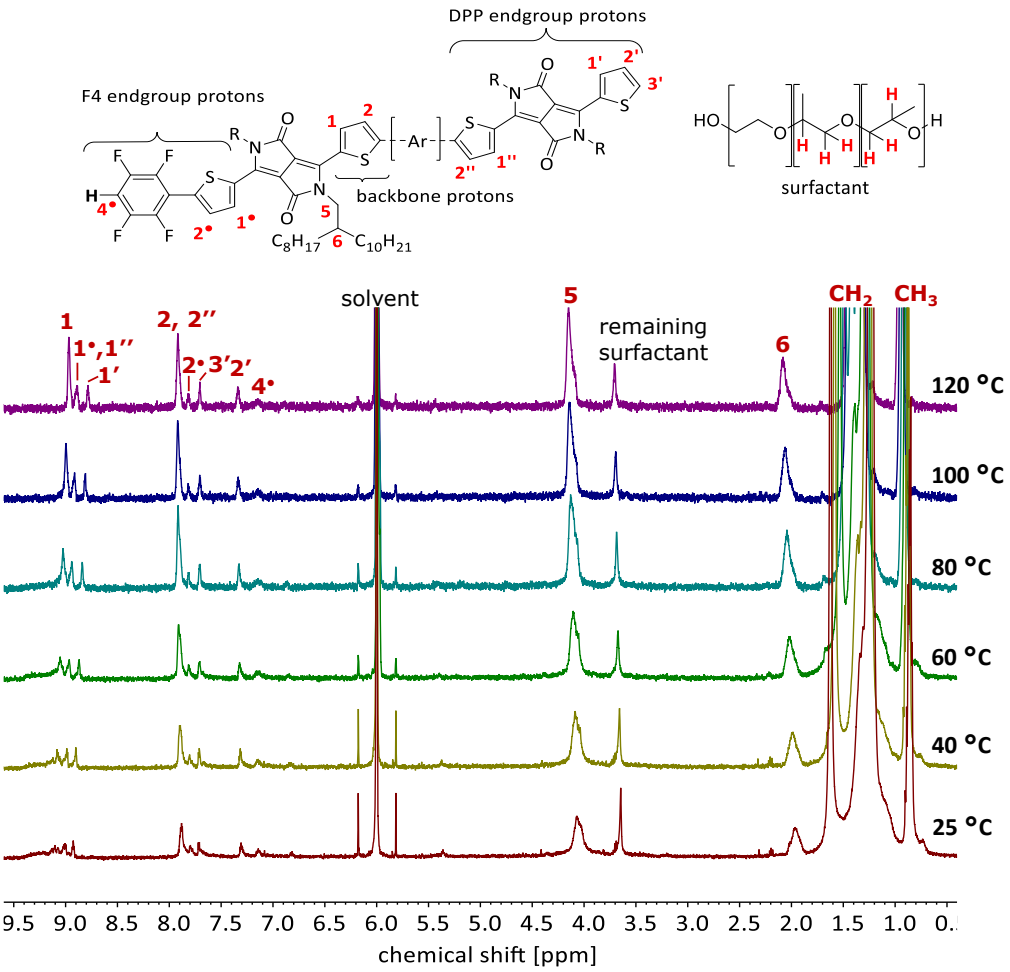

Figure 5.1: ^{1}H NMR spectrum of entry **3.46** in $C_2D_2Cl_4$ at various temperatures. The ratio between the integral intensities for protons within the aromatic region was independent of the measurement temperature for measurements conducted at 80 °C and higher.

To quantify the molecular weight of entry **3.46** by NMR end group analysis and the composition of polymers with specific terminal groups to each other, integral intensities of proton signals of each of the 3 spin systems were compared to each other. Therefore, the integrals of the non-superimposed signals **1**, **2•** and **1'**-**3'** as representatives of each spin systems were taken. Signals **2•** and **2'** appear to be suitable as integral reference since their clear doublet splitting suggests no additional underlying signals. In this instance, **2•** has been chosen and was compared with proton signals of each spin system (table 5.2). Comparing the integral intensity of **2•** and **1'**, the ratio of DPP to F4 termina is approximated to be 2:1.

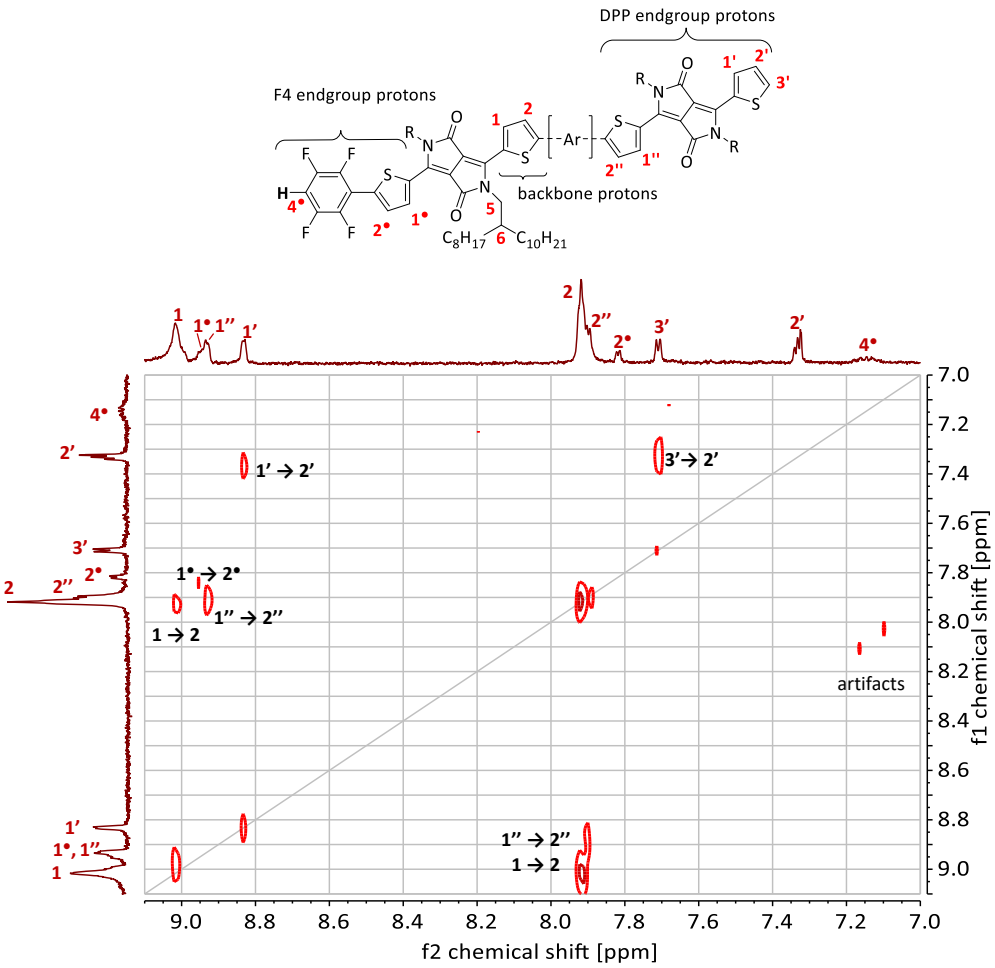

Figure 5.2: COSY spectrum of entry **3.46** in $C_2D_2Cl_4$ at 120 °C. R = 2-Octyldodecyl.

Table 5.2: Measured ^{1}H peak integral intensities of miniemulsion polymerised PDPPF4 (entry **3.46**). R = 2-Octyldodecyl.

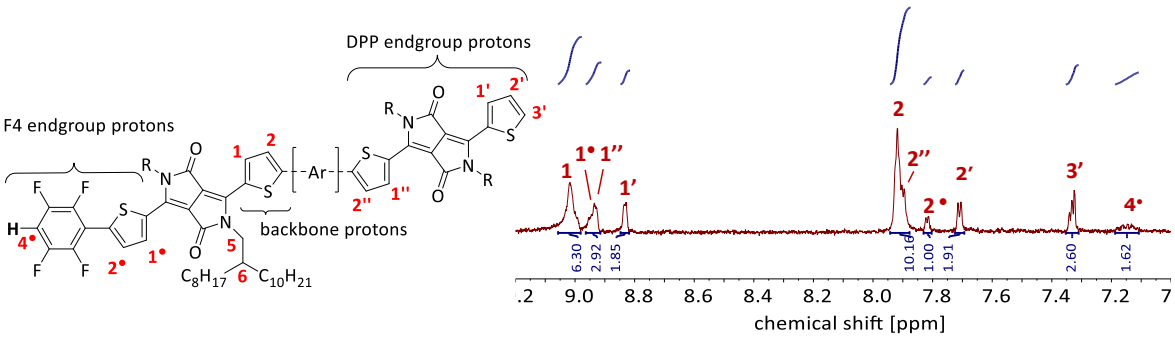

signal	integral	signal	integral
backbone		**DPP end group**	
1	6.3	**1'**	1.9
F4-H end group		**2'**	1.9
2•	1.0	**3'**	2.6

$$M_n = \frac{\frac{\sum backbone\ proton\ integrals}{\#\ backbone\ protons}}{\frac{\sum end\ group\ proton\ integrals}{\#\ end\ group\ protons}} \cdot \mathrm{M_{repeating\ unit}}$$

$$= \frac{\frac{2 \cdot 6.3}{2}}{\frac{5 \cdot 1.9 + 3 \cdot 1.0}{5+3}} \cdot 1008\ g\ mol^{-1} = 4.1\ kg\ mol^{-1} \quad (6)$$

The polymer backbone proton integral intensity was measured for signal **1** and was assumed to be the same as for backbone signal **2**. The two spin systems **‘** and **‘’** were taken into account for the DPP termina and an integral intensity of 1.9 was assumed for all signals since signals **1’’** and **2’’** are superimposed by other signals. The molecular weight was calculated according to equation 6 resulting in M_n = 4.1 kg mol^{-1}. This result obtained by end group analysis is somewhat lower than the HT-GPC analysis in trichlorobenzene ($M_{n,TCB}$ = 6.8 kg mol^{-1}) and less than half as much as measured by THF-GPC at 35 °C ($M_{n,THF}$ = 9.5 kg mol^{-1}) indicating an overestimation of M_n by GPC due to the larger apparent hydrodynamic volume of the conjugated polymer compared to the narrow polydispersity polystyrene standards used for GPC calibration. The integral intensity for signal **3’** suggests an underlying signal for which no correlations were observed in figure 5.2.

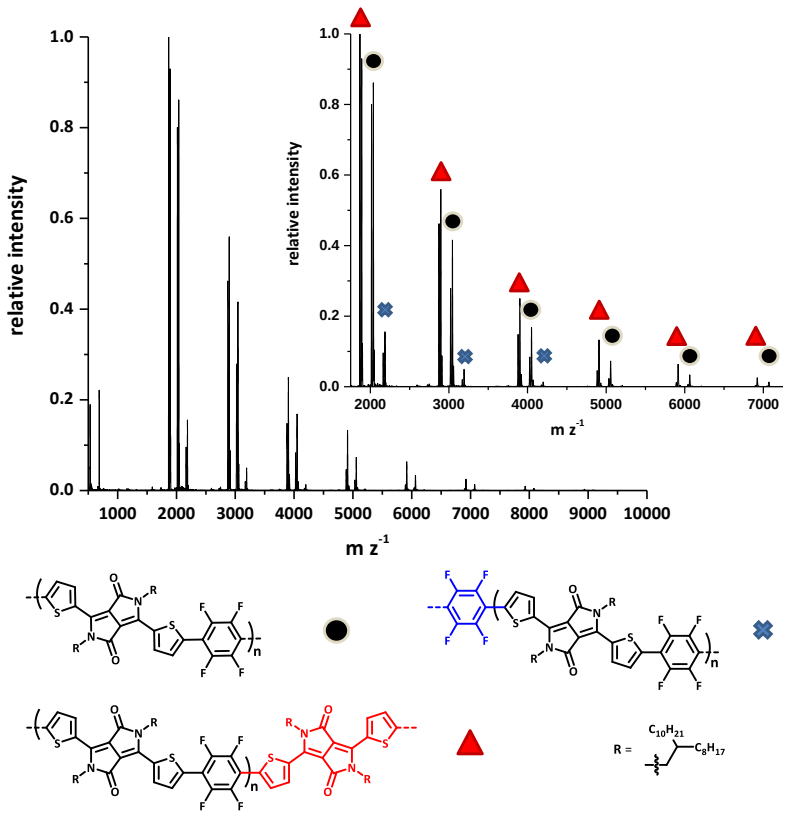

Figure 5.3: MALDI-TOF-MS spectra of entry **3.46**. Unless otherwise stated, polymer chains bear proton end groups.

The MALDI-TOF-MS spectrum of PDPPF4 polymerised in miniemulsion (entry **3.46**) is presented in figure 5.3. For the majority of peaks, m/z values of ionised polymer-sodium aggregates were detected accompanied by less intense peaks of ionised polymer-proton aggregates. Three different species are depicted and were differentiated by polymers terminated by both monomer moieties (●), only DPP (▲) or only tetrafluorobenzene (x). This concludes that the DArP of PDPPF4 in miniemulsion results in the absence of defects corroborating the findings by high temperature NMR spectroscopy.

.

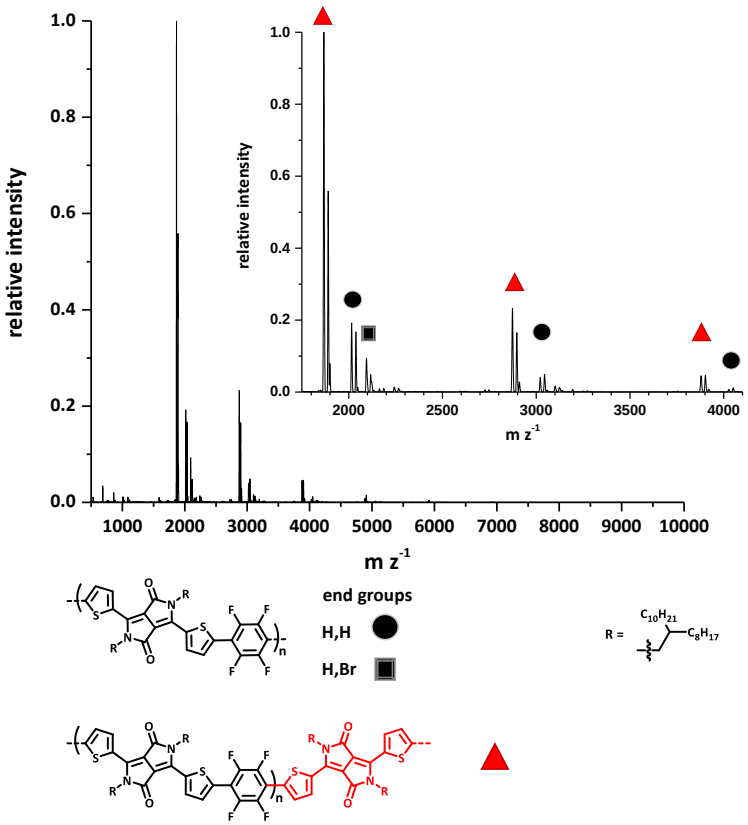

Figure 5.4: MALDI-TOF-MS spectrogram of entry **3.42** with a decreased phosphine ligand to palladium catalyst ratio of 1:1. Unless otherwise stated, polymer chains bear proton end groups.

Entry **3.42** with a decreased phosphine ligand to palladium ratio (P(*o*-anisyl)$_3$ to Pd_2dba_3 ratio 1:1, table 3.17) was analysed by MALDI-TOF-MS (figure 5.4) since previous reports discussed the presence of homo-coupling defects if sub-stoichiometric amounts of phosphine ligand were employed.[85] Figure 5.4 presents peaks for PDPPF4 terminated by DPP and tetrafluorobenzene end groups alike (● and ▣). An additional peak indicates the presence of bromine end groups to a marginal degree that cannot be quantified by MALDI-

TOF-MS. To confirm the absence of defect structures such as DPP-DPP homo couplings, further analysis by COSY is required.

The MALDI-TOF-MS analysis of PDPPF4 polymerised in solution (entry **3.56**) presents a different polymerisation outcome (figure 5.5). The expected copolymer species (● and ▲) were observed together with their bromine end group analogues (▣ and ▣). Additional peaks reveal either DPP-DPP groups within the PDPPF4 polymer backbone (◆) or DPP homopolymer.

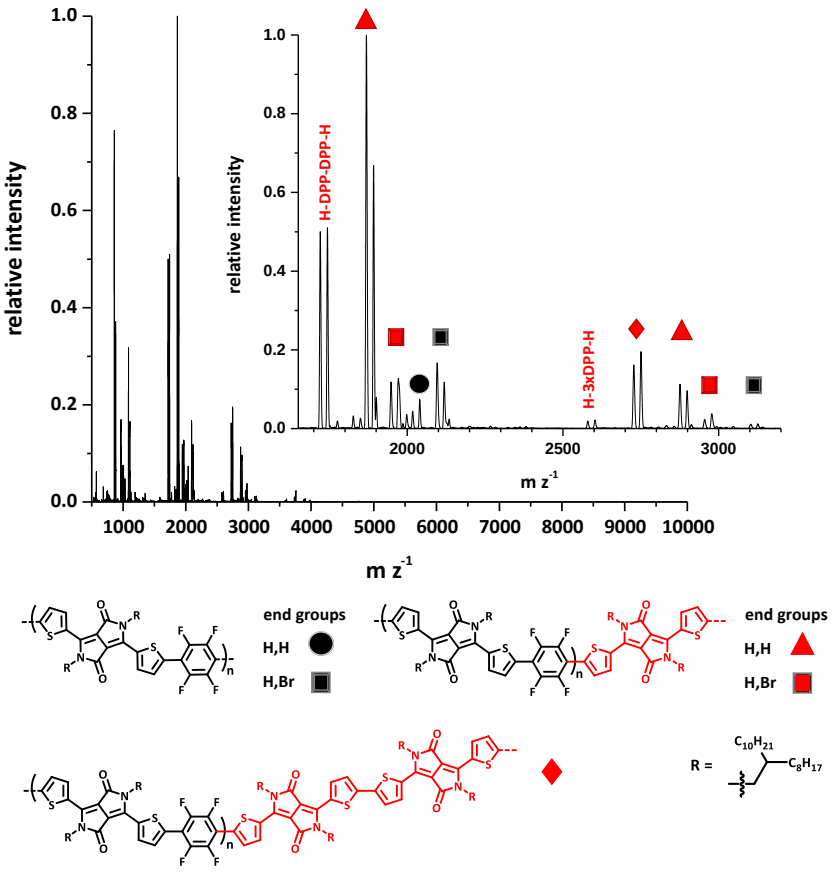

Figure 5.5: MALDI-TOF-MS spectra of entry **3.56.** Unless otherwise stated, polymer chains bear proton end groups.

The COSY NMR spectra of entry **3.46** (red) and **3.56** (green) were superimposed to verify already assigned proton signals and to determine the additional proton signals for solution polymerised PDPPF4 (figure 5.6). DPP homo couplings are reported to give rise to a distinguishable signal at δ = 7.50 ppm (**2‡**)[85] and an additional end group spin system indicated by the dagger (**‡**) symbol. The overlay of the two COSY graphs aids to distinguish

the latter from a regular DPP end group spin system showing a slight higher field shift for the DPP homo coupling end group spin system. A further unassigned spin system (indicated by **?**) shows two signals at δ = 7.79 and 8.87 ppm with a corresponding cross-correlation. Analyses by ^{13}C and heteronuclear single quantum correlation (HSQC) NMR spectroscopy could facilitate understanding of the origin of the **?** signal pair but no sufficient peak intensities/correlations were observed. Further experiments were not conducted due to resource and time constraints after the 1st Covid-19 related lockdown.

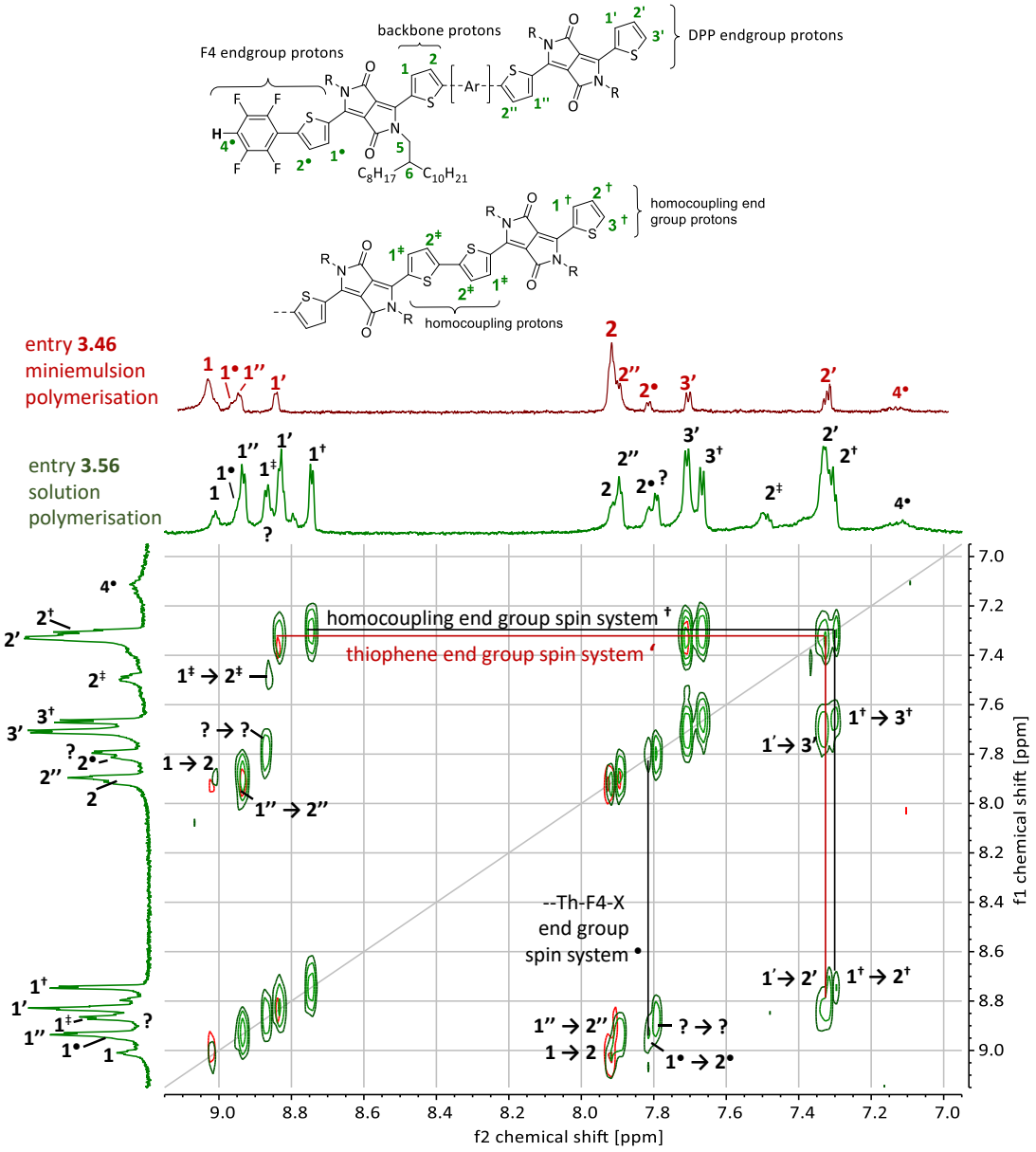

Figure 5.6: ^{1}H NMR (top) and COSY (bottom) spectra of entries **3.46** (red) and **3.56** (green) in $C_2D_2Cl_4$ at 120 °C. The region below 6.9 ppm was omitted for clarity. R = 2-Octyldodecyl.

Comparison between the integral intensities of backbone signal **1** ($\int_1$ = 1.0 as reference) and **2‡** ($\int_{2‡}$ = 1.4) suggests that most C-C bonds formed during the polymerisation occurred between two DPP units. The homo-coupling ratio presented here ($\int_{2‡}/(\int_1 + \int_{2‡})$ = 58 %) is greater than previously reported values (e.g. 6 – 12 %).[85] The elevated homo-coupling ratio can be explained by the different post-polymerisation purification procedures: The solution polymerisations in this body of work were not further purified by Soxhlet extraction for the sake of direct comparison with the miniemulsion polymerisations. The lack of this commonly utilised purification step removes impurities such as catalyst residues and low molecular weight compounds. Taking the MALDI-TOF-MS analysis of solution polymerised PDPPF4 (figure 5.5) into consideration, Soxhlet extraction would mostly remove the H-DPP-DPP-H dimer substantially decreasing the content of DPP homo-couplings. Hence, the values reported here are not directly comparable with previous reports. Moreover, the stoichiometric imbalance caused by the increased consumption of DPP monomer compared to the dibromotetrafluorobenzene monomer explains the low M_n obtained for entry **3.56**.

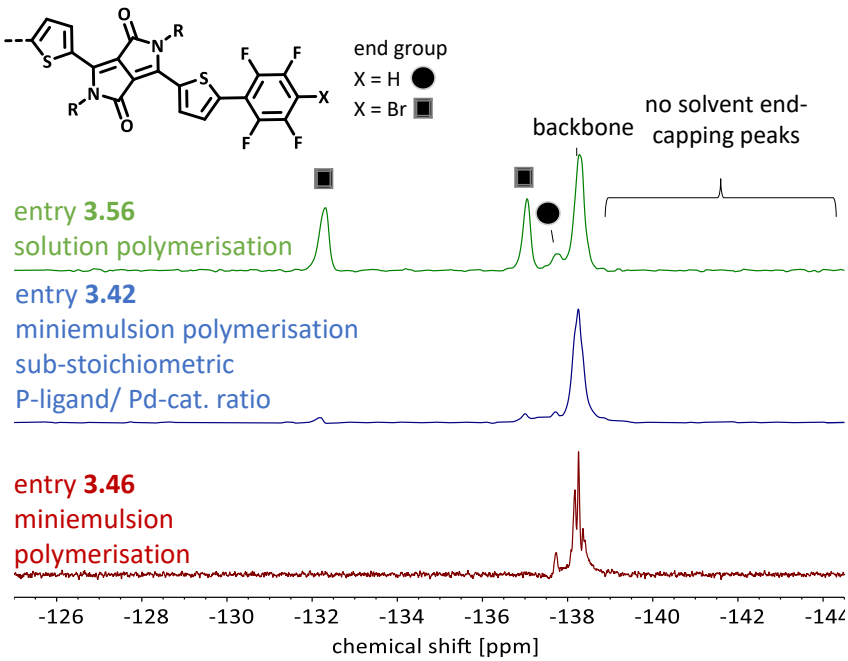

Figure 5.7: ^{19}F NMR spectra of entries **3.37**, **3.42** and **3.46** in $C_2D_2Cl_4$ at 120 °C. R = 2-Octyldodecyl.

Fluorine NMR spectroscopy of the discussed samples shows fluorine signals from within the polymer backbone at δ = - 138 ppm (figure 5.7). An additional set of signals (▣

and ●) is observed indicating the presence of bromotetrafluorobenzene terminal groups in case of solution polymerised PDPPF4 (green, entry **3.46**). Miniemulsion polymerised DPPPF4 shows no bromotetrafluorobenzene groups (red, entry **3.42**) and was observed to a lesser degree in case of sub-stoichiometric amounts of phosphine ligand employed (blue, entry **3.56**). These findings are corroborated by the MALDI-TOF-MS analysis of the PDPPF4 samples. Moreover, no solvent end-capping by p-xylene (i.e incorporation of solvent molecule onto polymer termina) is observed in figure 5.7 (expected chemical shift range indicated by bracket). C-H activation of commonly utilised solvents (e.g. toluene, chlorobenzene) was reported to lead to polymer chain end-capping resulting in decreased molecular weights in case of DArP.[137]

5.1.2. Poly(diketopyrrolopyrrole-*alt*-difluorobenzothiadiazole) - PDPPF2BT

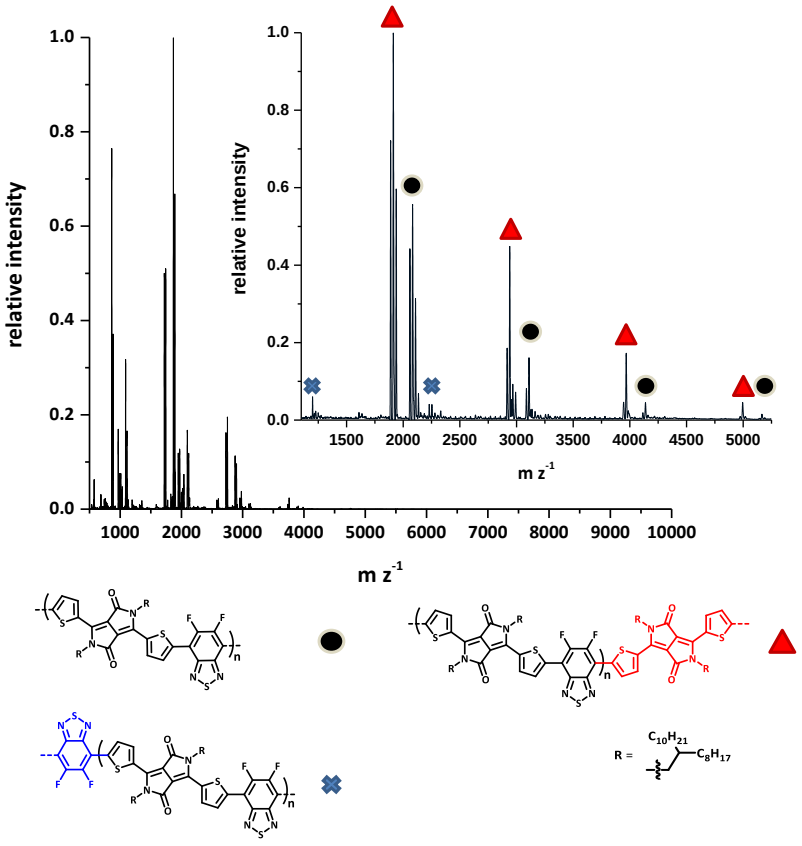

Figure 5.8: MALDI-TOF-MS spectra of entry **4.2**. Unless otherwise stated, polymer chains bear proton end groups.

The MALDI-TOF-MS analyses of PDPPF2BT polymerised in miniemulsion (entry **4.2**) and solution (entry **4.3**) are depicted in figure 5.8 and figure 5.9. The results indicate the same trend as observed for PDPPF4: The miniemulsion polymerisation gives polymers with molecular masses corresponding to the PDPPF2BT repeating unit or polymers bearing an additional DPP unit whereas the solution polymerisation results in an increased number of different polymer species. The additional peaks in case of entry **4.3** stem from bromine end groups (▣ and ▣) and DPP homo couplings (◆).

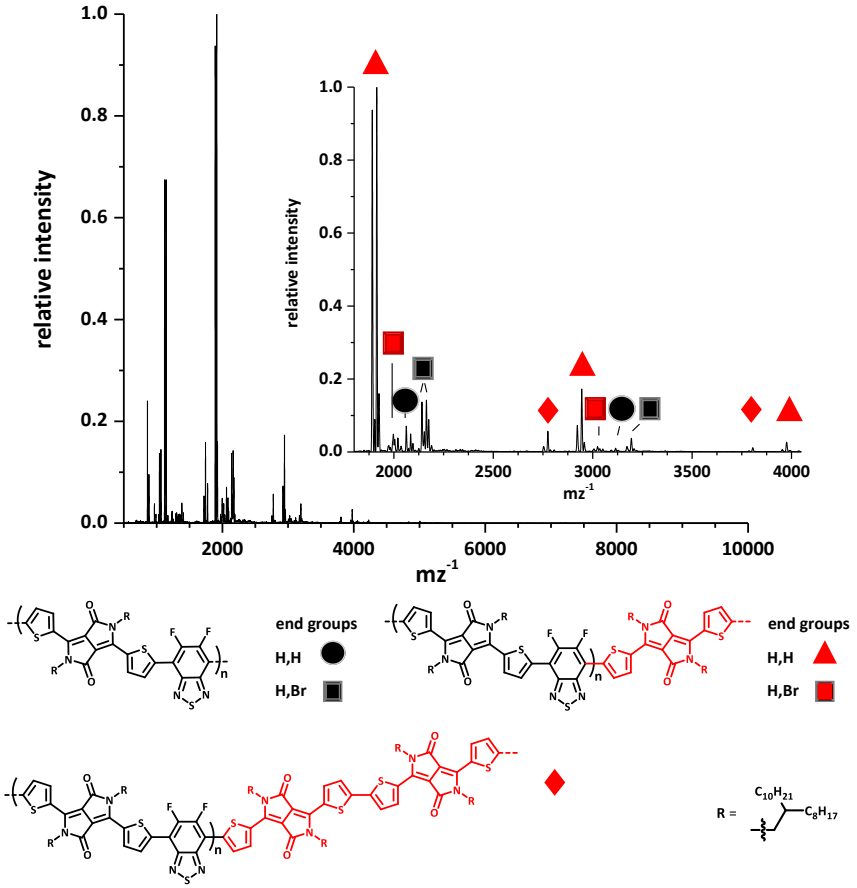

Figure 5.9: MALDI-TOF-MS spectrum of entry **4.3**. Unless otherwise stated, polymer chains bear proton end groups.

The ^{1}H NMR of entries **4.2** and **4.3** and COSY NMR spectra of entry **4.3** are depicted in figure 5.10. The region below 6.9 ppm has been omitted since this region is associated with the side chain protons (i.e. **5** and **6**). Pronounced peak broadening is observed for entry **4.2** due to the samples increased molecular weight (M_n = 11 kg mol^{-1}). Furthermore, no COSY cross-correlations were found for entry 4.2 despite increasing the concentration

if the sample and the number of scans performed. For entry **4.3**, The aromatic region of PDPPF2BT revealed similar patterns compared to PDPPF4 (e.g. the terminal thiophene spin system ' and homo coupling end group spin system †), whereas backbone protons **2** (8.3 – 8.5 ppm) are down field shifted compared to the backbone proton signals in PDPPF4 (7.9 ppm). The F2BT end group spin system • could not be unequivocally determined for both compounds and requires further investigation (e.g. ^{13}C NMR, HSQC/HMQC, HMBC, defined model compounds). Nonetheless, figure 5.10 presents the only reported proton peak assignment for PDPPF2BT to date.

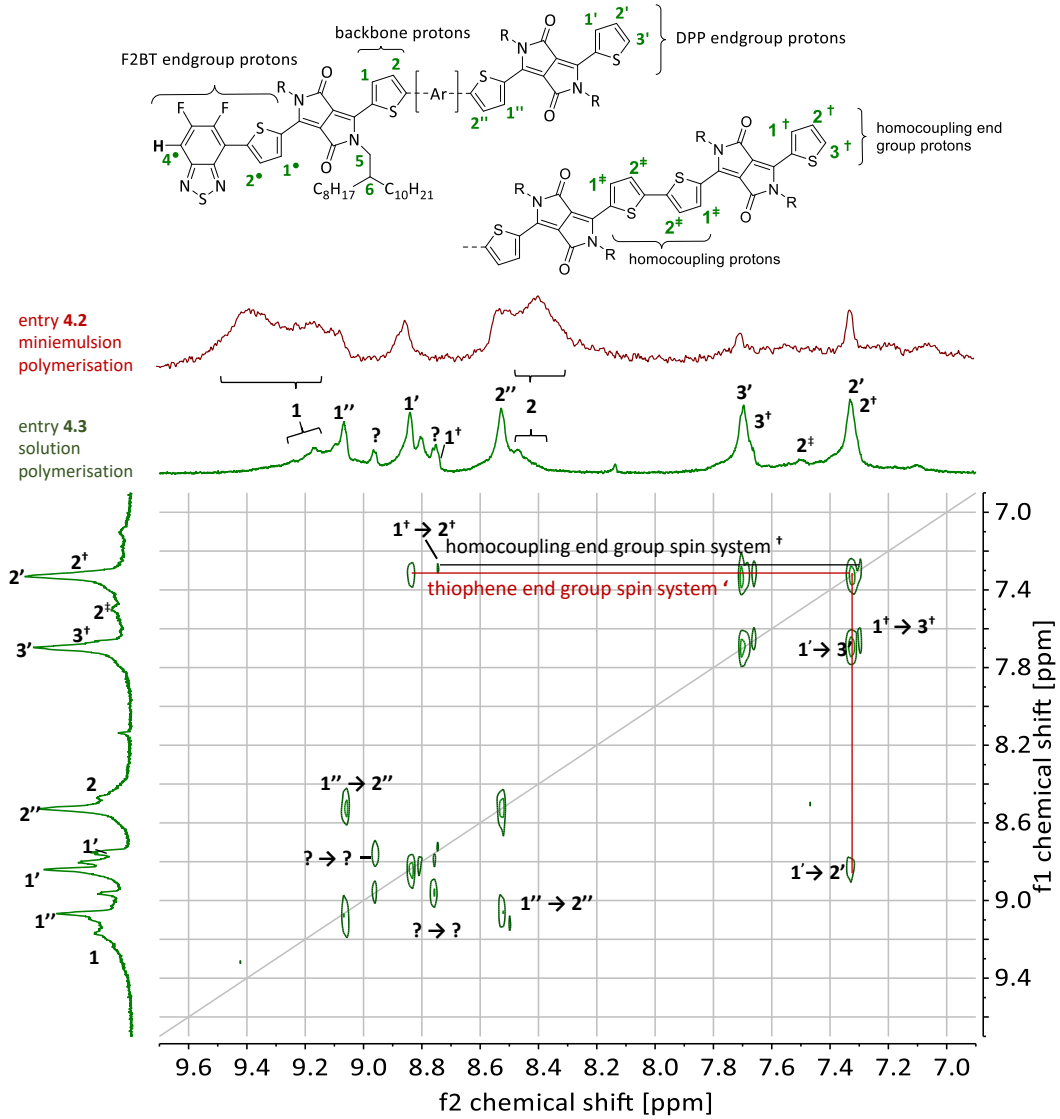

Figure 5.10: ^{1}H NMR (top) and COSY (bottom) spectra of entries **4.2** and **4.3** in $C_2D_2Cl_4$ at 120 °C.

The ^{19}F NMR spectrum of entry **4.2** shows the polymer backbone peak at δ = -124 ppm (figure 5.11). Additional signals (δ = -113 and -120 ppm, ▣) are observed for the solution polymerised batch (entry **4.3**) confirming the bromine end groups found by MALDI-TOF-MS. Moreover, no solvent end-capping by p-xylene is observed in figure 5.11 (expected chemical shift range indicated by bracket).

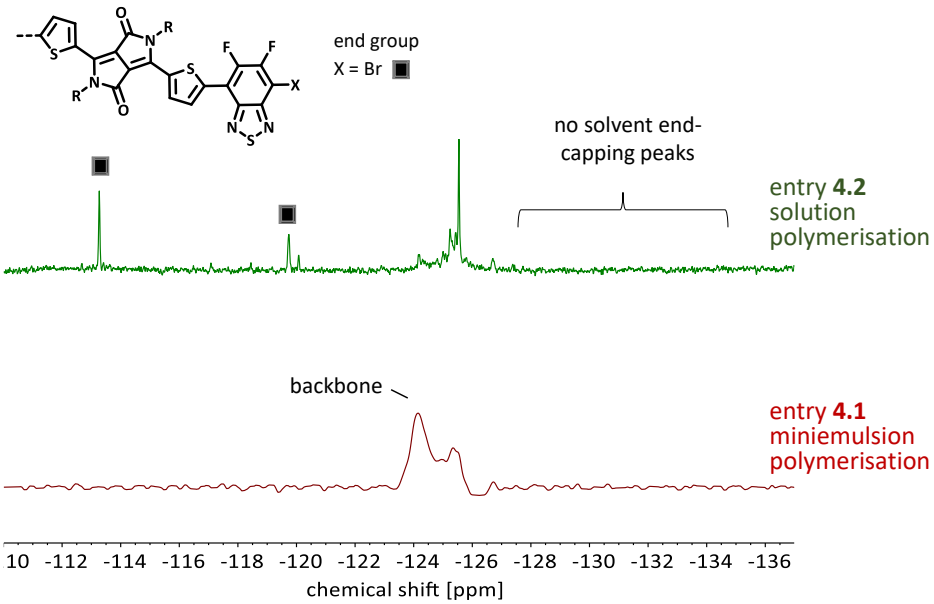

Figure 5.11: ^{19}F NMR spectra of entries **4.2** and **4.3** in $C_2D_2Cl_4$ at 120 °C.

5.1.3. Poly(diketopyrrolopyrrole-*alt*-thienothiophene) – PDPPTT

PDPPTT polymerised in miniemulsion (entry **4.5**) was analysed by MALDI-TOF-MS and exhibited a pattern of polymer species consisting of either the DPPTT repeating unit (●) or chains with one additional DPP group (▲, figure 5.12). A third sequence reveals DPP-DPP homo couplings (♦) in addition to H-DPP-DPP-H dimer. These homo couplings were also observed in the MALDI-TOF-MS spectra of solution polymerised PDPPTT (entry **4.6**, figure 5.13). Furthermore, bromine end groups were observed suggesting that hydrolysis of bromine chain ends occurs to a lesser degree within the solution polymerisation compared to the miniemulsion polymerisation.

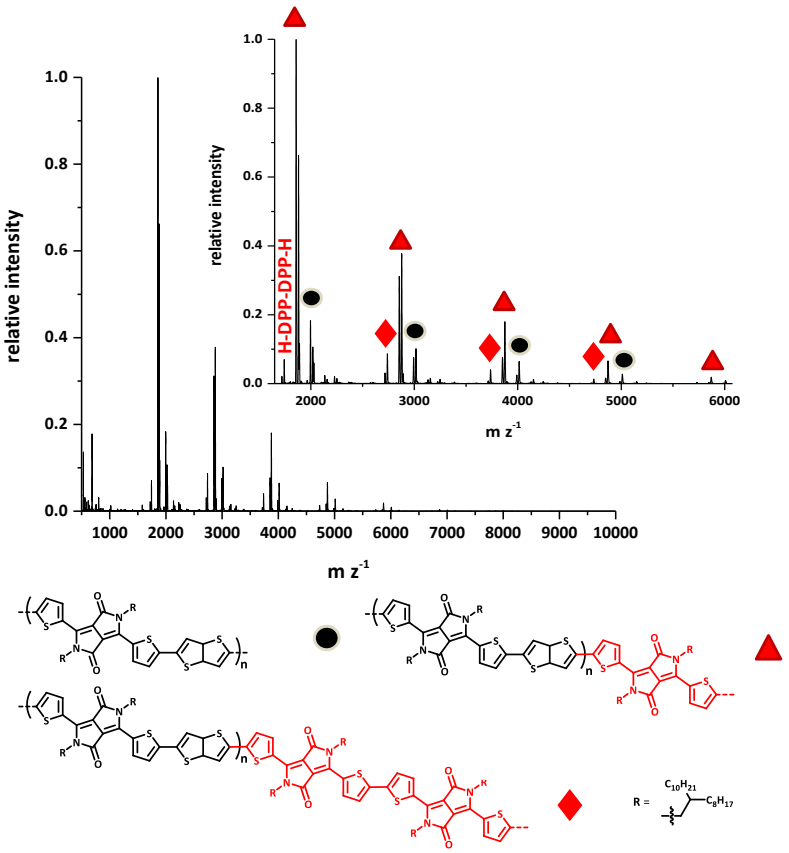

Figure 5.12: MALDI-TOF-MS spectra of entry **4.5**. Unless otherwise stated, polymer chains bear proton end groups.

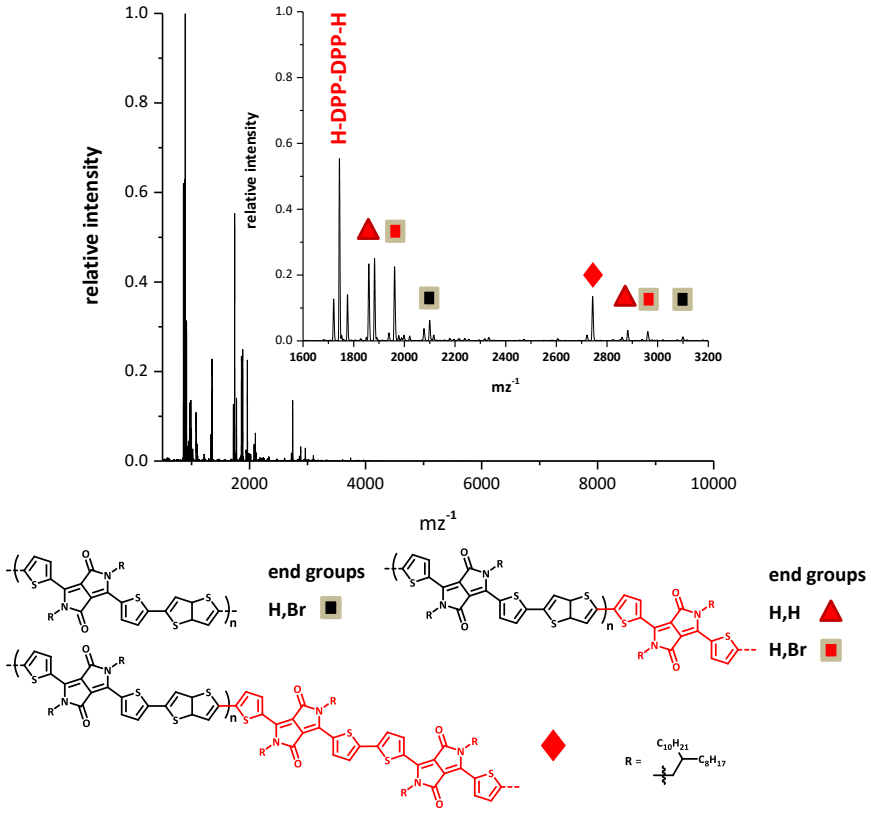

Figure 5.13: MALDI-TOF-MS spectra of entry **4.6**. Unless otherwise stated, polymer chains bear proton end groups.

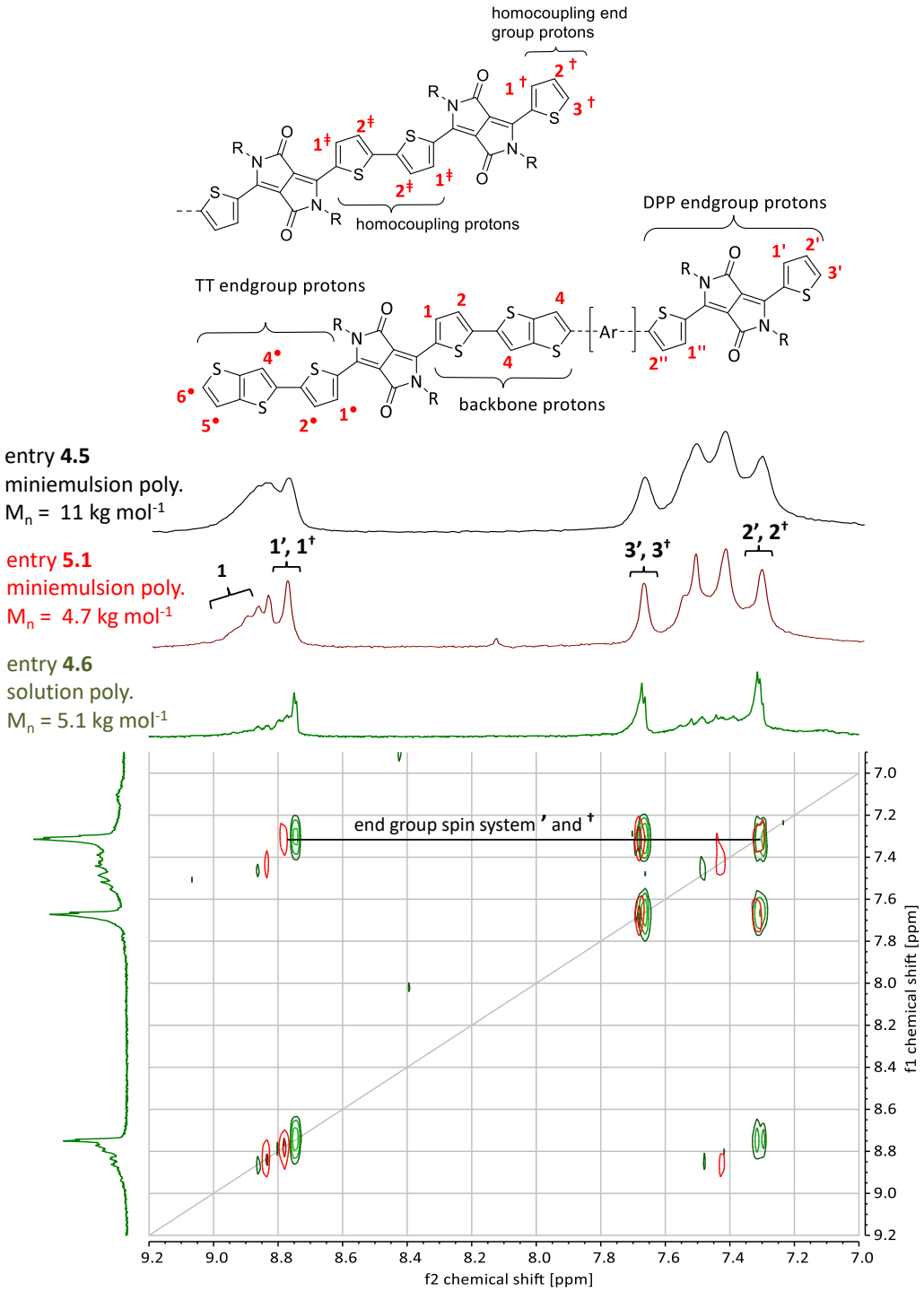

Figure 5.14: ^{1}H NMR (top) spectra of entries **4.5**, **4.6** and **5.1** and COSY (bottom) spectra of entries **4.5** and **4.6** in $C_2D_2Cl_4$ at 120 °C.

Both samples were further analysed by both high temperature ^{1}H and COSY NMR (figure 5.14). Entry **4.5** exhibited peak broadening due its increased molecular weight (M_n = 11 kg mol^{-1}) and showed no cross correlations in its COSY spectrum. Hence, an additional sample of miniemulsion polymerised PDPPTT with a lower molecular weight (entry **5.1**, M_n = 4.7 kg mol^{-1}) was prepared that exhibited similar contents of DPP homo couplings as

presented in figure 5.12. The correlation between the peaks at δ = 7.32, 7.67 and 8.78 ppm identify the protons belonging to the DPP end group (spin system ‘) and DPP homo coupling end group protons (spin system †). The DPP homo coupling protons **1**‡ and **2**‡ at δ = 7.46 and 8.85 ppm are assigned and correlate with each other but are superimposed by signals that cannot be further assigned. The assignment of the remaining spin systems (i.e. backbone protons **1** – **3**, DPP end group protons **1’’** and **2’’** and thienothiophene end group protons **4**• – **6**•) require a thorough investigation by high temperature ^{13}C NMR, HSQC/HMQC and HMBC in addition with defined model compounds. Hence, integral analysis to determine an absolute molecular weight by end group analysis and determination of end group ratios are not feasible.

5.1.4. Poly(diketopyrrolopyrrole-*alt*-thienopyrrolodione) - PDPPTPD

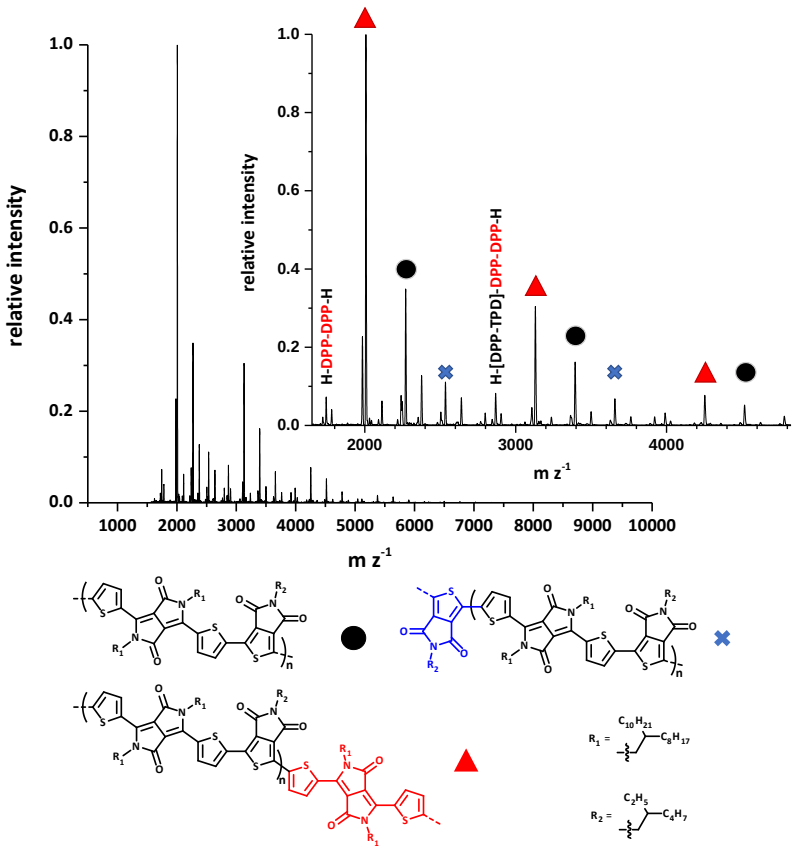

Figure 5.15: MALDI-TOF-MS spectra of entry **4.8.** Unless otherwise stated, polymer chains bear proton end groups.

The MALDI-TOF-MS analysis of PDPPTPD (entry **4.8**) polymerised in miniemulsion shows repeating patterns of three distinguishable polymer species (●, ▲, x) alongside two peaks accounting to DPP-DPP homo couplings (figure 5.15). The same patterns were observed for the solution polymerised polymer together with the DPP monomer, dimer and trimer (entry **4.9**, figure 5.16).

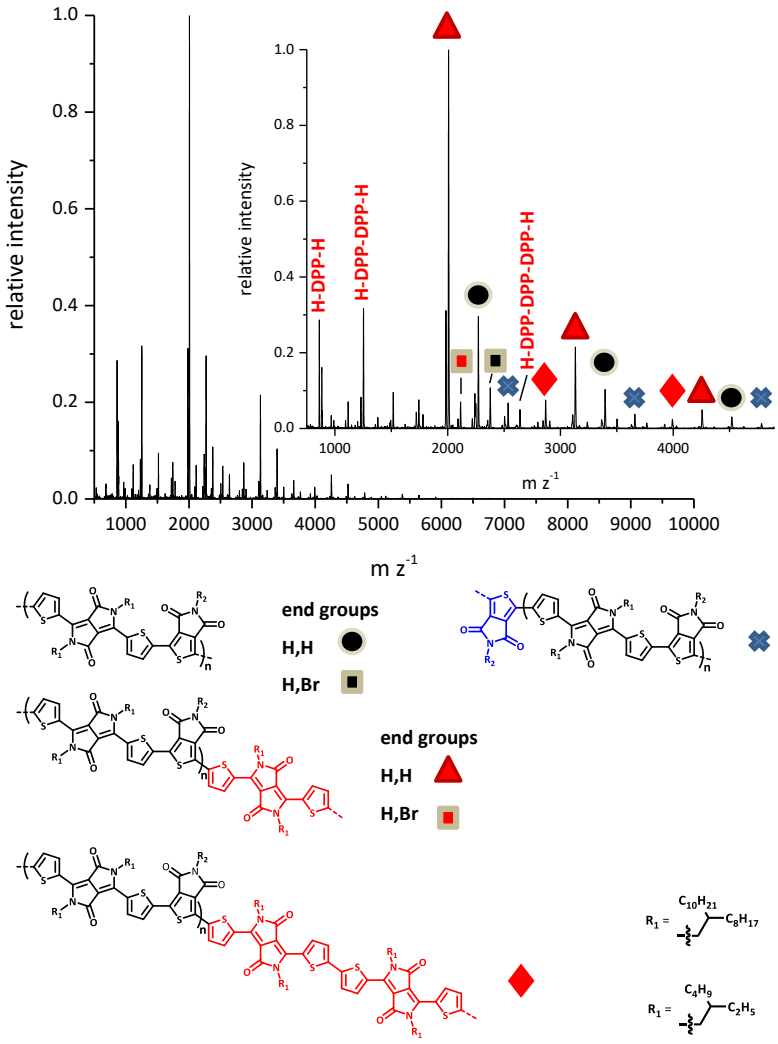

Figure 5.16: MALDI-TOF-MS spectra of entry **4.9**. Unless otherwise stated, polymer chains bear proton end groups.

High temperature ^{1}H NMR shows similar 1D spectra for both polymers since both the miniemulsion polymerisation and solution polymerisation yielded identical molecular weights (M_n = 4.1 kg mol^{-1}). The ^{1}H NMR spectrum of the solution polymerised batch (entry **4.9**) indicates a greater ratio of DPP homo couplings: Defined non-superimposed signals such as **1**‡ appear to be greater but cannot be quantified. Generally, quantification

of entities such as homo coupling content, end group ratio (i.e. TPD vs DPP) and end group determination were not possible due to overlapping signals.

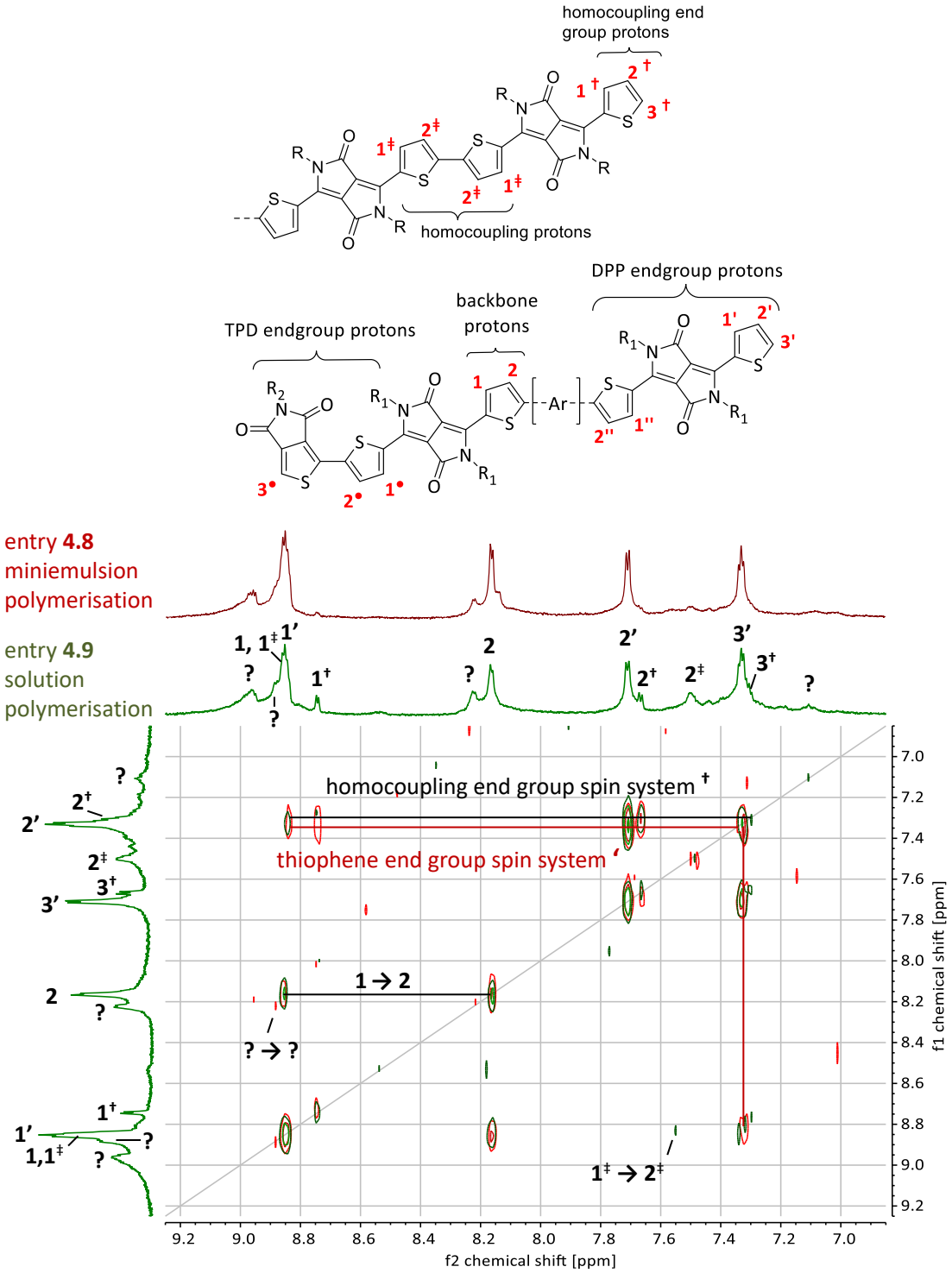

Figure 5.17: ^{1}H NMR (top) and COSY (bottom) spectra of entries **4.8** and **4.9** in $C_2D_2Cl_4$ at 120 °C.

5.1.5. Poly(naphthalene diimide-*alt*-tetrafluorobenzene) - PNDIF4

The MALDI-TOF-MS spectrum of entry **4.11** shows patterns of polymer chains made of the NDIF4 repeating unit (●, figure 5.18) or species containing an additional naphthalene (▲) or tetrafluorobenzene group (x). At higher degrees of polymerisation (≥ 4 repeating units), tetrafluorobenzene homo couplings (◆) occurred to a negligible degree. On the contrary, NDI homo couplings are observed for solution polymerised PNDIF4 (entry **4.12**, figure 5.19). Bromine end groups were observed only for the solution polymerised PNDIF4 batch and is in accordance with the findings of solution polymerised batches of the previously presented DPP copolymers.

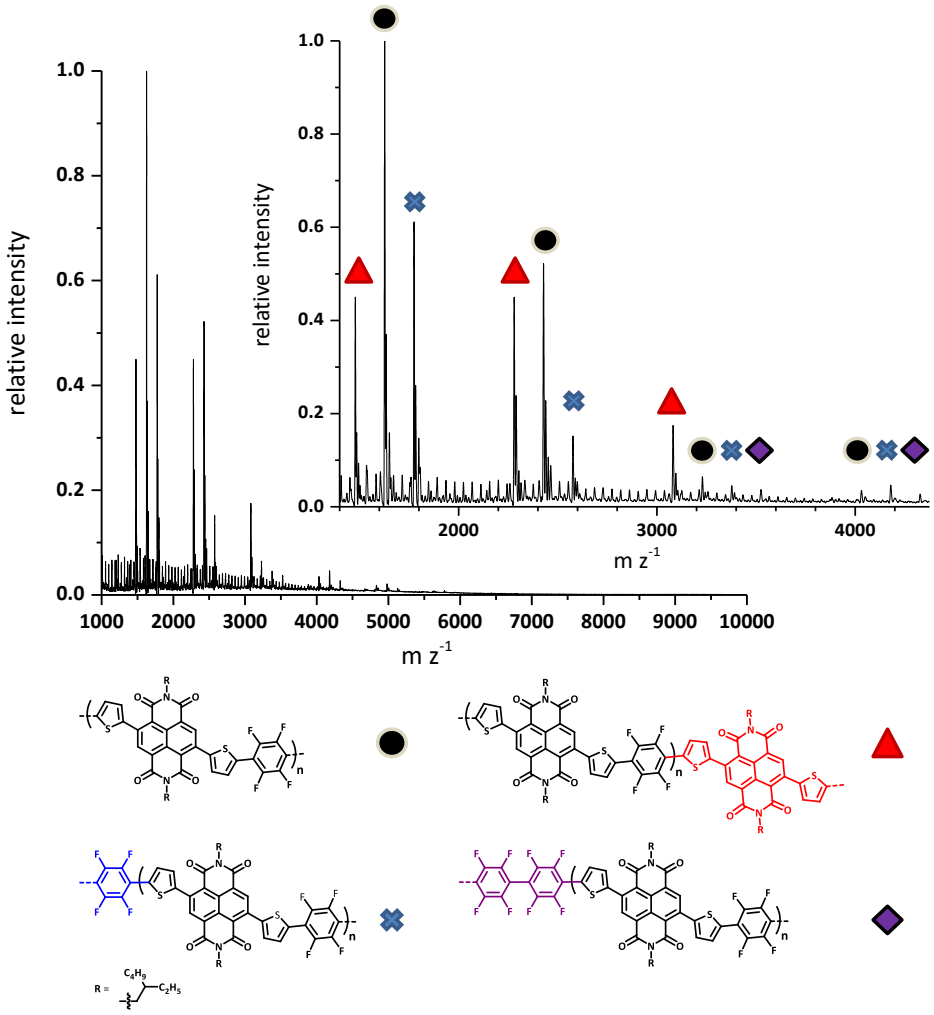

Figure 5.18: MALDI-TOF-MS spectra of entry **4.11**. Unless otherwise stated, polymer chains bear proton end groups.

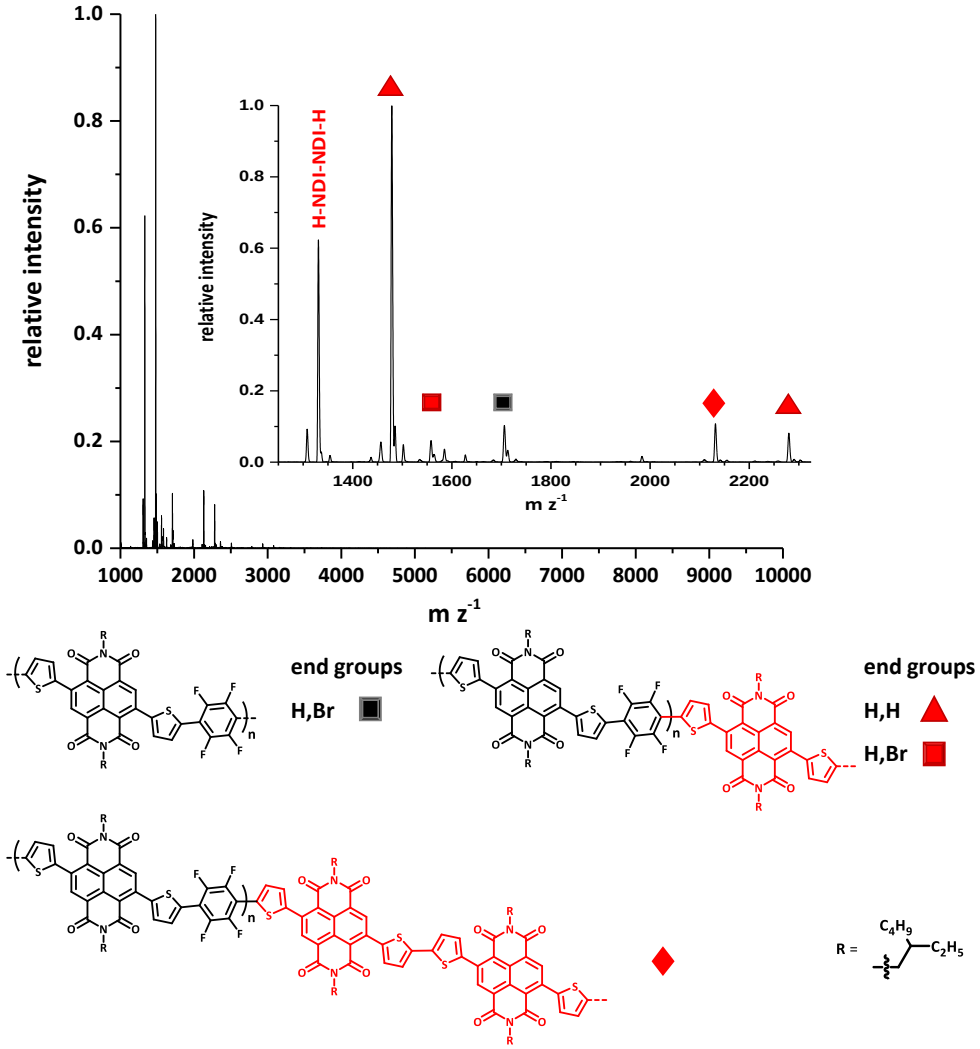

Figure 5.19: MALDI-TOF-MS spectra of entry **4.12**. Unless otherwise stated, polymer chains bear proton end groups.

High temperature ^{1}H NMR spectroscopy and COSY of PNDIF4 are presented in figure 5.20 and the proton signals were assigned according to a report of Sommer and co-workers.[126] Comparison between the two PNDIF4 batches reveal deviations especially for the naphthalene core protons **5** and **6** in the aromatic region between 8.78 ppm and 8.93 ppm (inlet in figure 5.20): The peak at δ = 8.80 ppm presumably belongs to the NDI homo coupling analogue of **5'**, followed by the homo coupling analogues of **5•** and **6'** at δ = 8.83 ppm and analogues of **5** and **6** at δ = 8.86 ppm. The four homo coupling signals at δ = 8.83 and 8.86 ppm are superimposed by the regular end group signals **5'**, **6'** and **5•** increasing the integral intensities of the two phenomenologically observed peaks for the solution polymerised batch. The peak of backbone signals **5** and **6** is less pronounced due to the low molecular weight obtained for entry **4.12** (M_n = 1.3 kg mol^{-1}).

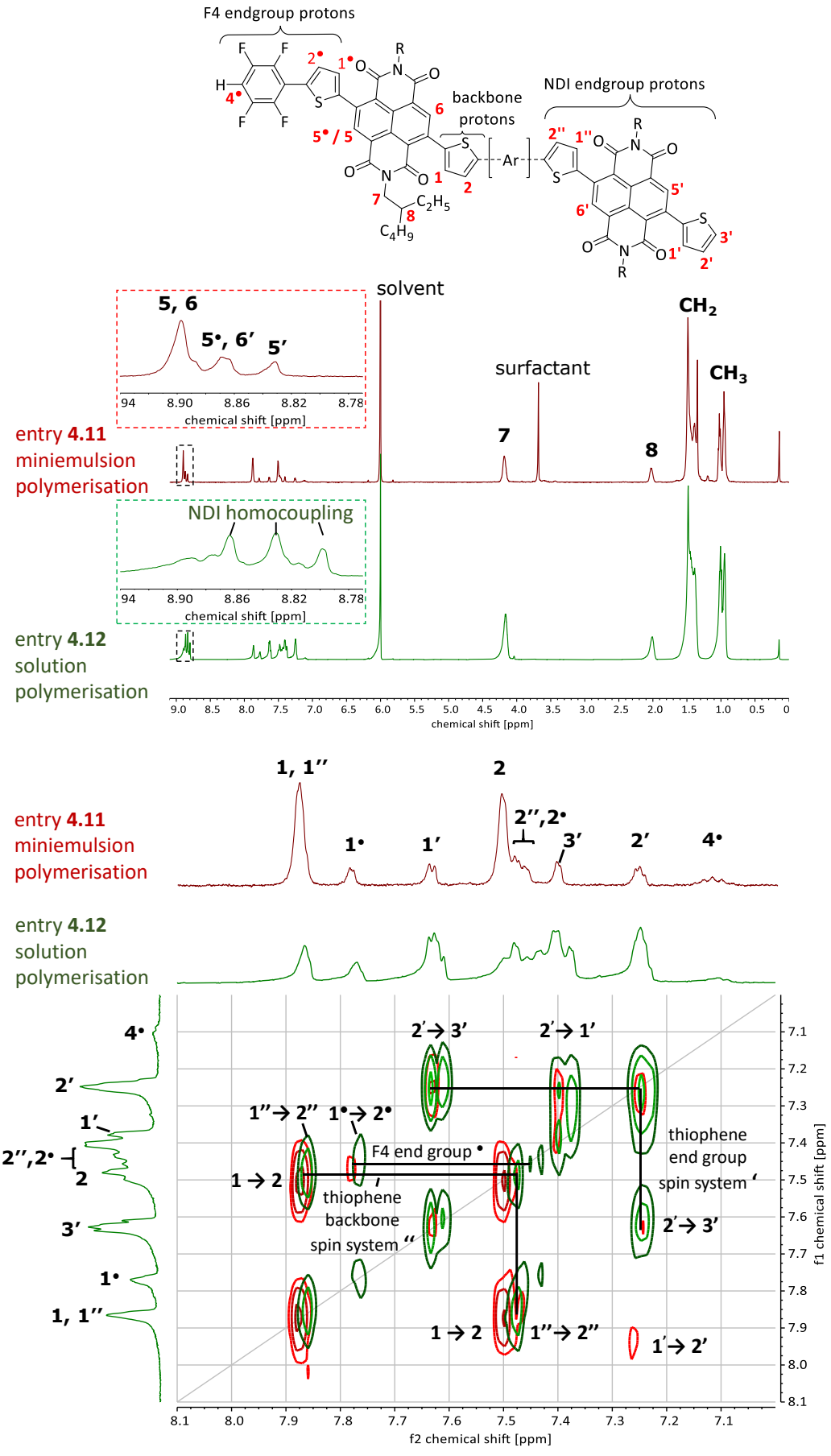

Figure 5.20: NMR and COSY spectra of PNDIF4 polymerised in miniemulsion (entry. **4.11**) and in solution (entry **4.12**). R = 2-Ethylhexyl.

The NDI homo coupling assignment is corroborated by MALDI-TOF-MS data presented for entries **4.11** and **4.12**, where NDI homo couplings were observed only for the solution polymerised polymer. An unambiguous assignment of the NDI homo coupling peaks requires further analysis, such as ^{1}H and ^{13}C correlations and a PNDIF4 model compound containing defined NDI-NDI groups. Quantification of the homo coupling content of entry **4.12** is not feasible due to the overlapping of the NDI homo coupling proton signal at δ = 8.86 ppm. To obtain the ratio between both the tetrafluorobenzene termina and NDI end groups, the integral intensities of the thiophene end group protons **1'** – **3'** (∫ = 1.0 as reference) were compared with the non-superimposed signal **1•** ($\int_{1\bullet}$ = 0.8). The measured integral intensities suggest a ratio of 5:4 between both terminal groups with a slight prevalence for NDI. End group analysis for entry **4.11** was performed according to equation 6 considering the integral intensities of the four backbone protons (i.e signals **1**, **2**, **5**, **6**, ∫ ≈ 4.3) and ten end group proton signals (i.e **1•**, **2•**, **4•**, **1'** – **3'**, **5'**, **6'**, **1''** and **2''**). The result of the end group analysis according to equation 6 (M = 4.6 kg mol^{-1}) indicates overestimation of the HT-GPC measurement (M_n = 5.6 kg mol^{-1}). This discrepancy between the molecular weights obtained by HT-GPC and NMR end group analysis is in accordance with the characterisation of PDPPF4 in section 5.3.1.

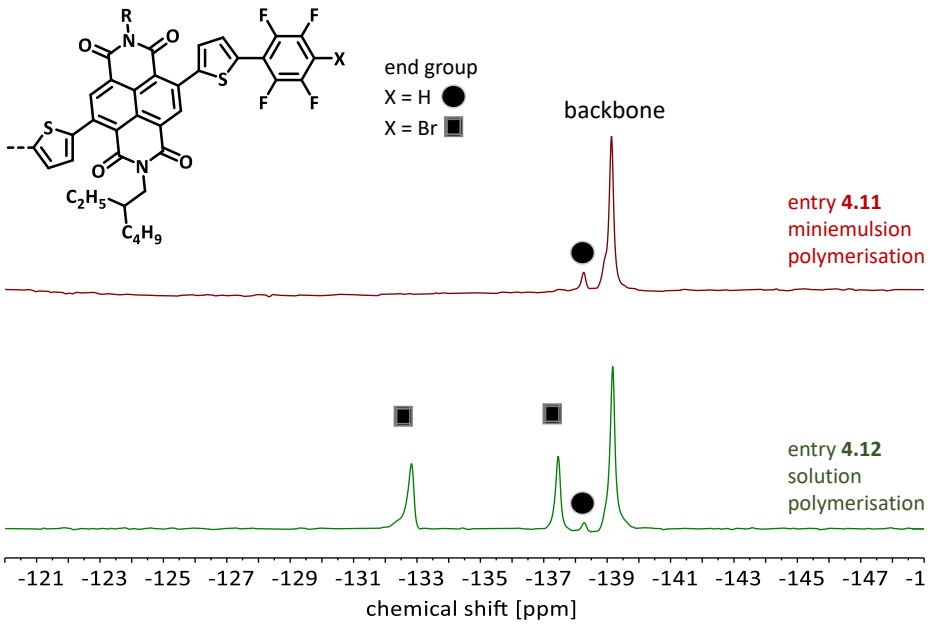

Figure 5.21: ^{19}F NMR spectra of entries **4.11** and **4.12** in $C_2D_2Cl_4$ at 120 °C. R = 2-Ethylhexyl.

The ^{19}F NMR spectra of entries **4.11** and **4.12** show a signal associated with the polymer backbone signal at δ = -139 ppm (figure 5.21). One additional peak is observed at δ = -138 ppm for the F4-H polymer terminal groups (●). For the solution polymerised batch, two peaks were observed at δ = -137 and -133 ppm (▣) confirming the bromine end groups found by MALDI-TOF-MS.

5.1.6. Poly(naphthalene diimide-*alt*-difluorobenzothiadiazole) - PNDIF2BT

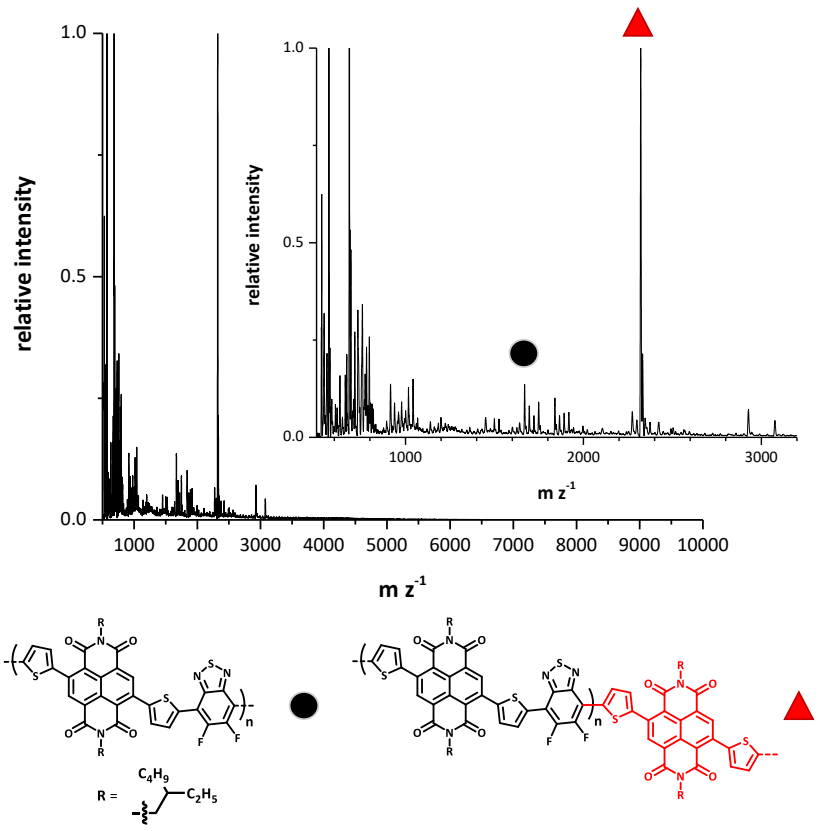

Figure 5.22: MALDI-TOF-MS spectra of entry **4.13**. Unless otherwise stated, polymer chains bear proton end groups.

The MALDI-TOF-MS measurement of entry **4.13** presents only two identifiable peaks for PNDIF2BT (●, ▲, figure 5.22). The solution polymerised analogue (entry **4.14**) reveals additional NDI homo couplings (◆) and bromine end groups (▣ and ▣, figure 5.23).

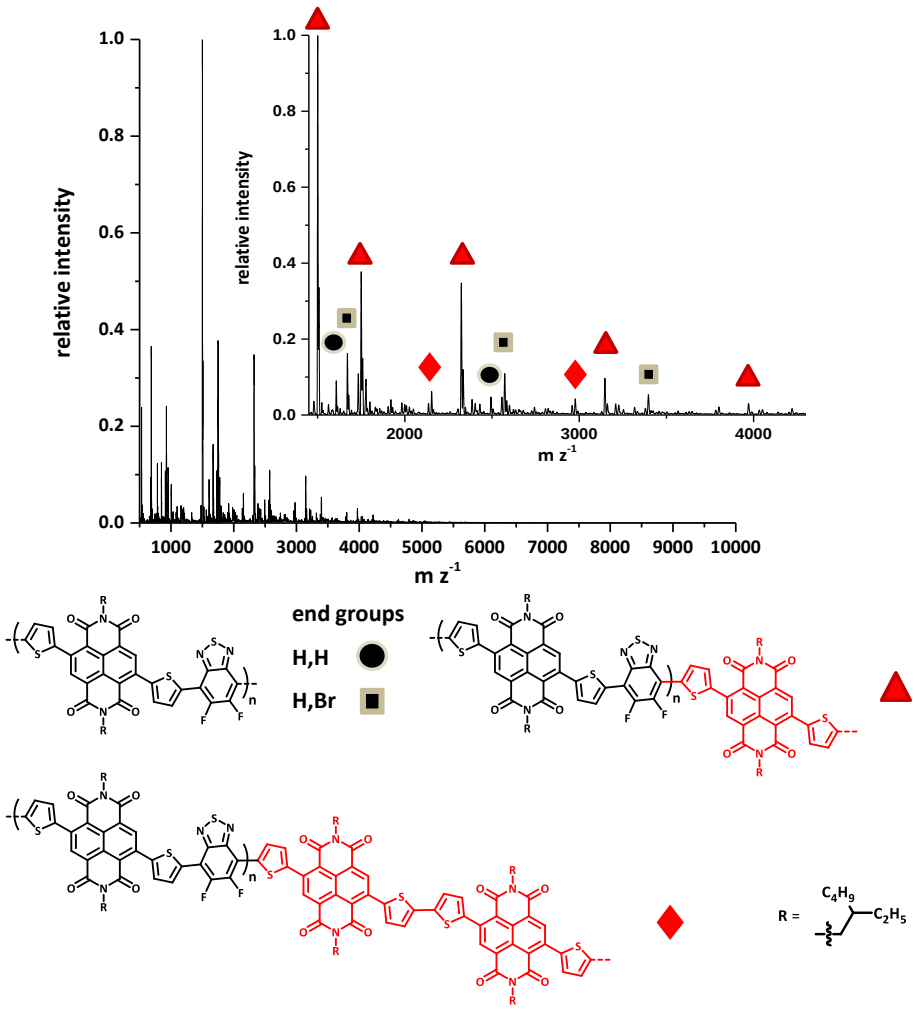

Figure 5.23: MALDI-TOF-MS spectra of entry **4.14**. Unless otherwise stated, polymer chains bear proton end groups.

The HT-NMR analysis of PNDIF2BT compares the ^{1}H and COSY spectra of the miniemulsion (red) and solution (green) polymerisation of PNDIF2BT (figure 5.24). The range in chemical shifts between the backbone protons **1** and **2** of PNDIF2BT is $\Delta\delta_{\mathbf{1\text{-}2\ PNDIF2BT}}$ ≈ 0.9 ppm and is almost as large as in case of PDPPF2BT ($\Delta\delta_{\mathbf{1\text{-}2\ PDPPF2BT}}$ ≈ 1.0 ppm) but substantially larger compared to PNDIF4 ($\Delta\delta_{\mathbf{1\text{-}2\ PNDIF4}}$ ≈ 0.4 ppm). On the contrary, the terminal thiophene spin system of PNDIF2BT shows a chemical shift range of $\Delta\delta_{\mathbf{1'\text{-}2'\ PNDIF2BT}}$ ≈ 0.4 ppm similar to PNDIF4 ($\Delta\delta_{\mathbf{1'\text{-}2'\ PNDIF4}}$ ≈ 0.4 ppm) rather than PDPPF2BT ($\Delta\delta_{\mathbf{1'\text{-}2'\ PDPPF2BT}}$ ≈ 1.1 ppm).

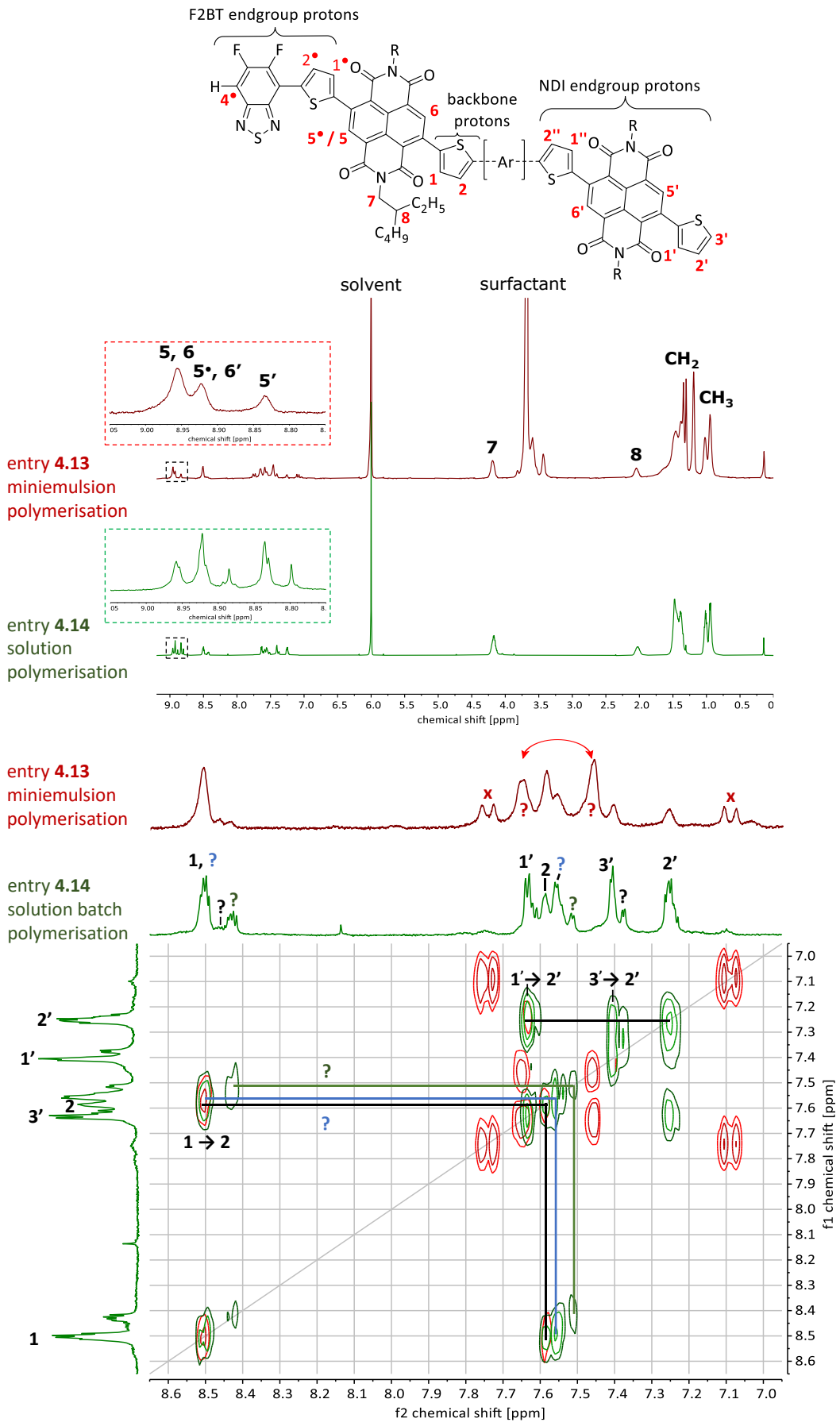

Figure 5.24: NMR and COSY spectra of PNDIF2BT polymerised in miniemulsion (entry. **4.13**) and in solution (entry **4.14**). R = 2-Ethylhexyl. **x** refers to Triton X aromatic proton signals.

These comparisons in chemical shifts suggest that amongst the four moieties presented here (i.e DPP, NDI, F4 and F2BT), DPP and difluorobenzothiadiazole are stronger electron withdrawing polymer building blocks compared to NDI and tetrafluorobenzene. This is corroborated by the fact that the chemical shift of backbone proton **1** has the greatest value in case of PDPPF2BT ($\delta_{1\ \mathbf{PDPPF2BT}}$ ≈ 9.4 ppm) whereas PNDIF4 reveals the lowest ($\delta_{1\ \mathbf{PNDIF4}}$ ≈ 7.9 ppm). The inlet zooming into the range between δ = 8.75 and 9.05 ppm reveals additional naphthalene proton signals for the solution polymerisation that are considered to arise from NDI homo coupling since their chemical shifts are identical to the ones observed for solution polymerised PNDIF4 at δ = 8.80 and 8.83 ppm. More signals were observed for the miniemulsion batch showing two spin systems with strong correlations between two peaks each. Those four peaks are not observed for the solution polymerisation and their origin is unknown. Further signal assignment of the end group spin systems ‘, ‘’, ● was not possible without further analysis by ^{13}C NMR, HSQC/HMQC, HMBC and model compounds with constituted of defined structures.

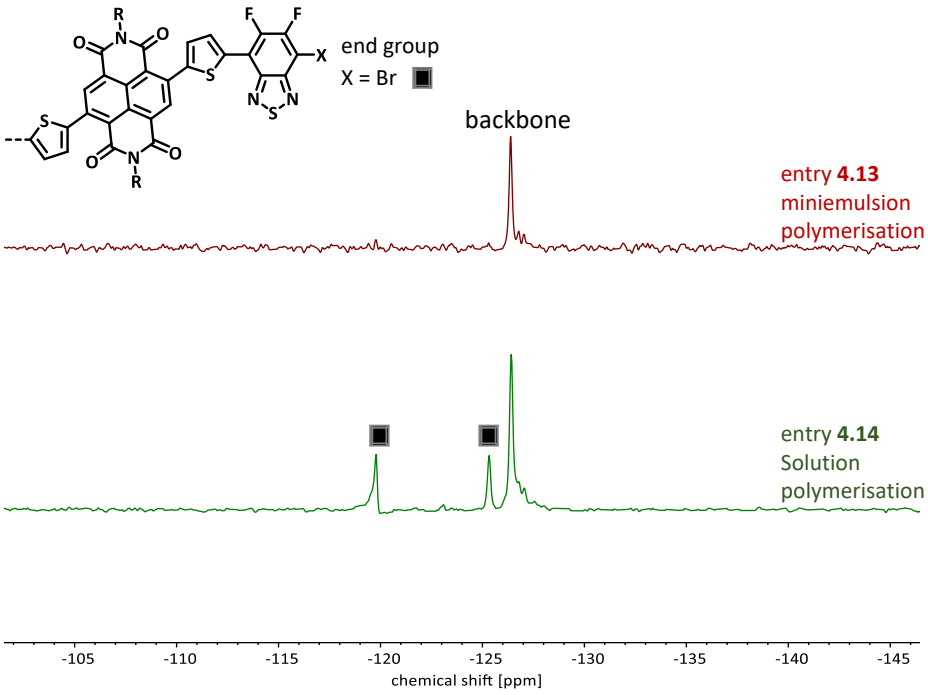

Figure 5.25: ^{19}F NMR spectra of entries **4.13** and **4.14** in $C_2D_2Cl_4$ at 120 °C. R = 2-Ethylhexyl.

The ^{19}F NMR spectra of entries **4.13** and **4.14** show a signal originating from within the polymer backbone signal at δ = -126 ppm (figure 5.25). Two peaks were observed at

δ = -120 and -125 ppm for the solution polymerised batch, confirming the bromine end groups found by MALDI-TOF-MS.

5.1.7. Poly(thienopyrrolodione-*alt*-tetrafluorobenzene) - PTPDF4 and Poly(thieno pyrrolodione-*alt*-difluorobenzothiadiazole) - PTPDF2BT

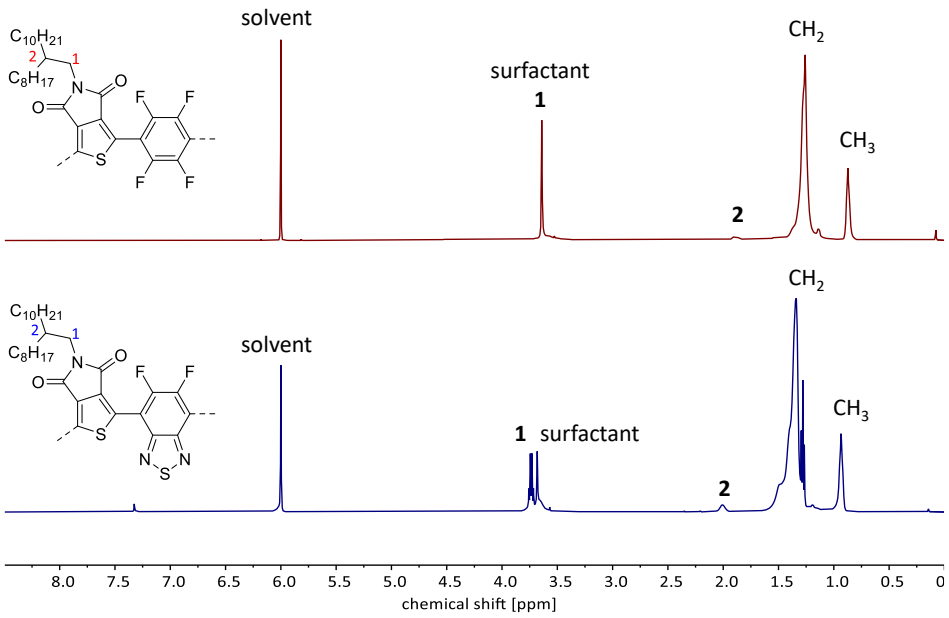

Figure 5.26: ^{1}H NMR spectra of entries **4.16** (top) and **4.18** (bottom) in $C_2D_2Cl_4$ at 120 °C.

The chemical structures of PTPDF4 and PTPDF2BT suggest no protons on the respective polymer backbones. Hence, the NMR analysis of both polymers was expected to be limited to the side chain protons and potential proton end group assignments. Figure 5.26 shows that only for PDPPF2BT (entry **4.18**) a terminal proton occurs. The findings suggest the prevalence of other polymer terminal groups but cannot be further evaluated due to lack of additional data. Both polymers show no signals in their MALDI-TOF-MS measurements presumably due to their elevated molecular weights ($M_{n\ PTPDF4}$ = 9.1 kg mol^{-1} and $M_{n\ PTPDF2BT}$ = 20 kg mol^{-1}).

5.1.8. Poly(benzodithiophene-*alt*-tetrafluorobenzene) - PBDTF4 and Poly(benzodi thiophene-*alt*-difluorobenzothiadiazole) - PBDTF2BT

MALDI-TOF-MS analysis of both miniemulsion (entry **4.21**) and solution polymerised PBDTF4 (entry **4.22**) are presented in figure 5.27 and figure 5.28. Entry **4.22** exhibits an additional pattern of tetrafluorobenzene homo couplings (◆).

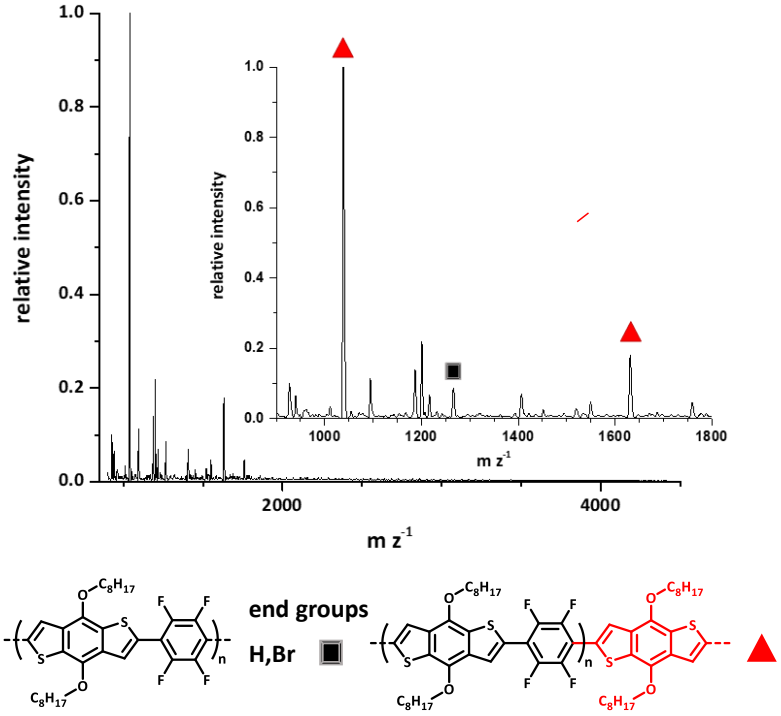

Figure 5.27: MALDI-TOF-MS spectra of entry **4.21**. Unless otherwise stated, polymer chains bear proton end groups.

In the case of PBDTF2BT, only the miniemulsion polymerisation batch (entry **4.23**, figure 5.29) was measured since no polymer was isolated from the solution polymerisation trial (entry **4.24**). Alongside proton side groups, bromine end groups were observed.

Because of the molecular weights obtained for both miniemulsion polymerisations ($M_{n\ BDTDF4}$ = 1.7 kg mol^{-1} and $M_{n\ BDTF2BT}$ = 1.7 kg mol^{-1}), no further analysis was performed by HT-NMR.

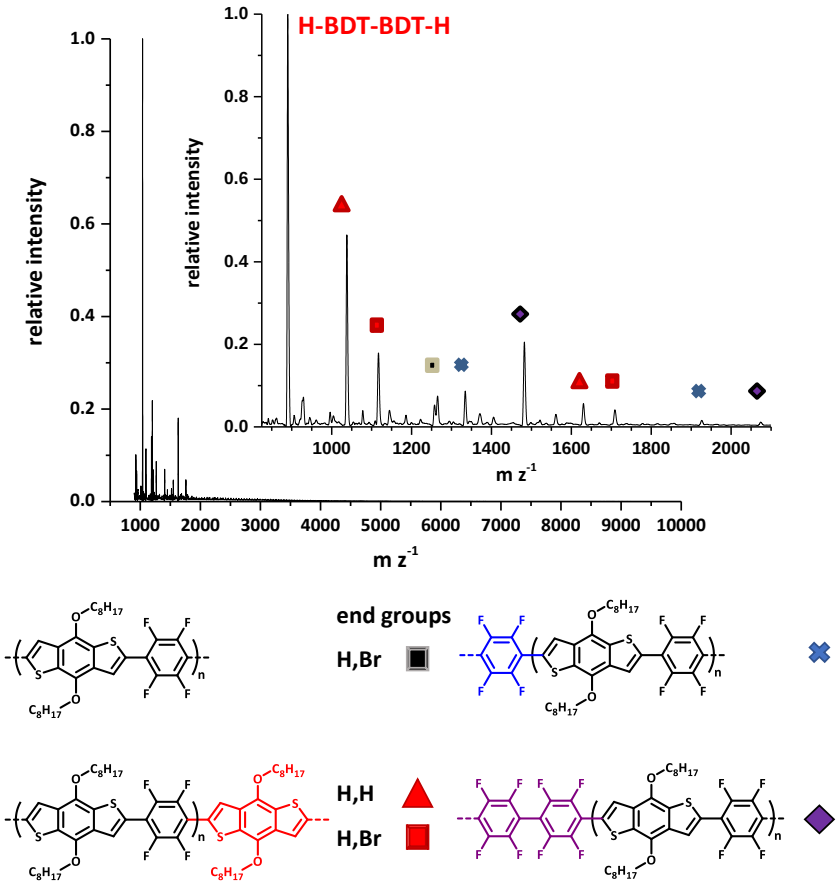

Figure 5.28: MALDI-TOF-MS spectrogram of **4.22**. Unless otherwise stated, polymer chains bear proton end groups.

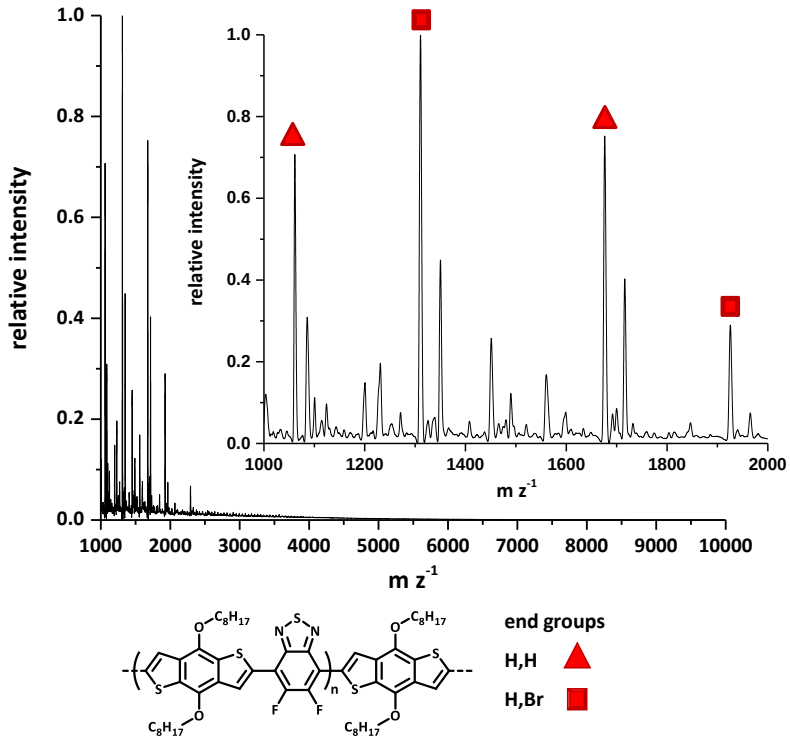

Figure 5.29: MALDI-TOF-MS spectrogra of entry **4.23**. Unless otherwise stated, polymer chains bear proton end groups.

5.2. Surfactant Removal by Dialysis

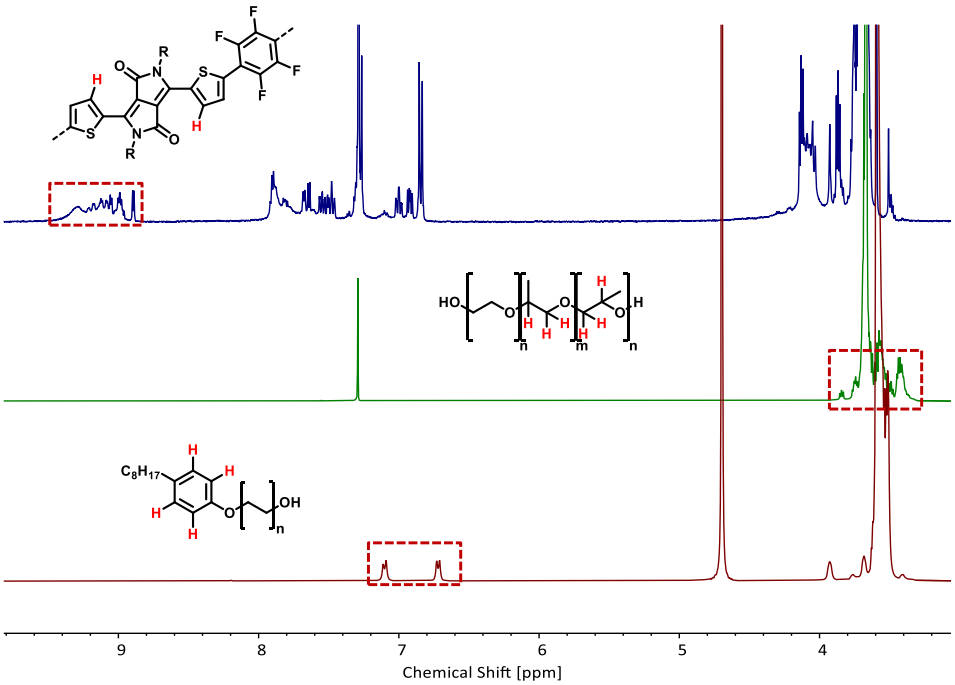

Figure 5.30: ^{1}H NMR spectra of entry **3.18** (blue, contains PDPPF4 and Triton X305), Synperonic F38 (green) and Triton X305 (red). The region below 3.0 ppm was omitted for clarity. The thiophene protons of PDPPF4 were compared against the surfactant's backbone protons to quantify the surfactant removal.

Removal of Triton X305 and the Synperonic F series was investigated to strip the CPNs from excess surfactant for subsequent application. While a surplus of surfactant facilitates the stability of the nanodroplets over the course of the miniemulsion polymerisation and the shelf life of the emulsion, the removal of the surfactant was considered essential to minimise the impact on OFET device performance (Chapter 6). For the dialysis of the CPNs, dialysis membranes were used with varying molecular weight cut-offs (MWCOs). To quantify the amount of surfactant removed, non-dialysed and dialysed samples were dried and subsequently dissolved in $CDCl_3$ for ^{1}H NMR analysis. The integration was normalised against the thienyl protons adjacent to the DPP core as depicted in figure 5.30. The amount of surfactant was then evaluated by integrating the signals of the backbone protons of the Synperonic F surfactants or the aromatic protons in case of Triton X305 (protons indicated in red in figure 5.30). Initial trials were conducted with MWCO 100 kg mol^{-1} tubes (Float-a-Lyzer®, cellulose ester membrane) for entries **3.18**

and **3.25** - **3.27** to compare the efficiency of removal for Triton X305 and the three Synperonic F38, F68 and F108 surfactants, respectively (table 5.3 and figure 5.31). For all four surfactants, their relative integral intensity of the remaining surfactant backbone protons tended to decrease with increasing dialysis time. According to the results presented in table 5.3, the remaining relative quantity of Triton X305 was 35 % after the first day of dialysis and subsequently decreased to 18 % after 3 days. A similar trend was observed for the Synperonic F surfactants decreasing from 39 % to 30 %, from 34 % to 16 % and 51 % to 16 % for F38, F68 and F108, respectively. Amongst the four surfactants, Synperonic F68 shows the least residual surfactant relative to PDPPF4 for this dialysis protocol.

Table 5.3: Relative remaining surfactant during and after dialysis with 100 kg mol^{-1} MWCO dialysis tubes of entries **3.18** and **3.25** - **3.27**.

entry	surfactant	remaining surfactant		
		1 day	2 days	3 days
3.18	Triton X305	35 %	28 %	18 %
3.25	Synperonic F38	39 %	37 %	30 %
3.26	Synperonic F68	34 %	19 %	16 %
3.27	Synperonic F108	51 %	37 %	31 %

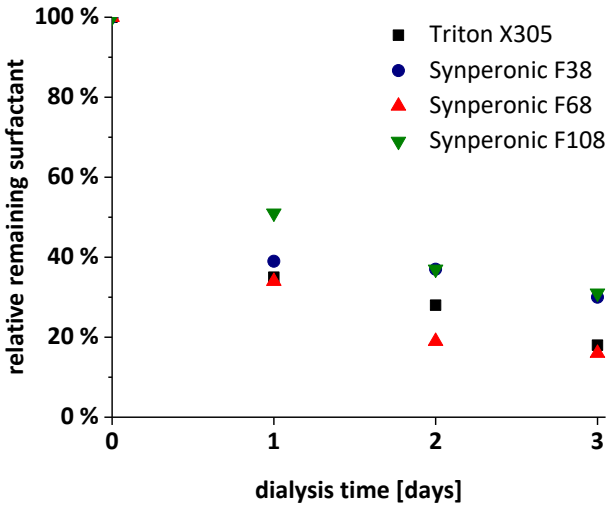

Figure 5.31: Normalised relative surfactant versus dialysis time for entries **3.18** and **3.25** - **3.27** dialysed with MWCO 100 kg mol^{-1} dialysis tubes.

In order to improve upon the ratio of total surfactant removed, 1000 kg mol^{-1} MWCO dialysis tubes were employed for entries **3.26** (Synperonic F68) and **3.27** (Synperonic F108) for prolonged dialysis times. The performance of the 1000 kg mol^{-1} MWCO dialysis tubes are presented and compared against the 100 kg mol^{-1} MWCO dialysis tubes in figure 5.32 and table 5.4 showing a total removal of 91 % in case of Synperonic F68 and 79 % for Synperonic F108. DLS data is not presented due to the elevated particle size dispersities measured already after reaction time for both entries.

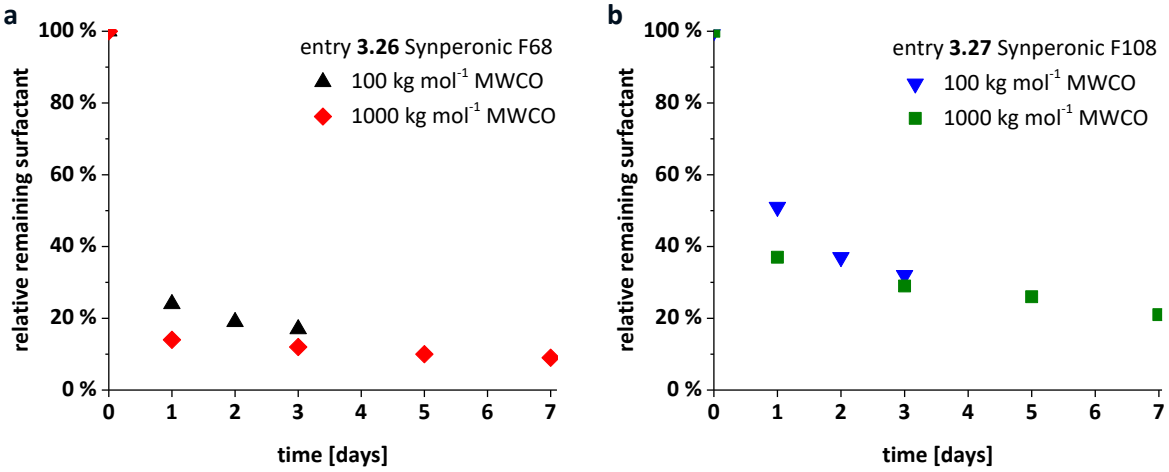

Figure 5.32: Relative remaining surfactant versus dialysis time for Synperonic F68 (entry **3.26**, a) and Synperonic F108 (entry **3.27**, b) for dialysis tubes with MWCO 100 and 1000 kg mol^{-1}.

Table 5.4: Remaining surfactant versus dialysis time quantified by NMR integral analysis for entries **3.26** and **3.27** with dialysis tubes of 100 and 1000 MWCO.

entry	surfactant	MWCO	remaining surfactant				
		[kg mol^{-1}]	1 day	2 days	3 days	5 days	7 days
3.26	Synperonic F68	100	34 %	19 %	16 %	-	-
		1000	14 %	-	12 %	10 %	9 %
3.27	Synperonic F108	100	51 %	37 %	31 %	-	-
		1000	37 %	-	29 %	26 %	21 %

To evaluate the impact of surfactant removal upon the particle size dispersities and emulsion stabilities, an additional set of nanoparticles containing Synperonic F68 were dialysed and measured for dispersions. These particle batches were prepared with elevated hydrophobe concentration ([hexadecane] = 0.85 M) since they gave lower PDIs (< 0.3) after

reaction rendering DLS measurements before and after dialysis valid. Quantification of the remaining surfactant for PDPPF2BT and PDPPTT was conducted in the same fashion as for PDPPF4 by NMR integral analysis. Table 5.5 presents the amount of remaining surfactant and the development of particle diameters and dispersities before and after dialysis for particles of PDPPF4, PDPPF2BT, PDPPTT, PNDIF4 and PNDIF2BT. The dialysis of PDPPF2BT and PDPPTT resulted in low amounts (9 % and 8 %) of residual Synperonic F68 as previously observed for PDPPF4 (entry **3.26**). The particle size dispersities increased in case of PDPPF2BT (entry **4.2**) and PDPPTT (entry **4.5**) indicating destabilisation of the dispersions upon surfactant removal. For the NDI copolymers (entries **4.11** and **4.13**), the integrals of the naphthalene protons (assigned as **5** and **6** in sections 5.1.5 and 5.1.6) were compared against the integrals of the Synperonic F68 backbone protons. The amount of the remaining surfactant is greater for both NDI copolymers compared to the presented DPP copolymers.

Table 5.5: Remaining surfactant quantified by NMR integral analysis for various copolymers with dialysis tubes of 1000 kg mol^{-1} MWCO and DLS analyses before and after dialysis.

entry	polymer	remaining surfactant	before dialysis size distribution[1] [nm]	PDI[1]	after dialysis size distribution[1] [nm]	PDI[1]
3.46	PDPPF4	18 %	282 ± 192 (95 %) 4013 ± 1163 (5 %)	0.27	215 ± 97 (100 %)	0.15
4.2	PDPPF2BT	9 %	192 ± 96 (100 %)	0.23	374 ± 100 (100 %)*	0.41
4.5	PDPPTT	8 %	153 ± 62 (100 %)	0.15	179 ± 100 (97 %) 2036 ± 952 (3 %)	0.23
4.11	PNDIF4	25 %	208 ± 95 (99 %) 4978 ± 619 (1 %)	0.18	157 ± 65 (100 %)*	0.16
4.13	PNDIF2BT	53 %	184 ± 97 (100 %)	0.20	162 ± 77 (99 %)* 31 ± 5 (1 %)	0.19

[1] DLS analysis of the size distribution and polydispersity index (PDI) at 25 °C. Integral ratios are presented in brackets. ***** Sample was subject to longer shelf-time prior to dialysis (~ ½ year, Covid-19 lockdown related). PDPPF4 (entry 3.38) and PDPPTT (entry 4.5) were dialysed prior to the 1st Covid-19 related lockdown and hence were analysed after lockdown upon their respective emulsion stabilities.

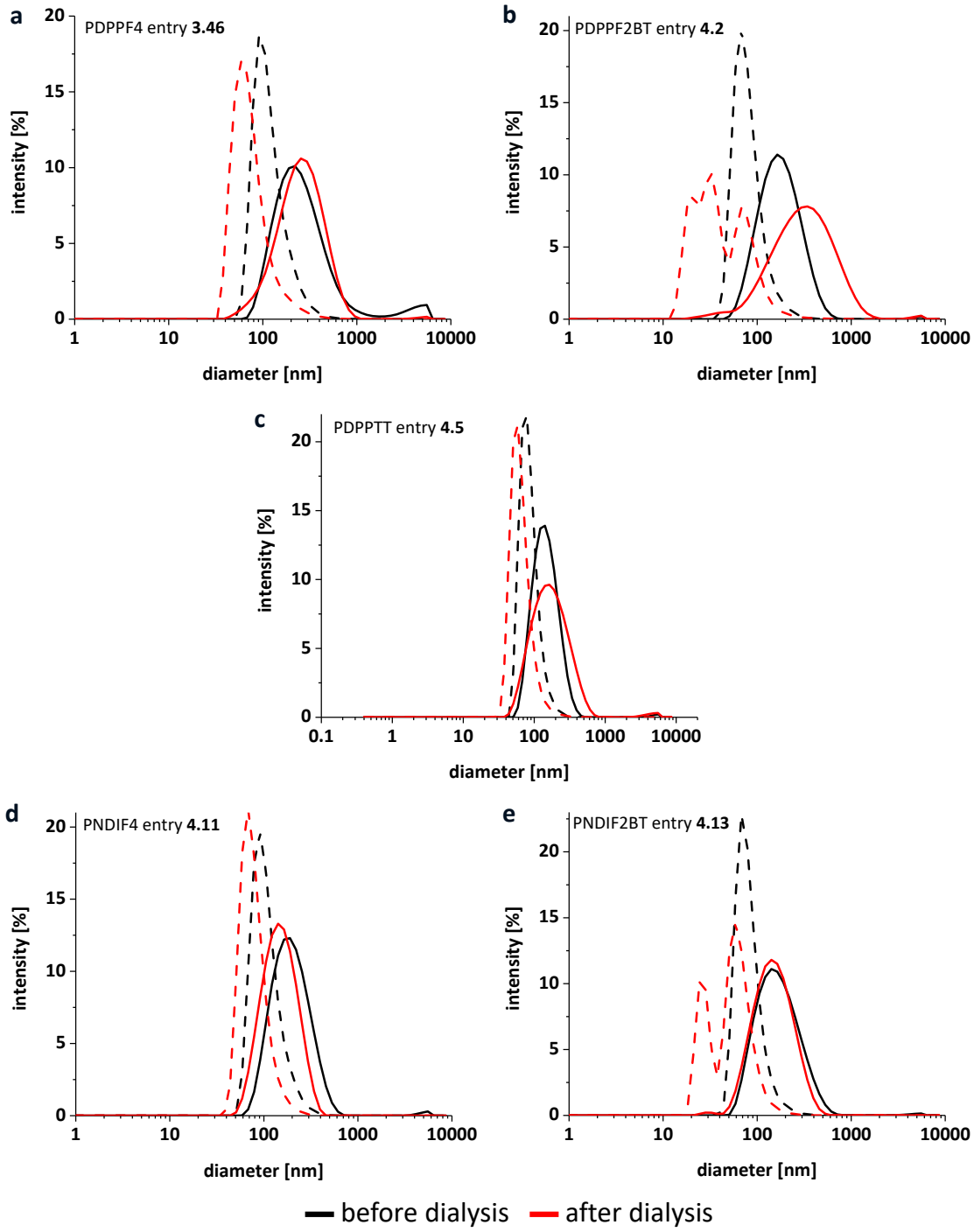

Figure 5.33: DLS number (dashed line) and intensity (straight line) distributions before and after dialysis of PDPPF4 (entry **3.46**, a), PDPPF2BT (entry **4.2**, b), PDPPTT (entry **4.5**, c), PNDIF4 (entry **4.11**, d) and PNDIF2BT (entry **4.13**, e).

Table 5.6 presents the DLS data for non-dialysed and dialysed batches of both samples and compares their DLS intensity size distributions and PDIs for those batches before and after their storage time. The non-dialysed PDPPF4 batch shows no change in particle diameter and dispersity indicating that this batch remained stable. The dialysed

PDPPF4 sample, on the contrary, showed a trimodal intensity distribution and an increased PDI. This result shows that the stability of the dialysed sample decreases upon surfactant removal and suggests prompt processing of dialysed particle batches. For PDPPTT (entry **4.2**), no destabilisation was observed for both the non-dialysed and dialysed batches indicating that emulsions can remain stable over prolonged times. Particle destabilisation upon dialysis might be either random or depends on the structure of the conjugated polymer backbone.

Table 5.6: Stability analysis of CPN batches of PDPPF4 (entry **3.46**) and PDPPTT (entry **4.5**) before and after a 6 months storage time.

entry	polymer	batch	no storage time		6 months storage	
			size distribution[1] [nm]	PDI[1]	size distribution[1] [nm]	PDI[1]
3.46	PDPPF4	non-dialysed	282 ± 192 (95 %) 4013 ± 1163 (5 %)	0.27	282 ± 150 (100 %)	0.23
		dialysed	215 ± 97 (100 %)	0.15	148 ± 83 (86 %) 20 ± 6 (11 %) 4267 ± 1000 (3 %)	0.45
4.5	PDPPTT	non-dialysed	153 ± 62 (100 %)	0.15	190 ± 109 (99 %) 4448 ± 903 (1 %)	0.23
		dialysed	179 ± 100 (97 %) 2036 ± 952 (3 %)	0.23	156 ± 142 (98 %) 4475 ± 930 (2 %)	0.24

[1] DLS analysis of the size distribution and polydispersity index (PDI) at 25 °C. Integral ratios are presented in brackets.

Additionally, the quantification of the remaining surfactant was conducted by DSC since the Synperonic F68 surfactant exhibits a melting point at 44 °C.[96] Figure 5.35 depicts the DSC traces of polymers PDPPF4, PDPPF2BT, PNDIF4 and PNDIF2BT before and after dialysis. To quantify the amount of residual surfactant, the melting heat of the surfactants ΔH within the respective samples were compared before and after the purification step. A similar trend is observed to the results of the NMR integral analysis: PDPPF2BT (entry **4.2**) shows the least remaining surfactant whereas the two NDI copolymers reveal greater contents of surfactant left. Overall, the ratios of remaining surfactant measured by DSC are in accordance with the data presented for NMR integral analysis except for PNIDF2BT

(entry **4.13**). For NDIF2BT, NMR integral analysis seems to overestimate the amount of residual Synperonic F68 (53 %) compared to the DSC analysis (25 %).

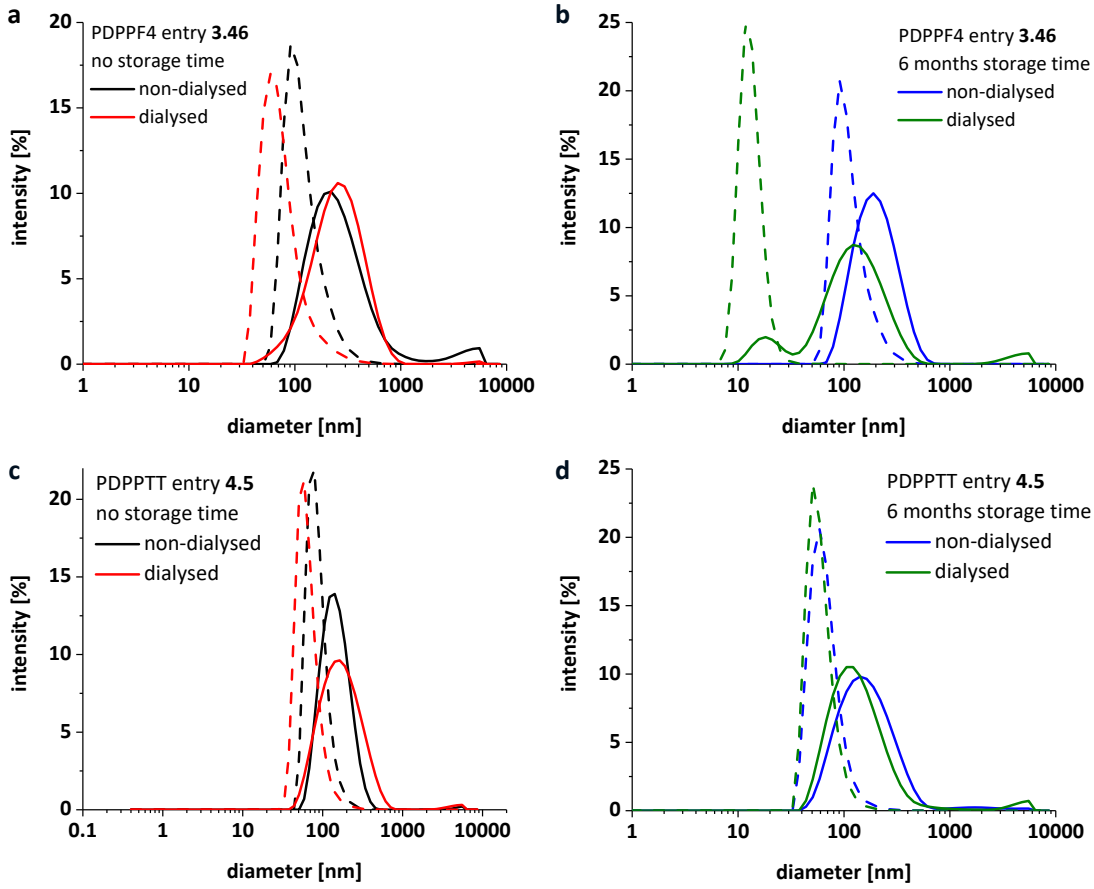

Figure 5.34 DLS number (dashed line) and intensity (straight line) distributions before (a and c) and after a shelf-time of 6 months (b and d) f PDPPF4 (entry **3.46**) and PDPPTT (entry **4.5**).

Table 5.7: Surfactant removal quantification by DSC.

entry			m_{DSC} [mg]	$\int m_{p,\ surfactant}$ [J g^{-1}]	ΔH [mJ]	remaining surfactant
3.46	PDPPF4	before dialysis	6.8	37.8	257	
		after dialysis	1.8	27.0	48.6	19 %
4.2	PDPPF2BT	before dialysis	5.7	42.3	241	
		after dialysis	2.4	14.4	34.7	14 %
4.11	PNDIF4	before dialysis	8.5	35.5	302	
		after dialysis	5.5	10.9	60.0	20 %
4.13	PNDIF2BT	before dialysis	5.6	36.6	205	
		after dialysis	2.1	20.4	42.8	21 %

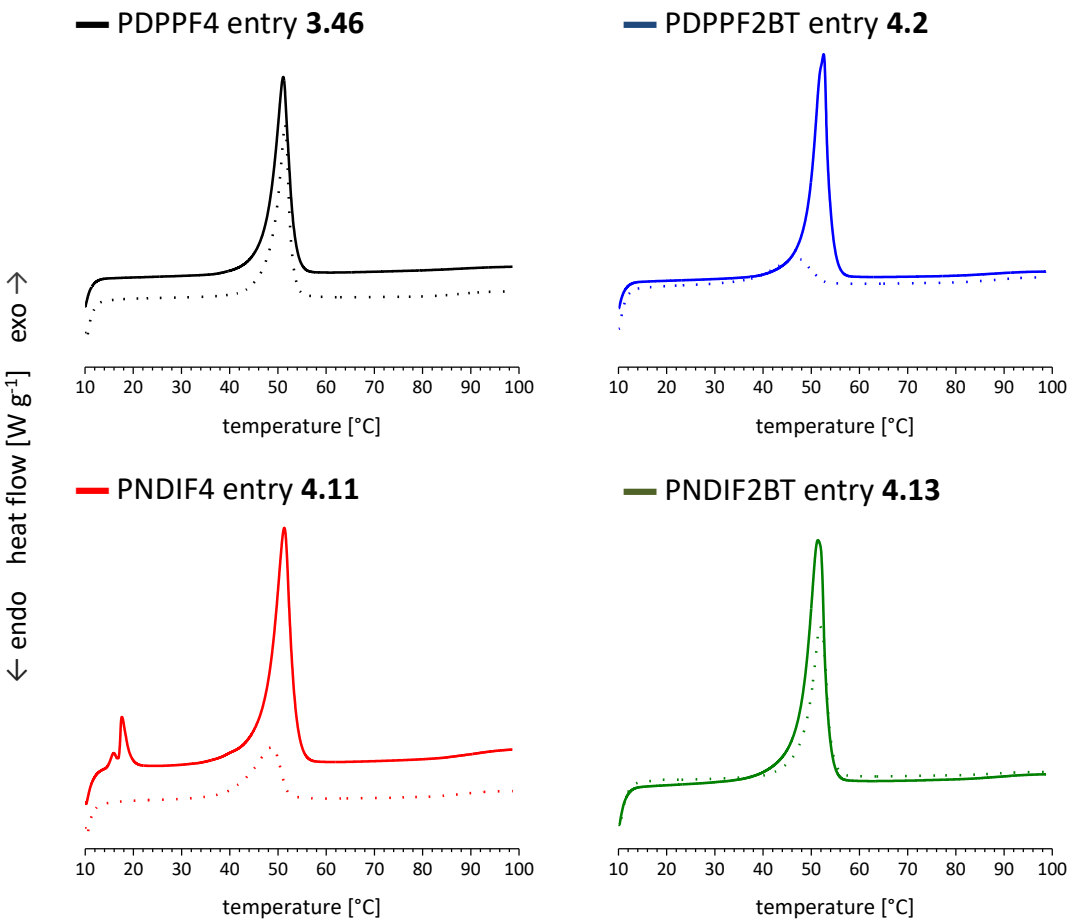

Figure 5.35: Quantification of surfactant removal by DSC. Sample before dialysis (straight line) and sample after (dashed line) dialysis.

5.3. Xylene Removal by Dialysis

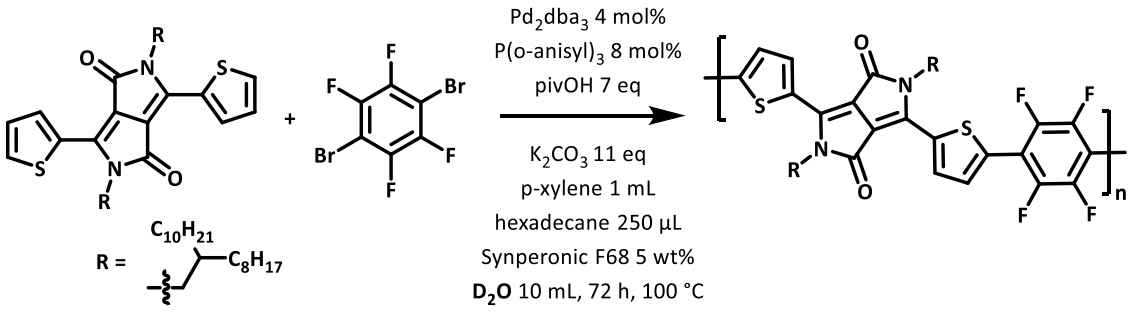

Scheme 5.1: DArP of DPPF4 in emulsion using D_2O as continuous phase.

Equally to the surfactant removal discussed in section 5.2, the removal of xylene was investigated by ^1H NMR techniques to quantify the removal of the solvent during the

dialysis process. Initial experiments with water as continuous phase indicated that the ^{1}H NMR water suppression experiment does not suffice to diminish the water peak. Hence, the optimised reaction conditions for entry **3.46** (section 3.4.8) were applied in D_2O as continuous phase (scheme 5.1). The molecular weight obtained for entry 5.1 is lower compared to entry 3.38, whereas particle sizes are in good agreement (table 5.8, figure 5.36).

Table 5.8: DArP of PDPPF4 in emulsion with D_2O as continuous phase.

entry	M_n[1] [kg mol^{-1}]	Đ[1]	size distribution[2] [nm]	PDI[2]
3.46	9.5	2.2	282 ± 192 (95 %) 4013 ± 1163 (5 %)	0.25
5.2	5.9	1.9	180 ± 74 (97 %) 2102 ± 758 (2 %) 4732 ± 727 (1 %)	0.15

Pd_2dba_3 4 mol%, P(*o*-anisyl)$_3$ 8 mol%, p-xylene 1mL, [monomer] 0.20 M, [hexadecane] 250 μL_{HD} mL_{xyl}^{-1}, K_2CO_3 11 eq., pivalic acid 7 eq., Synperonic F68 500 mg in 10 mL water at 100 °C for 72 h. GPC in THF vs. narrow polydispersity polystyrene standards. [2] DLS analysis of the size distribution and polydispersity index (PDI) at 25 °C. Integral ratios are presented in brackets.

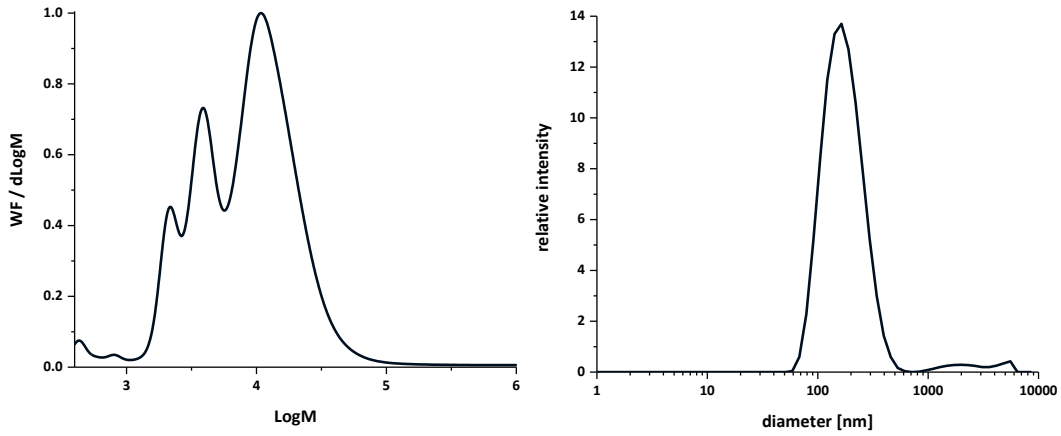

Figure 5.36: Normalised GPC trace (a) and DLS intensity distribution (b) of entry **5.2**.

The removal of xylene by dialysis was conducted in D_2O with 1000 kg mol^{-1} MWCO dialysis tubes and the samples were measured with ^{1}H NMR D_2O water suppression experiments. The integral of the thienyl protons of PDPPF4 were compared with the

integral of the aryl protons of p-xylene (figure 5.37). Table 5.9 presents that all p-xylene can be removed by dialysis over the course of 7 days.

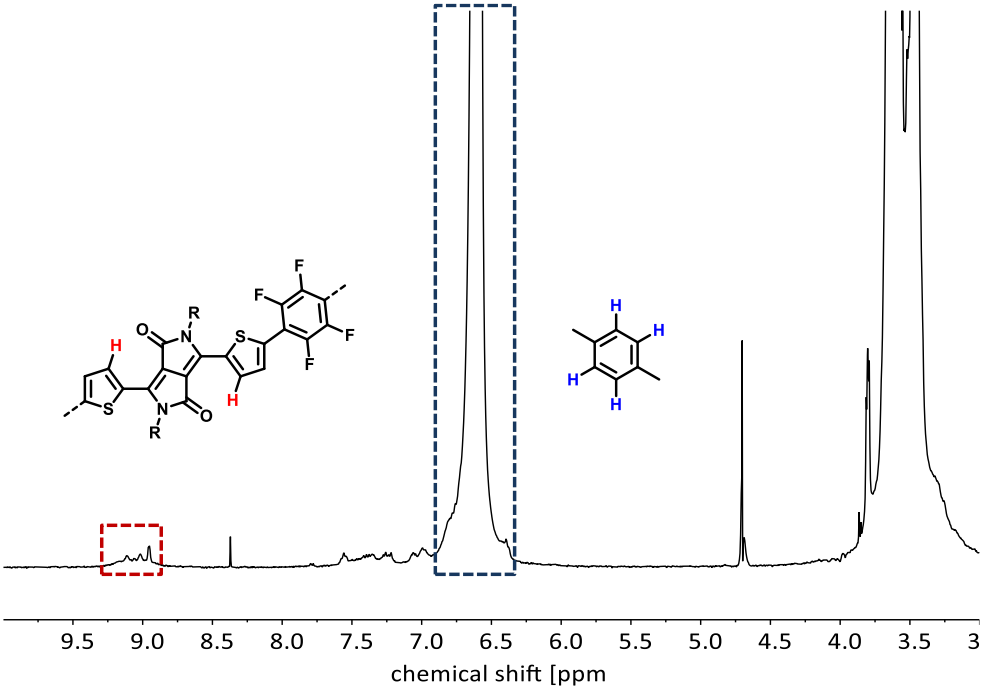

Figure 5.37: ^{1}H NMR spectra of entry **5.2** in D_2O. Region below 3.0 ppm emitted for clarity. The integral intensity of the thienyl protons of PDPPF4 were compared against the integral of the aryl protons of p-xylene to quantify the solvent removal.

Table 5.9: Remaining p-xylene during and after dialysis in D_2O of entry **5.2**.

remaining p-xylene				
start	1 day	3 days	5 days	7 days
100 %	88 %	14 %	2 %	0 %

5.4. UV/Vis Absorption Evaluation of the Polymers and Corresponding Polymer Nanoparticles

The UV/Vis absorption spectra of the polymers were measured as solution in chloroform, dispersed in water and as spin coated thin film (as spun) to investigate their absorption behaviour (figure 5.38 - figure 5.45). For the DPP containing copolymers, the first absorption band within 300 – 500 nm corresponds to the π-π* transition of the

polymers. The additional vibronic feature at longer wavelengths is the intramolecular charge transfer (ICT) band of the push-pull π-conjugated monomer units presented. All spectra were normalised on the maximum of their ICT bands. Comparing the polymers prepared in organic solvent with the miniemulsion polymerised compounds (graph a in figure 5.38 - figure 5.45), a molecular weight dependency becomes obvious whether λ_{max} is bathochromic or hypsochromic shifted. In most cases, the polymers isolated from the solution polymerisation resulted in a blue shift for λ_{max} in the absorption maxima over the corresponding miniemulsion analogues.

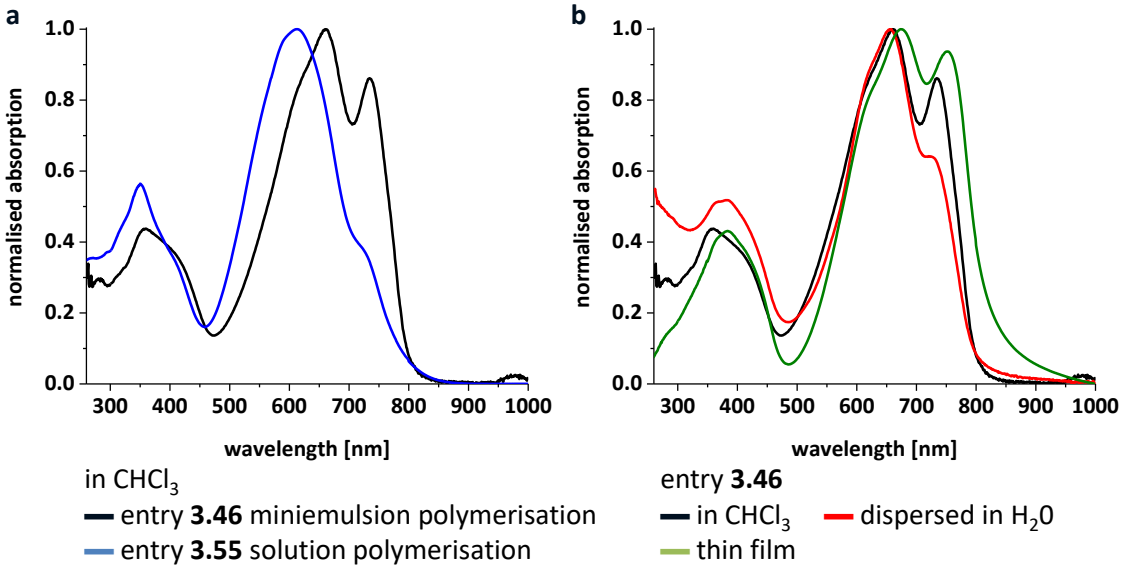

Figure 5.38: UV/Vis absorption of miniemulsion and solution polymerised PDPPF4 in chloroform (a). Miniemulsion polymerised PDPPF4 absorption measured in different media (b).

Table 5.10: λ_{A0}, λ_{A1}, λ_{onset}, A_1/A_0 and E_g of PDPPF4.

entry	M_n[1] [kg mol^{-1}]	measurement media	λ_{A0} [nm]	λ_{A1} [nm]	A_1/A_0	λ_{onset} [nm]	E_g [eV]
3.55	3.2	$CHCl_3$	612	-	-	790	1.57
3.46	9.5	$CHCl_3$	661	735	0.86	800	1.55
		H_2O	657	725	0.64	795	1.56
		thin film	674	752	0.94	820	1.51

[1] GPC in THF at rt vs. narrow polydispersity polystyrene standards.

PDPPF4 and PDPPF2BT show an additional peak that has been reported to correspond to aggregation due to π-π stacking (labelled as A_1 whereas $\lambda_{max\ ICT}$ is labelled A_0, figure 5.38 and figure 5.39).[85,121,133] Interestingly, the degree of aggregation is less pronounced within the CPNs dispersed in water compared to the respective polymers dissolved in chloroform (ratio A_1/A_0 in table 5.10 and table 5.11). A trend towards hypsochromic shifts for λ_{max} and λ_{onset} is observed comparing each sample dissolved in chloroform, dispersed in water and in solid state (as spun film) for all samples except PDPPF4 and PDPPF2BT (graph b in figure 5.40 - figure 5.45).

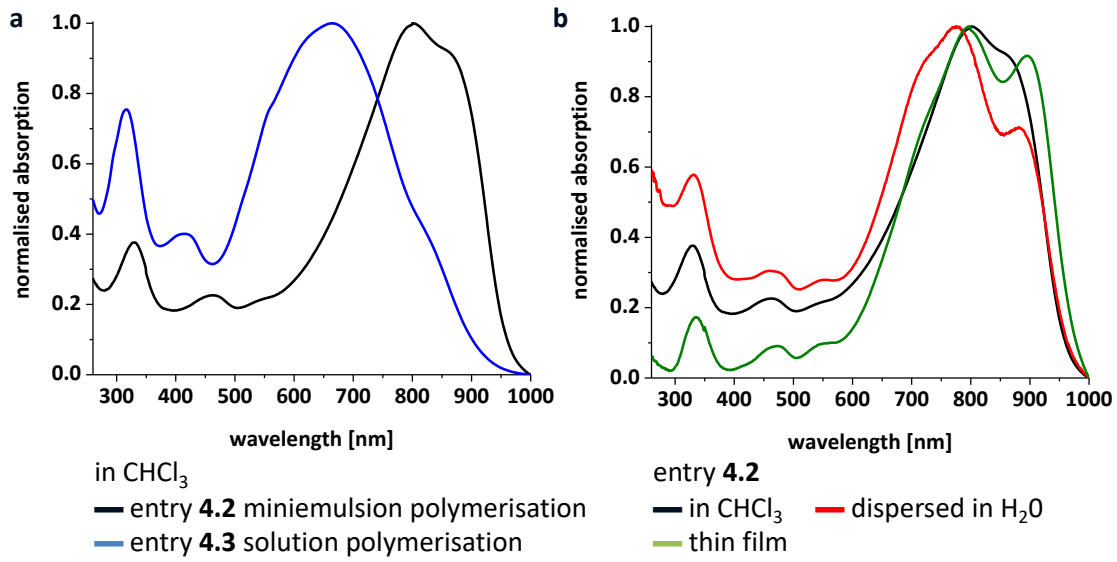

Figure 5.39: UV/Vis absorption of miniemulsion and solution polymerised PDPPF2BT in chloroform (a). Miniemulsion polymerised PDPPF2BT absorption measured in different media (b).

Table 5.11: λ_{A0}, λ_{A1}, λ_{onset}, A_1/A_0 and E_g of PDPPF2BT.

entry	M_n[1] [kg mol^{-1}]	measurement media	λ_{A0} [nm]	λ_{A1} [nm]	A_1/A_0	λ_{onset} [nm]	E_g [eV]
4.3	4.9	$CHCl_3$	665	-	-	914	1.36
4.2	11	$CHCl_3$	800	853	0.93	959	1.29
		H_2O	775	880	0.71	961	1.29
		thin film	798	895	0.92	974	1.27

[1] GPC in TCB at 120 °C vs. narrow polydispersity polystyrene standards.

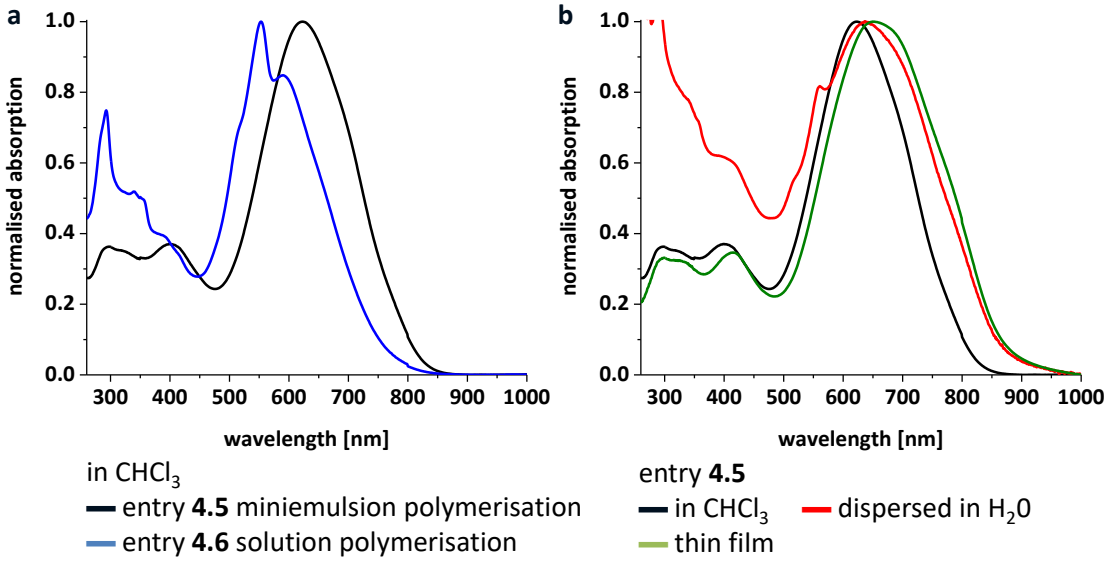

Figure 5.40: UV/Vis absorption of miniemulsion and solution polymerised PDPPTT in chloroform (a). Miniemulsion polymerised PDPPTT absorption measured in different media (b).

Table 5.12: λ_{max}, λ_{onset} and E_g of PDPPTT.

entry	M_n[1] [kg mol^{-1}]	measurement media	$\lambda_{max\ ICT}$ [nm]	λ_{onset} [nm]	E_g [eV]
4.5	5.6	$CHCl_3$	553	745	1.66
4.6	11	$CHCl_3$	623	792	1.57
		H_2O	636	851	1.46
		thin film	650	849	1.46

[1] GPC in TCB at 120 °C vs. narrow polydispersity polystyrene standards.

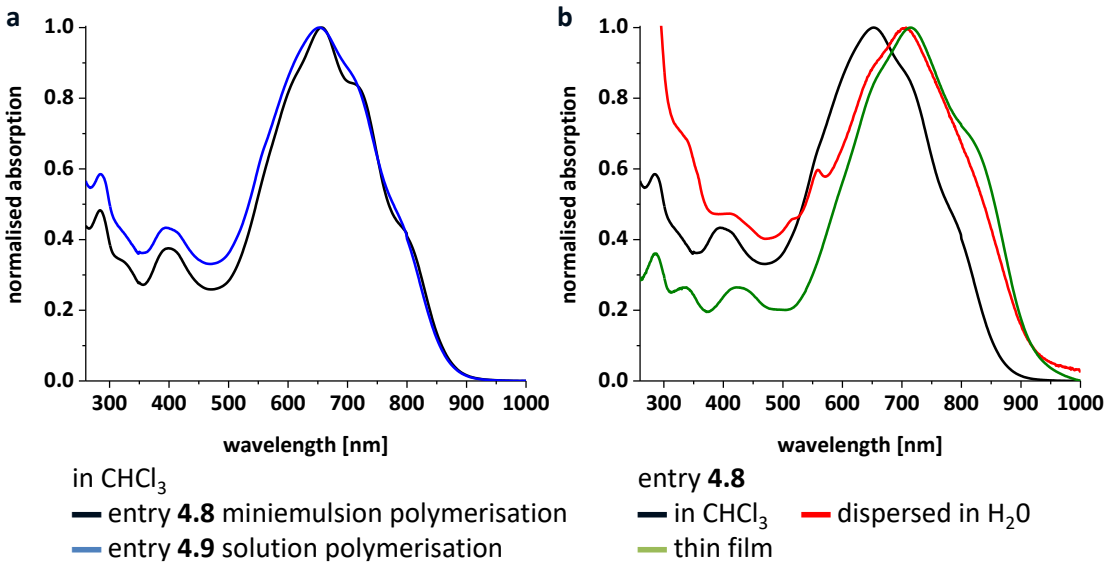

Figure 5.41: UV/Vis absorption of miniemulsion and solution polymerised PDPPTPD in chloroform (a). Miniemulsion polymerised PDPPTPD absorption measured in different media (b).

Table 5.13: λ_{max}, λ_{onset} and E_g of PDPPTPD.

entry	M_n[1] [kg mol^{-1}]	measurement media	$\lambda_{max\ ICT}$ [nm]	λ_{onset} [nm]	E_g [eV]
4.5	5.6	$CHCl_3$	652	863	1.44
4.6	11	$CHCl_3$	656	867	1.43
		H_2O	707	910	1.36
		thin film	715	916	1.35

[1] GPC in TCB at 120 °C vs. narrow polydispersity polystyrene standards.

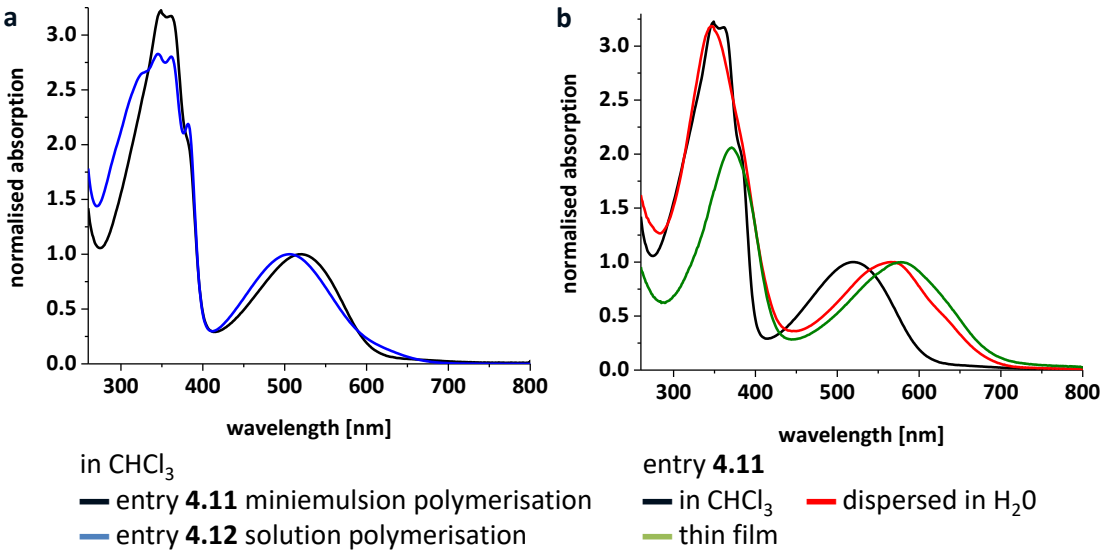

Figure 5.42: UV/Vis absorption of miniemulsion and solution polymerised PNDIF4 in chloroform (a). Miniemulsion polymerised PNDIF4 absorption measured in different media (b).

Table 5.14: λ_{max}, λ_{onset} and E_g of PNDIF4.

entry	M_n[1] [kg mol^{-1}]	measurement media	$\lambda_{max\ ICT}$ [nm]	λ_{onset} [nm]	E_g [eV]
4.12	1.3	$CHCl_3$	507	611	2.03
4.11	5.6	$CHCl_3$	521	606	2.05
		H_2O	566	689	1.80
		thin film	578	689	1.80

[1] GPC in TCB at 120 °C vs. narrow polydispersity polystyrene standards.

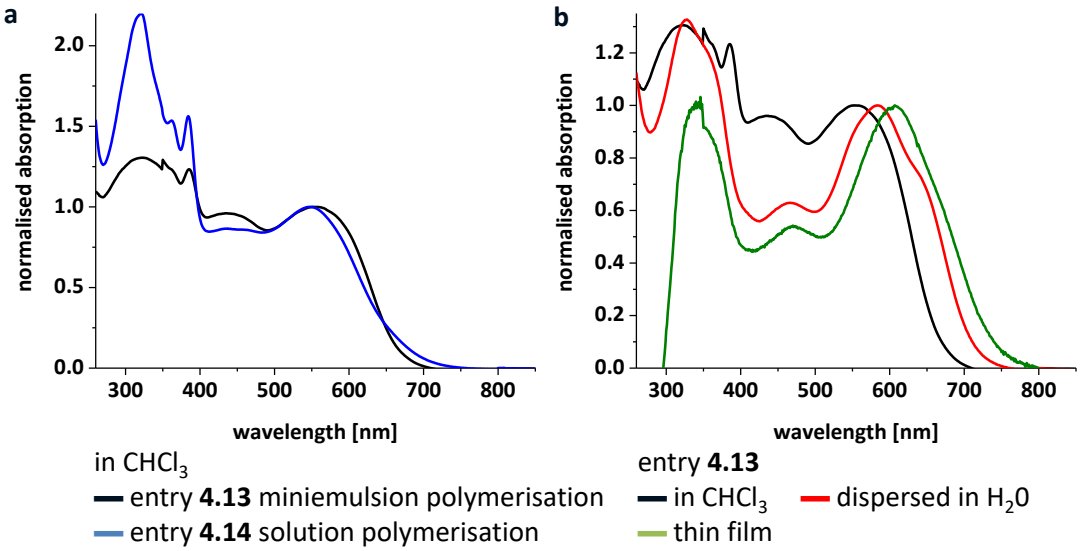

Figure 5.43: UV/Vis absorption of miniemulsion and solution polymerised PNDIF2BT in chloroform (a). Miniemulsion polymerised PNDIF2BT absorption measured in different media (b).

Table 5.15: λ_{max}, λ_{onset} and E_g of PNDIF2BT.

entry	M_n[1] [kg mol^{-1}]	measurement media	$\lambda_{max\ ICT}$ [nm]	λ_{onset} [nm]	E_g [eV]
4.14	1.8	$CHCl_3$	547	667	1.86
4.13	8.8	$CHCl_3$	553	665	1.86
		H_2O	583	709	1.75
		thin film	607	734	1.69

[1] GPC in TCB at 120 °C vs. narrow polydispersity polystyrene standards.

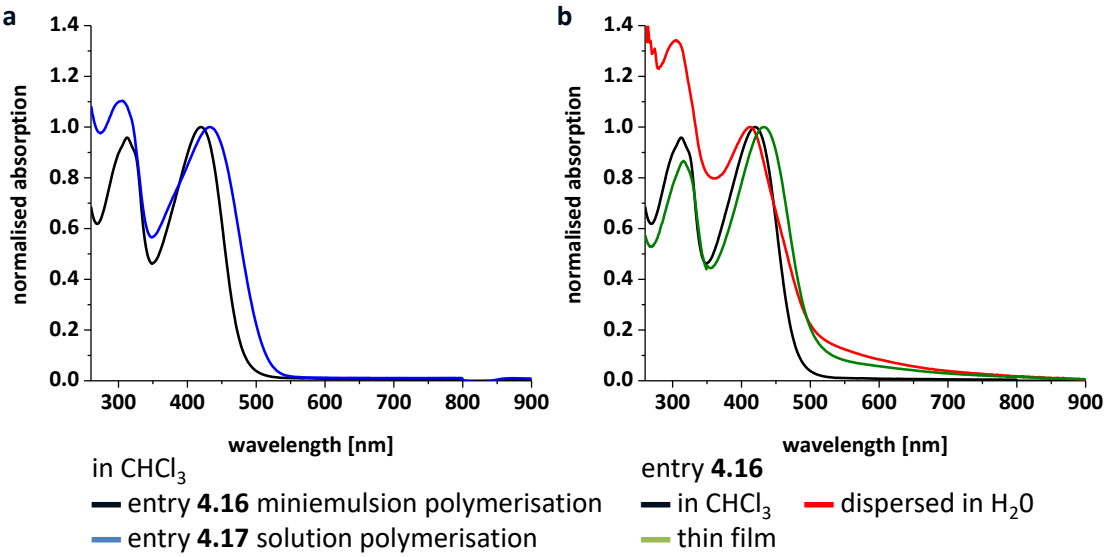

Figure 5.44: UV/Vis absorption of miniemulsion and solution polymerised PTPDF4 in chloroform (a). Miniemulsion polymerised PTPDF4 absorption measured in different media (b).

Table 5.16: λ_{max}, λ_{onset} and E_g of PTPDF4.

entry	M_n[1] [kg mol^{-1}]	measurement media	$\lambda_{max\ ICT}$ [nm]	λ_{onset} [nm]	E_g [eV]
4.17	4.3	$CHCl_3$	433	509	2.44
4.16	9.1	$CHCl_3$	412	478	2.59
		H_2O	420	504	2.46
		thin film	433	503	2.46

[1] GPC in TCB at 120 °C vs. narrow polydispersity polystyrene standards

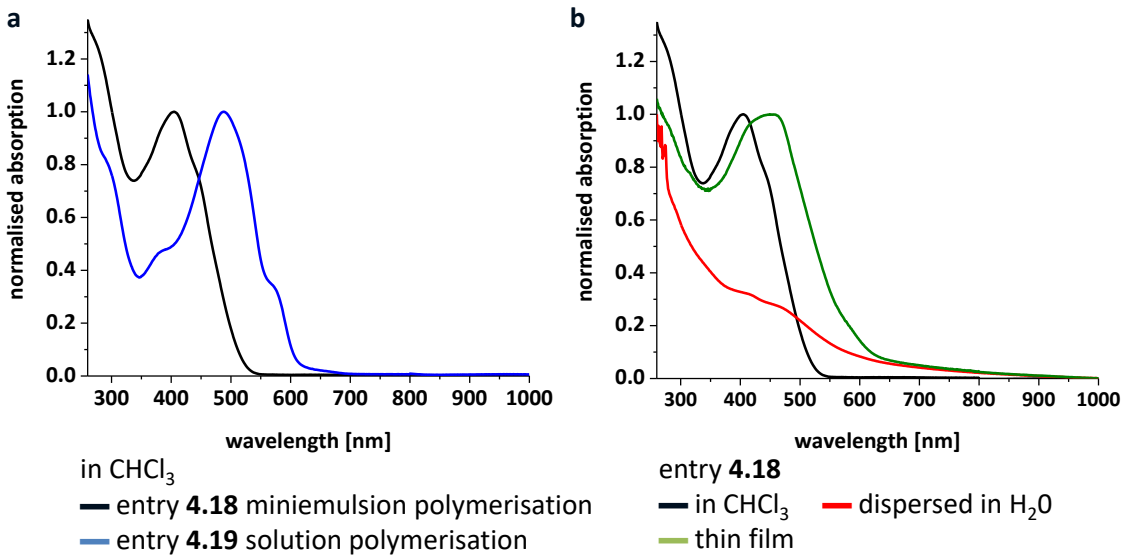

Figure 5.45:UV/Vis absorption of miniemulsion and solution polymerised PTPDF2BT in chloroform (a). Miniemulsion polymerised PTPDF2BT absorption measured in different media (b).

Table 5.17: λ_{max}, λ_{onset} and E_g of PTPDF2BT.

entry	M_n[1] [kg mol^{-1}]	measurement media	$\lambda_{max\ ICT}$ [nm]	λ_{onset} [nm]	E_g [eV]
4.19	11	$CHCl_3$	488	610	2.03
4.18	20	$CHCl_3$	405	506	2.45
		H_2O	-	607	2.04
		thin film	450	568	2.18

[1] GPC in TCB at 120 °C vs. narrow polydispersity polystyrene standards.

5.5. Scanning Transmission Electron Microscopy (STEM) Images

The objective of the STEM analysis was to verify the particle sizes and dispersities of the CPNs measured by DLS since previous reports revealed that anisotropic CPN shapes render DLS data insufficient to determine the particles actual dimensions.[1,3] CPN samples were prepared on a holey carbon grid and were thermally treated prior to measurement. The sample preparation and the image processing performed in Python are described in detail in section 8.1. The respective images of CPNs consisting of PDPPF4 (entry **3.46**), PDPPF2BT (entry **4.2**) and PDPPTT (entry **4.5**), their statistical evaluation of their equivalent diameters and particle shape eccentricities (0 implies circularity) are presented in figure 5.46, figure 5.47 and figure 5.48. The particle size analyses from TEM are coherently smaller than the DLS data presented (table 5.18). Moreover, the uncertainties seen from the DLS data are greater than those obtained by TEM. The statistical evaluation of the mean particle size was conducted through first removing particles of diameters smaller than 40 nm since particles relating to those diameters were assumed to be micelles. Micrometer sized CPN aggregates were observed for all samples (green arrow in figure 5.46) corroborating the second distribution in the micrometer regime observed by DLS. The presence of these aggregates indicates a stability issue of the CPN emulsions despite the elevated hexadecane concentration used ([hexadecane] = 0.85 M).

Table 5.18: DLS and TEM Size analyses of CPNs of PDPPF4, PDPPF2BT and PDPPTT.

entry	polymer	M_n[1] [kg mol^{-1}]	Đ[1]	size distribution[2] [nm]	PDI[2]	eq. diameter[3] [nm]
3.46	PDPPF4	7.2	1.7	282 ± 192 (95 %) 4013 ± 1163 (5 %)	0.25	133 ± 82
4.2	PDPPF2BT	11	2.2	192 ± 96 (100 %)	0.23	142 ± 80
4.5	PDPPTT	11	3.2	351 ± 297 (97 %) 4520 ± 897 (3 %)	0.35	159 ± 71

[1] GPC in TCB at 120 °C vs. narrow polydispersity polystyrene standards. [2] DLS analysis of the size distribution and polydispersity index (PDI) at 25 °C. Integral ratios are presented in brackets. [3] Particle size analysis from STEM data of over 1000 individual particles, processed in Python.

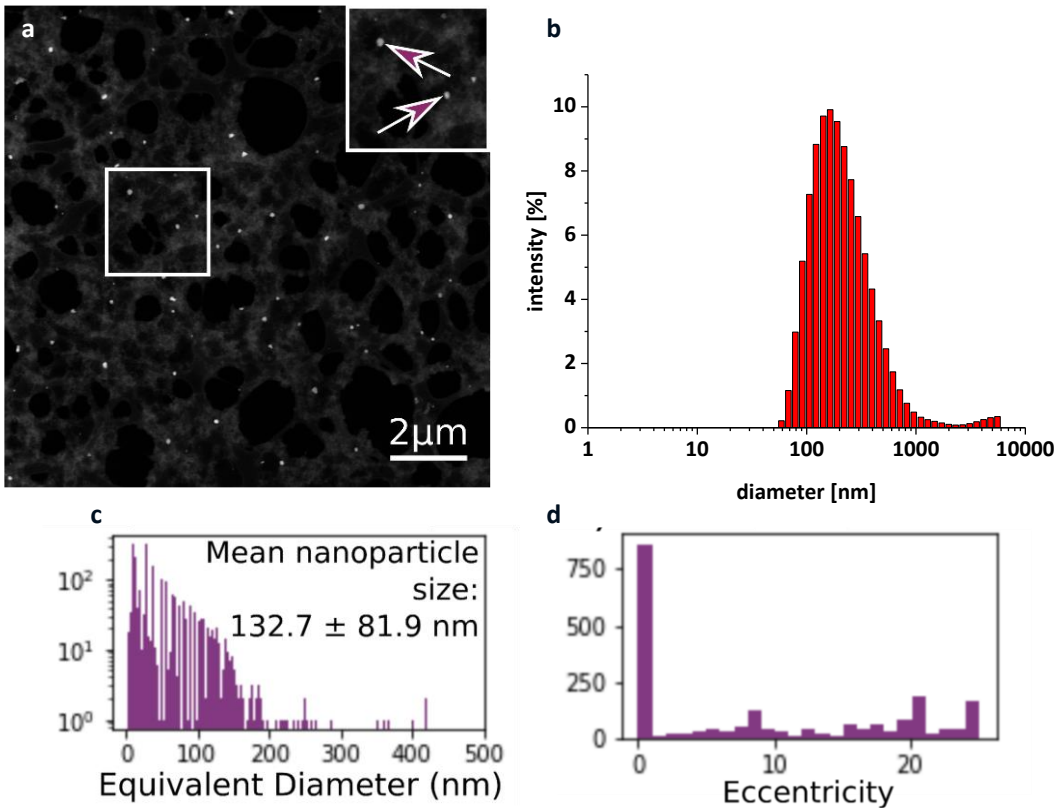

Figure 5.46: Annular dark field (ADF) STEM image of PDPPF4 CPNs (a). [2] DLS analysis of the intensity size distribution and polydispersity index (PDI) at 25 °C (b). Particle size analysis from STEM data of over 1000 individual particles, processed in Python (c). Eccentricities from particle size analysis (d).

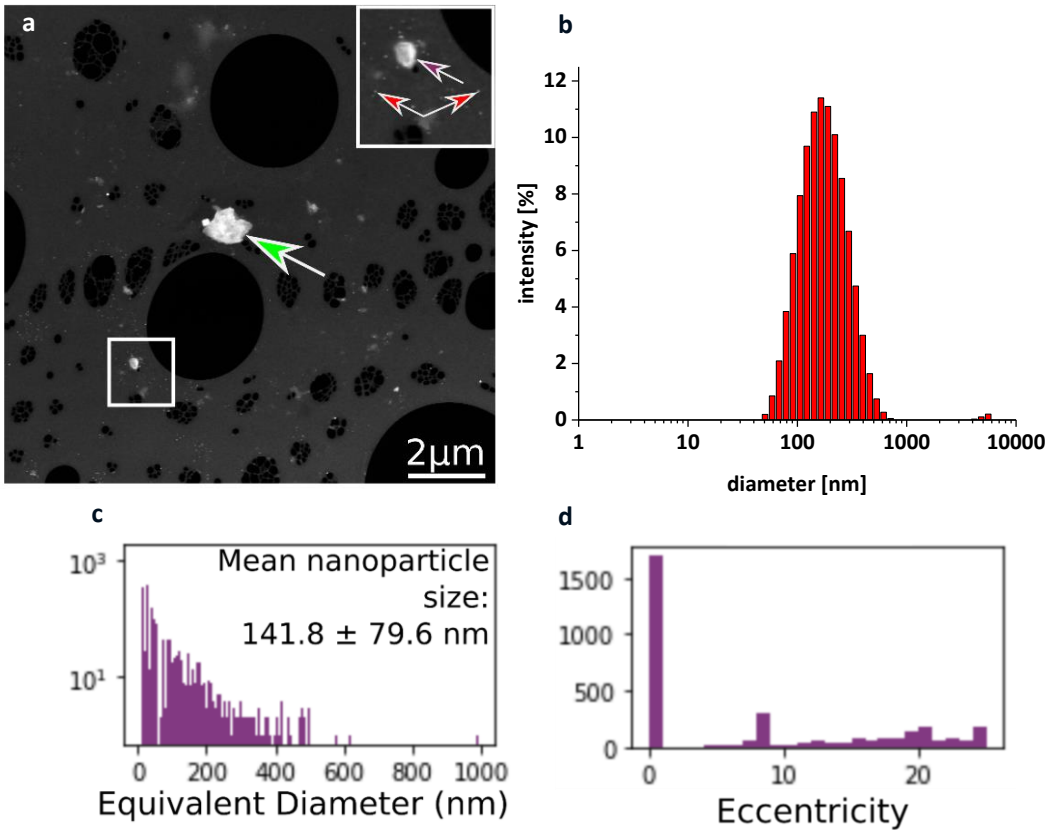

Figure 5.47: ADF STEM image of PDPPF2BT CPNs (a). [2] DLS analysis of intensity size distribution and polydispersity index (PDI) at 25 °C (b). Particle size analysis from STEM data of over 1000 individual particles, processed in Python (c). Eccentricities from particle size analysis (d).

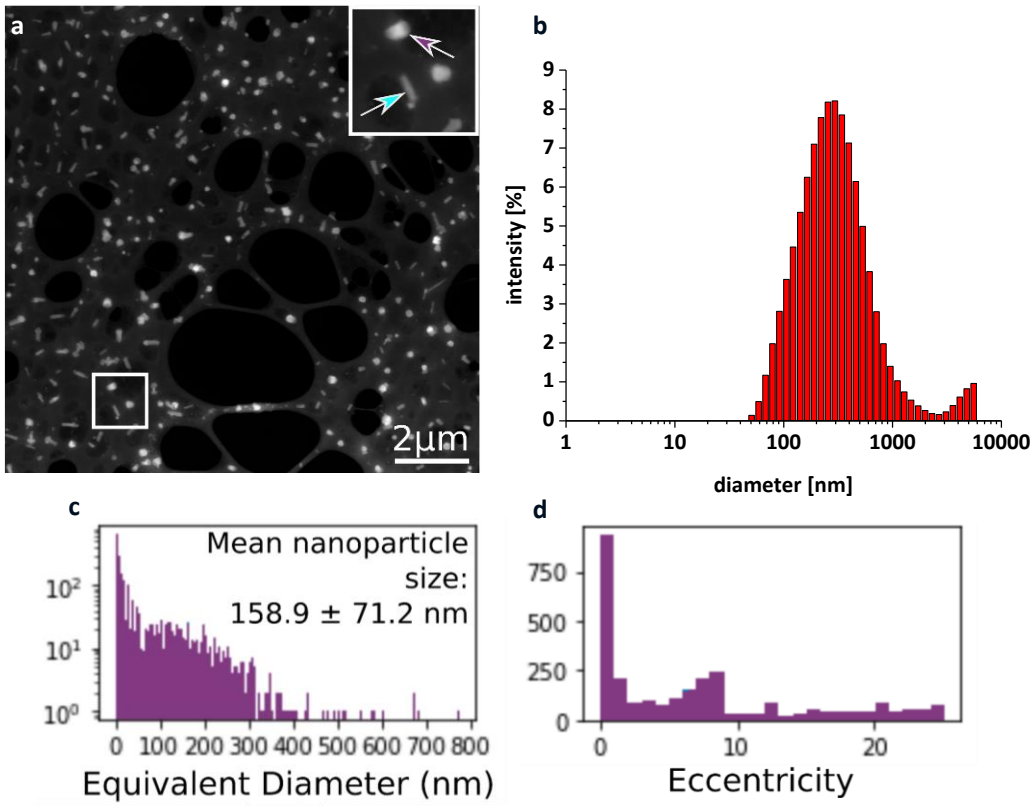

Figure 5.48: ADF STEM image of PDPPTT CPNs (a). [2] DLS analysis of intensity size distribution and polydispersity index (PDI) at 25 °C (b). Particle size analysis from STEM data of over 1000 individual particles, processed in Python (c). Eccentricities from particle size analysis (d).

The high population of nanoparticles possessing 0 eccentricity for CPNs made of PDPPF4 and PDPPF2BT implies circularity. On the contrary, PDPPTT shows the most rod-shaped nanoparticles. The anisotropic particle shapes seem to lead to overestimation of the particle size dispersity of entry **4.5** measured by DLS. It is noteworthy that PDPPTT particles were manufactured after the 1st Covid-related lockdown whereas PDPPF4 and PDPPF2BT were subject to longer shelf-times (6 moths) before their measurement. Hence, a particle shape evolution from anisotropic to isotropic shapes due to coalescence cannot be excluded. STEM analysis has demonstrated that the particles sizes obtained by DLS overestimate the diameter of the particles. This overestimation is attributed to solvent-induced particle swelling in case of the DLS measurements whereas the particles were subjected to vacuum during the STEM measurements causing a decrease of their diameter.

5.6. Thermal Properties of the Polymers obtained

Thermogravimetric analysis (TGA) was conducted to measure the onset of decomposition of the respective polymers (T_d) and are summarised in table 5.19. The TGA graphs for PDPPF4 and PDPPF2BT are presented in figure 5.49 and for the remaining DPP copolymers, NDI and TPD based polymers are illustrated in figure 5.50. The findings are in accordance with previous reports of polymers PDPPF4[85], PDPPF2BT[121], PDPPTT[122], PDPPTPD[138], PNDIF4[126] and PNDIF2BT[127]. Samples that were dialysed prior to their TGA measurements (i.e. PDPPF4 and PDPPTTPD) revealed lower residual amounts compared to the non-dialysed samples PDPPF2BT, PDPPTT, PNDIF4, PNDIF2BT, PTPDF4 and PTPDF2BT.

Table 5.19: Onset of decomposition determined by TGA.

entry	polymer	T_d [°C]
3.46	PDPPF4	406
4.2	PDPPF2BT	401
4.5	PDPPTT	376
4.8	PDPPTPD	401
4.11	PNDIF4	412
4.13	PNDIF2BT	462
4.16	PTPDF4	372
4.18	PTPDF2BT	413

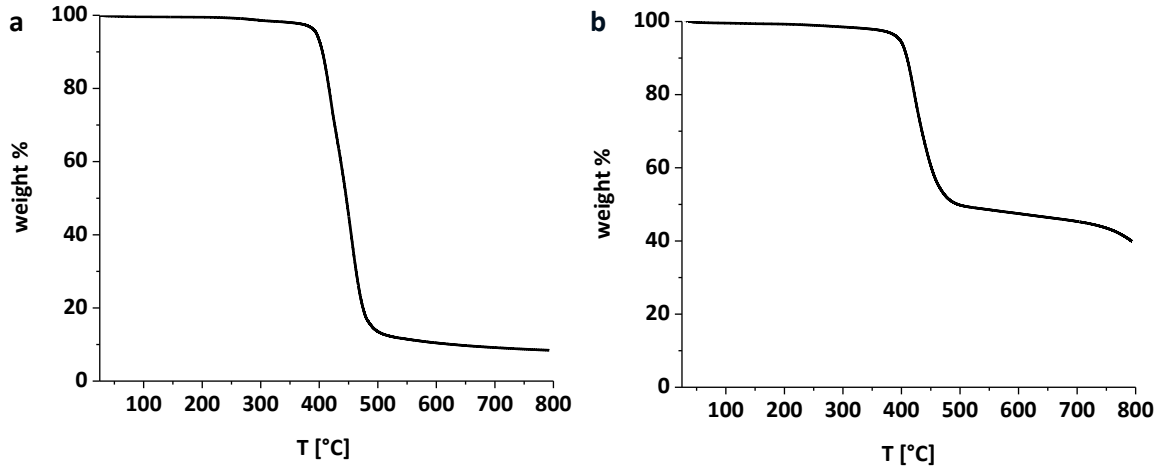

Figure 5.49: Thermogravimetric analysis of PDPPF4 (a), PDPPF2BT (b).

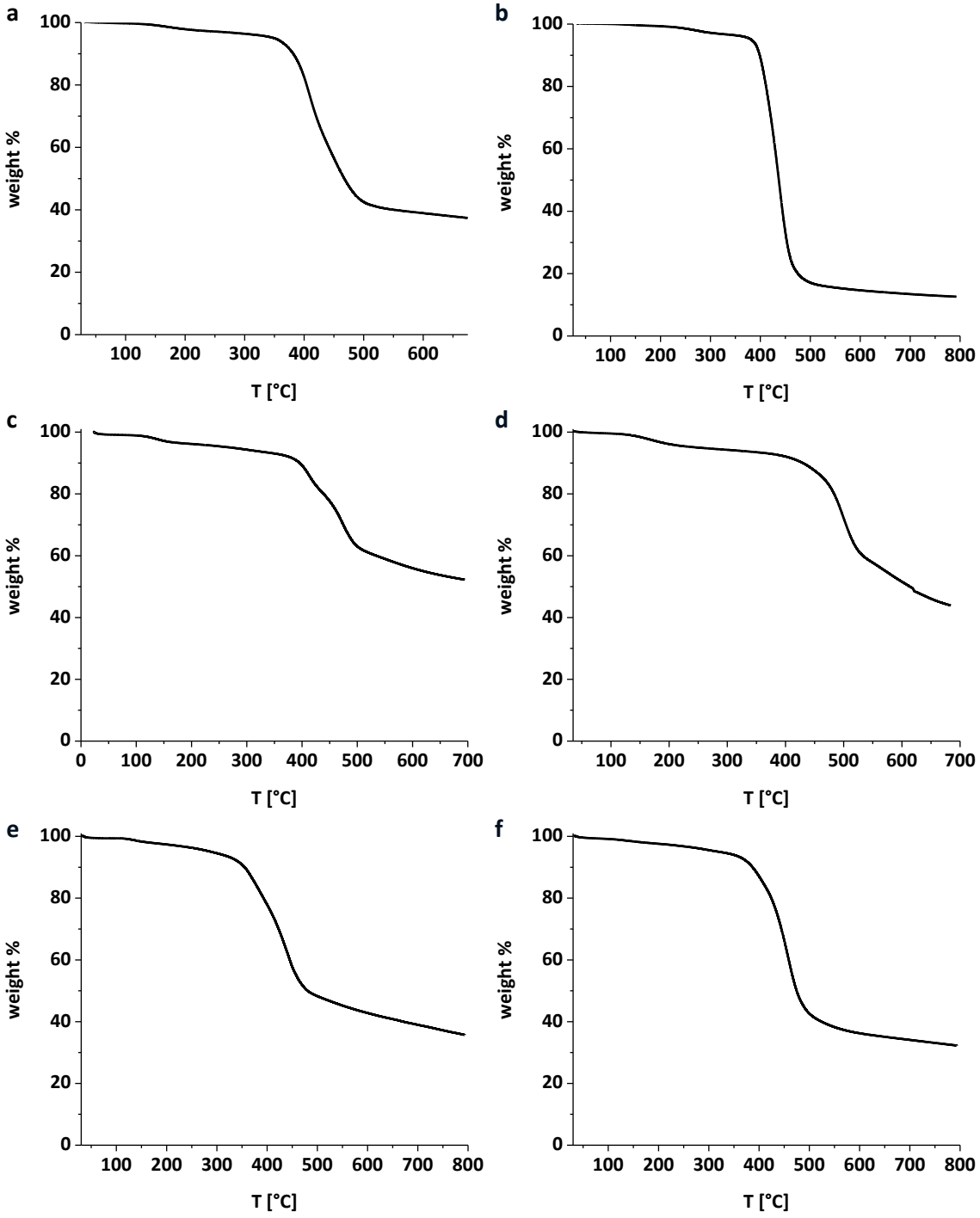

Figure 5.50: Thermogravimetric analysis of PDPPTT (a), PDPPTPD (b), PNDIF4 (c), PNDIF2BT (d), PTPDF4 (e) and PTPDF2BT (f).

Figure 5.51 (a) depicts the TGA graph of Synperonic F68 with an onset of decomposition at $T_{d,SynF68}$ = 378 °C. The similar decomposition temperature of the surfactant and the majority of conjugated polymers presented here render TGA impractical for quantification in surfactant removal studies. An additional decomposition is observed

for the graphs in figure 5.49 and figure 5.50 in a temperature range between 100 °C and 300 °C. These arise from non-volatile solvents such as hexadecane (figure 5.51 (b), $T_{d,HD}$ = 193 °C). Only one shake-centrifugation-decantation cycle (as described in section 3.4.1) with ethanol does not seem to suffice to remove these compounds entirely and indicates that repetition of the sample preparation cycle is required if total removal of remaining impurities is desired.

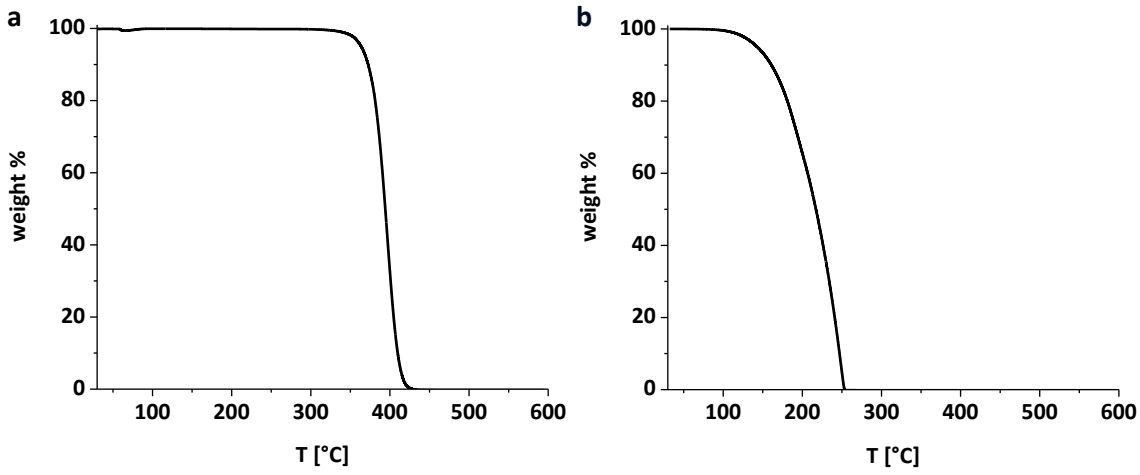

Figure 5.51: Thermogravimetric analysis of Synperonic F68 (a) and hexadecane (b).

6. Application of Conjugated Polymer Nanoparticles Prepared by Miniemulsion Polymerisation in Organic Field Effect Transistors

Aqueous dispersions of PDPPF4 were used to fabricate into OFETs to demonstrate the applicability of aqueous dispersions of conjugated polymers for application in electronic devices. To achieve thin film formation in a reproducible fashion, a suitable deposition technique was investigated and optimised. Further, the effect of the deposition medium on the charge carrier mobilities was investigated by deposition of the OSC layer from aqueous dispersions and the same polymer batch of PDPPF4 from chloroform solutions. Device fabrication and measurements were kindly provided and performed by Raja Usman Khan.

A previous report by Rahmanudin *et al*. demonstrated that increasing the hydrophilicity of the glass substrate allowed deposition of continuous films of aqueous CPN dispersions on ozone treated glass substrates.[55] Whilst SDS was employed as surfactant in the aforementioned report, Synperonic F68 was used for the synthesis of PDPPF4 dispersions in this work (entry **3.46**). Preliminary OSC film deposition trials on ozone treated glass substrates using **3.46** showed that the surface wetting before spin coating is crucial for the formation of coherent OSC thin films. Figure 6.1 presents optical microscopy and AFM images of a PDPPF4 thin film before and after annealing at 250 °C and subsequent washing with ethanol. Comparison of AFM images **g** and **h** reveals the melting of Synperonic F68 aggregates upon annealing ($T_{m,SynF68}$ = 44 °C).[96] Statistical analysis of the RMS roughness over the entire AFM images indicated that the PDPPF4 film becomes smoother after each treatment step (as cast 7 ± 1 nm, annealed 3 ± 3 nm, spin washed 2 ± 1 nm).

Based on these deposition trials OFET devices were fabricated as shown schematically in figure 6.2, based on the procedure reported by Rahmanudin *et al*.[55] An annealing temperature of 250 °C was chosen for PDPPF4 because previous reports suggested that the highest charge carrier mobility was found after crystallisation of the polymer within the thin film and that larger crystallite sizes and less grain boundaries were important.[78,85,139] The residual surfactant within the OSC layer was removed by washing the PDPPF4 thin film with ethanol and by spin coating and annealing at 100 °C to remove residual ethanol. Subsequent steps included the coating of PMMA as dielectric layer and

thermal evaporation of an aluminium gate electrode. To compare devices made from dispersions with those fabricated from solutions of the same polymer, PDPPF4 (entry **3.46**) was isolated from the emulsion (procedure described in section 8.4) and was dissolved in chloroform for the deposition *via* spin coating. Thus, the effect of the spin coating medium upon the charge carrier mobilities was directly compared.

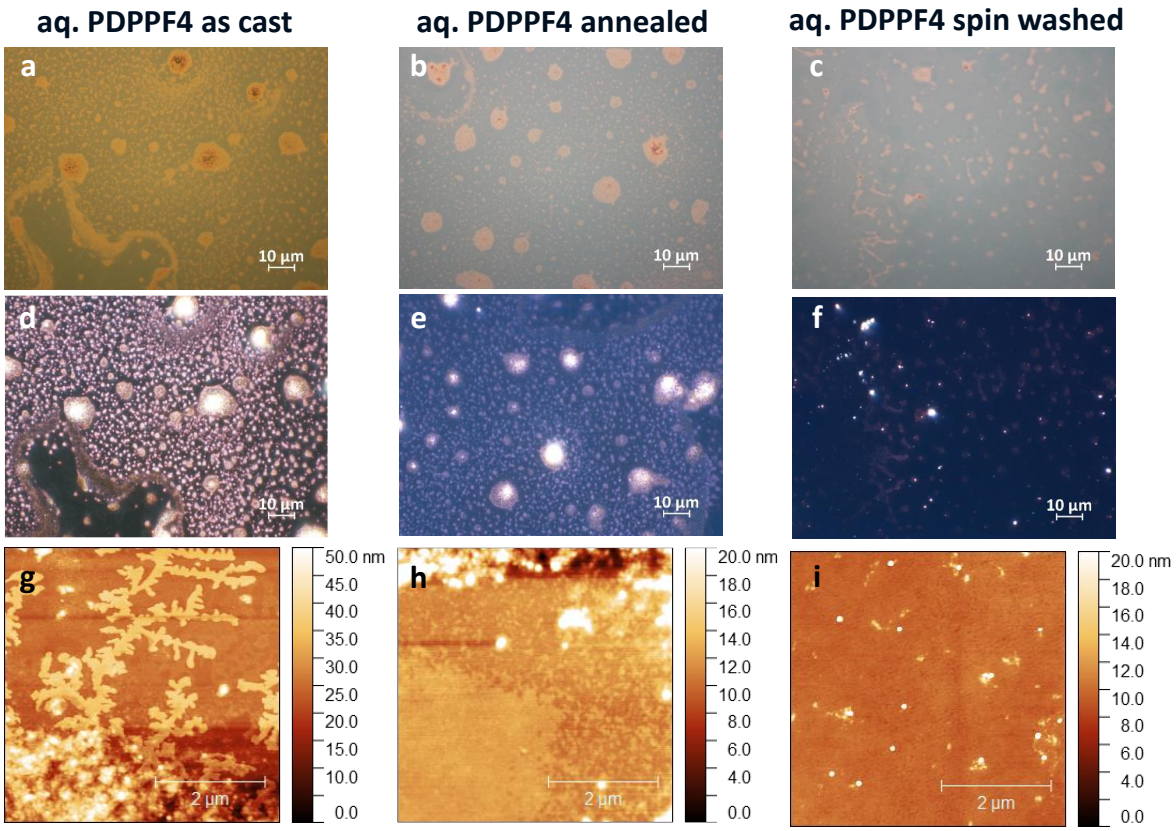

Figure 6.1. Optical bright field microscope images (a - c), optical dark field microscope images (d – f) and AFM measurements (g - i) of aqueous PDPPF4 dispersions (entry **3.46**) coated onto ozone treated glass substrates before and after thermal treatment and a subsequent spin wash step with ethanol.

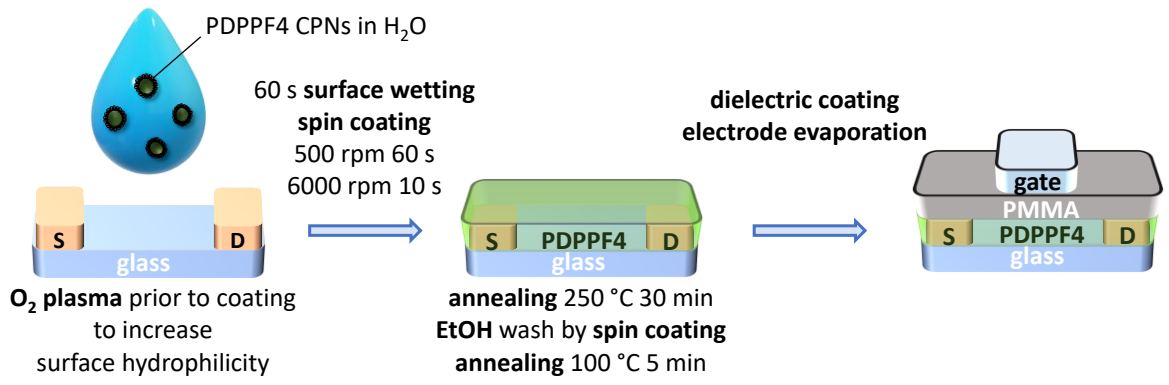

Figure 6.2: Schematic depiction of the OFET fabrication from aqueous PDPPF4 CPNs.

Table 6.1: Summary and comparison of saturation electron mobilities (μ_e), spin coating media, OFET architecture and synthesis method for PDPPF4 based OFETs annealed at 250 °C.

reference	M_n [kg mol^{-1}]	Đ	spin coating medium	μ_e [cm^2 V^{-1} s^{-1}]	OFET architecture[3]	C-C coupling
this work	9.5	2.2	aqueous	0.05 ± 0.00	BCTG	miniemulsion
entry **3.46**[1]			$CHCl_3$	0.05 ± 0.01		DArP
[78][1]	33	2.3	CB	0.01 ± 0.01	BGTC	DArP
[85][2]	11	1.5	$CHCl_3$	0.04 ± 0.01	BCTG	DArP
[139][2]	16	1.8	$CHCl_3$	1.25 ± 0.10	BGTC	Stille

Chlorobenzene (CB). [1] GPC in THF vs. narrow polydispersity polystyrene standards. [2] GPC in $CHCl_3$ vs. narrow polydispersity polystyrene standards. [3] bottom contact/top gate (BCTG), bottom gate/top contact (BGTC).

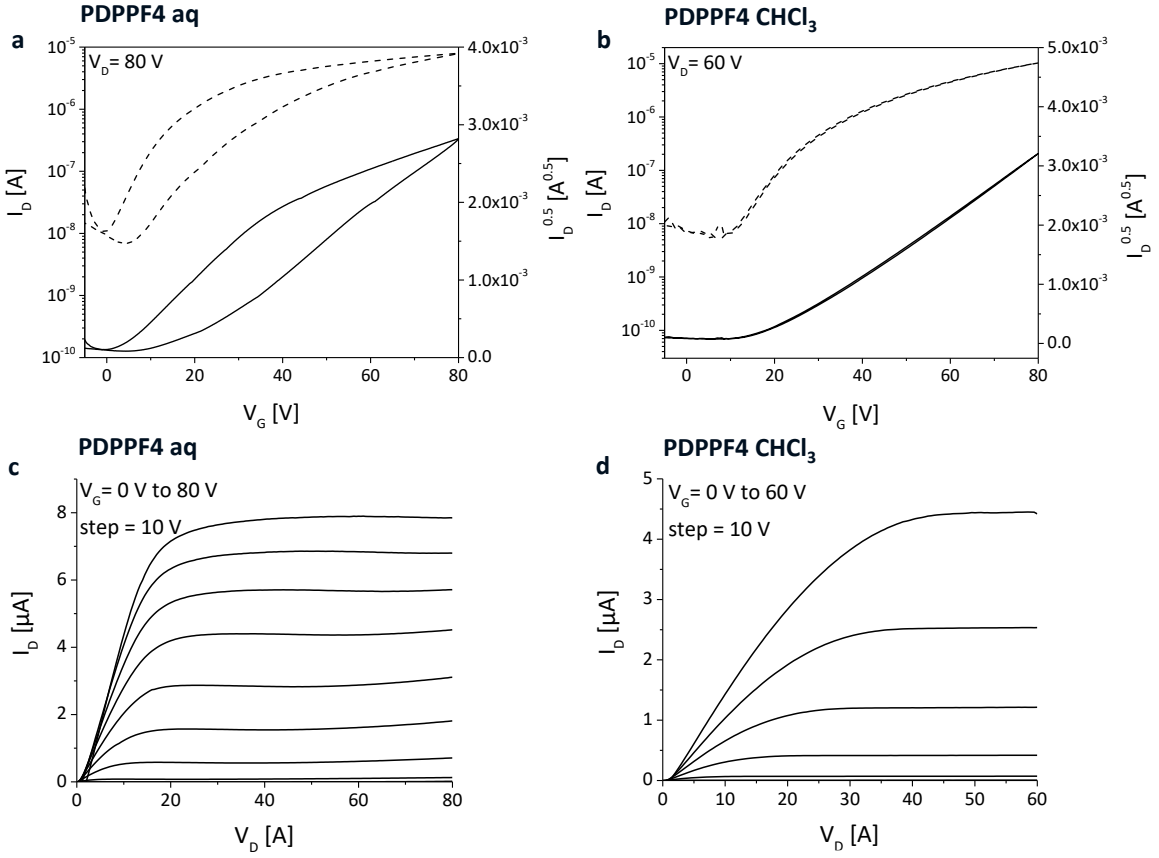

Figure 6.3: Representative transfer (a and b) and output (c and d) curves of PDPPF4 devices processed from aqueous dispersions or chloroform.

Measurements of the electron mobility within the saturation regime of the OFETs based on PDPPF4 processed by either aqueous dispersion or chloroform solution show similar values (table 6.1). Comparison of the transfer curves of both sets of OFET devices

emphasises the presence of hysteresis for devices only processed from aqueous dispersions of PDPPF4. The transfer curve hysteresis is most likely to be caused by remaining surfactant within the deposited OSC layer. Investigation of the surfactant removal by dialysis (section 5.2) has shown that a substantial amount of Synperonic F68 remains after dialysis (~ 10 %) and surfactant stripping by spin washing with ethanol is considered to have its limitations. Further studies are required upon the quantification of surfactant removal by spin washing and whether the surfactant stripping step needs improving to reduce the hysteresis. The measured electron mobilities for PDPPF4 synthesised by DArP are in good agreement with values reported by Wang *et al*.[78] and Sommer and coworkers[85], especially with the latter report using same device architecture and PDPPF4 of similar molecular weight.

Table 6.2: Summary of saturation electron mobilities (μ_e), threshold voltages (V_{th}) and on/off ratios of entries **3.46**, **4.2**, **4.5**, **4.11** and **4.13**.

entry	polymer	spin coating medium	μ_e [1] [$cm^2\ V^{-1}\ s^{-1}$]	V_{th} [V]	$I_{on/off}$
3.46	PDPPF4	aqueous	$5.13 \pm 0.17 \cdot 10^{-2}$	0.3 ± 2.1	10^4
		$CHCl_3$	$5.02 \pm 0.87 \cdot 10^{-2}$	22 ± 2.0	10^4
4.2	PDPPF2BT	$CHCl_3$	$1.82 \pm 0.89 \cdot 10^{-2}$	25 ± 1.5	10^5
4.5	PDPPTT	CB	$7.17 \pm 0.90 \cdot 10^{-3}$	46 ± 0.7	10^3
4.11	PNDIF4	DCB	$1.48 \pm 0.15 \cdot 10^{-3}$	-	8
4.13	PNDIF2BT	DCB	$0.36 \pm 0.26 \cdot 10^{-3}$	-	5

Chlorobenzene (CB), dichlorobenzene (DCB) [1] Averaged over up to 8 devices.

The electron mobilities of the other copolymers were measured by the same bottom contact/top gate device architecture as depicted in figure 6.2. The solvent used for the deposition by spin coating is indicated in table 6.2. Chlorobenzene and dichlorobenzene were used as solvents for the spin coating deposition step due to solubility limitations in chloroform for PDPPTT, PNDIF4 and PNDIF2BT. The OSC layers were annealed at 150 °C for 30 min for all copolymers except PDPPF4. The transfer and output curves for PDPPF2BT (entry **4.2**), PDPPTT (entry **4.5**), PNDIF4 (entry **4.11**) and PNDIF2BT (entry **4.13**) are presented in figure 6.4. OFETs fabricated with PNDIF4 and PNDIF2BT exhibit very low on/off current ratios due to elevated off currents and ambipolar behaviour. Hence, no threshold voltages have been extracted for OFETs made of entries **4.11** and **4.13**.

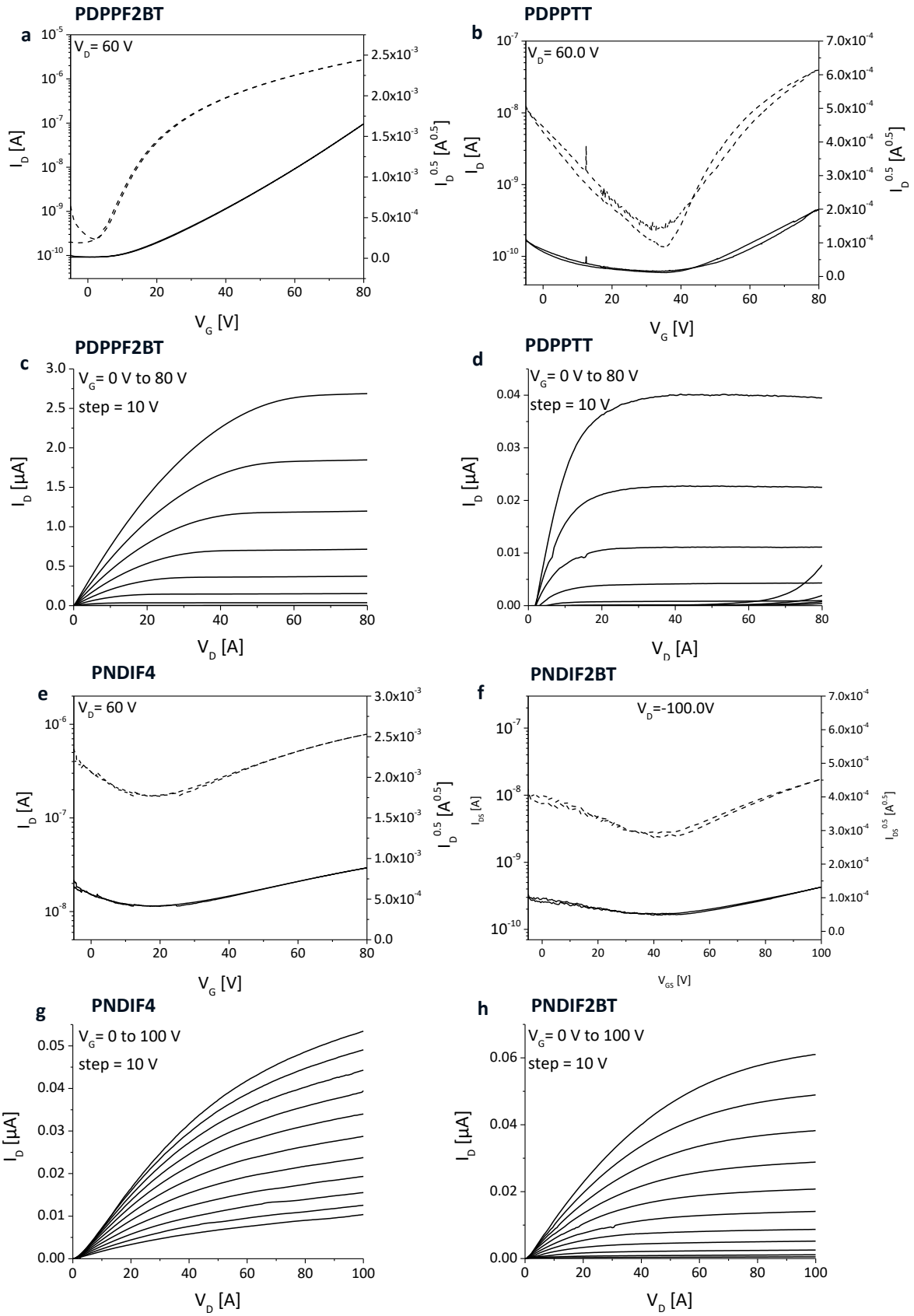

Figure 6.4: Representative transfer (a, b, e and f) and output (c, d, g and h) curves of PDPPF2BT, PDPPTT, PNDIF4 and PNDIF2BT devices processed from organic solvents.

7. Conclusion

The initial part of this work developed DArP of PDPPF4 in an *in-situ* miniemulsion polymerisation (Chapter 3). A summary of the most impactful and critical reaction parameters is presented in section 3.6. The optimised reaction conditions offer control over the molecular weight of the polymers, most notably by adjusting the pivalic acid and carbonate salt concentration (section 3.4.8). Thus, molecular weights of PDPPF4 $M_n \geq 10$ kg mol^{-1} could be obtained reproducibly by employing at least 5 equivalents (relative to the monomer) of pivalic acid and 8 equivalents of potassium carbonate. Control of the emulsion particle size dispersities was obtained by increasing the hexadecane concentration ([hexadecane] = 0.85 M) with particle sizes between 150 and 200 nm and moderate particle size dispersities (PDI < 0.3) in most cases (sections 3.4.2 and 3.4.3). Moreover, the particle size dispersities retained stable over the course of the reaction and for prolonged storage times (beyond 6 months, section 5.2). Changing the pre-catalysts from $Pd(OAc)_2$ to Pd_2dba_3 facilitated the applicability of miniemulsion DArP on a larger scope of substrates, whereas only PDPPF4 was polymerised when $Pd(OAc)_2$ was employed. Investigation of the comonomer structure including the C-H active monomers DPP, NDI, TPD and BDT with dibromotetrafluorobenzene and dibromodifluorobenzothiadiazole on the optimised miniemulsion DArP conditions (Chapter 4) demonstrated the scope of this novel synthesis procedure. The molecular weights obtained for DPP (M_n = 4.1 – 11 kg mol^{-1}), NDI (M_n = 5.6 – 8.8 kg mol^{-1}) and TPD (M_n = 9.1 – 20 kg mol^{-1}) containing copolymers suggest that electron deficient monomers polymerise better than BDT (M_n = 1.7 kg mol^{-1}).

Studies on homo coupling backbone defects caused by DArP revealed that the miniemulsion polymerisations gave in most cases higher molecular weights compared to the bulk polymerisations conducted in p-xylene under the same reaction conditions as those used for the miniemulsion (section 5.1). Conjugated polymers obtained *via* the miniemulsion DArP were defect-free (PDPPF4 and PDPPF2BT) or contained less homo coupling defects (PDPPTT, PDPPTPD, PNDIF4) than the analogous polymers prepared by bulk solution polymerisation. MALDI-TOF-MS proved to be an easily accessible method to qualitatively analyse the presence of polymer backbone defects in these polymers in conjunction with HT-NMR analyses. HT-NMR studies quantitatively confirmed the findings obtained by MALDI-TOF-MS, if all aromatic proton signals (between δ = 7.0 and 9.6 ppm)

were unequivocally assigned. An unambiguous proton peak assignment was feasible for polymers PDPPF4 (entry **3.46**) and PNDIF4 (entry **4.11**) rendering molecular weight determination by NMR end group analysis and quantification of the ratio of the chain terminal groups possible. The result of the end group analysis indicates an overestimation of the HT-GPC measurements. Comparison of integral intensities belonging to either DPP/NDI or tetrafluorobenzene end groups suggests a ratio of DPP to F4 termina of 2:1 and a slight prevalence for NDI in case of PNDIF4. With regards to the other polymers, the HT-NMR studies were partially inconclusive and will require the investigation of additional NMR techniques (^{13}C, HSQC) and model compounds to quantify the homo-coupling backbone defects. The question why the miniemulsion protocol gives superior materials to those prepared by solution polymerisations is content for debate and leaves an incentive for future work.

Further analysis by UV/Vis absorption (section 5.4) demonstrated that the characteristics of the polymers prepared by DArP in miniemulsion are in agreement with previous reports of these polymers synthesised by DArP, Suzuki-Miyaura or Stille cross couplings in solution.[85,121,122,126,127,133,138] Measurement of the thermal properties by TGA (section 5.6) revealed that the conjugated polymers obtained are thermally stable materials with elevated temperatures of decomposition ($T_d > 370$ °C). STEM analysis (section 5.5) indicated that DLS overestimates the particles diameter. This overestimation is attributed to solvent-induced particle swelling in case of the DLS measurements whereas the particles subjected to vacuum during the STEM measurements caused a decrease of their diameter. CPNs made of PDPPF4 and PDPPF2BT showed isotropic particle shapes whereas PDPPTT exhibited both spherical and lenticular shapes.

Aqueous dispersions of PDPPF4 were used to fabricate working OFETs and demonstrated the applicability of aqueous dispersions of conjugated polymers for application in electronic devices. This greener device fabrication approach reduces the usage of volatile organic compounds for the coating of the OSC layer (Chapter 6). OFETs made from both PDPPF4 in chloroform solution and dispersed as CPNs in water gave μ_e = 0.05 $cm^2 V^{-1} s^{-1}$. The results suggests that the presence of residual poloxamers (i.e Synperonic F68) does not impact charge carrier mobilities. This synthesis-to-device process in environmentally benign aqueous dispersions of conjugated polymers provides the

benefit of avoiding chlorinated solvents as well as a scalable process for the printing of electronic devices.

8. Experimental

8.1. Instrumentation

^{1}H **NMR** spectra at room temperature were recorded on a Bruker AVIII HD 400 at 400 MHz for ^{1}H nuclei. **High temperature NMR** measurements were performed on a Bruker AVII 500 with 500 MHz for ^{1}H nuclei and 126 MHz for ^{13}C nuclei. Chemical shifts are reported in ppm relative to the indicated residual solvent (i.e δ(CDCl3) = 7.26 ppm and δ($C_2D_2Cl_4$) = 6.00 ppm). The following abbreviations were used for the signal multiplicities: s = singlet, d = doublet, t = triplet, m = multiplet, dd = doublet of doublet. ^{19}F NMR spectra were recorded on a Bruker AVIII 400 at a frequency of 377 MHz for ^{19}F NMR and were referenced to an internal standard.

The molecular weights of polymers **3.9** – **3.32** were determined by **gel permeation chromatography** in THF at a flow rate of 1 mL min^{-1} at 35 °C, using an Viscotek GPCmax VE2001 solvent/sample module containing THF 2 · PL gel 10 µm MIXED-B + 1 · PL gel 500 A columns and a Viscotek VE3580 RI detector. Calibration of the system was based on low polydispersity PS standards (200 – 180 · 10^4 g mol^{-1}) from Polymer Laboratories. Samples from entry **3.33** onwards were measured in THF at a flow rate of 1 mL min^{-1} at 35 °C, using an Agilent 1260 Infinity II solvent/sample module consisting of a 2 · PL gel 10 µm MIXED-B columns + PL gel 10 µm guard column and an Agilent 1260 Infinity II G7162A 1260 RI detector. Calibration of the system was based on a low polydispersity PS standards kit (EasiVial® PS-M, 162 – 350 · 10^3 g mol^{-1}) from Agilent**. High temperature gel permeation chromatography** in 1,2,4-trichlorobenzene was performed at a flow rate of 1 mL min^{-1} at 120 °C with an Agilent 1260 High Temperature GPC System consisting of 3 · PL gel 5 µm MIXED-C + PL gel 5 µm guard columns and were calibrated by a low polydispersity PS standards kid (EasiVial® PS-H, 162 – 600 · 10^4 g mol^{-1}) from Agilent.

UV/Vis absorption spectra were recorded on an Agilent Varian Carry 5000 UV-Vis-NIR spectrophotometer. The samples were either diluted in water (CPNs) or dissolved in chloroform at room temperature.

Particle size analysis of the dispersions was completed using dynamic light scattering (DLS). The particle size distributions of diluted samples were measured at 25 °C using a

Malvern Zetasizer Nano ZS. The DLS results quoted are the average of three measurements. Samples were measured in a concentration regime between 0.1 – 0.2 mg mL^{-1} and were filtered through a 1 µm syringe filter (PTFE) prior to measurement. The PDI and mean particle size (z-average) were derived from a cumulant analysis according to ISO022412 (2017). The particle sizes were obtained from distribution analysis using a general purpose (non-negative least square (NNLS) algorithm.

Thermal properties were measured with a DSC 250 and Discovery SDT 650 from TA instruments with a heating rate of 10 °C min^{-1} in inert atmosphere.

MALDI-TOF-MS measurements were conducted with a Shimadzu Biotech Axima Confidence. The polymers were prepared in a dithranol matrix (1:1) and measured in positive polarity in linear mode calibrated against monodisperse poly(ethylene glycol), M_n = 6 kg mol^{-1}. The polymer solution (50 µL, 1 mg mL^{-1}) was mixed with 50 µL of a 10 mg mL^{-1} solution of the matrix (dithranol) in either THF/dichloromethane/chloroform. A drop of this solution was spotted onto a MALDI plate which had been pre-spotted with sodium iodide in THF (10 mg mL^{-1}).

Elemental analysis. compositions of carbon, hydrogen, nitrogen and sulphur atoms were measured using a Flash 2000 Organic Elemental Analyser (Thermo Scientific). Palladium was acid digested into solution and the solution was measured by a Thermo Scientific iCAP 6300 Duo ICP spectrometer.

Particle size analysis by scanning transmission electron microscopy. The polymer nanoparticles were kept as colloidal dispersion and stored in a desiccator prior to sample preparation. Samples were first sonicated for 5 minutes, before drop-casting onto clean holey carbon transmission electron microscopy (TEM) support grids (previously baked > 8 h at 120 °C), supplied by Agar. The grids were baked again for > 60 h at 120°C, prior to scanning transmission electron microscopy (STEM) characterisation. The STEM data was collected on a Thermo Fisher Tecnai TF300 STEM operating at 300 kV. STEM data was acquired with an electron dose rate of 443 electrons per square angstrom, a probe current of 195 pA, a semi-convergence angle of 4.5 mrad and an annular dark field (ADF) detector inner angle of 10.5 mrad. The data was processed using Python, where erroneous background signal was first removed through Python's image library (PIL) before thresholding the image for the highlighting of nanoparticles. After thresholding, the image is converted to binary and then the sorted regions of a NumPy array, corresponding to the areas of nanoparticles, have their properties measured *via* the *regionprops* function.

Statistical evaluation of the mean particle diameter was conducted through first removing particles of smaller than 40 nm and then evaluating the arithmetic mean with corresponding standard deviation.

Surface morphologies were measured with a Bruker Multimodal 8 atomic force microscope (AFM) in tapping mode.

OFET fabrication and characterization is identical to the procedure reported by Rahmanduin *et al*.[55] Top-gate/bottom-contact device OFETs were fabricated using corning glass as carrier substrate. The glass substrates were cleaned in acetone, 10 wt% DECON 90 solution, deionised water and isopropanol under sonication for 15 minutes. The cleaned glass substrates were subsequently treated by UV-ozone treatment for 5 minutes. Cr/Au source and drain electrodes were thermally evaporated under high vacuum (10^{-7} mbar) using a metal shadow mask with a patterned channel width = 1000 µm and length = 60 µm. To generate the hydrophilic surface for sufficient deposition of the CPNs by spin coating, the substrates were then treated with oxygen plasma for 3 minutes. PDPPF4 nanoparticle dispersions were dropped on the substrate and left for 60 s before spin coating at 500 rpm for 60 s and 6000 rpm for 10 s to form the OSC thin-film. The PDPPF4 thin-films were annealed at 250°C for 30 minutes under nitrogen and cooled down to room temperature. For the surfactant removal step, ethanol was dropped over the surface of the thin-film and left for 60s before spin-washing at 6000 rpm for 30s. The substrates were then annealed at 100 °C for 5 minutes and left under vacuum for 15 minutes to remove any remaining solvent. Poly(methyl methacrylate) (PMMA, M_w = 120 kg mol^{-1}) was spin-coated over the OSC thin-films from a butyl acetate solution (80 mg mL^{-1}) and the resulting dielectric layer was annealed at 80 °C for 30 minutes. The aluminum gate electrode (60 nm) was thermally evaporated on the dielectric layer using a metal shadow mask. The electrical properties of the OFETs were measured in the dark under ambient condition using an Agilent B1500 semiconductor parameter analyzer. The capacitance of C_i = 5.78 nF cm^{-2} for the PMMA dielectric was taken from the previous report.[55] In case of the chloroform/chlorobenzene/dichlorobenzene-processed devices, the OSCs were dissolved in the organic solvent (5 mg mL^{-1}) and filtered through a 1 µm filter (PTFE) followed by spin coating at 1000 rpm. All other steps were identical to the aqueous processed devices.

8.2. Chemicals

Table 8.1: Overview table of purchased monomers and polymerisation reagents used in this body of work.

chemical	supplier	purity
commercially available monomers		
4,7-Dibromo-5,6-difluoro-2,1,3-benzothiadiazole	Sigma-Aldrich	97 %
1,4-Dibromotetrafluorobenzene	Fluorochem	99 %
2,5-Dibromo-N-(2-ethylhexyl)-3,4-thiophenedicarboximide	TCI	> 98%
4,8-Bis-*n*-Octyloxybenzo[1,2-*b*:4,5-*b'*]dithiophene	TCI	> 98%
polymerisation reagents		
Potassium carbonate anhydrous	Fluka	> 99.5%
Sodium carbonate anhydrous	Fluka	> 99.5 %
Caesium carbonate anhydrous	Sigma-Aldrich	99 %
Silver carbonate	Sigma-Aldrich	> 99.9 %
N,N-Dimethyloctanamide	Fluorochem	95 %
N,N-Dimethylacetamide	Fluorochem	99 %
Pivalic acid	Fluorochem	98 %
Palladium(II) acetate	Acros Organics	99.9 % trace metal basis
Palladium(II) acetate trimer	Alfa Aesar	Pd 45.9 – 48.4 %
Palladium(II) acetate	Sigma-Aldrich	> 99.9 % trace metal basis
Tris(dibenzylidenaceton)dipalladium(0)	Acros Organics	97 %
Tris(4-methoxyphenyl)phosphine	Fluorochem	95 %
o-Xylene	Acros Organics	99 %
p-Xylene	Acros Organics	99 %
n-Hexadecane	Sigma-Aldrich	≥ 99.0 %
Sodium dodecyl sulphate	Sigma-Aldrich	≥ 99.0 %
Triton X165, X305, X405	Sigma-Aldrich	70 % in water
Synperonic F38, F68, F108	Croda	-

All chemicals mentioned in section 8.3 for the monomer syntheses were purchased by either Sigma-Aldrich, Alfa Aesar or Fluorochem. N-Bromosuccinimide was re-crystallised once from methanol prior to usage. The monomers, 1,4-dibromotetrafluorobenzene was used as received, 4,7-dibromo-5,6-difluoro-2,1,3-benzothiadiazole was crystallised from chloroform/methanol and 2,5-dibromo-N-(2-ethylhexyl)-3,4-thiophenedicarboximide was re-crystallised from chloroform/water. Column chromatography was performed using silica gel (60 Å, 230 - 400 mesh). Petroleum ether refers to the fraction obtained at 40-60 ˚C.

Deoxygenated solvents were prepared by freeze-pump-thaw cycles (minimum of three times) for the polymerisations using argon. Water has been filtered upon a resistivity of ≥ 16 megohm prior to usage. Surfactant removal was performed with Repligen 10 mL Float-a-Lyzer tubes that were washed and submerged in deionised water to remove the glycerine coating on the membrane prior to usage. The dialysate reservoir (1 L) was changed two times per day over the course of the dialysis time.

8.3. Monomer Syntheses

8.3.1. 1-Iodo-2-octyldodecane 3.8

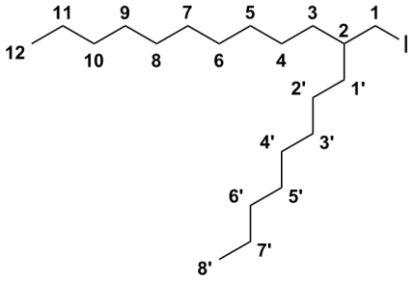

Imidazole (14.7 g, 215 mmol), 2-octyldodecanol (64.0 mL, 53.5 g, 180 mmol) and triphenylphosphine (56.4 g, 215 mmol) were added to a round bottom flask and dissolved in dichloromethane (300mL). The solution as cooled to 0°C and iodine (52.4 g, 206 mmol) was added portion wise. The solution was stirred at room temperature under ambient conditions for 16 h. Saturated aqueous $Na_2S_2O_3$ (50 mL) was added to obtain a clear yellow solution. The solution was filtered to remove the white precipitate. The organic phase was washed with H_2O and saturated aqueous NH_4Cl followed by drying of the organic layer over $MgSO_4$. After filtration, the solvent was removed under reduced pressure. The crude product was filtered through a short silica gel plug using petroleum ether. The title compound was obtained as clear liquid (60.8 g, 149 mmol, 83%). ^{1}H NMR (400 MHz, $CDCl_3$) δ [ppm] = 3.27 (d, *J* = 4.5 Hz, 2 H, H_1), 1.38-1.17 (m, 32 H, $H_{3\text{-}11}$ and $H_{1'\text{-}7'}$), 1.16-1.01 (m, 1 H, H_2), 0.88 (t, J = 6.7 Hz, 6 H, H_{12} and $H_{8'}$).

8.3.2. 3,6-Dithiophene-2-yl-2,5-dihydropyrrolo[3,4-c]pyrrole-1,4-dione 3.4

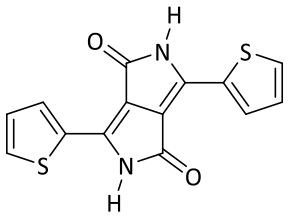

Potassium-*tert* butoxide (35.2 g, 314 mmol) and 2-thiophenecarbonitrile (19.0 mL, 16.2 g, 148 mmol) were dissolved in *tert*-amyl alcohol (200 mL) in a three-neck round bottom flask under a nitrogen atmosphere. The solution was heated up to 105 °C and succinic acid (8.9 mL, 9.9 g, 68 mmol) was added. After complete addition, the resulting slurry was stirred for 16h. The reaction was cooled to room temperature and methanol (50 mL) was added. Acetic acid was added to the slurry to obtain a pH of 7. The suspension was filtered, washed with hot methanol and twice with H_2O. The crude product was dried under vacuum and used without further purification (18.2 g, 60.4 mmol, 89%).

8.3.3. 2-Octyl-3,6-dithiophen-2-yl-2,5-dihydropyrrolo[3,4-c]pyrrole-1,4-dione 3.1

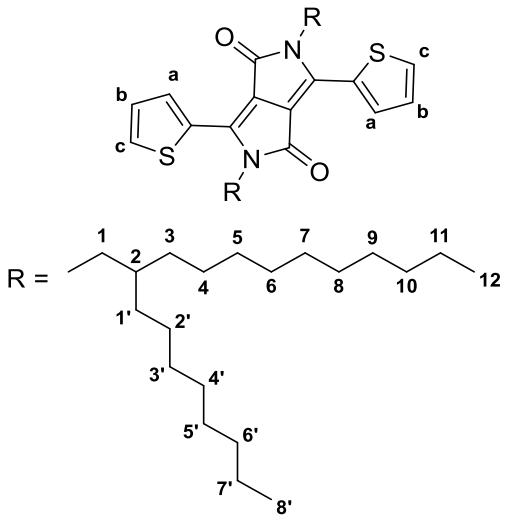

Potassium carbonate (32.0 g, 232 mmol) and 3,6-dithiophen-2-yl-2,5-dihydropyrrolo[3,4-c]pyrrole-1,4-dione (11.2 g, 37.2 mmol) were added to a two neck round bottom flask under an argon atmosphere. The solids were dissolved in anhydrous dimethylformamide (500 mL) and the solution was stirred at 120 °C for 3h. 1-Iodo-2-octyldodecane (60.8 g, 149 mmol) was added and the reaction mixture was stirred at 120 °C for 16h. After this, the solution was cooled to 0 °C and filtered. The filter cake was washed with chloroform until the solute was colourless. The crude product was purified by column chromatography [silica gel (60 Å, 230 – 400 mesh): chloroform/petroleum ether (1:1, v/v)]. To remove remaining impurities, the title compound was dissolved in a small amount of dichloromethane and precipitated in methanol. The precipitate was filtered and washed with cold methanol and subsequently dried under reduced pressure to give the title compound as red solid (7.62 g, 8.85 mmol, 24%). ^{1}H NMR (400 MHz, $CDCl_3$) δ [ppm] = 8.87 (dd, *J* = 3.9 Hz, 1.1 Hz, 2 H, $H_{\mathbf{c}}$), 7.61 (dd, *J* = 5.0 Hz, 1.1 Hz, 2 H, $H_{\mathbf{a}}$), 7.26 (dd, *J* = 5.1 Hz, 4.0 Hz, 2 H, $H_{\mathbf{b}}$), 4.02 (d, *J* = 7.7 Hz, 4 H, $H_{\mathbf{1}}$), 1.93-1.88 (m, 2 H, $H_{\mathbf{2}}$), 1.37 - 1.13 (m, 64 H, $H_{\mathbf{3-11}}$ and $H_{\mathbf{1`-7`}}$), 0.89 - 0.83 (m, 12 H, $H_{\mathbf{12}}$ and $H_{\mathbf{8`}}$).

8.3.4. 2,5-Dibromothieno[3,2-b]thiophene 4.4

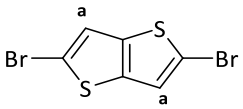

Thieno[3,2-b]thiophene (0.8 g, 5.7 mmol) was dissolved in DMF (11 mL) at 0 °C. *N*-Bromosuccinimide (2.1 g, 12 mmol) was added and the reaction mixture stirred for 4 h. Water was added and the mixture was extracted three times with ether. The organic phase was washed with water, dried over MgSO4 and the solvent was premoved under reduced pressure. Flash column chromatographical purification [silica gel (60 Å, 230 – 400 mesh): pentane] afforded the title compound (1.62 g, 5.4 mmol, 95 %) as a white solid (note: compound must be stored under argon at -20 °C to avoid decomposition). ^{1}H-NMR (400 MHz, $CDCl_3$): δ [ppm] = 6.31 (s, 2H).

8.3.5. 2,6-Bis(2-thienyl)naphthalene-1,4,5,8-N,N‘-bis(2-ethylhexyl) diimide 4.10

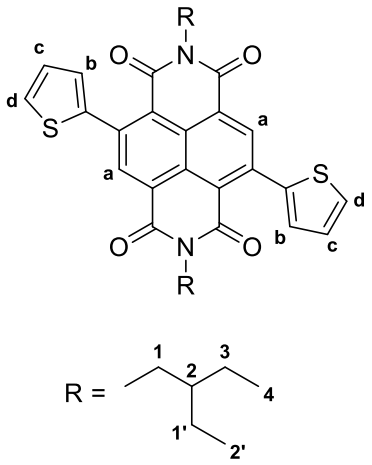

2,6-Dibromonaphthalene-1,4,5,8-N,N‘-bis(2-ethylhexyl) diimide (1.0 g, 1.5 mmol), dichlorobis(triphenylphosphine)palladium(II) (21 mg, $3.0 \cdot 10^{-3}$ mmol) and 2-(tributylstannyl)thiophene (1.4 g, 3.7 mmol) were prepared in a double-neck round bottom flask with a reflux condenser. The atmosphere was replaced by argon and anhydrous THF (35 ml) was added. The reaction mixture was stirred at reflux for 16 h and the organic solvent was evaporated. The resulting solid was recrystallised from hot isopropanol. An orange solid precipitated upon cooling to room temperature the product was isolated by filtration. The product was washed with cold isopropanol, methanol and dried in vacuo at 40 °C overnight. Yield (0.9 g, 1.4 mmol, 92%). ^{1}H NMR (400 MHz, $CDCl_3$) δ = 8.76 (s, 2H; H_a), 7.56 (dd, *J* = 5.1 Hz, 1.2 Hz, 2 H, H_d), 7.29 (dd, *J* = 3.6 Hz, 1.4 Hz, 2 H; H_b), 7.19 (dd, *J* = 5.1 Hz, 3.6 Hz, 2 H; H_c), 4.07 (d, *J* = 7.7 Hz, 4 H, H_1), 1.93 - 1.87 (m, 2H, H_2), 1.39 - 1.25 (m, 8 H, H_3 and $H_{1'}$), 0.92 – 0.85 (m, 12 H, H_4 and $H_{2'}$).

8.3.6. 5-(2-octyldodecyl)thieno[3,4]pyrrole-4,6-dione 4.15

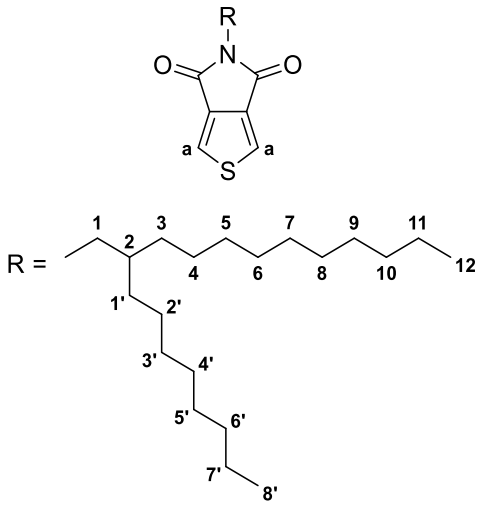

The compound 3,4-thiophenedicarboxilic acid (0.5 g, 2.8 mmol) and 2-hexyl-decanamine (1.0 mL, 0.8 g, 2.8 mmol) were prepared in a round bottom flask equipped with a Dean-Stark trap. The atmosphere was replaced by argon and the mixture was stirred at 200 °C overnight. The resulting brown mixture was cooled to room temperature and dissolved in dichloromethane. The extract was washed with water and brine and dried over anhydrous sodium sulphate. After filtration, the solvent was removed under reduced pressure. The crude product was purified by column chromatography [silica gel (60 Å, 230 – 400 mesh): chloroform/petroleum ether (1:1, v/v)]. To remove remaining impurities, the title compound was dissolved in a small amount of dichloromethane and the resulting solution was precipitated in water. The precipitate was filtered and washed with cold water and subsequently dried in vacuo at 40°C overnight to give the title compound as white solid (1.1 g, 2.4 mmol, 85 %). ^{1}H NMR (400 MHz, $CDCl_3$) δ = 7.73 (s, 2 H, H_a), 3,43 (d, J = 3.4 Hz 2H, H_1), 1.82 - 1.73 (m, 1 H, H_2), 1.34-1.11 (m, 32 H, $H_{3\text{-}11}$ and $H_{1'\text{-}7'}$), 0.84 - 0.76 (m, 6 H, H_{12} and $H_{8'}$).

8.4. General Procedure Direct Arylation Polycondensation in Emulsion

A general method for the preparation of the miniemulsion polymerisations is described in this report. Deviations from this procedure are mentioned in the discussion part for each particular polymerisation.

Surfactant (1-5 wt. %) and carbonate salt were loaded into a Schlenk tube and dissolved in deionised water (10 mL). The aqueous solution was then degassed by sparging with argon for 2 h. The monomers, pivalic acid, palladium catalyst and tris(4-methoxyphenyl)phosphine were added to a vial containing a stirring bar. This vial was transferred into an argon-filled glovebox and deoxygenated hexadecane and p-xylene (1.0 mL) were added. The vial was sealed with a Suba-seal and removed from the glovebox, the organic solution was stirred and sparged with argon before for 5 min before it was injected to the aqueous solution. The dispersion was stirred at 600 rpm until an emulsion has formed. The pre-emulsion was then further emulsified using a Cole-Parmer CPX 750 ultrasonic probe for 10 min with a fully immersed 6 mm tapered microtip and 21 % intensity. The formed emulsion was degassed by argon and subsequently transferred into an argon filled Young tube (25 mL), sealed and the reaction was stirred at the specified reaction temperature for 72 h.

To isolate the conjugated polymer from the dispersion for analysis, an aliquot (0.2 mL) of the dispersion was added to methanol (~ 50 mL). The vial tube was shaken for 12 h prior to centrifugation (18,000 rpm, 60 minutes) and the supernatant was decanted off. The pellet was dried under vacuum.

8.5. General Procedure Direct Arylation Polycondensation in Solution

2-Octyl-3,6-dithiophen-2-yl-2,5-dihydropyrrolo[3,4-c]pyrrol-1,4-dione (86.1 mg, 0.10 mmol), 1,4-dibromotetrafluorobenzene (30.8 mg, 0.10 mmol), potassium carbonate (152 mg, 1.10 mmol), pivalic acid (71.5 mg, 0.70 mmol), tris(dibenzylidenaceton)dipalladium(0) (3.66 mg, 4.00 µmol) and tris(4-methoxyphenyl)phosphine (2.82 mg, 8.00 µmol) were loaded into a screw cap vial containing a PTFE stirring bar. The vial was put under an argon atmosphere by three vacuum/argon purge cycles. Degassed p-xylene (0.50 mL) was added, and the solution was sparged with argon. The vial was sealed, and the reaction mixture was vigorously stirred at 100 °C for 72 h. The reaction mixture was cooled down to room temperature and diluted with chloroform (1.00 mL). The mixture was precipitated into methanol (20 mL) and the resulting precipitate was filtered. The product was further washed methanol and dried under vacuum.

9. References

1 D. Muenmart, A. B. Foster, A. Harvey, M.-T. Chen, O. Navarro, V. Promarak, M. C. McCairn, J. M. Behrendt and M. L. Turner, *Macromolecules*, 2014, **47**, 6531–6539.

2 J. M. Behrendt, J. A. Esquivel Guzman, L. Purdie, H. Willcock, J. J. Morrison, A. B. Foster, R. K. O'Reilly, M. C. McCairn and M. L. Turner, *React. Funct. Polym.*, 2016, **107**, 69–77.

3 J. D. Ruiz Perez and S. Mecking, *Angew. Chem. Int. Ed.*, 2017, **56**, 6147–6151.

4 K. H. Hendriks, W. Li, G. H. L. Heintges, G. W. P. van Pruissen, M. M. Wienk and R. A. J. Janssen, *J. Am. Chem. Soc.*, 2014, **136**, 11128–11133.

5 C. K. Chiang, C. R. Fincher, Y. W. Park, A. J. Heeger, H. Shirakawa, E. J. Louis, S. C. Gau and A. G. MacDiarmid, *Phys. Rev. Lett.*, 1977, **39**, 1098–1101.

6 C. W. Tang, *Appl. Phys. Lett.*, 1986, **48**, 183–185.

7 H. Koezuka, A. Tsumura and T. Ando, *Synth. Met.*, 1987, **18**, 699–704.

8 J. H. Burroughes, C. A. Jones and R. H. Friend, *Nature*, 1988, **335**, 137–141.

9 G. Horowitz, D. Fichou, X. Peng, Z. Xu and F. Garnier, *Solid State Commun.*, 1989, **72**, 381–384.

10 C. W. Tang and S. A. VanSlyke, *Appl. Phys. Lett.*, 1987, **51**, 913–915.

11 J. H. Burroughes, D. D. C. Bradley, A. R. Brown, R. N. Marks, K. Mackay, R. H. Friend, P. L. Burns and A. B. Holmes, *Nature*, 1990, **347**, 539–541.

12 T. M. Swager, *Macromolecules*, 2017, **50**, 4867–4886.

13 T. P. Kaloni, P. K. Giesbrecht, G. Schreckenbach and M. S. Freund, *Chem. Mater.*, 2017, **29**, 10248–10283.

14 D. Hashemi, X. Ma, R. Ansari, J. Kim and J. Kieffer, *Phys. Chem. Chem. Phys.*, 2019, **21**, 789–799.

15 K. Müllen and W. Pisula, *J. Am. Chem. Soc.*, 2015, **137**, 9503–9505.

16 J.-R. Pouliot, F. Grenier, J. T. Blaskovits, S. Beaupré and M. Leclerc, *Chem. Rev.*, 2016, **116**, 14225–14274.

17 N. S. Gobalasingham and B. C. Thompson, *Prog. Polym. Sci.*, 2018, **83**, 135–201.

18 Y. Zhao, Y. Guo and Y. Liu, *Adv. Mater.*, 2013, **25**, 5372–5391.

19 X. Zhang, H. Bronstein, A. J. Kronemeijer, J. Smith, Y. Kim, R. J. Kline, L. J. Richter, T. D. Anthopoulos, H. Sirringhaus, K. Song, M. Heeney, W. Zhang, I. McCulloch and D. M. DeLongchamp, *Nat. Commun.*, 2013, 4, 2238.

20 A. Teichler, J. Perelaer and U. S. Schubert, *J. Mater. Chem. C*, 2013, **1**, 1910.

21 W. Shockley, *Proc. IRE*, 1952, **40**, 1365–1376.

22 C. Reese and Z. Bao, *J. Appl. Phys.*, 2009, **105**, 024506.

23 H. Li, Y. Li, H. Li and J.-L. Brédas, *Adv. Funct. Mater.*, 2017, **27**, 1605715.

24 S. R. Thomas, P. Pattanasattayavong and T. D. Anthopoulos, *Chem. Soc. Rev.*, 2013, **42**, 6910.

25 B. Wang, P. Sonar, S. Manzhos and H. Haick, *Sens. Actuators B Chem.*, 2017, **251**, 49–56.

26 D. Khim, G.-S. Ryu, W.-T. Park, H. Kim, M. Lee and Y.-Y. Noh, *Adv. Mater.*, 2016, **28**, 2752–2759.

27 A. F. Paterson, S. Singh, K. J. Fallon, T. Hodsden, Y. Han, B. C. Schroeder, H. Bronstein, M. Heeney, I. McCulloch and T. D. Anthopoulos, *Adv. Mater.*, 2018, **30**, 1801079.

28 C. Liu, G. Li, R. Di Pietro, J. Huang, Y.-Y. Noh, X. Liu and T. Minari, *Phys. Rev. Appl.*, 2017, **8**, 034020.
29 H. Sirringhaus, *Adv. Mater.*, 2014, **26**, 1319–1335.
30 E. G. Bittle, H. W. Ro, C. R. Snyder, S. Engmann, R. J. Kline, X. Zhang, O. D. Jurchescu, D. M. DeLongchamp and D. J. Gundlach, *J. Polym. Sci. Part B Polym. Phys.*, 2017, **55**, 1063–1074.
31 Steven Abott, *Surfactant Science: Principles and Practice*, Creative Commons BY-ND, Attribution and No-Derivatives license, 2015.
32 D. Tuncel and H. V. Demir, *Nanoscale*, 2010, **2**, 484.
33 L. Feng, C. Zhu, H. Yuan, L. Liu, F. Lv and S. Wang, *Chem. Soc. Rev.*, 2013, **42**, 6620.
34 B. L. Liu, Ed., *Conjugated Polymers for Biological and Biomedical Applications*, Wiley-VCH Verlag GmbH & Co. KGaA, Weinheim, Germany, 2018.
35 C.-C. Shih, Y.-C. Chiu, W.-Y. Lee, J.-Y. Chen and W.-C. Chen, *Adv. Funct. Mater.*, 2015, **25**, 1511–1519.
36 C.-C. Shih, W.-Y. Lee, Y.-C. Chiu, H.-W. Hsu, H.-C. Chang, C.-L. Liu and W.-C. Chen, *Sci. Rep.*, 2016, **6**, 20129.
37 Z. J. Wang, S. Ghasimi, K. Landfester and K. A. I. Zhang, *Chem. Commun.*, 2014, **50**, 8177.
38 Y. Bai, L. Wilbraham, B. J. Slater, M. A. Zwijnenburg, R. S. Sprick and A. I. Cooper, *J. Am. Chem. Soc.*, 2019, **141**, 9063–9071.
39 F. Cicoira and C. Santato, Eds., *Organic electronics: emerging concepts and technologies*, Wiley-VCH Verlag GmbH & Co. KGaA, Weinheim, Germany, 2013.
40 P. Sarrazin, D. Chaussy, L. Vurth, O. Stephan and D. Beneventi, *Langmuir*, 2009, **25**, 6745–6752.
41 K. Landfester, N. Brechthold, F. Tiarks and M. Antonietti, 1999, 5222–5228.
42 J. Jeng, C.-A. Dai, W.-Y. Chiu, C.-S. Chern, K.-F. Lin and P.-Y. Young, *J. Polym. Sci. Part Polym. Chem.*, 2006, **44**, 4603–4610.
43 E. Hittinger, A. Kokil and C. Weder, *Angew. Chem. Int. Ed.*, 2004, **43**, 1808–1811.
44 H. Shirakawa, *Angew. Chem. Int. Ed.*, 2001, **40**, 2574–2580.
45 A. G. MacDiarmid, *Angew. Chem. Int. Ed.*, 2001, **40**, 2581–2590.
46 A. J. Heeger, *Angew. Chem. Int. Ed.*, 2001, **40**, 2591–2611.
47 J. Huber and S. Mecking, *Angew. Chem. Int. Ed.*, 2006, **45**, 6314–6317.
48 K. Müller, M. Klapper and K. Müllen, *Macromol. Rapid Commun.*, 2006, **27**, 586–593.
49 J. Pecher, J. Huber, M. Winterhalder, A. Zumbusch and S. Mecking, *Biomacromolecules*, 2010, **11**, 2776–2780.
50 M. C. Baier, J. Huber and S. Mecking, *J. Am. Chem. Soc.*, 2009, **131**, 14267–14273.
51 M.-T. Chen, D. A. Vicic, M. L. Turner and O. Navarro, *Organometallics*, 2011, **30**, 5052–5056.
52 D. Guest, M.-T. Chen, G. J. Tizzard, S. J. Coles, M. L. Turner and O. Navarro, *Eur. J. Inorg. Chem.*, 2014, **2014**, 2200–2203.
53 A. J. C. Kuehne, M. C. Gather and J. Sprakel, *Nat. Commun.*, 2012, **3**, 1088.
54 S. Kawaguchi and K. Ito, in *Polymer Particles*, ed. M. Okubo, Springer Berlin Heidelberg, Berlin, Heidelberg, 2005, vol. 175, pp. 299–328.
55 A. Rahmanudin, R. Marcial-Hernandez, A. Zamhuri, A. S. Walton, D. J. Tate, R. U. Khan, S. Aphichatpanichakul, A. B. Foster, S. Broll and M. L. Turner, *Adv. Sci.*, 2020, **7**, 2002010.
56 H. Dong, X. Fu, J. Liu, Z. Wang and W. Hu, *Adv. Mater.*, 2013, **25**, 6158–6183.

57 C. Szymanski, C. Wu, J. Hooper, M. A. Salazar, A. Perdomo, A. Dukes and J. McNeill, *J. Phys. Chem. B*, 2005, **109**, 8543–8546.
58 J. Pecher and S. Mecking, *Macromolecules*, 2007, **40**, 7733–7735.
59 B. S. Ong, Y. Wu, P. Liu and S. Gardner, *Adv. Mater.*, 2005, **17**, 1141–1144.
60 N. Kurokawa, H. Yoshikawa, N. Hirota, K. Hyodo and H. Masuhara, *ChemPhysChem*, 2004, **5**, 1609–1615.
61 I. O. Huyal, T. Ozel, D. Tuncel and H. V. Demir, *Opt. Express*, 2008, **16**, 13391.
62 C. Wu, B. Bull, C. Szymanski, K. Christensen and J. McNeill, *ACS Nano*, 2008, **2**, 2415–2423.
63 C. Wu, Y. Jin, T. Schneider, D. R. Burnham, P. B. Smith and D. T. Chiu, *Angew. Chem. Int. Ed.*, 2010, **49**, 9436–9440.
64 J.-S. M. Lee and A. I. Cooper, *Chem. Rev.*, 2020, **120**, 2171–2214.
65 H. Li, X. Wu, B. Xu, H. Tong and L. Wang, *RSC Adv.*, 2013, **3**, 8645.
66 J. Cho, S. Yoon, K. Min Sim, Y. Jin Jeong, C. Eon Park, S.-K. Kwon, Y.-H. Kim and D. S. Chung, *Energy Environ. Sci.*, 2017, **10**, 2324–2333.
67 J. Cho, K. H. Cheon, H. Ahn, K. H. Park, S.-K. Kwon, Y.-H. Kim and D. S. Chung, *Adv. Mater.*, 2015, **27**, 5587–5592.
68 D. Darwis, D. Elkington, S. Ulum, G. Bryant, W. Belcher, P. Dastoor and X. Zhou, *J. Colloid Interface Sci.*, 2013, **401**, 65–69.
69 M. Bag, T. S. Gehan, D. D. Algaier, F. Liu, G. Nagarjuna, P. M. Lahti, T. P. Russell and D. Venkataraman, *Adv. Mater.*, 2013, **25**, 6411–6415.
70 J. Cho, K. H. Cheon, J. Ha and D. S. Chung, *Chem. Eng. J.*, 2016, **286**, 122–127.
71 T. Bura, S. Beaupré, M.-A. Légaré, J. Quinn, E. Rochette, J. T. Blaskovits, F.-G. Fontaine, A. Pron, Y. Li and M. Leclerc, *Chem Sci*, 2017, **8**, 3913–3925.
72 L. G. Mercier and M. Leclerc, *Acc. Chem. Res.*, 2013, **46**, 1597–1605.
73 L. Ackermann, *Chem. Rev.*, 2011, **111**, 1315–1345.
74 S. I. Gorelsky, D. Lapointe and K. Fagnou, *J. Am. Chem. Soc.*, 2008, **130**, 10848–10849.
75 S. I. Gorelsky, *Coord. Chem. Rev.*, 2013, **257**, 153–164.
76 A. S. Dudnik, T. J. Aldrich, N. D. Eastham, R. P. H. Chang, A. Facchetti and T. J. Marks, *J. Am. Chem. Soc.*, 2016, **138**, 15699–15709.
77 G. Marzano, F. Carulli, F. Babudri, A. Pellegrino, R. Po, S. Luzzati and G. M. Farinola, *J Mater Chem A*, 2016, **4**, 17163–17170.
78 K. Wang, G. Wang and M. Wang, *Macromol. Rapid Commun.*, 2015, **36**, 2162–2170.
79 F. Grenier, K. Goudreau and M. Leclerc, *J. Am. Chem. Soc.*, 2017, **139**, 2816–2824.
80 L. Huo, J. Hou, H.-Y. Chen, S. Zhang, Y. Jiang, T. L. Chen and Y. Yang, *Macromolecules*, 2009, **42**, 6564–6571.
81 B. Zhao, K. Sun, F. Xue and J. Ouyang, *Org. Electron.*, 2012, **13**, 2516–2524.
82 J. Mei and Z. Bao, *Chem. Mater.*, 2014, **26**, 604–615.
83 X. Xu, Z. Li, O. Bäcke, K. Bini, D. I. James, E. Olsson, M. R. Andersson and E. Wang, *J Mater Chem A*, 2014, **2**, 18988–18997.
84 Jair Azael Esquivel Gusman, PhD Thesis, University of Manchester, 2016.
85 S. Broll, F. Nübling, A. Luzio, D. Lentzas, H. Komber, M. Caironi and M. Sommer, *Macromolecules*, 2015, **48**, 7481–7488.
86 S. K. Li and D. Chantasart, *J. Pharm. Sci.*, 2019, **108**, 350–357.
87 M. Wakioka, Y. Nakamura, M. Montgomery and F. Ozawa, *Organometallics*, 2015, **34**, 198–205.

88 Dow Chemical Company, Dow Surfactants Reference Chart, http://msdssearch.dow.com/PublishedLiteratureDOWCOM/dh_09b0/0901b803809b0065.pdf?filepath=surfactants/pdfs/noreg/119-01491.pdf?filepath=surfactants/pdfs/noreg/119-01491.pdf&fromPage=GetDoc, (accessed 7 April 2020).
89 W. A. Carole and T. J. Colacot, *Chem. - Eur. J.*, 2016, **22**, 7686–7695.
90 V. I. Bakhmutov, J. F. Berry, F. A. Cotton, S. Ibragimov and C. A. Murillo, *Dalton Trans.*, 2005, 1989.
91 I. P. Stolyarov, L. I. Demina and N. V. Cherkashina, *Russ. J. Inorg. Chem.*, 2011, **56**, 1532–1537.
92 P. Alexandridis and T. Alan Hatton, *Colloids Surf. Physicochem. Eng. Asp.*, 1995, **96**, 1–46.
93 A. Pitto-Barry and N. P. E. Barry, *Polym Chem*, 2014, **5**, 3291–3297.
94 M. Antonietti, *Prog. Polym. Sci.*, 2002, **27**, 689–757.
95 J. Delgado, M. S. El-Aasser and J. W. Vanderhoff, *J. Polym. Sci. Part Polym. Chem.*, 1986, **24**, 861–874.
96 H.-W. Tsui, J.-H. Wang, Y.-H. Hsu and L.-J. Chen, *Colloid Polym. Sci.*, 2010, **288**, 1687–1696.
97 M. Yu. Kozlov, N. S. Melik-Nubarov, E. V. Batrakova and A. V. Kabanov, *Macromolecules*, 2000, **33**, 3305–3313.
98 J. B. Kayes and D. A. Rawlins, *Colloid Polym. Sci.*, 1979, **257**, 622–629.
99 J. A. Baker and J. C. Berg, *Langmuir*, 1988, **4**, 1055–1061.
100 T. J. Aldrich, A. S. Dudnik, N. D. Eastham, E. F. Manley, L. X. Chen, R. P. H. Chang, F. S. Melkonyan, A. Facchetti and T. J. Marks, *Macromolecules*, 2018, **51**, 9140–9155.
101 X. Wang and M. Wang, *Polym Chem*, 2014, **5**, 5784–5792.
102 M. Wakioka, R. Takahashi, N. Ichihara and F. Ozawa, *Macromolecules*, 2017, **50**, 927–934.
103 E. Iizuka, M. Wakioka and F. Ozawa, *Macromolecules*, 2016, **49**, 3310–3317.
104 P. Izquierdo, J. Esquena, Th. F. Tadros, C. Dederen, M. J. Garcia, N. Azemar and C. Solans, *Langmuir*, 2002, **18**, 26–30.
105 P. Izquierdo, J. Esquena, T. F. Tadros, J. C. Dederen, J. Feng, M. J. Garcia-Celma, N. Azemar and C. Solans, *Langmuir*, 2004, **20**, 6594–6598.
106 E. J. Acosta, *Colloids Surf. Physicochem. Eng. Asp.*, 2008, **320**, 193–204.
107 S. Zarate-Muñoz, A. B. Troncoso and E. Acosta, *Langmuir*, 2015, **31**, 12000–12008.
108 K. Shinoda and H. Arai, *J. Phys. Chem.*, 1964, **68**, 3485–3490.
109 M. Zerfa, S. Sajjadi and B. W. Brooks, *Colloids Surf. Physicochem. Eng. Asp.*, 2001, **178**, 41–48.
110 A. Kumar, S. Li, C.-M. Cheng and D. Lee, *Ind. Eng. Chem. Res.*, 2015, **54**, 8375–8396.
111 G. S. Hamilton, in *Encyclopedia of Reagents for Organic Synthesis*, ed. John Wiley & Sons, Ltd, John Wiley & Sons, Ltd, Chichester, UK, 2001, p. rp176.
112 A. Punzi, M. A. M. Capozzi, S. Di Noja, R. Ragni, N. Zappimbulso and G. M. Farinola, *J. Org. Chem.*, 2018, **83**, 9312–9321.
113 D. Whitaker, J. Burés and I. Larrosa, *J. Am. Chem. Soc.*, 2016, **138**, 8384–8387.
114 A. Seidell and W. Linke, *Solubilities of Inorganic Compounds (2nd ed.)*, D. Van Nostrand Company, 1919.
115 K. Shinoda and H. Saito, *J. Colloid Interface Sci.*, 1968, **26**, 70–74.
116 R. Matsidik, H. Komber and M. Sommer, *ACS Macro Lett.*, 2015, **4**, 1346–1350.
117 F. J. Schork and J. Guo, *Macromol. React. Eng.*, 2008, **2**, 287–303.

118 J. Kuwabara, W. Tsuchida, S. Guo, Z. Hu, T. Yasuda and T. Kanbara, *Polym. Chem.*, 2019, **10**, 2298–2304.
119 A. K. Leone, E. A. Mueller and A. J. McNeil, *J. Am. Chem. Soc.*, 2018, **140**, 15126–15139.
120 R. M. Pankow and B. C. Thompson, *Polym. Chem.*, 2020, **11**, 630–640.
121 J. Lee, M. Jang, S. M. Lee, D. Yoo, T. J. Shin, J. H. Oh and C. Yang, *ACS Appl. Mater. Interfaces*, 2014, **6**, 20390–20399.
122 Y. Li, S. P. Singh and P. Sonar, *Adv. Mater.*, 2010, **22**, 4862–4866.
123 J. Li, Y. Zhao, H. S. Tan, Y. Guo, C.-A. Di, G. Yu, Y. Liu, M. Lin, S. H. Lim, Y. Zhou, H. Su and B. S. Ong, *Sci. Rep.*, 2012, **2**, 754.
124 J. C. Bijleveld, R. A. M. Verstrijden, M. M. Wienk and R. A. J. Janssen, *J. Mater. Chem.*, 2011, **21**, 9224.
125 J.-R. Pouliot, L. G. Mercier, S. Caron and M. Leclerc, *Macromol. Chem. Phys.*, 2013, **214**, 453–457.
126 A. Luzio, D. Fazzi, F. Nübling, R. Matsidik, A. Straub, H. Komber, E. Giussani, S. E. Watkins, M. Barbatti, W. Thiel, E. Gann, L. Thomsen, C. R. McNeill, M. Caironi and M. Sommer, *Chem. Mater.*, 2014, **26**, 6233–6240.
127 C. An, H. Makowska, B. Hu, R. Duan, W. Pisula, T. Marszalek and M. Baumgarten, *RSC Adv.*, 2018, **8**, 16464–16469.
128 A. Nitti, F. Debattista, L. Abbondanza, G. Bianchi, R. Po and D. Pasini, *J. Polym. Sci. Part Polym. Chem.*, 2017, **55**, 1601–1610.
129 B. Zhang, PhD Thesis, University of Kentucky Libraries, 2018.
130 P. Shen, H. Bin, Y. Zhang and Y. Li, *Polym Chem*, 2014, **5**, 567–577.
131 C. Duan, A. Furlan, J. J. van Franeker, R. E. M. Willems, M. M. Wienk and R. A. J. Janssen, *Adv. Mater.*, 2015, **27**, 4461–4468.
132 F. Lombeck, F. Marx, K. Strassel, S. Kunz, C. Lienert, H. Komber, R. Friend and M. Sommer, *Polym. Chem.*, 2017, **8**, 4738–4745.
133 A. Luzio, F. Nübling, J. Martin, D. Fazzi, P. Selter, E. Gann, C. R. McNeill, M. Brinkmann, M. R. Hansen, N. Stingelin, M. Sommer and M. Caironi, *Nat. Commun.*, 2019, **10**, 3365.
134 A. E. Rudenko and B. C. Thompson, *J. Polym. Sci. Part Polym. Chem.*, 2015, **53**, 135–147.
135 M. Orbach, J. Choudhury, M. Lahav, O. V. Zenkina, Y. Diskin-Posner, G. Leitus, M. A. Iron and M. E. van der Boom, *Organometallics*, 2012, **31**, 1271–1274.
136 Z. Ahmadi and J. S. McIndoe, *Chem. Commun.*, 2013, **49**, 11488.
137 R. Matsidik, H. Komber, A. Luzio, M. Caironi and M. Sommer, *J. Am. Chem. Soc.*, 2015, **137**, 6705–6711.
138 C.-W. Ge, C.-Y. Mei, J. Ling, F.-G. Zhao, H.-J. Li, L. Liang, J.-T. Wang, J.-C. Yu, W. Shao, Y.-S. Xie and W.-S. Li, *J. Polym. Sci. Part Polym. Chem.*, 2014, **52**, 2356–2366.
139 J. H. Park, E. H. Jung, J. W. Jung and W. H. Jo, *Adv. Mater.*, 2013, **25**, 2583–2588.